EVALUATION AND IMPROVEMENT OF MASS SPECTROMETRY BASED STRATEGIES FOR PROTEIN POST-TRANSLATIONAL MODIFICATION ANALYSIS

By

Li Cui

A DISSERTATION

Submitted to
Michigan State University
in partial fulfillment of the requirements
for the degree of

Chemistry – Doctor of Philosophy

2014

ABSTRACT

EVALUATION AND IMPROVEMENT OF MASS SPECTROMETRY BASED STRATEGIES FOR PROTEIN POST-TRANSLATIONAL MODIFICATION ANALYSIS

By

Li Cui

Protein post-translational modifications (PTMs), such as phosphorylation, glycosylation, oxidation and methylation, play critical roles in a variety of intra- and intercellular activities, such as cell growth, division, migration and apoptosis. Dysregulation of PTMs may induce various diseases including cancer and diabetes. Mass spectrometry (MS) based proteomics has gained popularity in identifying, characterizing and quantifying proteins with PTMs.

Successful structural elucidation of proteins with PTMs largely replies on obtaining fragmentation information from tandem mass spectrometry (MS/MS) of peptides resulting from protein digestion. This dissertation partially focuses on improving the knowledge of phosphopeptide fragmentation chemistry during collision induced dissociation (CID)-MS/MS. Abundant neutral losses of 98 Da are often observed upon ion trap CID-MS/MS of phosphopeptides. Two competing fragmentation pathways are involved in this process, namely the direct loss of H_3PO_4 and the combined losses of HPO_3 and H_2O. They produce product ions with different structures but the same m/z values, potentially limiting the utility of CID-MS^3 for phosphorylation site localization. Furthermore, phosphate group rearrangement reactions in CID-MS/MS (phosphate groups transfer from one phosphorylated site to another hydroxyl group in the peptide) increase the ambiguity for assigning phosphate groups. In this dissertation, factors influencing the competing fragmentation and phosphate group rearrangement

reactions during CID-MS/MS of phosphopeptides have been systematically evaluated using a synthetic phosphopeptide library by varying a number of peptide properties. Both competing fragmentation and phosphate group rearrangement reactions were found to be most problematic for CID-MS/MS of phosphopeptide ions with limited proton mobility. The relative contribution of each competing neutral loss pathway was quantified in a series of regioselective ^{18}O-phosphate ester labeled phosphopeptides by comparing the abundance of the -100 Da ($-H_3PO_3{}^{18}O$) versus -98 Da ($-(HPO_3+H_2O)$) neutral loss product ions formed upon CID-MS/MS.

MS-based methods have also been extensively used for characterization and quantification of proteins containing methionine oxidation. Here parathyroid hormone (PTH), which is responsible for regulation of circulating calcium concentration in plasma, has been analyzed. The oxidation kinetics of PTH was first investigated *in vitro* with H_2O_2. The obtained oxidized forms of PTH were characterized by CID-MS/MS. It was found that methionine residues in PTH can mainly be oxidized to sulfoxides. An immuno-LC-MS/MS assay was then successfully developed for simultaneous quantification of native, truncated and oxidized forms of PTH in clinical plasma samples by employing heavy isotope labeled protein and peptide standards. The results from this immuno-LC-MS/MS assay analysis were compared to those from traditional PTH immunoassays to evaluate the effect of oxidation on the detection of PTH using traditional PTH immunoassays.

ACKNOWLEDGEMENTS

This dissertation would not have been completed without the support and help from the following folks. I owe my genuine gratitude to you.

Foremost, I would like to thank my advisor, Dr. Gavin Reid for your guidance in completing my doctoral research. Thank you very much for giving me the wonderful opportunity to work on these fascinating projects. Your enthusiasm, curiosity and pursuit of excellence for science have greatly infected me. I also greatly appreciate the guidance from my knowledgeable, thoughtful and encouraging committee, Dr. Merlin Bruening, Dr. Babak Borhan and Dr. David Weliky. I am very lucky to have you on my committee.

I sincerely thank my collaborators, Ipek Yapici and Dr. Babak Borhan at MSU, for helping me in the synthesis of ^{18}O labeled amino acids and for an enjoyable collaboration experience. I would also like to thank Ipek as a great friend for always bringing your positive energy to me. I thank the industry experts from DiaSorin for their funding and experience support and providing the clinical samples for the PTH project, especially John Wall, for you sacrificing several weekends to come to MSU and help me with sample processing.

I would like to give my special appreciation to the current and previous Reid's lab members. I deeply thank the current lab members Dr. Todd Lydic and Shuai Nie for your support when writing up my dissertation. I thank all the current and previous lab members who have overlapped with me in the lab, Dr. Cassie Fhaner, Kristen Reese and many others. Your support in and out of the lab is very important for me to go

through five years of graduate school. My special thanks go to Dr. Scott Smith, Dr. Yali Lu and Dr. Xiao Zhou for training me in proteomics work, for your guidance in my early graduate school life and for your helpful advice in preparing all my qualification examples. I would also like to thank Yongle Pang from Dr. Merlin Bruening's lab and Yueli Liu from Dr. Dana Spence's lab for teaching me how to use the HPLC.

I am truly grateful for my family and friends giving me all their generous love and support. I thank all my fantastic friends to be there for me whenever I need. Without the joy you have brought to me, without your shoulders I have cried on and without the hands you have given me, I would not have gone so far in my Ph.D. study. I specially would like to thank Zhenzhen Wang and Xiaonan Kou for your great support during the toughest time I have been through in graduate school. Finally yet importantly, I thank my parents for their unconditional love, encouragement and support in life. Without my mom's caring in the last several months, I would not have completed all the experiments and writing of this dissertation.

TABLE OF CONTENTS

LIST OF TABLES x

LIST OF FIGURES xi

LIST OF SCHEMES xvii

KEY TO ABBREVIATIONS xviii

CHAPTER ONE
An Overview of Mass Spectrometry Based Methods for Proteome Analysis 1
1.1 Introduction 1
1.2 Summary of Recent Improvements for MS-based Proteomics 4
1.2.1 Advancements in Protein Purification, Separation and Digestion Methods 4
1.2.2 Advancements in MS Instrumentation 6
1.2.3 Advances in MS Spectra Interpretation by Algorithms for Protein Identification 10
1.2.4 Development of New Dissociation Methods for MS/MS 11
1.3 Tandem Mass Spectrometry 11
1.3.1 CID 11
1.3.1.1 High-energy CID 14
1.3.1.2 Low-energy CID (Slow Activation) 14
1.3.1.3 Low-energy CID (Very Slow Activation) 14
1.3.1.4 Enhanced Cleavage of Protonated Peptides Ions in CID 15
1.3.1.5 Neutral Losses from Protonated Peptide Ions in CID 17
1.3.1.6 Peptide Sequence Scrambling in CID 19
1.3.1.6.1 Sequence Rearrangement Through Cyclization 19
1.3.1.6.2 Factors Influencing Peptide Sequence Scrambling 20
1.3.1.6.3 Effect of Sequence Scrambling on Confidence of Peptide Sequence Identification 20
1.3.1.7 Negative ionization mode CID 21
1.3.2 Electron-driven dissociations 22
1.3.2.1 ECD 22
1.3.2.1.1 General Introduction to ECD 22
1.3.2.1.2 Peptide Fragmentation Mechanism in ECD-MS/MS 22
1.3.2.1.3 Advantages and Disadvantages of ECD for Peptide Analysis 23
1.3.2.1.4 Alternative ECD Strategies 24
1.3.2.2 ETD 24
1.3.2.2.1 General Introduction to ETD 24
1.3.2.2.2 Advantages and Disadvantages of ETD 25
1.3.2.2.3 Negative ETD 26
1.3.2.3 EDD 26
1.3.3 Photon Dissociation 27

1.3.3.1 IRMPD 27
1.3.3.1.1 General Introduction of IRMPD 27
1.3.3.1.2 Characteristics of IRMPD 27
1.3.3.2 UVPD 28
1.3.3.2.1 General Introduction to UVPD 28
1.3.3.2.2 193 nm Photodissociation 29
1.3.3.2.3 Other UVPDs 30
1.3.4 Tandem Mass Spectrometry of Phosphorylated Peptides 31
1.3.4.1 Importance of Phosphorylation in Biological Systems 31
1.3.4.2 Challenges Associated with Phosphoproteomics 32
1.3.4.3 Phosphopeptide Fragmentation in CID 32
1.3.4.3.1 Neutral Losses in CID-MS/MS of Phosphopeptides 32
1.3.4.3.2 Phosphate Group Rearrangement in CID-MS/MS of Phosphopeptides .. 36
1.3.4.3.3 Negative Ionization Mode CID-MS/MS of Phosphopeptides 36
1.3.4.4 Phosphopeptide Fragmentation in Electron-Driven Dissociations 37
1.3.5 Tandem Mass Spectrometry of Peptides Containing Glycosylation 37
1.3.5.1 Significance of Glycosylation in Biological Systems 38
1.3.5.2 Categories of Glycosylation 38
1.3.5.3 Challenges and Strategies for Glycopeptide Analysis 39
1.3.5.4 Fragmentation of Glycopeptides in CID-MS/MS 40
1.3.5.5 Fragmentation of Glycopeptides in Electron-driven Dissociation and Photon Dissociation 41
1.3.5.6 Negative Ionization Mode Fragmentation of Acidic Glycopeptides 42
1.3.6 Tandem Mass Spectrometry of Peptides Containing Oxidized Methionine 42
1.3.6.1 Biological Significance of Methionine Oxidation in Proteins 42
1.3.6.2 MS/MS Fragmentation of Peptides Containing Methionine Oxidation 43
1.4 Algorithms for Peptide Identification 45
1.4.1 General Procedures that Algorithms Use for Peptide Identification 45
1.4.2 Database Search Algorithms 47
1.4.3 De Novo Sequencing Algorithms 48
1.4.4 PTM Identification Algorithms 48
1.4.5 Incorporation of Peptide Fragmentation Rules in Algorithms 49
1.5 Aims of this Dissertation 51

CHAPTER TWO
Examining Factors that Influence Erroneous Phosphorylation Site Localization via Competing Fragmentation and Rearrangement Reactions during Ion Trap CID-MS/MS and -MS^3 52
2.1 Introduction 52
2.2 Results and Discussion 54
2.2.1 Abundant Competing Fragmentation and Phosphate Group Rearrangement Ions can be Observed from CID-MS/MS of Multiply Protonated Peptide Precursor Ions 54
2.2.2 CID-MS^3 can Result in Erroneous Phosphorylation Localization Due to Competing Fragmentation or Rearrangement Reactions 59
2.2.3 Factors that Influence the Amplitude of Phosphate Group Rearrangement 65

2.2.4 Competing Fragmentation or Rearrangement Reactions can Result in Erroneous CID-MS/MS Phosphorylation Site Localizations in Phosphopeptides Containing Multiple Donors and Acceptors 80
2.3 Conclusions 85

CHAPTER THREE
Quantification of Competing H_3PO_4 versus HPO_3+H_2O Neutral Losses from Regioselective ^{18}O-Labeled Phosphopeptides 99
3.1 Introduction 99
3.2 Results and Discussion 103
3.2.1 Quantification of Competing Fragmentation Pathways 103
3.2.2 Examination of Factors that Influence the Competing Side Chain Fragmentation Pathways 108
3.2.3 Competing Fragmentation Pathways in HCD-MS/MS 111
3.2.4 The Source of Water in the Combined Neutral Loss Pathway 115
3.3 Conclusions 122

CHAPTER FOUR
Experimental Methods for Chapters Two and Three 123
4.1 Materials 123
4.2 Phosphopeptides 126
4.2.1 Fmoc Solid-Phase Peptide Synthesis (SPPS) 126
4.2.2 Synthesis of Regioselective ^{18}O-Labeled Phospho-serine and threonine Peptides 128
4.2.3 On-resin SPPS of Regioselective ^{18}O-Labeled Phospho-serine and -threonine Peptides 136
4.3 Multistage Tandem Mass Spectrometry Analysis of Phosphopeptides 137
4.3.1 Phosphopeptide Sample Preparation 137
4.3.2 Mass Spectrometry 137
4.4 Quantitative Analysis 138
4.4.1 Quantitative Analysis of Product Ion Abundances in Phosphate Group Rearrangement Reactions (Chapter Two) 139
4.4.2 Quantitative Analysis of Competing Fragmentation Pathways for Product Ions with Neutral Loss of 98 Da (Chapter Three) 140

CHAPTER FIVE
Characterization of Full Length, Truncated and Oxidized Variants of Parathyroid Hormone and Development of an Immuno-LC-MS/MS Assay for their Detection in Biological Samples 141
5.1 Introduction 141
5.2 Results and Discussion 145
5.2.1 Characterization of Full Length and Truncated PTH by LC-MS Bottom-up Approach 145
5.2.2 Oxidation Profiles of Full Length and Truncated PTH 149
5.2.3 Separation of Full Length, Truncated and Oxidized Variants of PTH 152
5.2.4 MS and CID-MS/MS for Top-down Characterization of Full Length, Truncated and Oxidized Variants of PTH 154

5.2.5 Development of an Immuno-LC-MS/MS Assay for Full Length, Truncated and Oxidized Variants of PTH in Biological Samples 163
5.3 Conclusions 178

CHAPTER SIX
Experimental Methods for Chapter Five 180
6.1 Materials 180
6.2 Isotope-labeled Peptides 181
6.2.1 Fmoc Solid-Phase Peptide Synthesis (SPPS) 181
6.3 Comparison of Different Proteolytic Enzymes for PTH Digestion 182
6.3.1 Trypsin Digestion 182
6.3.2 Glu-C Digestion 183
6.3.3 Arg-C Digestion 183
6.4 Oxidation Profiles of PTH 183
6.4.1 *In Vitro* Oxidation of WHO_PTH 1-84 and ^{15}N_PTH 7-84 183
6.4.3 Glu-C Digestion of Oxidized PTH 184
6.5 Preparation and Purification of Oxidized Variants of PTH 184
6.5.1 Oxidation of ProSpec_ PTH 1-84 and ProSpec_PTH 7-84 184
6.5.2 Purification of Oxidized ProSpec_PTH Variants 185
6.6 Quantification of the ^{15}N_PTH and PTH Variants 185
6.6.1 Trypsin Digestion of WHO_PTH and ^{15}N_PTH 185
6.6.2 Trypsin Digestion of ^{15}N_PTH and PTH Variants 186
6.7 Immuno-LC-MS/MS Assay for PTH 186
6.7.1 Immuno-affinity Enrichment of PTH in Plasmas 186
6.7.2 Recovery Yields of PTH Variants in Immuno-LC-MS/MS 187
6.7.3 Trypsin Digestion of Enriched PTH by Immuno-affinity Approach 187
6.8 Mass Spectrometry 188
6.8.1 ESI-MS and CID-MS/MS Analysis of $^{13}C_6{}^{15}N_1$Leu Labeled Peptides and Purified Oxidized PTH Variants 188
6.8.2 LC-ESI-MS and LC-ESI-MS/MS Analysis of PTH Digests in Immuno-LC-MS/MS Assay 188
6.9 Data Analysis 192
6.9.1 *In Vitro* Oxidation Profiles of PTH Methionine Residues 192
6.9.2 Determination of the Actual Quantity of ^{15}N_PTH and PTH Variants 192
6.9.3 Recovery Yields of PTH Variants in Immuno-LC-MS/MS 192
6.9.4 Quantification of PTH Native and Oxidized Variants in Patient Plasma . 193

BIBLIOGRAPHY 195

LIST OF TABLES

Table 2.1 Summary of Ascore LTQ MS/MS and Dscore LTQ MS/MS and MS^3 phosphorylation site localization results for a library of synthetic phosphopeptide sequences. (Ascore: * indicates the assigned phosphorylation site; Dscore: # indicates the assigned phosphorylation site for MS/MS; * indicates the assigned site for MS^3; Ascore/Dscore sequences are indicated in bold text if they were incorrectly assigned; Ascore/Dscore values are indicated in bold text if they were not confidently (>95% confidence) assigned; When two phosphorylation sites exist, the assigned site is labeled in red text.) 87

Table 4.1 Common amino acid building blocks used for solid-phase peptide synthesis. 125

Table 6.1 Tryptic PTH peptide 'inclusion list' precursor ions, retention times and 'targeted' CID-MS/MS product ions. 191

LIST OF FIGURES

Figure 1.1 Generic procedure for MS-based proteomics. Stage 1: The tissues or cells are lysed and fractionated by centrifugation and SDS-PAGE is used for separating the proteins. Stage 2: Proteases digest the separated proteins into peptides. Stage 3: The peptide mixture is separated using LC. Stage 4: ESI is employed for ionization of the peptides and the multiply protonated peptide precursor ions are then analyzed by a mass spectrometer to generate MS spectra. Stage 5: MS/MS or further MS^n are performed on the isolated precursor ions to induce fragmentation for peptide sequence analysis[6]. 3

Figure 2.1 ESI-LTQ ion trap CID-MS/MS product ion spectra for the doubly protonated precursor ions of the phosphopeptides (A) GRApYPVPAPSGGLHAAVR and (B) GRApYPVPAPAGGLHAAVR. ■ = +80Da (+HPO_3), ∆ = –98Da (–H_3PO_4 or –(H_2O+HPO_3)); □ = –80Da (–HPO_3); ° = –18Da (–H_2O). 57

Figure 2.2 ESI-LTQ ion trap CID-MS/MS product ion spectra from the doubly protonated precursor ions of the phosphopeptides (A) GRASPVPAPpYGGLHAAVR and (B) GRAAPVPAPpYGGLHAAVR. ■ = +80 Da (+HPO_3), ∆ = –98 Da (–H_3PO_4 or –(H_2O+HPO_3)); □ = –80 Da (–HPO_3); ° = –18 Da (–H_2O). 58

Figure 2.3 ESI-LTQ ion trap CID-MS^3 product ion spectra for the doubly protonated $[M+2H-98]^{2+}$ neutral loss product ions from the doubly protonated phosphopeptides (A) GRApYPVPAPSGGLHAAVR from Figure 2.1 and (B) GRASPVPAPpYGGLHAAVR from Figure 2.2. ● = +18 Da (–H_2O); ♦ = +17 Da (+NH_3); □ = –80 Da (–HPO_3); ° = –18 Da (–H_2O);); * = –17 Da (–NH_3). 60

Figure 2.4 ESI-LTQ ion trap CID-MS/MS and -MS^3 product ion spectra of GRApTPVPAPSGGLHAAVR. (A) CID-MS/MS of the doubly protonated precursor ion and (B) CID-MS^3 of the $[M+2H-98]^{2+}$ neutral loss product ion from panel A. ■ = +80 Da (+HPO_3); ● = +18 Da (–H_2O); ♦ = +17 Da (+NH_3); ∆ = –98 Da (–H_3PO_4 or –(H_2O+HPO_3)); □ = –80 Da (–HPO_3); ° = –18 Da (–H_2O). 63

Figure 2.5 ESI-LTQ ion trap CID-MS/MS and -MS^3 product ion spectra of GRApSPVPAPSGGLHAAVR. (A) CID-MS/MS of the doubly protonated precursor ion and (B) CID-MS^3 of the $[M+2H-98]^{2+}$ neutral loss product ion from panel A. ■ = +80 Da (+HPO_3); ● = +18 Da (–H_2O); ♦ = +17 Da (+NH_3);

Δ = –98 Da (–H_3PO_4 or –(H_2O+HPO_3)); □ = –80 Da (–HPO_3); ° = –18 Da (–H_2O). 64

Figure 2.6 Average % phosphate group rearrangement for the doubly protonated ($[M+2H]^{2+}$) precursor ions of the synthetic phosphopeptide library $GX_1AX_2PVPAPX_3GGLHAAVX_4$, where X_1 = R, K or G; X_2 = pY, pT or pS; X_3 = S, T or Y and X_4 = R, K or G, acquired by ion trap CID-MS/MS using ESI-LTQ (dark blue) or ESI-LTQ Velos (light blue) mass spectrometers. Average rearrangement ratios were calculated from the observed $y_{10}^{\blacksquare}$, y_{10}, $y_{12}^{\blacksquare}$, y_{12}, $y_{14}^{\blacksquare}$, y_{14} and $b_4^{\square}$, b_4, $b_6^{\square}$, b_6 $b_8^{\square}$, b_8 product ions. Error bars show the standard deviation of the individual % phosphate group rearrangements determined from each product ion. 66

Figure 2.7 Average % phosphate group rearrangement for the doubly protonated ($[M+2H]^{2+}$) precursor ions of the synthetic phosphopeptide library $GX_1AX_2PVPAPX_3GGLHAAVX_4$, where X_1 = R, K or G; X_2 = pY, pT or pS; X_3 = S, T or Y and X_4 = R, K or G, acquired by ion trap CID-MS/MS using ESI-LTQ (dark blue) or ESI-LTQ Velos (light blue) mass spectrometers. Average rearrangement ratios were calculated only using the observed $y_{10}^{\blacksquare}$, y_{10}, $y_{12}^{\blacksquare}$, y_{12}, $y_{14}^{\blacksquare}$ and y_{14} product ions. Error bars show the standard deviation of the individual % phosphate group rearrangements determined from each product ion. 67

Figure 2.8 Average % phosphate group rearrangement for the doubly protonated ($[M+2H]^{2+}$) precursor ions of several synthetic phosphopeptide libraries acquired by ion trap CID-MS/MS using ESI-LTQ. Average ratios were calculated from all $y^{\blacksquare}$, $y^{\blacksquare\blacksquare}$ and y-type product ions. (A) $y_4^{\blacksquare}$, $y_6^{\blacksquare}$, $y_7^{\blacksquare}$, $y_8^{\blacksquare}$ ions were observed for the LFX_1GHPEX_2LER peptides (where X_1 = pS, pT or pY, and X_2 = S, T or Y), (B) $y_8^{\blacksquare}/y_8^{\blacksquare\blacksquare}$,$y_9^{\blacksquare}/y_9^{\blacksquare\blacksquare}$, $y_{10}^{\blacksquare}/y_{10}^{\blacksquare\blacksquare}$, $y_{11}^{\blacksquare}/y_{11}^{\blacksquare\blacksquare}$, $y_{12}^{\blacksquare}/y_{12}^{\blacksquare\blacksquare}$, $y_{13}^{\blacksquare}/y_{13}^{\blacksquare\blacksquare}$ ions were observed for the $GX_1QELDVKPX_2AX_2PQER$ peptides (where X_1 = pSpS, pTpT or pYpY, and X_2 = S, T or Y) and (C) $y_8^{\blacksquare}$, $y_{10}^{\blacksquare}$ ions were observed for the $X_1PLPAPPRPFLX_2R$ peptides (where X_1 = pS, pT or pY, and X_2 = S, T or Y). Error bars show the standard deviation of the individual % phosphate group rearrangements determined from each of product ion. 69

Figure 2.9 Average % phosphate group rearrangement for the singly protonated ($[M+H]^{+}$) precursor ions of the synthetic phosphopeptide library $GX_1AX_2PVPAPX_3GGLHAAVX_4$, where X_1 = R, K or G; X_2 = pY, pT or pS; X_3 = S, T or Y and X_4 = R, K or G, acquired by ion trap CID-MS/MS using MALDI-LTQ XL mass spectrometer. Average rearrangement ratios were calculated from the observed $y_{10}^{\blacksquare}$, y_{10}, $y_{12}^{\blacksquare}$, y_{12}, $y_{14}^{\blacksquare}$, y_{14} and $b_4^{\square}$, b_4, $b_6^{\square}$, b_6 $b_8^{\square}$, b_8 product ions. Error bars show the standard deviation of the individual % phosphate group rearrangements determined from each product ion. ... 72

Figure 2.10 Average % phosphate group rearrangement for the doubly protonated ($[M+2H]^{2+}$) precursor ions of the synthetic phosphopeptide library $GX_1AX_2PVPAPX_3LHAAVX_4$, where X_1 = R or K; X_2 = pS or pSpS; X_3 = SGG, SSG or SSS and X_4 = R or K, acquired by ion trap CID-MS/MS using ESI-LTQ (dark blue) or ESI-LTQ Velos (light blue) mass spectrometers. Average ratios were calculated from all observed $y^{\blacksquare}$, $y^{\blacksquare\blacksquare}$ and y-type product ions. Error bars show the standard deviation of the individual % phosphate group rearrangements determined from each product ion. 75

Figure 2.11 ESI-LTQ ion trap CID-MS/MS of the doubly protonated precursor ion from the doubly phosphorylated peptide GRApSpSPVPAPSSLHAAVR. Panel (A) shows the full product ion mass spectrum. An expanded region of the product ion spectrum from panel (A) is shown in panel (B), while panel (C) shows an expanded region of the high resolution product ion spectrum acquired using an LTQ Orbitrap Velos mass spectrometer. ■ = +80Da ($+HPO_3$); ∆ = –98Da ($-H_3PO_4$ or $-(H_2O+HPO_3)$); □ = –80Da ($-HPO_3$); ° = –18Da ($-H_2O$). 76

Figure 2.12 ESI-LTQ ion trap CID-MS/MS of the doubly protonated precursor ion from the doubly phosphorylated peptides (A) GRApSpSPVPAPSSSLHAAVR and (B) GRApSpSPVPAPSSSLHAAVK. ■ = +80Da ($+HPO_3$); ∆ = –98Da ($-H_3PO_4$ or $-(H_2O+HPO_3)$); □ = –80Da ($-HPO_3$); ° = –18Da ($-H_2O$). 78

Figure 2.13 Average % phosphate group rearrangement versus Ascore and Dscore ratios for the LTQ CID-MS/MS doubly protonated ($[M+2H]^{2+}$) precursor ions from the synthetic phosphopeptide library $GX_1AX_2PVPAPX_3LHAAVX_4$, where X_1 = R, K or G; X_2 = pS, pSpS, pT, pY or pYpY; X_3 = SGG , TGG, YGG, SSG or SSS and X_4 = R, K or G. The x-axis shows the average % phosphate group rearrangement for each peptide. The y-axis shows the ratio of Ascore (blue) and Dscore (red) values determined from the triply and doubly protonated precursor ions (*i.e.*, the ratio of Ascore 3+/2+ or Dscore 3+/2+) for each phosphopeptide in the library. 84

Figure 3.1 (A) CID-MS/MS product ion spectra for the doubly protonated precursor ions of the phosphopeptides GRApSPVPAPSGGLHAAVR. The blue colored inserts (i) show the isolation spectra for the precursor ions, while the red colored inserts (ii) show expanded regions of the spectra for the neutral losses of $H_3PO_3{}^{18}O$ and (HPO_3+H_2O). ∆ = –100/98 Da ($-H_3PO_3{}^{18}O$ or $-(HPO_3+H_2O)$); □ = ‑80 Da (‑HPO_3); ° = –18 Da ($-H_2O$); * = –17 Da ($-NH_3$). (B) CID-MS/MS product ion spectra for the doubly protonated precursor ions of the phosphopeptides ALQAPHSPpTK. The blue colored inserts (i) show the isolation spectra for the precursor ions, while the red colored inserts (ii) show expanded regions of the spectra for the neutral

losses of $H_3PO_3{}^{18}O$ and (HPO_3+H_2O). Δ = –100/98 Da (–$H_3PO_3{}^{18}O$ or –(HPO_3+H_2O)); □ = ‒80 Da (‒HPO_3); ° = –18 Da (–H_2O); * = –17 Da (–NH_3). 106

Figure 3.2 Quantification of competing neutral loss pathways from CID-MS/MS of singly and doubly protonated ^{18}O labeled pS and pT phosphopeptide ions. Green and red bars indicate the % of the combined losses, while gray bars indicate the % of direct losses. Peptide pairs labeled in blue have same basic sequences but differ in the identity of the phosphorylated residue (*i.e.*, pS and pT). □ = –80 Da (–HPO_3); ○ = –18 Da (–H_2O). M: Mobile Proton; P: Partially Mobile Proton; N: Non-mobile Proton. 109

Figure 3.3 HCD-MS/MS product ion spectra for the doubly protonated precursor ions of the phosphopeptides (A) GRApSPVPAPSGGLHAAVR and (B) ALQAPHSPpTK. The red colored inserts show expanded regions of the spectra for the neutral losses of $H_3PO_3{}^{18}O$ and (HPO_3+H_2O). Δ = –100/98 Da (–$H_3PO_3{}^{18}O$ or –(HPO_3+H_2O)). 113

Figure 3.4 Comparison of the % combined neutral losses from CID-MS/MS (red) and HCD-MS/MS (blue) of the doubly protonated ^{18}O labeled pS and pT phosphopeptide ions. 114

Figure 3.5 Quantification of competing neutral loss pathways from CID-MS/MS of singly and doubly protonated ^{18}O labeled pS and pT phosphopeptide methyl esters. The underlined residues were methyl esterified. Green and red bars indicate the % of the combined losses, while gray bars indicate the % of direct losses. Peptide pairs labeled in blue have same basic sequences but differ in the identity of the phosphorylated residue (*i.e.*, pS and pT). □ = –80 Da (–HPO_3); ° = –18 Da (–H_2O). M: Mobile Proton; P: Partially Mobile Proton; N: Non-mobile Proton..... 117

Figure 3.6 CID-MS/MS product ion spectra for the doubly protonated precursor ions of the phosphopeptides (A) AASDAIPPApTPKADAPIDK and (B) AAADAIPPApTPKADAPIDK. Δ = –100/98 Da (–$H_3PO_3{}^{18}O$ or –(HPO_3+H_2O)); ° = –18 Da (–H_2O). 120

Figure 3.7 Quantification of competing neutral loss pathways from CID-MS/MS of doubly protonated ^{18}O labeled AAADAIPPApTPKADAPIDK and AAADAIPPApTPKADAPIDK methyl ester phosphopeptide ions. The underlined residues were methyl esterified. Red bars indicate the % of the combined losses, while gray bars indicate the % of direct losses. □ = –80 Da (–HPO_3); ° = –18 Da (–H_2O). 121

Figure 5.1 LC-MS of trypsin digested PTH 1-84. (A) General LC chromatography of trypsin digested PTH 1-84; (B) Extracted MS ion current for triply charged PTH 1-13; (C) Extracted MS ion current for doubly charged PTH 14-20; (D) Extracted MS ion current for PTH 1-20; Insert (i) shows the averaged MS scans for PTH 1-13 while (i) shows the averaged MS scans for PTH 14-20. 147

Figure 5.2 LC-MS of Glu-C digested PTH 1-84. (A) General LC chromatography of Glu-C digested PTH 1-84; (B) Extracted MS ion current for quadruply charged PTH 5-19; Insert spectrum shows the averaged MS scans for PTH 5-19. 148

Figure 5.3 Oxidation profiles of PTH 1-84 (A) and PTH 7-84 (B). Oxidation was performed in PBS buffer with 12 mM H_2O_2 at 37 ºC. The length of time is shown as the x-axis while y-axis shows the percentage of each of the forms at certain time point calculated based on the MS intensity of quadruply charged PTH 5-19 (A) and PTH 7-19 (B) ions. 151

Figure 5.4 HPLC separation of native and oxidized forms of PTH 1-84 (A) and PTH 7-84 (B). Oxidation was performed in PBS buffer with 12 mM H_2O_2 at 37 ºC for 1 h for PTH 1-84 and 30 min for PTH 7-84. 153

Figure 5.5 ESI-MS and CID-MS/MS of $[M+11H]^{11+}$ of PTH 1-84 (A), PTH 1-84M8(O) (B), PTH 1-84M18(O) (C) and PTH 1-84M8(O)M18(O) (D). The b ions labeled in red can be used for localizing methionine sulfoxide(s). 155

Figure 5.6 ESI-MS and CID-MS/MS of $[M+11H]^{11+}$ of PTH 7-84 (A), PTH 7-84M8(O) (B), PTH 7-84M18(O) (C) and PTH 7-84M8(O)M18(O) (D). The b ions labeled in red can be used for localizing methionine sulfoxide(s). 159

Figure 5.7 Workflow for the Immuno-LC-MS/MS PTH Assay 164

Figure 5.8 Response curves of immuno-LC-MS/MS for PTH 1-84 represented by PTH 1-13 (A) and PTH 14-20 (B). The x-axis is the initial concentration of PTH in the sample and the y-axis is the monitored fragment ion (y_{11}^{2+} for PTH 1-13 and y_5^+ for PTH 14-20) intensity in CID-MS/MS. 166

Figure 5.9 LC-MS/MS extracted currents for monitored fragments of PTH 1-13 and PTH 1-13M(O) (A); PTH 7-13 and PTH 7-13M(O) (B); PTH 14-20 (C) and PTH 14-20M(O) (C). 168

Figure 5.10 Immuno-LC-MS/MS assay results from patient samples 170

Figure 5.11 The relative recoveries of different variants of PTH in immuno-LC-MS/MS 172

Figure 5.12 Oxidation of PTH in different sets of patient samples. The percentage of oxidation was calculated by taking the sum concentration of PTH 1-13M(O), PTH 7-13M(O) and PTH 14-20M(O) divided by the sum concentration of all native and oxidized peptides. There were 41 samples in set A collected from site 1, and 29 samples in set B and 4 samples in set C collected from site 2. 174

Figure 5.13 The effect of oxidation on the PTH detection of traditional PTH assays. X-axis shows the percentage of oxidation while the y-axis shows the concentration differences in pg/mL. The percentage of oxidation was calculated by taking sum concentration of PTH 1-13M(O), PTH 7-13M(O) and PTH 14-20M(O) divided by the sum concentration of all native and oxidized peptides. The concentration difference was calculated by subtracting the concentration of PTH 1-13 obtained in the immuno-LC-MS/MS assay from the detected PTH concentration in the traditional assay. 177

LIST OF SCHEMES

Scheme 1.1 Nomenclature of peptide backbone fragment ions[60] 13

Scheme 1.2 Fragmentation pathways in CID-MS/MS of phosphopeptides 35

Scheme 3.1 Competing pathways for the CID-MS/MS gas-phase fragmentation reactions of protonated phosphopeptide ions. (A) Competition between H_3PO_4 loss side chain fragmentation and amide bond cleavage pathways, (B) competition within side chain fragmentation pathways involving the loss of H_3PO_4 or the combined losses of HPO_3 and H_2O, and (C) intramolecular phosphate group (HPO_3) transfer (*i.e.*, rearrangement or 'scrambling'). 102

Scheme 4.1 Synthesis process for Fmoc-Serine(^{18}O-TBDMS) (A) and Fmoc-L-Threonine(^{18}O-TBDMS) (B). 130

KEY TO ABBREVIATIONS

MS: mass spectrometry; MS/MS: tandem mass spectrometry

MS^n: multi-stage mass spectrometry

ESI: electrospray ionization

MALDI: matrix-assisted laser desorption/ionization

DESI: desorption electrospray ionization

CID: collision induced dissociation

CAD: collision activated dissociation

HCD: higher energy collisional dissociation

ETD: electron transfer dissociation

ECD: electron capture dissociation

niECD: negative-ion ECD

NETD: negative ETD

ETcaD: supplemental collisional activation strategy

UVPD: ultraviolet photodissociation

IRMPD: infrared multiphoton dissociation

FWHM: full width at half maximum

FT: fourier transform

ICR: ion cyclotron resonance

TOF: time of flight

QqQ: triple quadrupole mass spectrometer

PIM: process-induced modification

PTM: post-translational modification

SCX: strong cation-exchange

MOAC: metal oxide affinity chromatography

HPLC: high performance liquid chromatography

LC: liquid chromatography

UPLC: ultra performance liquid chromatography

SPPS: solid-phase peptide synthesis

PTH: parathyroid hormone

PTH1R: PTH receptor type 1

CHAPTER ONE

An Overview of Mass Spectrometry Based Methods for Proteome Analysis

1.1 Introduction

Although the human genome has already been sequenced in primary nucleotide form, the functional proteins transformed from DNA have not yet been fully characterized[1]. A common approximation for the number of genes in the human genome is 23,000. This may be enormous in number; however, it is not when compared with the two to three orders of magnitude greater number of proteins present the in proteome[2]. The sheer number of proteins in mammals, which is mainly due to the great variety of posttranslational modifications (PTMs), makes the complete characterization of the proteome exceedingly difficult[1]. PTMs are the chemical modifications to the side chains of amino acids within proteins, which include phosphorylation, glycosylation, oxidation, methylation, ubiquitination, and hundreds of others[1].

Analysis of the complex proteome samples requires the state-of-art technologies. Due to the advantages of mass spectrometry (MS), including high sensitivity, accuracy, information density and efficient analysis of large data sets and complex samples, this technology has been widely employed in proteomics for identification, characterization and quantification of proteins[3], especially after the development of the soft ionization techniques, matrix-assisted laser desorption/ionization (MALDI)[4] and electrospray ionization (ESI)[5] in the late 1980s. However, this is not to say that MS can provide us with all the desired information of a complex protein sample in a single analytical run[6]. Proteins in biological tissues and fluids exist not only in a great variety in terms of

molecular masses and PTMs, but also in dramatically different levels of abundance, spanning more than five orders of magnitude[7, 8]. MS has been most effective when employed for analysis of small sets of isolated proteins[6]. Thus sample fractionation, enrichment and separation techniques are often required prior to MS analysis. Figure 1.1 showed a typical workflow for MS-based proteomics using a so called “bottom-up” approach[6]. There are generally five stages involved in the whole process. Firstly, the tissues or cells of interest are lysed and fractionated by centrifugation. Protein mixtures are then extracted using an appropriate buffer. One- or two-dimensional gel electrophoresis is then employed to separate the proteins according to their electrophoretic mobility. The second stage involves protease digestion of the separated proteins into peptides, usually by trypsin. In the third stage, the peptides in the mixture are separated using liquid chromatography (LC) for further separation. For on-line LC-MS, ESI is commonly used for ionization of peptides to produce ions carrying multiple charges. The multiply protonated peptide precursor ions are then analyzed by a mass spectrometer first at the MS stage, which reveals the mass to charge (m/z) information of the peptide. With accurate measurement of peptide masses, and knowledge of the amino acid sequence for the protein of interest, these ions might be assigned to certain peptide sequences. However, very likely, multiple peptide sequences can be matched to one ion in the MS spectrum. Therefore tandem mass spectrometry (MS/MS) or further multi-stage mass spectrometry (MS^n) is needed to induce fragmentation of the isolated peptide precursor ions. Peptide ions with identical m/z can be then differentiated by analyzing the characteristic product ions that are formed by MS/MS or MS^n.

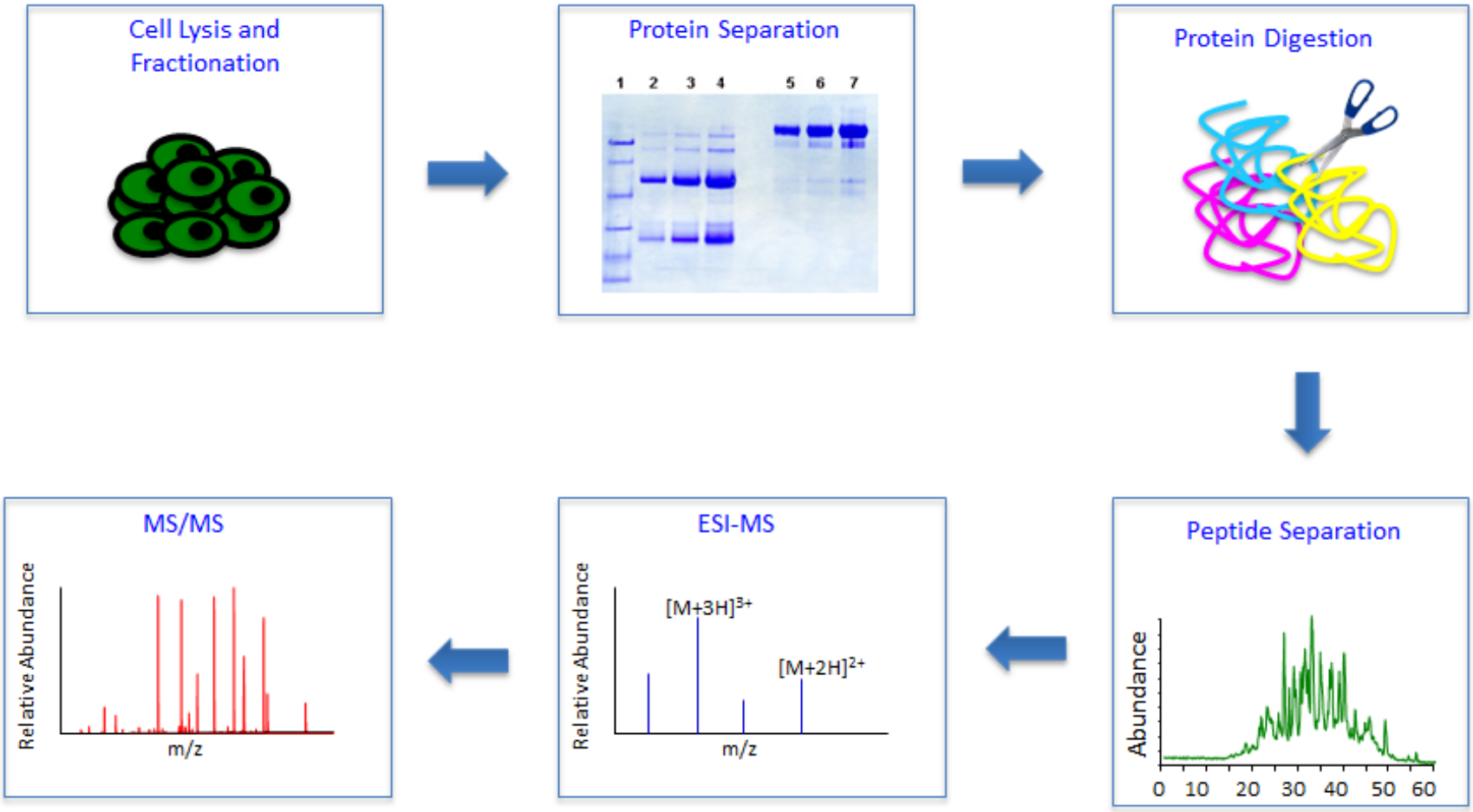

Figure 1.1 Generic procedure for MS-based proteomics. Stage 1: The tissues or cells are lysed and fractionated by centrifugation and SDS-PAGE is used for separating the proteins. Stage 2: Proteases digest the separated proteins into peptides. Stage 3: The peptide mixture is separated using LC. Stage 4: ESI is employed for ionization of the peptides and the multiply protonated peptide precursor ions are then analyzed by a mass spectrometer to generate MS spectra. Stage 5: MS/MS or further MS^n are performed on the isolated precursor ions to induce fragmentation for peptide sequence analysis[6].

1.2 Summary of Recent Improvements for MS-based Proteomics

1.2.1 Advancements in Protein Purification, Separation and Digestion Methods

There has been a significant amount of effort devoted toward improving the technologies for MS-based proteomics using the "bottom-up" approach. "Bottom-up" refers to the process of obtaining the protein sequence and structure information by putting peptide fragments together. Endoproteases necessarily play a critical role to generate the "appropriate" set of peptide fragments. A number of factors have to be considered before defining the peptides as "appropriate". First of all, the length of the peptides should neither be too short or too long. An average length of 8-9 residues is considered as a reasonable length for the "appropriate" peptides in MS analysis[9]. If the peptides are too long, it increases the complexity of the MS/MS or MS^n spectra especially considering that the fragmentation pattern of different peptides are often varied. More detailed discussion about how peptides fragment will be included in later sections. Oppositely, if the peptides are too short, there will be too many pieces in the "jigsaw puzzle", which makes it difficult to see the whole structure of the protein. Secondly, basic residues, *i.e.* arginine (Arg), lysine (Lys) and histidine (His), are required to efficiently protonate peptides by ESI or MALDI in the typically used positive ionization mode. Trypsin has been the primary choice for digesting proteins of interest in most studies (*2*). It efficiently cleaves the protein at the C-terminal side of Arg and Lys residues, except when Arg or Lys residues are bound to C-terminal proline (Pro). This insures the cleaved peptides have at least one basic residue. Additionally, tryptic peptides have an average length of 8.4 residues[9], which is a "appropriate" length for MS analysis at the normal mass range from 150-2000 m/z. Unfortunately, Arg and Lys

residues are not evenly distributed throughout proteins[10]. If long regions of sequence without Arg or Lys residues are present in the protein of interest, use of trypsin alone is not sufficient to achieve full sequence coverage. Therefore, several other endoproteases have been identified for protein digestion, such as chymotrypsin, Arg-C, Lys-C, Glu-C, Lys-N and Asp-N. Those enzymes cleave the proteins at different sites respectively and are widely recognized to improve sequence coverage when used in conjunction with trypsin[9]. However, the problems of low specificity, high cost and low efficiency have prevented them from being widely employed in proteomics. Certainly, further efforts to develop new enzymes that overcome these limiting factors would be valuable for improving the sequence coverage of proteins.

One of the great hurdles in MS-based proteomics is sample complexity. Commonly used advanced separation techniques have been employed and improved to solve this problem. Two-dimensional gel electrophoresis (2DE) has been well developed for more than three decades for separating protein mixture[6]. For proteins separated in 2DE, they can be excised along with the gel and digested for MS analysis. Despite the initial success in coupling 2DE with MS to identify abundant proteins in cells, the dynamic range of the proteins that can be identified by this method is limited[6, 7]. Therefore, more effort has been given to develop gel-free MS-based proteomics[2] to overcome the drawbacks of 2DE based proteomics, such as long duration of analysis, under representation of the less soluble membrane proteins[11] and an inability to detect lower abundant proteins. Nevertheless, separation of a complex protein mixture remains a daunting issue in the gel free approaches. Multidimensional protein identification technology (MudPIT)[12], which involves a combination of strong cation-

exchange (SCX) chromatography and reverse-phase columns to separate the peptide mixture prior to MS analysis, has been developed to improve the resolution power of peptide separations[3]. The complex peptide mixtures are first introduced into high capacity SCX resins and fractionated according to their isoelectric points. Each peptide fraction is then further separated by high resolution reverse phase columns. Advances in LC instrumentation have also been achieved to aid the analysis of complex protein samples. Ultra performance liquid chromatography (UPLC) characterized by high pressure and low flow rate has been recently developed. It has begun to achieve more popularity in LC-MS based proteomics because of its inherent advantages of better sensitivity and faster chromatography when compared to conventional high performance liquid chromatography (HPLC)[2, 13]. The drawbacks for UPLC include the high cost of instrumentation and that the current data acquisition rates of the mass spectrometer may not be able to adequately accommodate the sharp peaks in UPLC.

1.2.2 Advancements in MS Instrumentation

In parallel to improvements in the upstream analytical methods, additional advances in MS technology have dramatically sped up the development of MS-based proteomics. Recent improvements have been achieved in four primary areas: ionization techniques, ion transmission efficiency, mass detection efficiency and activation/dissociation technologies [2, 8]. ESI has gained more popularity than MALDI in proteomics because of its ability to be readily coupled to on-line LC systems. Numerous other soft ionization techniques have been applied to proteomics since the advent of ESI and MALDI. Ambient ionization refers to a series of direct ionization techniques that occur at ambient environments that require few or no sample

preparation steps, such as desorption electrospray ionization (DESI)[14, 15]. It has attracted widespread attention and approximately 40 ambient ionization methods have been described in the literature to date[16]. However, only a few of ambient ionization designs have been commercialized. This is partially due to the complexity and non-repeatability of the instrument designs.

Recent improvement in ion optics has improved the ion transmission from the ionization source to the mass spectrometer, which greatly facilitates the analysis of low abundance proteins/peptides. For instance, the implementation of the “S-lens” on ion-trap mass spectrometers increased their sensitivity by five times compared to traditional tube lens/skimmer optics[17].

More importantly, advancements in mass analyzers have significantly altered the world of mass spectrometers. The pursuit of mass analyzers with high resolution and accuracy has always been a focus in the MS field. These advances enable researchers to acquire mass spectra with improved accuracy, resolution and mass range, which facilitates the interpretation of spectra and the subsequent understanding of peptide fragmentation pathways. Better understanding of the peptide fragmentation chemistry ultimately helps achieve better understanding of the structure of proteins/peptides of interest. High mass accuracy makes two fragments ions with close masses distinguishable, which helps with correct interpretation of the spectra; while high resolution resolves two adjacent peaks, which enables isotopic labeling techniques to investigate the peptide fragmentation pathways. Mass analyzers can be divided into three categories based on their resolution (calculated using full width at half maximum (FWHM)): low resolution quadrupoles and quadrupole ion traps (< 2,000), medium

resolution time of flight (TOF) (10,000-60,000) and high resolution analyzers, Fourier-transform ion cyclotron resonance (FT-ICR) and Orbitrap (>100,000)[2].

The linear ion trap has been the most widely used mass analyzer to date owing to its advantages of low price and high efficiency. The recent development of a dual-pressure ion trap mass spectrometer achieved great improvement in the number of proteins and peptides detected in complex mixtures[17]. It comprises a linear ion trap operated at higher pressure for more efficient trapping and fragmenting of the precursor ions of interest, and another linear ion trap operated in low pressure for detecting the fragments with higher resolution[17]. Moreover, the recently introduced Orbitrap mass spectrometer[18] achieved a competitive resolution power compared to FT-ICR, but with the advantage of a more affordable price. The Orbitrap Elite marketed by Thermo Fisher Scientific achieved a resolution power of 240,000 at m/z 400[19] by employing the enhanced form of Fourier Transformation (eFT)[20] and reduction of the delay between ion injection and start of ion transient detection[19]. Moreover, it incorporated three different dissociation methods into one instrument: collision induced dissociation (CID), electron transfer dissociation (ETD) and higher energy collisional dissociation (HCD), which are beneficial for structural elucidation of proteins and peptides. A recent updated version of Orbitrap mass spectrometer, Orbitrap Fusion, has achieved an even higher resolution power (450,000 at m/z 200) and has been successfully employed for highly efficient proteome analysis[21].

TOF, which combines relatively high resolution, low price and short analysis time, has been a popular choice to be directly coupled to on-line LC in many proteomics studies. Additionally, the combination of MALDI with TOF was proposed as the most

promising mass spectrometer for future biological studies[8]. To overcome the limitation that MALDI cannot be coupled to on-line LC system, a strategy has been developed involving deposition of the droplets coming out of LC onto the MALDI plate sequentially along with the matrix solution. The MALDI plate was allowed to dry and then inserted into the mass spectrometer for off-line analysis[8, 22]. By this approach, the samples preserved on the plate can be subjected to analysis over an extended period of time, therefore it enables acquisition of high quality MS/MS spectra on low abundance targets[8]. Moreover, several different dissociation methods can be applied to analyze one peptide ion of interest using this strategy.

TOF mass analyzers can theoretically reach unlimited mass ranges and thus have been widely used in “top-down” proteomics[23-27]. “Top-down” proteomics involves direct analysis of the intact protein precursor ions and interpretation of the MS/MS spectra for protein sequence and PTM information[28, 29]. The molecular weight of the intact protein is usually large and the MS/MS spectra are very complicated to interpret due to the presence of massive peptide fragments[30]. Therefore it requires mass analyzers with both high resolution and high mass range[2]. The FT-ICR mass analyzer has been initially used in characterization of intact proteins in proteomics because of its high resolving power [26, 28, 29, 31, 32]. Recently, the Orbitrap mass analyzer has also been increasingly employed in top-down proteomic analysis[33, 34]. The initial version of the Orbitrap analyzer could only analyze intact proteins as large as 30 kDa[35, 36]. This limitation was overcome by the later versions[19, 36]. A large protein, enolase (46.64 kDa), has been successfully detected and resolved by the Orbitrap Elite instrument[19].

Undoubtedly, we may envision that future improvements in MS instrumentation will continuously benefit the field of proteomics.

1.2.3 Advances in MS Spectra Interpretation by Algorithms for Protein Identification

Due to the great mixture complexity of proteins in biological systems, one typical LC-MS/MS run can generate thousands of spectra with peptide information. Manual interpretation of the data is heavily time consuming, which has led to the development of automatic data processing algorithms. Both database search algorithms, such as frequently used Sequest[37], Mascot[38], OMSSA[39] and X!Tandem[40], and de novo sequencing algorithms, such as PepNovo[41] and PEAKS[42] identify the peptide sequence by matching the peaks in experimental spectra to *in silico* fragments. The use of these algorithms greatly speeds up the proteomics data analysis process. Unfortunately, these algorithms are less successful when interpreting spectra with limited sequence coverage fragments. Ideally, if the simulated fragmentation pattern matches perfectly with the observed fragmentation pattern, there will be no ambiguity in determining the peptide sequence. However, theoretical rules employed in these algorithms for predication of peptide fragmentation are often simplistic and do not consider all actual patterns of peptide fragmentation. Moreover, a full understanding of peptide fragmentation rules has not yet been achieved despite decades of research in this field.

Section 1.3 in this chapter will discuss the status of ongoing efforts to systematically characterize peptide sequence- and modification-dependent fragmentation patterns.

1.2.4 Development of New Dissociation Methods for MS/MS

State-of-the-art proteomics largely relies on MS/MS for structure elucidation of peptides and proteins. Therefore, it is critical to identify a dissociation method that can provide fragment ions containing all relevant structural information. In addition to collision induced dissociation (CID)[43], traditionally the most widely used dissociation method in MS/MS-based proteomics, electron-driven dissociation and photodissociation methods have also gained in popularity. As these new dissociation techniques develop, including electron capture dissociation (ECD)[44, 45], electron transfer dissociation (ETD)[46], infrared multiphoton dissociation (IRMPD)[47, 48], and ultraviolet photodissociation (UVPD)[47, 49, 50], the understanding of their respective protein and peptide fragmentation rules is also increasing, which greatly facilities peptide and protein analysis. It is generally accepted that these recently employed dissociation methods are complementary to CID for improving sequence coverage of peptides or proteins. These new dissociation methods are still limited by a number of factors, such as accessibility of the required MS instrumentation, ease of instrument maintenance, and efficiency and speed of analysis. More detailed discussion about the mechanism and application of each of the above dissociation methods is included in the following section.

1.3 Tandem Mass Spectrometry

1.3.1 CID

The use of CID, also known as collision activated dissociation (CAD), was first implied at the original report describing a mass spectrometer by J.J. Thomson in 1913[51, 52]. Modern CID work was pioneered by Jennings[53] and McLafferty and

Bryce[54] in the 1960's. Initially, CID was primarily employed in the analyis of small molecules and hadn't been widely implemented for protein characterzition untill the 1980's after the development of MALDI and ESI enabled the ionization of large biological molecules[43]. In CID-MS/MS of peptide or protein ions, kinetic energy is transformed to internal energy upon collisions with neutral gas molecules such as He, N_2 or Ar [43, 54, 55]. Upon sufficient internal energy accumulation, the precursor ions undergo charge-directed or charge-remote fragmentation processes to form mainly b- and y- type product ions[56, 57]. The nomenclature for peptide product ions was determined by the cleavage sites within the peptide backbone[58, 59]. Cleavages at amide bonds give rise to b ions containing the N-terminal ends of the peptide and y ions containing the C-terminal ends. Similaly, fragmentation of the C_α-C and N-C_α bonds, generate a- and x- ions, and c- and z- type ions, respectively, as shown in Scheme 1.1.

.

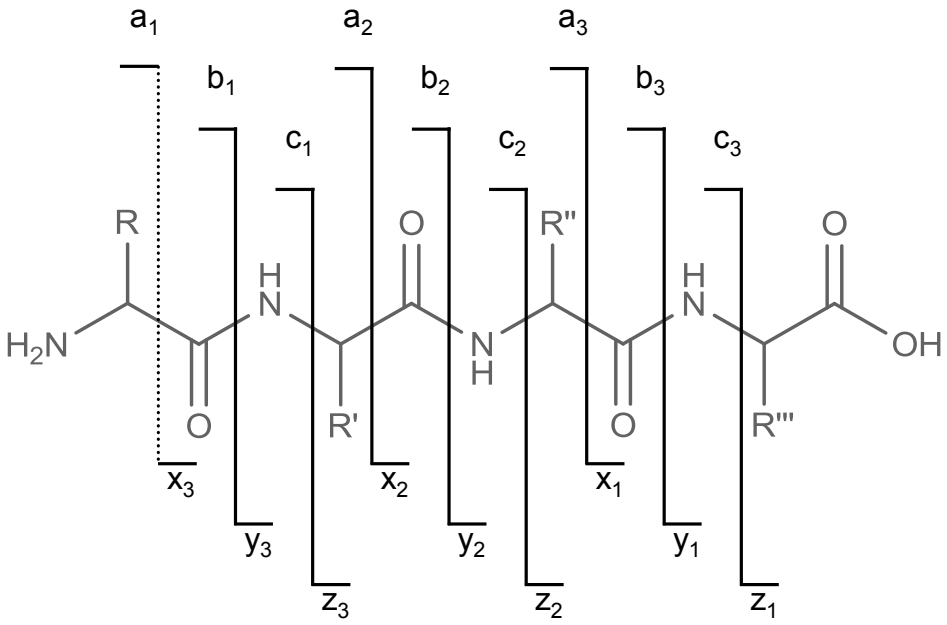

Scheme 1.1 Nomenclature of peptide backbone fragment ions[60]

1.3.1.1 High-energy CID

CID can be divided into three main categories according to the activation time scale and the collision energy[43]. High-energy CID is the first kind of CID that was described. It involves kilo-electron-volt kinetic energy, which can be achieved in sector-based instruments and tandem TOF instruments. With only a few collisions required, high-energy CID occurs in a time scale of a few microseconds. High-energy CID has been used for peptide characterization in proteomics for its merit of enabling cleavage of amino acid side chains in addition to amide bond cleavage[61], which is helpful for distinguishing isomeric residues. However, it has relatively low efficiency, typically less than 10%, due to its short dissociation time and low efficency for the collection of product ions[43].

1.3.1.2 Low-energy CID (Slow Activation)

The second category of CID is referred as low-energy CID induced by slow activation, which is typically performed on quadrupole and other multipole instruments. The most frequently used instruments in slow activation induced low-energy CID are a triple quadrupole mass spectrometer (QqQ) or a quadrupole time of flight mass spectrometer (Q-TOF). Slow activation induced low-energy CID occurs in a few hundred microseconds to a few milliseconds with elevated gas pressure (Ar or N_2) to allow tens to hundreds of collisions. The collision energy used here is up to 100 electon volts. The longer activation time allows low-energy CID efficiency to reach up to 50%[43, 55, 62]. A so called higer-energy CID (HCD), which was recently enabled on the high resolution Orbitrap instrument using N_2 as the collision gas, also falls into this category[63].

1.3.1.3 Low-energy CID (Very Slow Activation)

The third category of CID is also called low-energy CID, but induced by very slow activation. As the name implies, its collision duration is tens to hundreds of miliseconds. Ion trap intrstruments are often employed for this category of low-energy CID, to trap precursor ions for an extended period of time so that sufficient energy can be accumulated by the precursor ions to induce fragmentation. This kind of CID is also known as ion trap CID. It usually employs He as the collision gas. Since the ions have to be trapped for a relatively long time, they can only be excited to a few electron volts of kinetic energy; however, it is this characteristic that enables ion trap CID efficiency to reach up to 50-100%[43].

1.3.1.4 Enhanced Cleavage of Protonated Peptides Ions in CID

The low-energy CID have been more prominently explored than high-energy CID due to their high efficieny and readily available instrumentation. A review by Paizs and Suhai summarized in detail the various fragmentation pathways of peptide ions by CID [57]. Activation occurring at the time scale of low-energy CID is actually longer than the time scale for unimolecular fragmentation[30, 60], which allows the energy transferred into peptide presursor ions to redistribute along the peptide backbone and results in cleavage through the lowest energy pathway[30]. Consequently, the b- and y- types of product ions are not obtained in equal intensities. Several studies have reported the occurrence and the mechanisms of enhanced cleavages at N-terminal to Pro and C-ternimal to aspartic acid (Asp)[64-71].

The enhanced cleavages at Xaa (any amino acid) -Pro were proposed to be related to the special cyclic pyrrolidine ring structure of Pro residues[72]. Because the imide bond of Pro has relatively higher proton affinity than the normal amide bond and

the attack on the Pro carbonyl carbon by the neighboring carbonyl oxygen is hindered due to the ring structure, cleavages to the Pro C-terminal are reduced while to its C-terminal are enhanced[64, 71]. The carboxylic groups at the side chains of Asp residues were found to be involved in the enhanced cleavages at Asp-Xaa[67]. A number of different mechanisms have been proposed for this phenomenon, but the acutal process remains uncertain[57].

Enhanced cleavages have been found to be closely related to the proton mobility of the precursor ions, which was defined by the mobile proton model[69, 73, 74]. In this mobile proton model, peptide precursor cations have generally been classified into three categories according to their ability to mobilize proton(s)[71], namely, mobile (# of protons > # of Arg+ Lys+ His), partially mobile (# of Arg < # of protons ≤ # of Arg+ Lys+ His) and non-mobile (# of protons ≤ # of Arg). Besides those primary preferred cleavages, other secondary enhanced fragmentations have also been observed in various investigations. Kapp *et. al.* reported the effect of specific pairwise interactions on preferential cleavage after performing a statistical study on a large set of peptides. Cleavage between the Asp-Pro bonds was found to be the most dominant one for all Asp-Xaa cleavages, but was only the most dominant one for all Xaa-Pro cleavages within peptide presursor ions under non-mobile protonated ion conditions[71]. In another statistical study conducted by Tabb and co-workers, the formation of b ions at the C-terminal to His were found to be increased[64]. Tsaprailis *et. al.* further investigated the enhanced cleavage of His and proposed a mechanism involving an atypical b ion structure. Dominant complementary b^+/y^+ product ions cleaved between the His-Pro amide bond were observed in doubly protonated peptide precursor ions containing

Arg[75]. Huang and co-workers found that cleavages of Asp-Xaa bonds are more prominent in doubly protonated peptide precursor ions that contained internal basic residues than those that did not. The basic residue effect was most predominant for Arg, followed by Lys and lastly His, which were in good correlation with their proton mobility classification. It again suggested a mechanism in which the acidic hydrogen on the Asp side chain induced enhanced cleavage when protons were localized to basic residues[76]. Moreover, the enhanced cleavage was observed at glutamic acid (Glu)-Xaa bonds of non-mobile peptide precursor ions, but the phenomenon was not as extensive as that of Asp-Xaa[76].

In addition to the effects of common amino acid residues on peptide fragmentation patterns, PTMs are also found to influence the peptide fragmentation pathways in terms of enhanced cleavage. For example, enhanced cleavages at the C-terminal side of phosphorylated serine (Ser) and threonine (Thr) residues were found in non-mobile peptide precursor ions[77]. Gehrig and co-workers proposed a nucleophilic attack mechanism involving phosphate oxygen attacking to the neighboring C_α of peptide backbone[77].

1.3.1.5 Neutral Losses from Protonated Peptide Ions in CID

There are generally two categories of fragments generated upon dissociation of peptide ions. One category is sequence ions that provide information concerning the amino acid composition of the peptides, like the b and y ions produced during CID-MS/MS. Non-sequence ions, however, often exist as side products during the fragmentation process. These include product ions with water or ammonium neutral losses. The presence of these non-sequence ions increases the complexity of spectra

interpretation, especially when they dominate the overall fragmentation. The production of these neutral loss ions is also related to the characteristics of CID, which fragment peptides ions in the lowest energy pathway. Water losses can be initiated from the C-terminal COOH group[78, 79], side chain COOH groups of Asp and Glu[57], side chain OH groups from Ser and Thr[80, 81], and backbone amide oxygens[79, 81]. Ammonium losses usually result from protonated side chains of Lys[82, 83], Arg[57], asparagine (Asn) and glutamine (Gln)[57, 84].

The fragmentation chemistry of peptides containing PTMs can be very different from their unmodified forms[85]. For instance, abundant non-sequence ions with neutral loss of phosphate or meta-phosphate groups are observed in the MS/MS spectra of phosphorylated peptides. This is due to the activation energy barrier for cleaving phosphate groups (< 20 kcal/mol) being much lower than that needed for amide bond cleavage (~ 40 kcal/mol)[80, 86-88]. Beneficially, this neutral loss of the phosphate group can be treated as a characteristic property of phosphopeptides, which makes the phosphopeptide easily distinguished from other peptides. However, sometimes these non-sequence ions are so intense that the abundance of other sequence ions is greatly suppressed. In this case, sequence identification becomes problematic due to a lack of information[60]. Studies have demonstrated that this neutral loss process highly depends on the proton mobility of the precursor peptide ions[60]. Generally, it is more dramatic in peptide ions with lower charge states and more basic residues, which are under non-mobile conditions. Localizing the correct position of a PTM is critical in terms of studying the proteins' biological functions. However, it is often difficult to localize the position of the PTMs when abundant non-sequencing ions are present in the spectra.

Another example is characterization of glycosylation. Due to the lability of glycans, CID-MS/MS of glycosylated peptides produces abundant peaks from cleavage of glycans and less abundant peaks from peptide backbone cleavage [89, 90]. That makes analysis of glycosylation a challenging task. Furthermore, peptides with process-induced modifications (PIMs) could also result in neutral losses upon CID[85]. For example, methionine (Met)- and S-alkyl cysteine (Cys)-containing peptides, which are often oxidized to sulfoxide forms, may produce a dominant neutral loss of alkyl sulfenic acid (RSOH)[91-95].

1.3.1.6 Peptide Sequence Scrambling in CID

1.3.1.6.1 Sequence Rearrangement Through Cyclization

During low energy CID-MS/MS, non-conventional fragments with elimination of internal amino acid residues and relocation of C-terminal residues to the N-terminus of a peptide's original sequence have been identified[96-100]. This phenomenon has been called peptide sequence scrambling / rearrangement / permutation. It was proposed that the scrambling involves a cyclization of b ions head-to-tail and reopening at different positions[97, 100]. In CID-MS/MS, the resultant y ions exist only in a linear form while b ions may exist in two forms: linear structures with a five-membered oxazolone ring at the C-terminal side[101, 102] and macrocycle structures. The macrocycle structures were formed by N-terminal nitrogen attacking the carbonyl carbon of the oxazolone of linear structure b ions[100]. The macrocycle ring may then reopen at various amide bonds, which produces b ion isomers that are not distinguishable from its original sequence[96-98]. The above proposed mechanism was supported by the fact that N-acetylation of the N-terminal nitrogen inhibited the sequence scrambling[97].

1.3.1.6.2 Factors Influencing Peptide Sequence Scrambling

Instrumentation has a strong impact on peptide sequence scrambling due to the influence of activation time scales. It is found to be more predominant in ion-trap CID (very slow activation) than triple quadrupole CID (slow activation)[98]. Relatively slow activation gives the fragment ions more time to rearrange and generate new forms of fragments. Sequence scrambling was further affected by the properties of the peptides themselves. Yague *et. al.* reported that elimination of the internal amino acids was found to be more favorable for amino acids with aliphatic side chains[97]. Doubly protonated b ions were observed to produce more scrambling products than singly charged b ions[97, 99], which could be due to the fact that doubly charged species more readily form macrocycle structures and/or singly charged cyclic b ions do not fragment as readily as doubly charged ones[97]. Interestingly, Jia *et. al.* found that deletion of internal amino acids due to sequence scrambling was also observed with singly charged b ions in multi-stage CID (i. e. MS^3)[103]. They also reported that the enhanced cleavage rules, which were mentioned in section 1.3.1.4, can influence the selectivity of b ions macrocycle ring opening.

1.3.1.6.3 Effect of Sequence Scrambling on Confidence of Peptide Sequence Identification

With the presence of scrambled b ions suggesting incorrect primary peptide sequences, it becomes difficult to identify the original primary peptide sequence. Peptide sequence scrambling was first investigated based on specific model peptides, and therefore its effect on the confidence of peptide sequence identification needs to be evaluated on numerous naturally occurring peptides. In a study performed by

Saminathan *et. al.*, of 43 tryptic peptides investigated, 35% showed evidence of scrambled b ions with relative low abundance ranging from 8% to 16%. However, the accuracy of peptide and protein identification by Mascot was not negatively affected by sequence scrambling in these cases[104]. Yu *et. al.* statistically evaluated the peptide sequence scrambling of greater than 4,500 tryptic peptides from a published proteomics study. Peptide sequence scrambling was found to increase with longer sequences and higher charge states. They also found that among peptides with higher-confidence matches (at least five ions were assigned to the original sequence), only an average 20% of masses in the spectra could be assigned to the original sequences and a third of the remaining unassigned products ions may be caused by sequence scrambling[105]. With an estimation of such a high rate of scrambling, the authors questioned whether considering the peptide permutation would increase the confidence of the peptide identification. Unfortunately, the number of peptides that they were able to analyze was not adequate to answer this question.

1.3.1.7 Negative ionization mode CID

CID can also be performed in negative ionization mode to fragment peptide anions. The Bowie research group and others have conducted intensive studies on how peptide ions fragment in negative CID[106]. Unfortunately, abundant neutral losses from the side chains of amino acids are observed in negative CID of peptides, such as CH_2O and MeCHO losses from Ser and Thr residues, respectively, H_2S losses from Cys residues, water losses and ammonium losses[107, 108]. Additionally, phosphate group rearrangement reactions was found in negative ionization mode CID of phosphopeptides[109]. These unfavorable fragmentation pathways do not provide an

advantage for negative ionization mode CID over positive ionization mode CID in peptide characterization. Nevertheless, negative ionization mode CID is generally a strategy of interest for analyzing acidic peptides that are not ionized well in positive ionization mode, and therefore it has been used in characterization of phosphorylated[110-112] and glycosylated peptides[113]. More detailed discussion will be included in the following sections when describing the fragmentation chemistry of peptides containing PTMs.

1.3.2 Electron-driven dissociations

1.3.2.1 ECD

1.3.2.1.1 General Introduction to ECD

McLafferty and co-workers first developed ECD on an FT-ICR instrument[44]. Following the peptide precursor cation capturing a soft electron, i. e. low energy electron (<0.2 eV)[114], a cation radical site is generated. This promotes fragmentation at N-C_α bonds of the peptide precursor ions generating c- and z- type product ions. ECD efficiency strongly depends on the efficiency of capturing electrons. The electron capture efficiency is related to the capture cross section, which is proportional to the square of the ion charge[115]. Since the maximized capture also requires a minimum kinetic energy difference between the electron and peptide precursor ion, the electron's energy needs to be kept low so that there can be sufficient time for the electron to be captured by the peptide precursor ions[114, 116]. ECD is mainly enabled on FT-ICR instruments because of their ability to trap low energy electrons and allowing sufficient interaction between the electrons and peptide precursor ions[117].

1.3.2.1.2 Peptide Fragmentation Mechanism in ECD-MS/MS

Of the different fragmentation mechanisms proposed for ECD, the Cornell mechanism and the Utah–Washington mechanism have become most well-known[118]. In the Cornell mechanism proposed by McLafferty and co-workers, the electron is captured on a positively charged site and it subsequently promotes a hydrogen transfer to the amide oxygen through a relaxation process. The thus formed carbon-centered aminoketyl radical intermediate initiates a cleavage of the N–C_α bond at its right side[44]. The Utah–Washington mechanism suggests that the electron is directly captured onto the amide group, forming an aminoketyl radical anion. The formed radical anion is either first neutralized by proton transfer from a charged site and then initiates bond cleavage between N–C_α[119] or initiates the cleavage first and then proton transfer[120].

1.3.2.1.3 Advantages and Disadvantages of ECD for Peptide Analysis

ECD occurs in less than 10^{-12} s, which only allows direct bond dissociation to form c- and z- type odd-electron product ions[117]. This short time scale does not permit redistribution of intra-molecular vibrational energy over all degrees of freedom, to induce the fragmentation of the weakest bonds as occurred in CID. Consequently, peptide bonds are cleaved evenly and PTMs are preserved on their original sites in ECD, which is advantageous in sequencing peptides and localizing PTM sites[121, 122]. Due to the high S-S affinity for H• atoms, S-S bonds are preferably cleaved in ECD. This fragmentation is not favored in low energy dissociations[123], but is very useful in identifying the presence and location of the S-S bonds[117]. However, the limitation of ECD not being amenable to ion trap instruments without additional modifications confines its range of application. In addition, the electron will neutralize

singly charged peptide precursor ions and thus ECD is not applicable to these ions. For doubly charged ions, the efficiency of ECD is 20% or less. Fortunately, the efficiency rises up to 80-100% for more than doubly charged peptide ions[118].

1.3.2.1.4 Alternative ECD Strategies

Taking advantage of ECD being able to be coupled to FT-ICR instruments with high mass resolution, ECD has been actively employed in top-down proteomics to fragment intact proteins. However, due to the high order structure of proteins and non-covalent interactions within the protein, ECD is not efficient in fragmenting large proteins (>20 kDa)[30]. Activated ion (AI) ECD was developed by Horn and co-workers to address this challenge[124]. The protein precursor ions were simultaneously heated during ECD, which increased the number of backbone fragments from the protein.

Negative-ion ECD (niECD) has been developed to enable ECD analysis of peptide anions for better sequencing of acidic peptides that are ionized more efficiently in negative ionization mode[125]. In niECD, peptide anions can capture 3.5~6.5 eV electrons, which induces dissociation similar to ECD.

1.3.2.2 ETD

1.3.2.2.1 General Introduction to ETD

ETD was first introduced on an ion trap instrument in 2004[46]. Unlike CID, where fragmentation is induced by collisions between isolated precursor ions and an inert gas, ETD occurs via ion/ion reactions[126]. An electron carried by a reagent anion transfers to multiply charged peptide cations upon collision, which results in an odd-electron cation that undergoes radical-driven cleavage primarily at N-C_α bonds to generate c-and z-type product ions[46]. It follows a similar pattern of fragmentation as

ECD[127]. However, ETD occurs in an ion trap where gas pressure is several orders of magnitude higher than that of ECD. Faster collisional cooling reduces more energetic fragmentation routes[118].

Reagent anions for donating the electron are critical in ETD. Chemicals which have low electron affinity have been introduced for chemical ionization (CI) to generate ETD reagent ions[116]. Anthracene was initially employed[46] and later several other reagents were evaluated for ETD[128, 129]. The most successful reagent used so far is fluoranthene, which has an electron transfer efficiency about 40%[130].

1.3.2.2.2 Advantages and Disadvantages of ETD

ETD has become the most widely spread electron-driven dissociation in proteomics for several reasons. First, its ability to be employed on a low cost ion trap mass spectrometer makes it accessible for a large number of researchers. Secondly, it yields unselective cleavages throughout the entire peptide backbone, which facilitates the sequencing of the peptide amino acid composition[131]. Moreover, modification sites of peptides can been easily localized due to the ability of ETD to preserve the labile PTMs on corresponding fragments[132].

However, ETD also suffers from several limitations. The most prominent limitation is that the fragmentation efficiency of ETD is strongly dependent on the charge intensity of the peptide ions, *i.e.* the lower the ratio of residues/charge, the higher the ETD fragmentation efficiency[129]. Due to the nature of ETD fragmentation, it cannot be used for singly charged peptide precursor ions. For that reason, ETD is coupled with ESI rather than MALDI. Spectra for ETD-MS/MS of doubly charged peptide precursor ions are dominated by electron-transfer charge reduced product ions ($[M+2H]^{+\bullet}$) instead

of fragment ions, which limits the usage of ETD for doubly charged peptide precursor ions. To overcome this limitation, a supplemental collisional activation strategy (ETcaD) was proposed in which CID was performed on those non-dissociated $[M+2H]^{+\bullet}$ ions to generate more c- and z-type fragments so that the sequence coverage of the peptide can be improved[133]. However, since ETcaD involves implementation of CID fragmentation, neutral losses of labile PTMs may be observed in ETcaD. Moreover, ETcaD results in new fragments with H atom loss or gain from typical c- and z-type fragments, which increases the difficulty for assigning the fragments by database search algorithms[131].

1.3.2.2.3 Negative ETD

Negative ETD (NETD) has been developed to analyze peptide anions. Radical cations, such as $Xe^{+\bullet}$, $C_{16}H_{10}^{+\bullet}$, can be employed in NETD to abstract an electron from peptide anions to generate free-radical sites, which then induce fragmentation of the C_{α}-C bond to yield a- and x-type product ions[134, 135]. Additionally, residue-specific neutral losses from amino acids were observed in NETD spectra. Moreover, product ions with PTMs attached were also observed, which were beneficial for PTM localization[136]. In general, the NETD serves as a complementary tool for using ETD on acidic peptides that are ionized well in negative ionization mode.

1.3.2.3 EDD

EDD is another commonly utilized electron-driven dissociation. For the same purpose as niECD and NEDT, EDD is introduced for analyzing peptide anions. Electrons with energy >10 eV colliding with the peptide anions results in electron detachment from the precursor ions instead of capturing the electron as in niECD. The

charge-reduced peptide radical anions are then dissociated at the C_α-C bond to produce a- and x- type product ions[137, 138]. As an electron-driven dissociation, EDD also has the feature of non-selective fragmentation throughout the peptide backbone and preservation of the labile PTMs[116]. However, the efficiency of EDD is lower than other electron-driven dissociations, *i.e.* ECD and ETD[116].

1.3.3 Photon Dissociation

1.3.3.1 IRMPD

1.3.3.1.1 General Introduction of IRMPD

IRMPD was explored very early in the development of tandem mass spectrometry. It involves precursor ions absorbing tens or hundreds of low-energy (0.12 eV/photon) IR (mainly CO_2 laser, wavelength: 10.6 μm) photons[47]. With enough internal energy accumulated in this process, precursor ions are induced to fragment. Given that IRMPD is a slow-heating process occurring on a millisecond scale, it produces mainly b- and y- type product ions similar to CID. IRMPD was first enabled on FT-ICR instruments to take advantage of ion trapping for longer irradiation time and high vacuum for a lower cooling rate[139-141]. Later, it was incorporated into ion trap instruments, which greatly improved the popularity of IRMPD in proteomics[48, 142].

1.3.3.1.2 Characteristics of IRMPD

The primary advantage of IR activation compared to CID is that it is a non-resonant process and independent of trapping voltage. Consequently, the product ions from primary fragmentation can further be activated by photons and induce secondary fragments. This is beneficial for generating more fragment ions for peptide sequencing without employing multi-stage tandem mass spectrometry[47]. In addition, IRMPD does

not have the limitation of low mass cut-off like CID, so low mass fragments can be detected. Moreover, the product ions observed in IRMPD of multiply charged peptide precursor ions are mainly singly charged, which simplifies the spectra and makes the interpretation of spectra easier[47, 143, 144]. Furthermore, nearly all molecules have the ability to absorb photons in the IR range to some extent. This non-selective feature ensures the wide application of IRMPD[47].

IRMPD efficiency in the ion trap is a function of He gas pressure [48, 145]. With increased pressure, the efficiency of IRMPD decreases because bath gas collides with precursor ions causing them to lose energy that has been absorbed through IR irradiation[146]. Alterative IRMPD strategies have been developed to increase its efficiency in ion traps. In one case, IRMPD was enabled on an ion trap with lower He gas pressure, i. e. the low pressure cell in the dual pressure linear ion trap[144]. In another study, a multi-pass optical arrangement was used to increase the photon absorption and thus promoted more efficient fragmentation[142]. Moreover, the temperature of the He gas was elevated to assist the dissociation process[146]. CID has also been combined with IRMPD to simultaneously activate the precursor ions to increase the fragmentation efficiency[147].

1.3.3.2 UVPD

1.3.3.2.1 General Introduction to UVPD

Similar to IRMPD, UVPD also employs photon absorption to induce subsequent dissociation. Unlike IRMPD, however, the photons in UVPD have energies ranging from 3 eV to 124 eV with corresponding wavelengths from 400 nm to 100 nm. Many different lasers with various wavelengths can be employed for UVPD. Of these, 157 nm (F_2

excimer) and 193 nm (ArF excimer) are most popular for peptide fragmentation due to the fact that these two wavelengths are closest to the two maximum absorbance wavelengths of peptides in the range of 250 nm to 100 nM [50]. Photodissociation has been reviewed at length in a recent paper and thus will not be discussed further here[47].

The energy of UV range photons is much higher than that of IR and is comparable with the peptide bond dissociation energy (3-4 eV)[50]. Therefore, only a few photons or even a single photon are required to dissociate the peptide precursor ions[49]. In other words, it is a more efficient energy deposition process requiring much shorter irradiation time, on the nanosecond to microsecond timescale[148], which makes UVPD amenable to on line LC-MS/MS strategies. The fragmentation pattern of peptides dissociated by UVPD varies according to the wavelength of the laser used. As a general feature of photodissociation, UVPD has a wide range of instrument implementation. Time-of-flight, FT-ICR and ion trap mass spectrometers can all be modified to be used for photon dissociation[49, 50, 148].

1.3.3.2.2 193 nm Photodissociation

193 nm photodissociation has been successfully employed in high-throughput proteomic workflows. Enzymatic peptides were fragmented efficiently with only a 5 ns laser pulse, producing a wide range of product ions including a, b, c, x, y, and z ions as well as a few lower abundance w and v side-chain loss ions and some immonium ions[149]. Only a few scans are needed for averaging to get high quality spectra, which increases the analysis duty cycle significantly[47]. Both the rich sequencing product ions

and high efficiency characteristics are advantageous compared to CID or electron-driven dissociation alone.

Negative ion mode 193 nm photodissociation of singly and multiply charged peptide anions produces abundant a- and x-type product ions as well as d and w side-chain loss ions, which often cover the entire peptide sequence[150]. This shows a great potential for improving the analysis of acidic peptides by 193 nm photodissociation.

1.3.3.2.3 Other UVPDs

Peptide precursor ions excited by 157 nm photons are initially cleaved at the C_α-C bond yielding a- and x- type product ions through radical directed dissociation[151]. Subsequent secondary fragmentation processes can produce an even wider variety of fragment ions, such as d, v and w-type ions[152]. Through these secondary fragment ions, isoleucine and leucine residues in peptides can be differentiated[153]. Interestingly, the disulfide bonds, which are usually left intact during CID fragmentation, can be efficiently cleaved upon 157 nm photon activation[154]. 157 nm photodissociation has been widely used for peptide and protein characterization[49].

One of the distinct features of UVPD compared with IRMPD is that absorbance of UV photons is more selective than that of IR photons. It often requires a chromophore moiety for efficient absorbance of the UV light[47]. Therefore, it is quite common that enhanced fragmentation will be observed for peptides with chromophores. For example, in UVPD at 266 nm, peptide precursor ions containing the tryptophan (Trp), tyrosine (Tyr), or phenylalanine (Phe) residues require shorter time for completely fragmenting the precursor ions and the enhanced cleavages are induced near the aromatic residues[155]. Derivatization of the peptide with a chromophore containing reagent

absorbing 355 nm photons is necessary for UVPD of peptides at 355 nm[156]. Even though selective absorbance of photons is a challenge, it is also an advantage for the fact that it enables the selective detection of certain residues through enhanced cleavages[148].

1.3.4 Tandem Mass Spectrometry of Phosphorylated Peptides

1.3.4.1 Importance of Phosphorylation in Biological Systems

Perhaps the most important PTM is protein phosphorylation. It has been estimated that one third of the proteins in a given mammalian cell may undergo phosphorylation at some point during their lifetime[157]. Protein phosphorylation primarily modifies Ser, Thr and Tyr residues by attaching phosphate groups to the hydroxyl groups on the side chains of these amino acids[158]. Generally, proteins can be phosphorylated by kinases leading to protein activation, and become inactivated upon dephosphorylation by phosphatases[158]. This dynamic reversible process constitutes one of the most important regulatory mechanisms in cells. It is involved in regulating numerous cellular activities, such as cellular growth, cell division, and apoptosis[158]. Protein phosphorylation has been implicated in critical steps in cell signaling networks by regulating protein activity, cellular location and dynamic interactions with other proteins[159-161]. Due to the important role that phosphorylation plays, alteration of protein phosphorylation can lead to the onset and progression of diseases including cancer[162-165], diabetes[166], Alzheimer's disease [167, 168] and rheumatoid arthritis[168, 169]. Developing an understanding of how phosphorylation regulates cellular activities may provide the scientific community with insights into potential drug targets.

1.3.4.2 Challenges Associated with Phosphoproteomics

There are many challenges associated with phosphoproteomics. First, many different structural isomeric forms of phosphoproteins exist, which are due to the sheer number of potential phosphorylation sites on a given protein, increasing the complexity of a sample[170]. In addition, the low stoichiometry of phosphoproteins makes them difficult to observe if a whole cell sample is directly analyzed. Moreover, protein phosphorylation is a reversible process characterized by short lifetime that reduces the chance of obtaining proteins in their phosphorylated state[170, 171]. As a result, there are no universal techniques that can ensure the detection of all phosphorylation sites in proteins.

Large-scale detection, characterization and quantitation of phosphorylation sites are mainly carried out by MS. The merits of MS-based proteomics also applies to MS-phosphoproteomics[172]. In the 'bottom-up' approach of phosphoproteomics, phosphopeptide enrichment is usually employed after SCX [173, 174] to address the challenges associated with low stoichiometry of phosphoproteins. Immobilized metal ion affinity chromatography (IMAC) is one of the most widely used non-covalent enrichment methods[175, 176]. Recently, metal oxide affinity chromatography (MOAC), such as titanium dioxide and zirconium dioxide chromatography, have become increasingly popular because of their high specificity for capturing phosphopeptides[177-179]. Because a recent review[175] has summarized this topic comprehensively, this aspect will not be further discussed in detail here.

1.3.4.3 Phosphopeptide Fragmentation in CID

1.3.4.3.1 Neutral Losses in CID-MS/MS of Phosphopeptides

The success of conventional phosphoproteomic analysis strategies for the large-scale detection, characterization and quantitation of protein phosphorylation is highly dependent on the use of MS/MS methods to identify the sequence and localize the site of modification to a specific amino acid residue within proteolytic peptides[116, 173]. CID in ion trap mass spectrometers has been the most widely used ion activation/dissociation method for MS/MS of phosphopeptides[116]. One of the limitations associated with the use of CID-MS/MS for phosphopeptide identification and characterization, however, is the often dominant 'non-sequence' neutral loss of 80 Da (HPO_3) and/or 98 Da (H_3PO_4) from the protonated phosphopeptide precursor ions, and their b- and y-type 'sequence' ions[180]. Under non-mobile and partially mobile protonation conditions, these neutral losses can compete with amide bond cleavage reactions such that sequence ions (required for peptide identification) are suppressed (Scheme 1.2 A). In such cases, multistage MS/MS (MS^3 or 'psuedo'-MS^3) strategies to further dissociate the -98 Da neutral loss product ion have been widely employed to obtain additional sequence information for phosphopeptide sequence identification and localization[173, 181-186]. However, Palumbo *et. al.*, and others, using simple model peptide sequences, have previously reported that the loss of 98 Da can also occur via the combined losses of HPO_3 from a phosphorylated Ser or Thr amino acid residue and H_2O from another site within the peptide sequence; e.g., the hydroxyl side chain of an unmodified serine or Thr residue (Scheme 1.2 B), the carboxyl side chain of Asp and Glu residues, or the C-terminus[180, 187]. This competing HPO_3+H_2O neutral loss fragmentation pathway yields a -98 Da neutral loss product ion with the same m/z value as that formed via the direct loss of H_3PO_4, but with a different product ion structure

(e.g., dehydration at the site of an unmodified Ser or Thr rather than at the originally phosphorylated residue). If this occurs to a major extent, the site of phosphorylation could be incorrectly assigned. As the extent to which this competing fragmentation reaction contributes to the -98 Da neutral loss product ion abundance cannot be directly determined, it was previously proposed that MS^3 cannot be used for confident and unambiguous phosphate site localization for *a priori* unknown phosphopeptides[187].

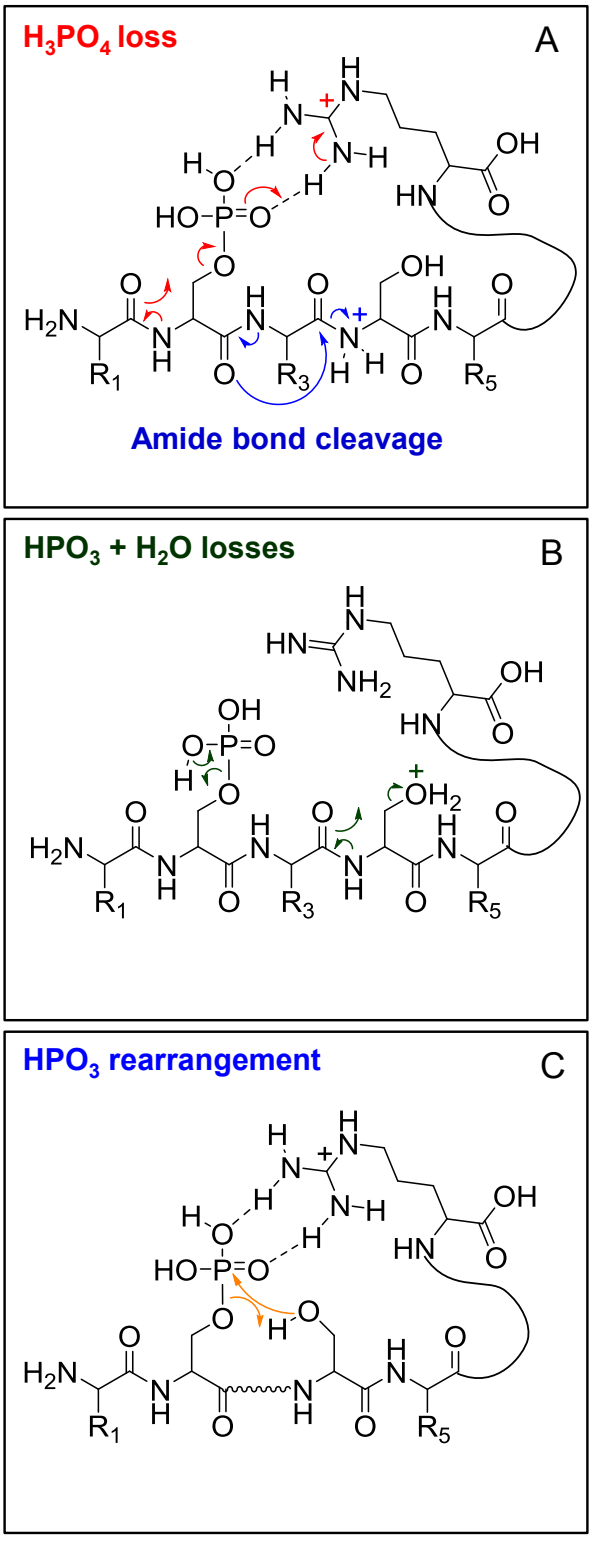

Scheme 1.2 Fragmentation pathways in CID-MS/MS of phosphopeptides

1.3.4.3.2 Phosphate Group Rearrangement in CID-MS/MS of Phosphopeptides

Palumbo *et. al.* initially reported that protonated phosphopeptide ions can undergo a rearrangement reaction prior to fragmentation during the relatively long (*i.e.*, msec) activation timescales associated with ion trap CID-MS/MS, that results in intramolecular transfer (*i.e.*, 'scrambling') of the phosphate group to another Ser, Thr or Tyr residue within the sequence[187] (Scheme 1.2 C). Similar to the H_3PO_4 and HPO_3 losses described above, phosphate group scrambling reactions were shown to be most prevalent under non-mobile and partially mobile protonation conditions. Under conditions when extensive scrambling does occur, the observed product ion spectrum may contain abundant product ions where the phosphate group is located at the incorrect site(s), and could therefore potentially result in erroneous phosphorylation site localization in *a priori* unknown phosphopeptides. However, note that no apparent phosphate group rearrangement has been observed to date in quadrupole CID-MS/MS conditions including HCD, likely due to the short (*i.e.*, μsec) activation timescales associated with these experiments[187].

1.3.4.3.3 Negative Ionization Mode CID-MS/MS of Phosphopeptides

The discussion above has focused on the use of MS/MS in positive ionization mode, in which precursor cations are induced to fragment. As discussed earlier, phosphopeptides have relatively low isoelectric points and thus tend to ionize better in negative ionization mode[188]. The intensity of phosphopeptide precursor ions dramatically increases in negative ionization mode MS compared to that in positive ionization mode[188]. However, in negative ionization mode CID-MS/MS, phosphopeptides with phosphoserine (pS) or phosphothreonine (pT) tend to undergo

characteristic neutral losses of H_3PO_4 while phosphopeptides containing phosphotyrosine (pY) have characteristic neutral loss of HPO_3[111]. Moreover, characteristic low-mass fragments of $H_2PO_4^-$, PO_3^- and PO_2^-, and high-mass fragments of $[M\text{-}nH\text{-}79]^{(n-1)-}$ are also commonly observed[189]. A recent study also showed that phosphate groups on pY within monoanions can transfer to another site with hydroxyl or carboxyl groups and then undergo rearrangement to form fragments with neutral loss of H_3PO_4[189]. This study questioned the utility of neutral loss of H_3PO_4 in pY as diagnostic information to distinguish pY from pS and pT containing phosphopeptides. Unfortunately, CID-MS/MS in negative ionization mode also yields dominant product ions with neutral losses of H_3PO_4 and HPO_3, which generate little information useful for assigning phosphorylation site.

1.3.4.4 Phosphopeptide Fragmentation in Electron-Driven Dissociations

Alternatively, electron transfer dissociation (ETD)-MS/MS has been used for phosphoprotein analysis[46]. ETD has become a powerful tool for sequencing phosphopeptides due to its ability to preserve the phosphate group during MS/MS[131]. As stated earlier, the efficiency of ETD highly depends on the charge state of peptides. Usually, it is only highly effective for peptides with charge states ≥ 3+[190]. ECD has also been widely acclaimed for phosphopeptide analysis[157, 191]. However, it is specific for use in instruments that employ magnetic fields for ion confinement[131], which limits its application.

Recently, the NETD technique for analyzing phosphopeptides has also been established[135]. This new strategy enables ETD on analysis of peptide anions[192].

1.3.5 Tandem Mass Spectrometry of Peptides Containing Glycosylation

1.3.5.1 Significance of Glycosylation in Biological Systems

Another important PTM is protein glycosylation. It is estimated that more than half of all proteins in nature are glycosylated. Almost all proteins in human serum are glycoproteins[193]. Glycoproteins commonly exist in biological systems and have critical biological functions. Due to the characteristic properties of the glycan chains in glycoproteins, which include high branching ability, various linkage types and chemical properties of carbohydrates[194], glycosylated proteins are involved in coordination of most intra- and intercellular processes[195, 196] through regulating protein interactions, such as regulation of immune functions[197] and processes of cell division, migration and adhesion[193, 195]. Dysfunction of glycosylation has been found in various diseases, ranging from cancer, autoimmune, diabetes, and Alzheimer's disease to hematologic disorders[198, 199]. Consequently, effort has been devoted to profile protein glycosylation for discovery of disease diagnostic biomarkers.

1.3.5.2 Categories of Glycosylation

Glycosylation can be divided into four categories according to the forms of glycans and their linkage to the protein substrates[200]. The most common and well-known type is N-linked glycans attached to the side chain of Asn residues. N-linked glycans can be further divided into three groups according to the substitution of the monosaccharide residues in the common trimannosyl-chitobiose inner core structure[201]. Another common type of glycosylation is O-linked glycans anchored to hydroxyl side chains of Ser or Thr residues. There are a large number of O-linked glycan variants built on at least 8 different core structures[202]. However, they are generally less complicated than N-linked glycans[201]. The third category of

glycosylation involves attaching glycosylphosphatidylinositol anchors to the carboxyl terminus of certain membrane proteins. The last category is C-glycosylation, in which glycans are attached to Trp residues of certain membrane or secreted proteins[203].

1.3.5.3 Challenges and Strategies for Glycopeptide Analysis

Due to the diversity of glycans resulting from the identity, number and linkage structure of the monosaccharides, as well as varying degree of glycosylation site occupation of the protein, glycoprotein analysis thus remains a great challenge[200]. MS-based analysis of glycoproteins has been widely employed based on the same reasons for using MS for other PTM characterization and quantification, such as high sensitivity, efficiency and information density. Due to the complexity of biological samples, enrichment and purification procedures are often introduced to clean up the sample. Lectin affinity chromatography in combination with other techniques has been widely used for extracting and concentrating glycoproteins and glycopeptides from the sample mixture[196, 202, 204-207].

In the “bottom-up” approach, where glycoproteins were digested into peptides, glycans can be removed before enzyme digestion though chemical release, β-elimination and enzyme release[208]. Hydrazine is employed to remove both N-linked and O-linked glycans[209, 210]. O-linked glycans are usually released through β-elimination with alkali[211] while N-linked glycans are often removed by Protein-N-glycosidase F (PNGase F)[200, 208, 212]. The cleaved glycans are then introduced into MS for structural elucidation, which includes identification and characterization of each monosaccharide unit, determination of the monosaccharide sequence, determination of linkage structure and identification of other groups such as sulphate[208].

Glycan removal strategies simplify the MS/MS spectra for glycopeptide fragmentation because they enable separate characterization of glycans and peptide sequences. However, one of the most important aspects in MS-base glycosylation analysis is identifying the site of glycosylation. In this case, it is necessary to preserve the glycan on the peptides so that fragments with gylcans attached can be generated in MS/MS[208]. Alternatively, localization of glycosylation site can also be achieved by derivatization of reducing terminal site of glycopeptides after glycan removal.

1.3.5.4 Fragmentation of Glycopeptides in CID-MS/MS

Slow heating, low energy excitation methods, such as CID and IRMPD, have been employed for fragmenting glycopeptides[213]. CID has also been most widely used in glycosylation analysis. Similar to phosphopeptide fragmentation in ion trap CID-MS/MS, the most dominant fragment for glycopeptides is cleavage of the glycosidic bond instead of peptide bond cleavage[214]. These fragments are useful for confirming the identity of glycosylated peptides, but also make obtaining glycosylated peptide sequence information and localization of the glycan units challenging. CID-MS^3 can be applied to fragment deglycosylated peptide ions to generate fragments for sequencing the peptide[215, 216]. However, unlike CID-MS^3 of the characteristic -98 Da neutral loss ion from phosphopeptide fragmentation, it is very challenging to make this sequential fragmentation process of glycopeptides automatic during the LC-MS/MS analysis due to the complexity of glycans[213]. In triple quadrupole CID, there are both fragment ions from glycosidic bond cleavage and peptide bond cleavage, which enables the sequencing of the peptide backbone[217]. Unfortunately, the glycan units are not

retained on the fragments from the peptide backbone cleavage. In this case, it is still not possible to localize the site of glycosylation [213].

1.3.5.5 Fragmentation of Glycopeptides in Electron-driven Dissociation and Photon Dissociation

Electron-driven dissociation, like ETD and ECD, overcomes the limitations of CID for glycopeptide analysis. It produces fragments from the cleavage of the peptide backbones with the glycans retained so that the site of glycosylation can be readily identified[218-220]. While these methods provide information concerning the glycosylation site, they also suffer from the drawbacks of low fragmentation efficiency (approximately 20%), and limited mass range up to m/z 1400 due to the nature of ETD[221]. ECD and ETD do not produce many fragments from glycosidic bond cleavage, and thus are not useful to characterize the linkage structure of glycans[213]. However, given that they produced fragments that are complementary to CID fragmentation of glycopeptides, the combination of CID and electron-driven dissociations is proven beneficial for complete glycopeptide analysis[218, 221, 222].

IRMPD of glycopeptides generates similar fragmentation patterns as those of CID, which are dominated by fragmentation of glycosidic bonds. Charge state, charge carrier and glycan composition influence the fragmentation of N-linked glycopeptides in IRMPD[223]. UVPD has also recently become attractive for glycopeptide analysis. Zhang and Reilly reported that 157 nm photon dissociation of glycopeptides showed unique advantages of generating both peptide and glycan fragments. Abundant cross-ring glycan fragments were also observed, which were not detected in low energy CID-MS/MS[213]. These fragments provided information for glycan composition and linkage

as well as primary peptide sequence using a single dissociation technology. More details about dissociation of glycosylated peptide ions using different dissociation strategies can be found in a recent review[224].

1.3.5.6 Negative Ionization Mode Fragmentation of Acidic Glycopeptides

For glycopeptides with sialylated glycans, negative mode ionization is more efficient than positive mode. Thus it is favorable to analyze these acidic glycopeptides in negative ionization mode especially when they are present in a mixture with other basic peptides[224]. Fragmentation of glycopeptides in negative ionization mode has been investigated by different dissociation methods. Deguchi *et. al.* reported that CID-MS/MS of glycopeptide anions with neutral and sialylated N-glycans were found to yield complementary fragments to CID-MS/MS of their positive ions[225]. The same research group proposed that a combination of negative ionization mode CID and positive ionization mode ECD-MS^n can be used for direct assignment of O-glycan glycosylation sites and characterization of peptide amino acid sequence[226]. Nwosu et. al. also reported that negative ionization mode CID-MS/MS produced glycan fragments and peptide backbone fragments. 193 nM photon dissociation has also been employed for analysis of glycopeptide anions[227, 228]. O-linked glycopeptides produced fragments that retained the labile glycans, product ions resulted from glycosidic bond cleavages and from less common cross-ring cleavages upon UVPD[228].

1.3.6 Tandem Mass Spectrometry of Peptides Containing Oxidized Methionine

1.3.6.1 Biological Significance of Methionine Oxidation in Proteins

Methionine residues within proteins contain sulfur atoms in their side chains, which are susceptible to oxidation by reactive oxygen species (ROS), such as H_2O_2,

HOCl, smoke, reduced transition metals, UV light and ozone[229, 230], resulting in the formation of methionine sulfoxides and/or sulfones. Methionine sulfoxides can be reduced back to methionines by reductases[231]. This enzymatic cyclic redox process not only regulates the activity of proteins but also scavenges some ROS species to protect organisms[231, 232]. Notably, methionine oxidation does not have an apparent effect on the biological function of some proteins while it changes others significantly[232]. For instance, studies have shown that methionine oxidation has a direct effect on the activity of calmodulin (CAM), a protein that regulates calcium concentration, which then subsequently activates many other proteins, such as the transcription factors Nrf-2, NFAT and NFjB[231]. Furthermore, accumulation of methionine sulfoxide could indicate a disruption of homeostasis in oxidative stress *in vivo*. Methionine oxidation has been found associated with the onset of several diseases, such as age-related degenerative diseases[233] including Alzheimer's disease[232].

Because of the critical role methionine oxidation can play in biological systems, there is a driving need for identification, characterization and quantification of methionine oxidation. Again, MS coupled with LC has been the most powerful tool for studying site-specific methionine oxidation of proteins. It follows the same workflow as general MS-based proteomics. Notably, methionine oxidation can also be induced from sample handling process, which potentially affects the quantification and identification of methionine oxidation *in vivo*. Fortunately, the process induced methionine oxidation can be minimized by proper control of sample handling process[234].

1.3.6.2 MS/MS Fragmentation of Peptides Containing Methionine Oxidation

Methionine sulfoxide shows a mass increase of 16 Da while methionine sulfone shows a mass increase of 32 Da, corresponding to the addition of one or two oxygen atoms to the native form of methionine, respectively. These mass increases in a full MS spectrum therefore could be used as an indication of oxidation[231]. Methionine sulfoxide containing peptides could also be diagnosed by the characteristic neutral loss of methane sulfenic acid (CH_3SOH, 64Da) from the side chain of methionine sulfoxide upon CID-MS/MS of their protonated ions[235]. This neutral loss is the dominant fragmentation process under low proton mobility conditions[91], which is similar to phosphate group neutral loss from phosphorylated peptides. Both charge-remote and charge-directed mechanisms have been proposed for the -CH_3SOH loss[57]. Deuterium labeling experiments on model peptides showed that this neutral loss mainly occurred through charge-remote process involving a cis-1,2 elimination for peptide ions under non-mobile or partially protonated conditions, while was induced primarily through a charge-directed process, which was initiated by a mobile proton mobilization and a subsequent nucleophilic attack reaction, for those under mobile protonation conditions[91].

While identification of the presence of methionine sulfoxide can be achieved by CID, it is also essential to localize the position of methionine oxidation because only certain sites of oxidation affect the activity of the protein[231]. As electron-driven dissociations have the ability to retain the labile sulfoxide side chain, they have been used as complementary strategies for analysis of methionine sulfoxide to determine the location of the modifications[236].

Generally, analysis of methionine oxidation by MS/MS is less challenging than phosphorylation and glycosylation owing to the fact that there are no scrambling issues, as in the case of phosphate groups, and no complicated PTM forms as in the case of glycans. Thus only a few publications have reported studies on the fragmentation pattern of methionine sulfoxide containing peptides in MS/MS. Also, to date there has been even less interest in using photodissociation for fragmenting methionine sulfoxide containing peptides. Further study of methionine sulfoxide containing peptides using photodissociation could be expected to be an area of future interest for the MS research community.

1.4 Algorithms for Peptide Identification

1.4.1 General Procedures that Algorithms Use for Peptide Identification

Data obtained by LC-MS workflows in proteomics is massive and complex. Manual interpretation is not practical and thus data are usually processed automatically by algorithms. There are generally two types of algorithms employed for peptide identification, characterization and quantification, which are database search algorithms and de novo sequencing algorithms[237].

Spectra collected from the instruments need to be preprocessed before being interpreted by algorithms. The spectra first undergo deconvolution and are transferred into readable format for the algorithms containing ion m/z and abundance information[238]. Several issues are involved in spectra deconvolution[237]. First of all, background noise is filtered out according to the peak intensities[239]. Moreover, both isotope and charge state deconvolution can be easily performed if mass resolution is high enough for individual isotope peaks to be resolved, which simplifies the spectra

and reduces interferences[240, 241]. If multiple scans were collected for one precursor ion, these spectra can be averaged and normalized before scoring. This is especially helpful for algorithms that determine scores based on intensities of the fragments. In addition, low quality spectra can be filtered out to save data processing time later on[242]. Each algorithm requires certain data formats as input. The standard formats that have been used are primarily mzXML and mzData[237]. Data conversion software is also available to transform the data format to fulfill the requirements of certain algorithms.

A number of parameters need to be specified for each algorithm before performing spectra interpretation. These parameters include, but are not limited to, the desired database to search against, dissociation methods for fragmenting the peptides, mass accuracy of the instruments and fixed and variable modifications[237]. The above information is essential as it will affect the outcome of the interpretation. For instance, as discussed in the previous sections, different dissociation methods produce different types of product ions. It is possible sometimes that a b_n ion overlaps with a z_m ion. These two types of ions are usually induced by different dissociation methods. With the fragmentation method noted, the algorithm can identify the fragments easily with less ambiguity.

After raw spectra are preprocessed and parameters are set up, the algorithm uses a function to match the peptide fragments in real MS/MS spectra with theoretical fragments of the candidate peptides to result in a best-fit peptide sequence. The function that algorithms use varies in detail from one to another. Most popularly, probability based score functions have been implemented in peptide identification

algorithms. The result of the search needs to be tested or validated. The false discovery rate (FDR) approach has been widely employed for this purpose[243]. In this method, the acquired spectra are searched against a random database[38] or reverse sequences of the real database[244]. By comparison of the original score distribution and reversed or randomized database score distribution, the confidence level of the identification can be determined[237].

1.4.2 Database Search Algorithms

There have been a large number of database search algorithms developed since the 1990's. In this type of search, the database used for searching contains proteins with known sequence information. With the enzyme used for protein digestion noted, the m/z values of precursor ions in the MS spectra are matched with those of the theoretical enzymatic peptides. A number of matches can result especially when the resolution and mass accuracy of the instrument are not high enough. The fragments in MS/MS are then matched with the theoretical fragments generated from the peptide candidates. Scoring and validation follows the match to yield the best fit peptide sequence to a spectrum[245]. The first database search algorithm, Sequest, for peptide identification based on MS/MS data used a cross-correlation function to match the fragments in the spectra to the theoretical values[37]. Later on, probability based scoring functions were used in database search algorithms, such as the well-known Mascot[38]. Following the pioneering work of Mascot and Sequest, which have been made commercially available, many similar algorithms have been developed to overcome certain limitations of these algorithms[237, 243]. Among those, OMSSA[39], X!Tandem[40] and Andromeda[246] are well recognized.

Database search algorithms increase the number of peptide identifications by taking the advantage of known protein sequences. However, sometimes undiscovered proteins can also be detected in an LC-MS/MS workflow. In this case, database search algorithms cannot assign the acquired spectra confidently or correctly. De novo sequencing algorithms have been developed to address this issue.

1.4.3 De Novo Sequencing Algorithms

De novo sequencing algorithms do not rely on any known protein sequence information and consider all possible combinations of amino acids with the same m/z values as the precursor ions. This is beneficial for identifying new peptides and proteins. PEAKS[42] and PepNovo[41] represent the early and well-recognized work in this area. Given that a great number of possible identities exist for any detected precursor ions, it is quite a time consuming and challenging process for the de novo sequencing algorithms to assign the correct peptide sequences[237]. Peptides assigned with a high confidence level by multiple database search algorithms have been used to evaluate the performance of de novo sequencing algorithms. Usually only 30-45% of the peptides can be correctly identified[247]. The ‘Sequence tag’ concept was then introduced into de novo sequencing to increase the number of identifications and to reduce the analysis time[247-250]. Nevertheless, no significant advances have been made in improving the identification of peptide sequences by de novo sequencing algorithms and thus will not be discussed in details here.

1.4.4 PTM Identification Algorithms

Due to the importance of PTMs in proteomics, algorithms have been developed to handle the task of intensive data analysis of proteome with PTMs. There are

algorithms designed for the analysis of various types of PTMs, such as InsPect[250],and MODa[251], as well as algorithms designed for specific type of PTMs including many for phosphorylation localization[252]. Among those, PTM Score[173], Ascore[253], PhosphoScore[254] and PhosphoRS[255] and Mascot Delta Score[256] are most well-known. Despite the great effort in phosphorylation analysis, successful localization of phosphorylation sites remains a challenge, especially when multiple residues within the sequence can be phosphorylated and multiple phosphorylation sites exist. A deeper understanding of the fragmentation mechanisms of PTMs will certainly aid the development of more confident peptide identification.

1.4.5 Incorporation of Peptide Fragmentation Rules in Algorithms

As discussed earlier in this chapter, peptides do not fragment homogenously throughout the peptide backbone. These fragmentation patterns vary according to the dissociation methods used, peptide sequence, peptide precursor ion charge states, ion polarity and PTMs. These variations in peptide fragmentation patterns, such as missed cleavages and dominant neutral losses, are great challenges that peptide identification algorithms face for assigning the correct peptide sequences. Many developed algorithms have been adapted to accommodate these factors.

Most algorithms were first developed based on peptide fragmentation in CID, mainly considering b- and y- types of product ions. With increasing numbers of proteomics studies conducted by electron-driven dissociations and photodissociations, there has been a great need for algorithms to incorporate other types of product ions. Many algorithms have enabled the searching of c- and z-type product ions from ETD

spectra, such as SpectrumMill[191] and OMSSA[257]. A new algorithm designed specifically for processing ETD data, ZCore[258], has also been developed.

Incorporating enhanced cleavages rules of peptides fragmentation into database search and scoring algorithms can potentially increase the confidence of peptide assignment and subsequently achieve a reliable and comprehensive protein identification and characterization, particularly for peptides that currently yield low or insignificant search scores. Unfortunately, few algorithms have fully taken into account these rules. To date, peptide sequence permutation and phosphate group rearrangement have not been considered by the algorithm development research community. Notably, neutral loss ions have been weighted differently by many algorithms to help with the peptide sequence assignment, such as PepNovo[41] and MODa[251].

A lack of communication and mutually shared knowledge between those who study peptide fragmentation and those who develop algorithms has hindered the progress in computational sequencing of peptides. Improving the calculation functions that are used by the various peptide identification algorithms may influence the output results to some extent, but the key to advance the field of algorithm-based peptide identification is to improve the fundamental understanding of the peptide fragmentation chemistry, especially for peptides with PTMs. The fragmentation rules were developed individually by different research groups, sometimes based on only a few model peptides. On one hand, model peptides simplify various properties of the peptides, which enables more direct obervation of the fragmentation patterns. On the other hand, the MS research community is largely interested in peptide fragmentation rules that are

universal to large set of proteomics data. Hence, it is necessary to evaluate these rules systematically in a large library containing representative peptide spectra before defining them as “golden rules” to be included in protein/peptide identification algorithms

1.5 Aims of this Dissertation

The aims of this dissertation include:

1. Design and synthesis of a library of phosphopeptides containing various amino acid compositions, phosphorylated residues and potential phosphorylated residues.
2. Examination of factors that influence erroneous phosphorylation site localization via competing fragmentation and rearrangement reactions during ion trap CID-MS/MS and -MS^3 using the synthetic phosphopeptide library.
3. Development of a regioselective ^{18}O-labeling strategy to synthesize ^{18}O-phosphate ester labeled phosphopeptides
4. Quantification of competing H_3PO_4 versus HPO_3+H_2O side chain neutral losses from protonated phosphopeptide ions during CID-MS/MS using ^{18}O labeled phosphopeptides.
5. Preparation, purification and characterization of full length, truncated and oxidized variants of PTH by CID -MS/MS.
6. Development of an immuno-LC-MS/MS assay for the quantification of oxidation variants of full length, truncated and oxidized variants of PTH at pg/mL levels.

CHAPTER TWO

Examining Factors that Influence Erroneous Phosphorylation Site Localization via Competing Fragmentation and Rearrangement Reactions during Ion Trap CID-MS/MS and -MS^3

2.1 Introduction

Subsequent to the initial report about phosphate group rearrangement reactions[187], as discussed in chapter one, Aguiar *et. al*.[259] and Mischerikow *et. al*.[260] each performed separate studies to evaluate the potential impact of phosphate group rearrangement reactions on the confidence for automated phosphorylation site localization in large scale CID-MS/MS datasets. Aguiar *et. al.* used the Ascore algorithm[253] to analyze data from sequential CID and electron transfer dissociation (ETD)[174, 191] on a synthetic phosphopeptide library and a Lys-C generated yeast digest, while Mischerikow *et. al.* employed the MSQuant[261] PTM scoring algorithm to analyze data from CID and ETD with supplemental activation (*i.e.*, ETcaD) on trypsin- and Lys-N-generated phosphopeptides from a human cell lysate. In both studies, ETD was employed for comparison with CID as it has been shown that no rearrangement reactions occur when using this ion activation method[187]. In the former study, analysis of the CID-MS/MS spectra acquired from the doubly protonated precursor ions from the synthetic phosphopeptide library revealed only minimally abundant phosphate group transfer reaction product ions. An average of two 'site determining' ions were observed

---

The results described in this chapter were published in: Cui, L. and Reid, G.E., Examining Factors that Influence Erroneous Phosphorylation Site Localization via Competing Fragmentation and Rearrangement Reactions during Ion Trap CID-MS/MS and -MS^3. *Proteomics* **2013**, 13, 964-973.

for the incorrect species (one more than would be expected by chance), while an average of eight were observed for the correct site localization, and fewer than 1% of the peptides had both a significant Ascore value and were assigned to the incorrect position. This result was entirely consistent with the originally reported observation of minimal rearrangement from the doubly protonated precursor ion of one of the members (LFpTGHPESLER) of this library[187]. For the proteome-wide dataset in the former study conducted by Aguiar *et. al.*, ETD and CID fragmentation agreed as to the site localization for 93% of the phosphopeptides[259], while in the later study performed by Mischerikow *et. al.*, assignment of the phosphate group positions were identical for 74% of the phosphopeptide ions for which complementary CID and ETcaD sequencing information was obtained[260]. It was noted in the later study that this result was not surprising given that the majority of the peptides contained within the dataset possessed mobile protons, consistent with the original observation of minimal rearrangement occurring under these conditions. For the remaining 26% of the sequenced phosphopeptides, no signs of relocation were observed. Instead, it was noted that the peptides exhibited ambiguity in their site localization predominantly due to factors including inefficient fragmentation, or poor spectrum quality.

While these studies reasonably concluded that phosphate group rearrangement reactions have a statistically insignificant effect on the confidence of phosphorylation site localizations in large-scale phosphorylation datasets, the formation of abundant rearrangement product ions could still result in erroneous phosphorylation site assignments in individual (potentially biologically or functionally important) peptides. It is also possible that the properties of the phosphopeptides identified from large scale

datasets are biased toward those that do not undergo extensive rearrangement, and therefore yield more confident site localizations. However, the factors that influence the magnitude of competing fragmentation or phosphate group rearrangement reactions (e.g., the precursor ion proton mobility, the identity and number of the 'donor' and 'acceptor' residues, their positional relationship within the sequence, ion activation time scales, etc.), and their individual effect on phosphorylation site localization using available PTM scoring algorithms, have not been systematically explored. The study reported in this chapter focuses on evaluating these factors.

2.2 Results and Discussion

2.2.1 Abundant Competing Fragmentation and Phosphate Group Rearrangement Ions can be Observed from CID-MS/MS of Multiply Protonated Peptide Precursor Ions

A library of peptides with the general sequence $GX_1AX_2PVPAX_3GGLHAAVX_4$ (where X_1 = R, K or G, X_2 = pS, pT or pY, X_3 = S, T or Y, and X_4 = R, K or G; adapted from the sequence of a peptide from Hypothetical protein LOC57648 that was previously reported from a large scale prosphoproteome analysis dataset[173]), was initially synthesized to evaluate some of the factors affecting competing fragmentation reactions and phosphate group rearrangement. A typical LTQ CID-MS/MS spectrum for the doubly protonated (non-mobile) precursor ion of the pY containing peptide GRApYPVPAPSGGLHAAVR (pYSR) is shown in Figure 2.1 A. The dominant product ion in this spectrum corresponds to the loss of 98 Da from the precursor ion. As the pY residue cannot directly lose H_3PO_4 from its side chain, this product must be formed from the competing combined losses of HPO_3 (where the superscript □ indicates the loss of

80 Da) and H_2O (where ○ indicates the loss of 18 Da), or the loss of H_3PO_4 following a rearrangement reaction. The potential rearrangement sequence ions observed in this spectrum above the level of the noise were $y_9^{■}$, $y_{10}^{■}$, $y_{11}^{■}$, $y_{12}^{■}$, $y_{13}^{■}$ and $y_{14}^{■}$ (where the superscript ■ indicates the addition of 80 Da), and $b_4^{□}$, $b_6^{□}$ and $b_8^{□}$. From these abundances, as well as those of the observed non-rearranged ions, an average rearrangement ratio of 43.4% for the $y_n^{■}$ ions and 31.1% for the $b_4^{□}$ ions was determined, with a combined average % rearrangement for the spectrum of 39.7%. However, each of these ions (both rearranged and non-rearranged) could potentially overlap with other product ions present at the same m/z in the low resolution LTQ MS/MS spectra For example, by examining the CID-MS/MS spectrum obtained at high resolution and accurate mass using the LTQ Orbitrap Velos (data not shown), the $y_9^{■}$ (m/z 1007.47), $y_{11}^{■}$ (m/z 1175.56) and $y_{13}^{■}$ (m/z 1371.68) ions were each found not to be present, but instead corresponded to the M+1 isotope peaks of the y_{10}^{o} (m/z 1006.54), y_{12}^{o} (m/z 1174.63) and y_{14}^{o} (m/z 1370.75) ions. Thus, upon excluding these abundances, the average rearrangement for the 'real' $y_n^{■}$ ions (*i.e.*, $y_{10}^{■}$, $y_{12}^{■}$ and $y_{14}^{■}$) was determined to be 12.5%, such that the combined average rearrangement for this spectrum was reduced to 21.7%. For other peptides, rearrangement and overlapping ions were both found to be present at a given m/z value (see below). Note also that $b_n^{□}$ rearrangement ions could also be formed via the direct loss of HPO_3 from the pY residue, or via the combined losses of HPO_3 and H_2O (where the H_2O loss occurred from the complementary fragment ion). To determine the extent to which the $b_4^{□}$, $b_6^{□}$ and $b_8^{□}$ ions in Figure 2.1 A originated via the direct neutral loss of meta-phosphate, rather than the rearrangement process, a peptide lacking the 'acceptor' Ser residue, *i.e.*,

GRApYPVPAPAGGLHAAVR, was synthesized and subjected to CID-MS/MS (Figure 2.1 B). For this peptide, the $b_4^{\square}$, $b_6^{\square}$ and $b_8^{\square}$ ions (average HPO_3 loss of 12.8%) can only be formed from the direct neutral loss process. Thus, the difference in the abundances of these ions between Figure 2.1 A and Figure 2.1 B can be attributed as most likely being due to the rearrangement process. Taking this into account, the actual corrected average rearrangement for the peptide was determined to be 15.35%. A similar trend was observed for another pair of peptides in which the 'donor' and 'acceptor' positions were switched relative to their positions in Figure 2.1 (*i.e.*, GRASPVPAPpYGGLHAAVR (SpYR) and GRAAPVPAPpYGGLHAAVR) (Figure 2.2), indicating that for this particular peptide sequence, the position of donor and acceptor does not significantly affect the extent of rearrangement.

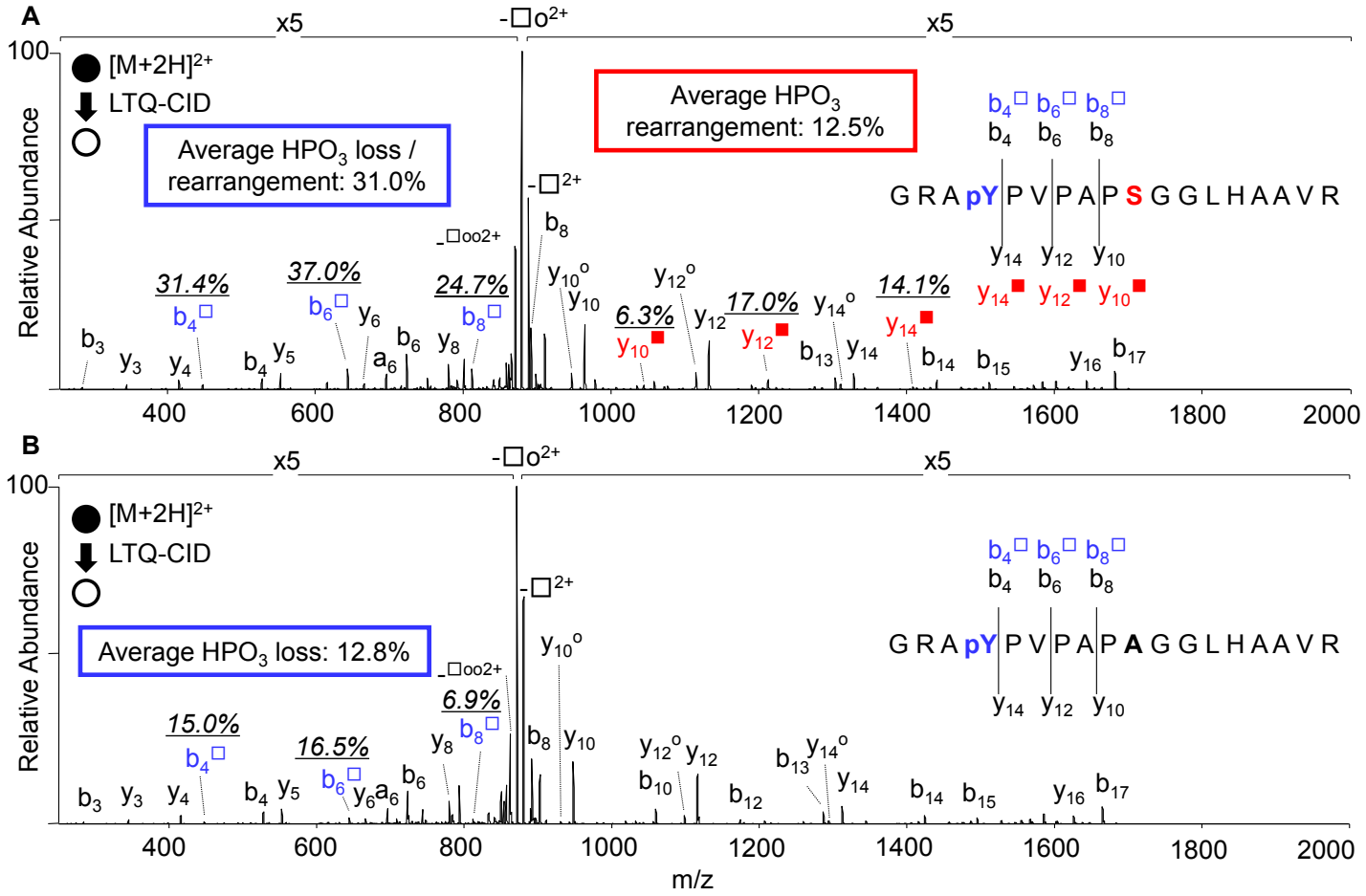

Figure 2.1 ESI-LTQ ion trap CID-MS/MS product ion spectra for the doubly protonated precursor ions of the phosphopeptides (A) GRApYPVPAPSGGLHAAVR and (B) GRApYPVPAPAGGLHAAVR. ■ = +80Da (+HPO_3), Δ = –98Da (–H_3PO_4 or –(H_2O+HPO_3)); □ = –80Da (–HPO_3); ° = –18Da (–H_2O).

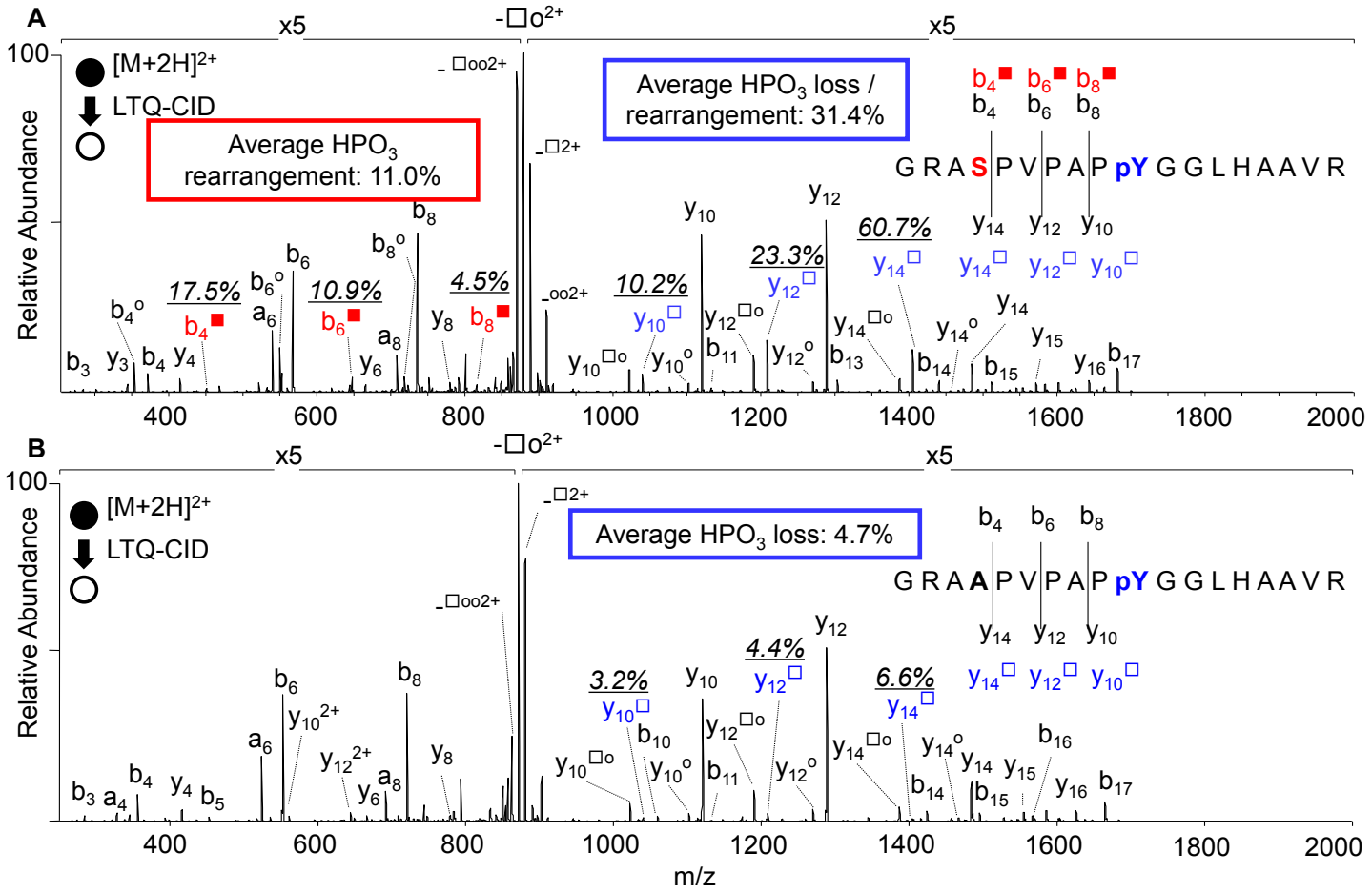

Figure 2.2 ESI-LTQ ion trap CID-MS/MS product ion spectra from the doubly protonated precursor ions of the phosphopeptides (A) GRASPVPAPpYGGLHAAVR and (B) GRAAPVPAPpYGGLHAAVR. ■ = +80 Da (+HPO_3), Δ = –98 Da (–H_3PO_4 or –(H_2O+HPO_3)); □ = –80 Da (–HPO_3); ° = –18 Da (–H_2O).

2.2.2 CID-MS^3 can Result in Erroneous Phosphorylation Localization Due to Competing Fragmentation or Rearrangement Reactions

Given the abundant -98 Da neutral loss product ions observed in the spectra in Figure 2.1 and Figure 2.2, the pYSR and SpYR peptides were also subjected to CID-MS^3 (Figure 2.3). The product ions in these spectra are labeled where the pY has lost 80 Da and the Ser residue has lost 18 Da, for a combined loss of 98 Da (another other major site of dehydration for the spectra in Figure 2.3 is at the C-terminus). Note however, that these assignments are the same as if the original site of phosphorylation was at the Ser residue, which had directly lost H_3PO_4. Therefore, upon subjecting the MS^3 spectra of these two peptides to analysis using the PhosphoScore PTM site localization algorithm, the sites of phosphorylation were confidently, but incorrectly, assigned to the Ser residues, with a maximum Dscore value of 1 (a Dscore value greater than 0.01 indicates a 95% confidence level for phosphorylation site localization[254])(

Table 2.1). This erroneous assignment is due to the fact that while current PTM scoring algorithms correctly recognize that pY residues cannot lose H_3PO_4, they incorrectly assume that 98 Da losses can only arise from pS or pT, rather than counting the attribution of the combined losses of 80 Da from the pY residue and 18 Da from Ser or Thr residues (or other sites within the peptide). Importantly therefore, for phosphorylation site assignments based on CID-MS^3 of -98 Da neutral loss product ions from phosphoproteome-wide datasets, all peptides containing pY, and at least one other Ser or Thr residue, will be incorrectly assigned.

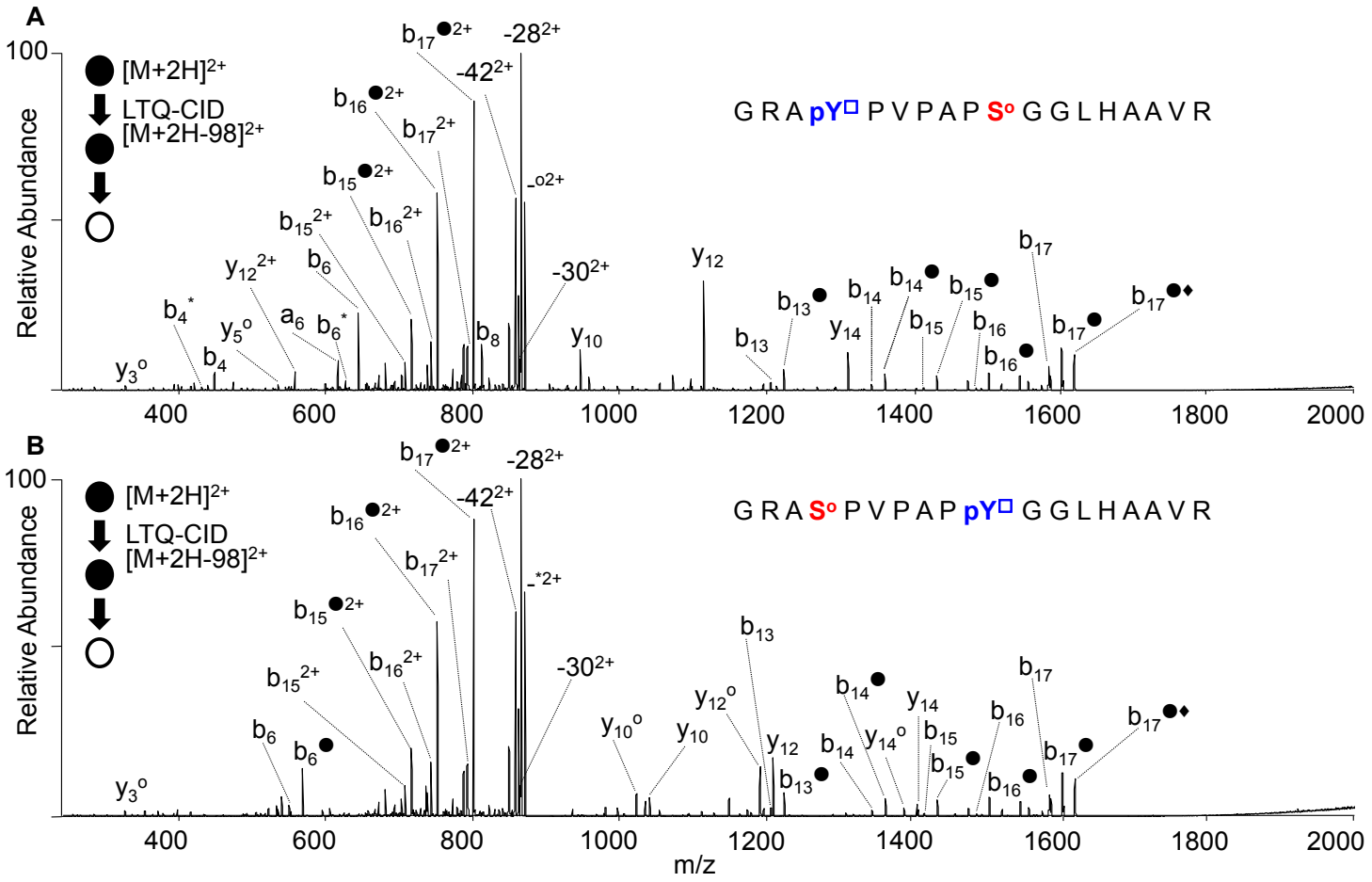

Figure 2.3 ESI-LTQ ion trap CID-MS^3 product ion spectra for the doubly protonated $[M+2H-98]^{2+}$ neutral loss product ions from the doubly protonated phosphopeptides (A) GRApYPVPAPSGGLHAAVR from Figure 2.1 and (B) GRASPVPAPpYGGLHAAVR from Figure 2.2. ● = +18 Da ($–H_2O$); ♦ = +17 Da ($+NH_3$); □ = –80 Da ($–HPO_3$); ° = –18 Da ($–H_2O$);); * = –17 Da ($–NH_3$).

Next, to investigate whether pS and pT containing peptides can also yield incorrect site localizations from analysis of their CID-MS^3 spectra, the doubly protonated precursor ions of the pT containing GRApTPVPAPSGGLHAAVR (pTSR) (Figure 2.4) and pS containing GRApSPVPAPSGGLHAAVR (pSSR) (Figure 2.5) peptides were also subjected to MS/MS and MS^3. For both peptides, while the dominant loss of 98 Da can also occur via the combined -HPO_3 and -H_2O fragmentation pathway, the spectra are labeled assuming that the loss occurred as -H_3PO_4, *i.e.*, directly from the phosphoamino acid residue. Analysis of the pTSR peptide MS^3 spectra using the PhosphoScore algorithm resulted in a confident (Dscore 0.0140), but incorrect, assignment of the phosphate group to the Ser residue. This was likely due to the fact that the product ions formed via the competing fragmentation pathway (e.g., y_{10}^o, y_{12}^o and y_{14}^o) were all higher in abundance than the expected y_n ions. In contrast, for the pSSR peptide, where the y_n^o ions were lower in abundance, the site of phosphorylation was confidently assigned (Dscore 0.0268) to the correct position. A summary of the Dscore CID-MS^3 phosphorylation site localization results for all the phosphopeptide sequences examined in this study are shown in

Table 2.1 at the end of this chapter. Based on these results, the ability to correctly assign the sites of phosphorylation in pT and pS containing peptides (that also contain at least one other Ser or Thr residue) in phosphoproteome-wide MS^3 datasets, will depend heavily on the relative abundance of the observed direct loss and competing loss product ions. When the latter ions are more abundant, the incorrect phosphorylation site is most likely to be assigned. Unfortunately, for unknown phosphopeptides, it is not possible to know the extent to which these competing pathways occur. Therefore, consistent with the conclusions made in the original

report[187], CID-MS^3 cannot be used for unambiguous phosphorylation site characterization.

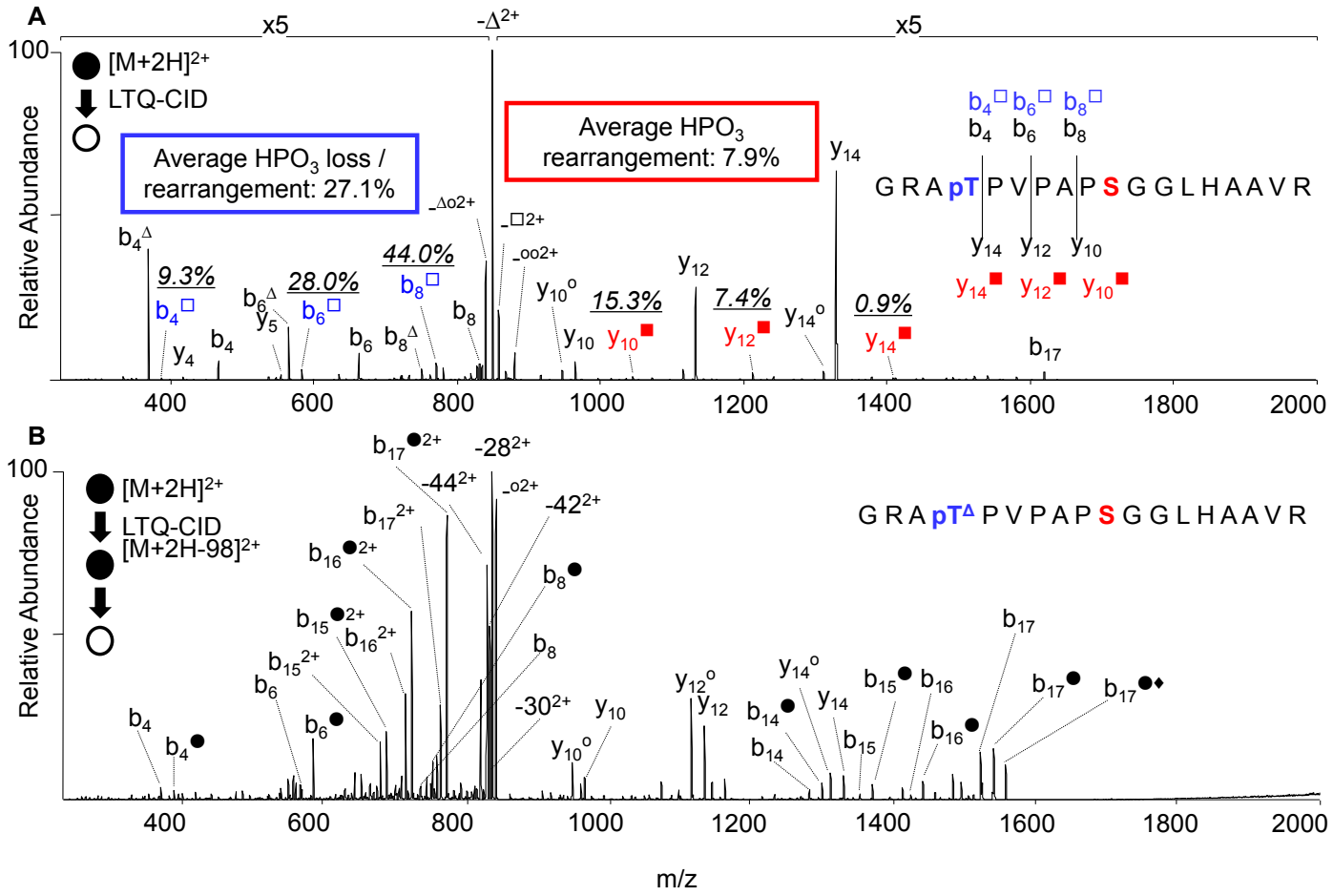

Figure 2.4 ESI-LTQ ion trap CID-MS/MS and -MS^3 product ion spectra of GRApTPVPAPSGGLHAAVR. (A) CID-MS/MS of the doubly protonated precursor ion and (B) CID-MS^3 of the $[M+2H-98]^{2+}$ neutral loss product ion from panel A. ■ = +80 Da (+HPO_3); ● = +18 Da (–H_2O); ♦ = +17 Da (+NH_3); Δ = –98 Da (–H_3PO_4 or –(H_2O+HPO_3)); □ = –80 Da (–HPO_3); ° = –18 Da (–H_2O).

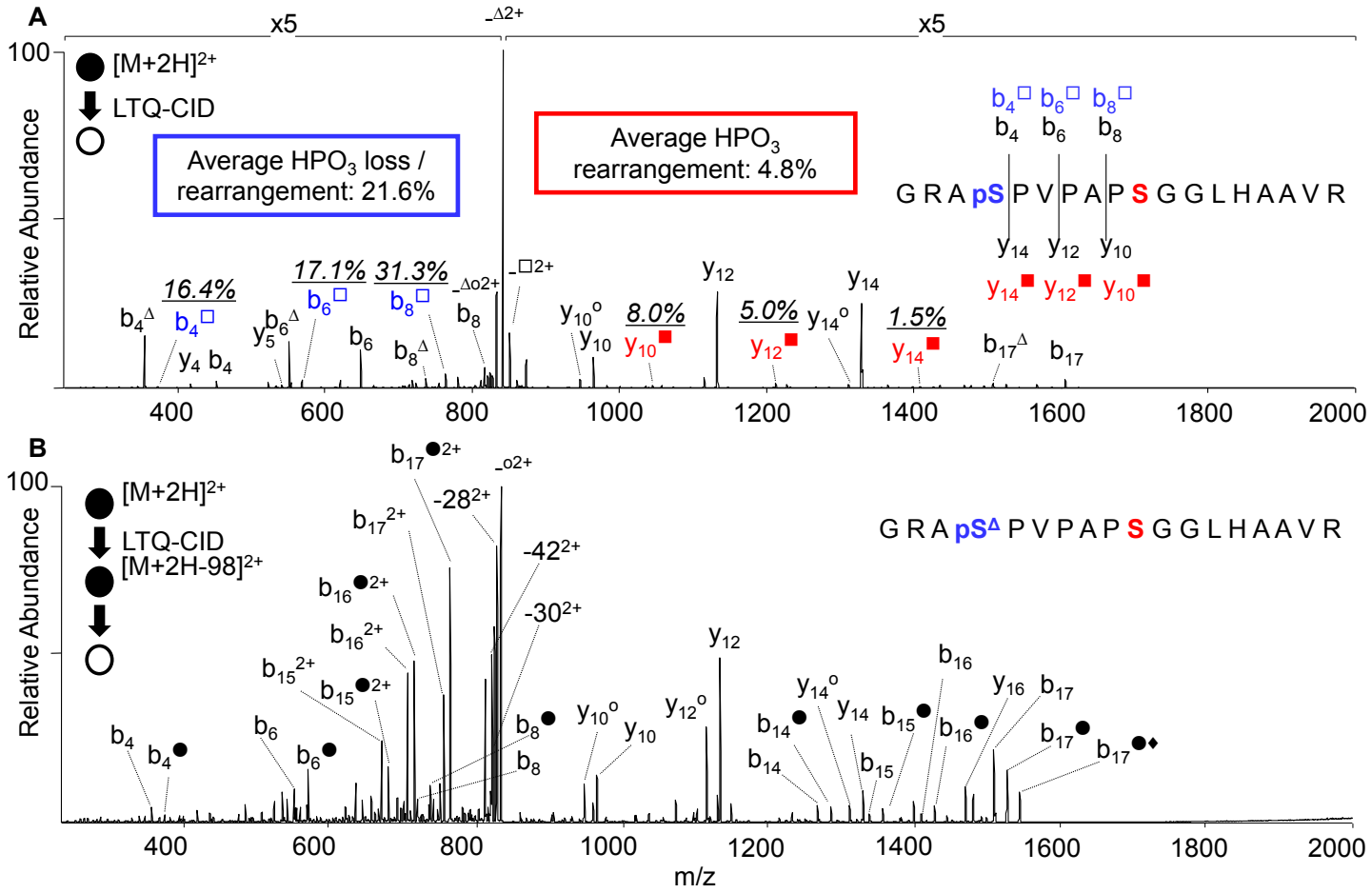

Figure 2.5 ESI-LTQ ion trap CID-MS/MS and -MS^3 product ion spectra of GRApSPVPAPSGGLHAAVR. (A) CID-MS/MS of the doubly protonated precursor ion and (B) CID-MS^3 of the $[M+2H-98]^{2+}$ neutral loss product ion from panel A. ■ = +80 Da ($+HPO_3$); ● = +18 Da ($-H_2O$); ♦ = +17 Da ($+NH_3$); Δ = –98 Da ($-H_3PO_4$ or $-(H_2O+HPO_3)$); □ = –80 Da ($-HPO_3$); ° = –18 Da ($-H_2O$).

2.2.3 Factors that Influence the Amplitude of Phosphate Group Rearrangement

2.2.3.1 'Donor' and 'Acceptor' Identity

The % average rearrangement reactions observed for the doubly protonated precursor ions of several members of the $GX_1AX_2PVPAX_3GGLHAAVX_4$ peptide library, acquired using ion trap CID-MS/MS in both LTQ (light blue) and LTQ Orbitrap Velos (dark blue) mass spectrometers, and taking into account the ratios of all the observed $y_n^{\blacksquare}/(y_n^{\blacksquare} + y_n)$ and $b_n^{\square}/(b_n^{\square} + b_n)$ ions, are shown in Figure 2.6. From the first 9 peptides in Figure 2.4, it can be seen that while the average rearrangement ratios varied quite widely (approximately 3-20%) depending on the identity of the 'donor' phosphoamino acid residue and 'acceptor' amino acid residue, Ser was observed as the best 'acceptor' residue (followed by Thr and Tyr), while pY was the best 'donor' residue (followed by pT and pS). As described above, the competing fragmentation pathway involving the direct neutral loss of meta-phosphate from the phosphoamino acid can also contribute to the $b_n^{\square}$ ion abundances, thereby potentially over estimating the extent to which phosphate group rearrangement reaction actually occurs. Therefore, the average rearrangement reaction ratios were also determined based only on the $y_n^{\blacksquare}/(y_n^{\blacksquare} + y_n)$ ion abundance ratios (Figure 2.7). Consistent with the results described for the pYSR peptide in Figure 2.1, the average % rearrangement determined using this method were somewhat lower in magnitude, indicating that competing fragmentation and rearrangement reactions were occurring in each case.

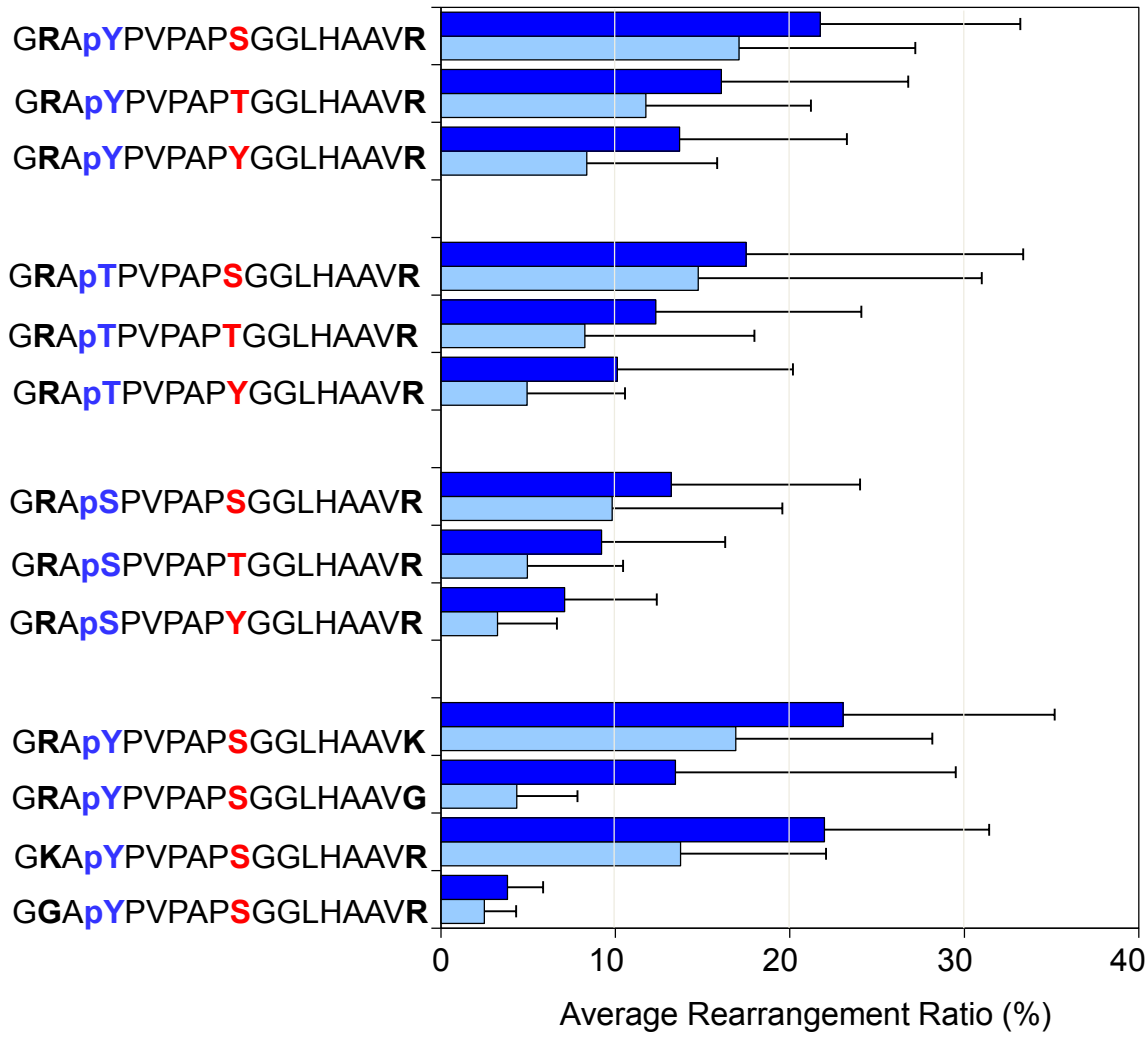

Figure 2.6 Average % phosphate group rearrangement for the doubly protonated ($[M+2H]^{2+}$) precursor ions of the synthetic phosphopeptide library $GX_1AX_2PVPAPX_3GGLHAAVX_4$, where X_1 = R, K or G; X_2 = pY, pT or pS; X_3 = S, T or Y and X_4 = R, K or G, acquired by ion trap CID-MS/MS using ESI-LTQ (dark blue) or ESI-LTQ Velos (light blue) mass spectrometers. Average rearrangement ratios were calculated from the observed $y_{10}^{\blacksquare}$, y_{10}, $y_{12}^{\blacksquare}$, y_{12}, $y_{14}^{\blacksquare}$, y_{14} and $b_4^{\square}$, b_4, $b_6^{\square}$, b_6 $b_8^{\square}$, b_8 product ions. Error bars show the standard deviation of the individual % phosphate group rearrangements determined from each product ion.

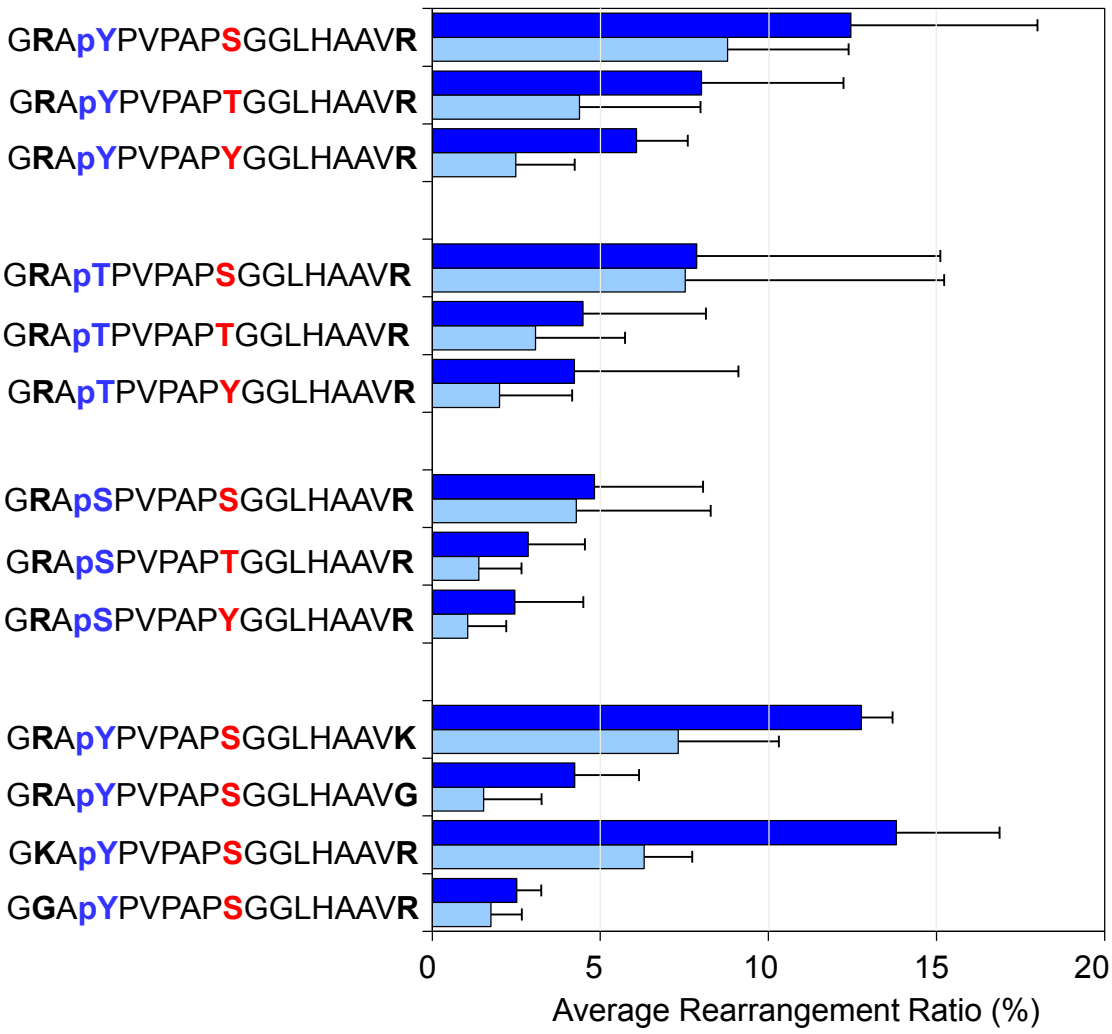

Figure 2.7 Average % phosphate group rearrangement for the doubly protonated ($[M+2H]^{2+}$) precursor ions of the synthetic phosphopeptide library $GX_1AX_2PVPAPX_3GGLHAAVX_4$, where X_1 = R, K or G; X_2 = pY, pT or pS; X_3 = S, T or Y and X_4 = R, K or G, acquired by ion trap CID-MS/MS using ESI-LTQ (dark blue) or ESI-LTQ Velos (light blue) mass spectrometers. Average rearrangement ratios were calculated only using the observed $y_{10}^{\blacksquare}$, y_{10}, $y_{12}^{\blacksquare}$, y_{12}, $y_{14}^{\blacksquare}$ and y_{14} product ions. Error bars show the standard deviation of the individual % phosphate group rearrangements determined from each product ion.

To examine whether the above results regarding donor and acceptor preferences could be extrapolated to other phosphopeptides, three additional phosphopeptide libraries (LFX_1GHPEX_2LER, GX_1X_1QELDVKPX_2AX_2PQER, X_1PLPAPPRPFLX_2R (where X_1 = pS, pT or pY, and X_2 = S, T or Y) were synthesized, and their doubly protonated precursor ions were then analyzed by LTQ CID-MS/MS. The average % rearrangement ratios calculated for each library are shown in Figure 2.8. Consistent with the results discussed in Figure 2.6, the acceptor preference for these three libraries was determined to be Ser > Thr > Tyr. In contrast, however, pS was observed to be the best 'donor' in each these three libraries. Further studies aimed at determining the specific factors (e.g., peptide sequence, gas-phase conformation, etc.) that influence the donor preference associated with phosphate group rearrangement reactions are warranted, by statistical analysis of a larger set of different phosphopeptide sequences.

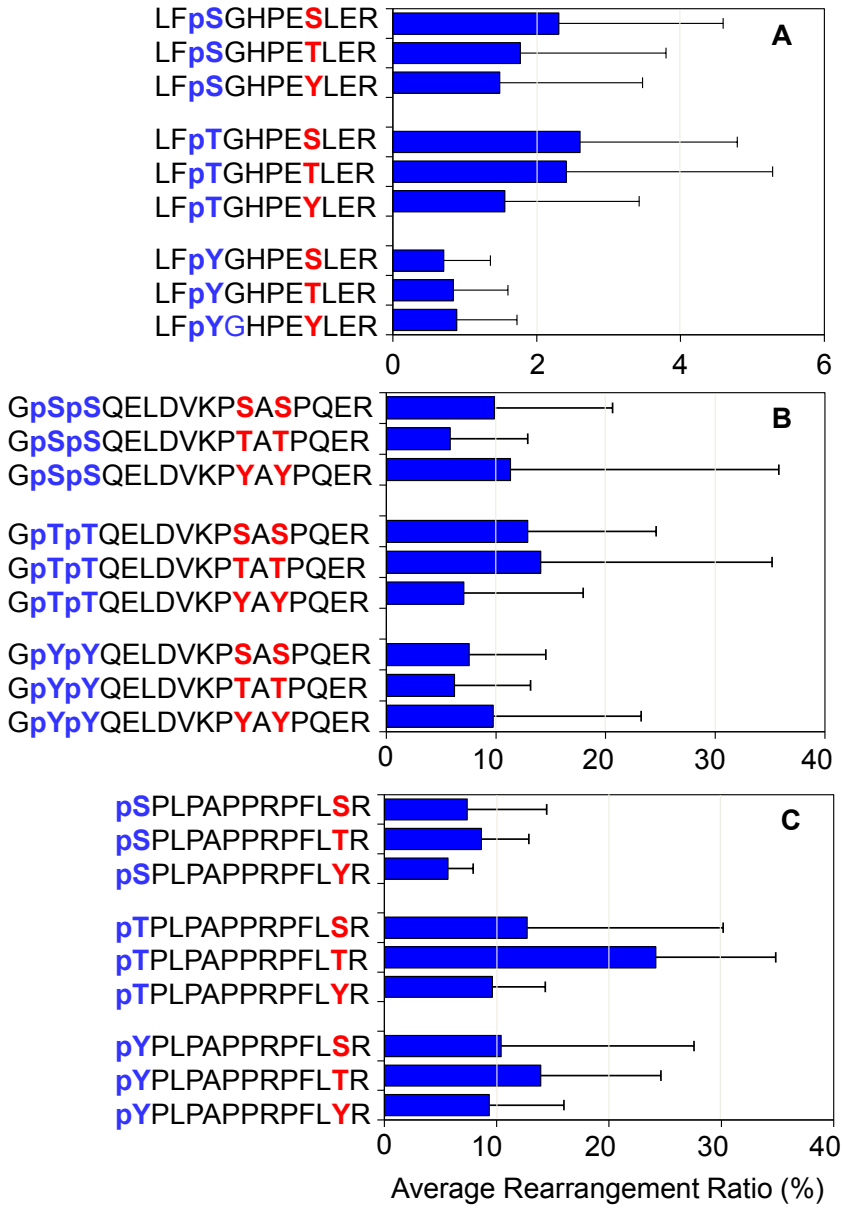

Figure 2.8 Average % phosphate group rearrangement for the doubly protonated ($[M+2H]^{2+}$) precursor ions of several synthetic phosphopeptide libraries acquired by ion trap CID-MS/MS using ESI-LTQ. Average ratios were calculated from all $y^{\blacksquare}$, $y^{\blacksquare\blacksquare}$ and y-type product ions. (A) $y_4^{\blacksquare}$, $y_6^{\blacksquare}$, $y_7^{\blacksquare}$, $y_8^{\blacksquare}$ ions were observed for the LFX_1GHPEX_2LER peptides (where X_1 = pS, pT or pY, and X_2 = S, T or Y), (B) $y_8^{\blacksquare}/y_8^{\blacksquare\blacksquare}$,$y_9^{\blacksquare}/y_9^{\blacksquare\blacksquare}$, $y_{10}^{\blacksquare}/y_{10}^{\blacksquare\blacksquare}$, $y_{11}^{\blacksquare}/y_{11}^{\blacksquare\blacksquare}$, $y_{12}^{\blacksquare}/y_{12}^{\blacksquare\blacksquare}$, $y_{13}^{\blacksquare}/y_{13}^{\blacksquare\blacksquare}$ ions were observed for the $GX_1QELDVKPX_2AX_2PQER$ peptides (where X_1 = pSpS, pTpT or pYpY, and X_2 = S, T or Y) and (C) $y_8^{\blacksquare}$, $y_{10}^{\blacksquare}$ ions were observed for the $X_1PLPAPPRPFLX_2R$ peptides (where X_1 = pS, pT or pY, and X_2 = S, T or Y). Error bars show the standard deviation of the individual % phosphate group rearrangements determined from each of product ion.

2.2.3.2 Proton Mobility

The occurrence and magnitude of phosphate group rearrangement has been shown to be highly dependent on the proton mobility of the phosphopeptide precursor ion. Non-mobile peptides are more likely to undergo a greater rearrangement than those in the partially mobile state, while precursor ions in the mobile protonation state rarely undergo rearrangement to any appreciable extent[187]. The proton mobility of a peptide can be varied in two ways, *i.e.*, by changing the charge state of the precursor ion while maintaining the sequence of the peptide, or by varying the number of basic residues within the peptide but maintaining the same charge state. To examine these effects within the $GX_1AX_2PVPAX_3GGLHAAVX_4$ peptide library, CID-MS/MS of all the peptides in Figure 2.6 were also acquired from their singly protonated precursor ions using a MALDI LTQ XL mass spectrometer. Interestingly, while these ions are all classified as non-mobile, *i.e.*, the same as that of the doubly protonated precursor ions, the average rearrangement ratios for all the peptides (see Figure 2.9) were approximately double that observed in Figure 2.6. This is likely due to the presence of two arginine residues but only a single proton making these precursor ions 'more non-mobile' compared to the doubly protonated precursors. A pair of peptides GRApYPVPAPSGGLHAAVK and GKApYPVPAPSGGLHAAVR, in which one of the arginine residues was substituted for lysine were also synthesized then subjected to CID-MS/MS from their doubly protonated precursor ions. As seen in Figure 2.6, despite now being in a partially mobile protonation state, this pair of peptides yielded about the same % rearrangement as the doubly protonated non-mobile GRApYPVPAPSGGLHAAVR peptide. However, analysis of the doubly protonated precursor ions from glycine substituted peptides

(GRApYPVPAPSGGLHAAVG and GGApYPVPAPSGGLHAAVR), also classified as being partially mobile, resulted in substantially lower rearrangement ion ratios. Finally, CID-MS/MS of the triply protonated partially mobile precursor ion of the GRApYPVPAPSGGLHAAVR peptide, as well as all the other peptides in this library, resulted in the observation of negligible (<1%) rearrangement products. Thus, proton motility distributions within a given non-mobile or partially mobile proton motility classification can substantially influence the extent of rearrangement reactions that are observed.

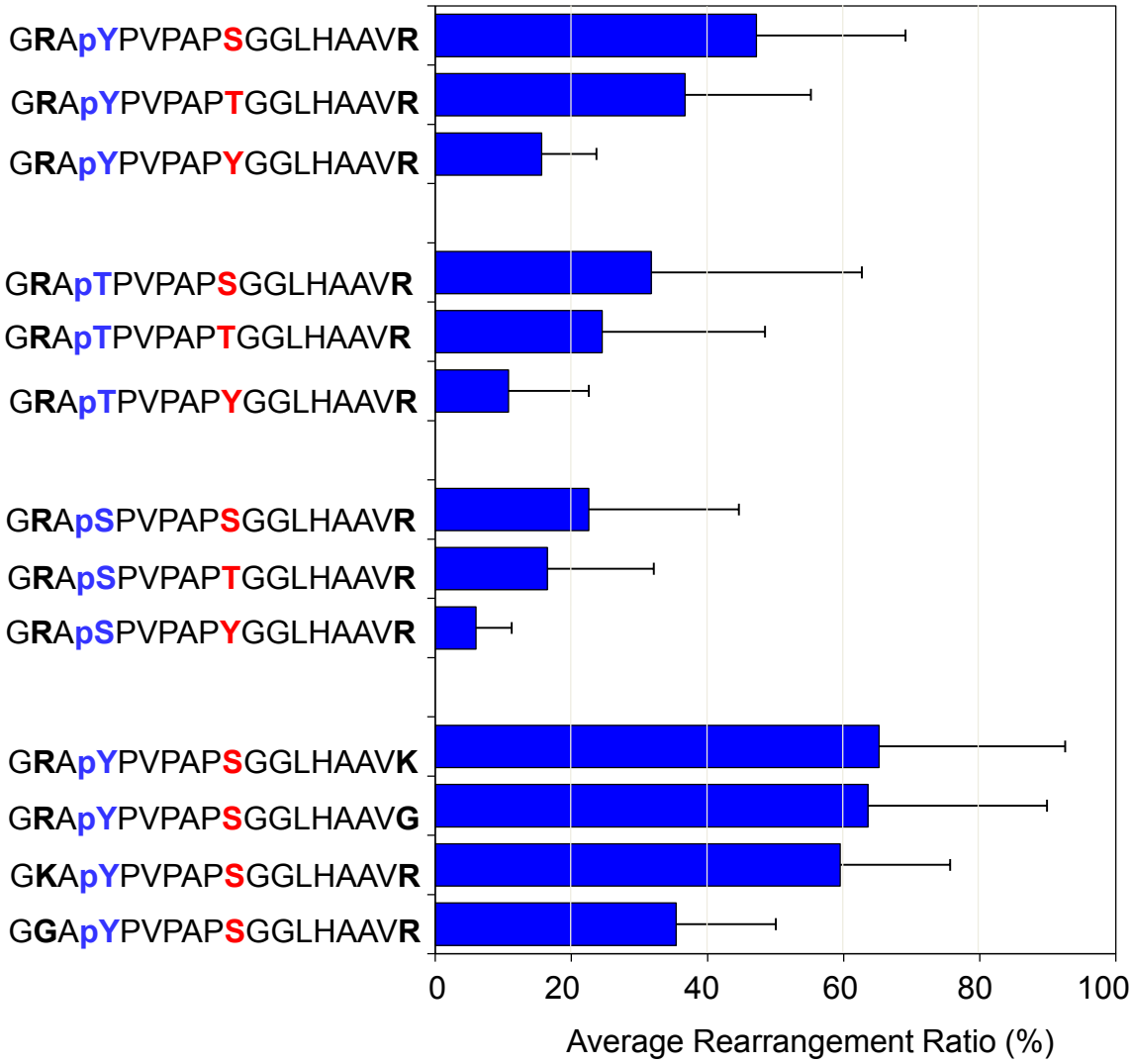

Figure 2.9 Average % phosphate group rearrangement for the singly protonated ($[M+H]^+$) precursor ions of the synthetic phosphopeptide library $GX_1AX_2PVPAPX_3GGLHAAVX_4$, where X_1 = R, K or G; X_2 = pY, pT or pS; X_3 = S, T or Y and X_4 = R, K or G, acquired by ion trap CID-MS/MS using MALDI-LTQ XL mass spectrometer. Average rearrangement ratios were calculated from the observed $y_{10}^{\blacksquare}$, y_{10}, $y_{12}^{\blacksquare}$, y_{12}, $y_{14}^{\blacksquare}$, y_{14} and $b_4^{\square}$, b_4, $b_6^{\square}$, b_6 $b_8^{\square}$, b_8 product ions. Error bars show the standard deviation of the individual % phosphate group rearrangements determined from each product ion.

2.2.3.3 Number of Donors and Acceptors

The above phosphopeptide library examined phosphate group rearrangement reactions in peptides containing only a single donor and acceptor. Following that, how the rearrangement ratio can change upon increasing the number of donors and acceptors as investigated. Figure 2.10 shows the average % rearrangement ratios determined by CID-MS/MS from the doubly protonated precursor ions of a $GX_1AX_2PVPAPX_3LHAAVX_4$ phosphopeptide library, where X_1 = R or K; X_2 = pS, pSpS; X_3 = SGG, SSG or SSS and X_4 = R or K. From these results, rearrangement ratios were observed to increase with an increased number of donors and acceptors. For example, from the GRApSpSPVPAPSSLHAAVR (Figure 2.11) and GRApSpSPVPAPSSSLHAAVR (Figure 2.12 A) peptides containing two potential 'donors' and two or three potential 'acceptors', respectively, average % rearrangement ratios of 42.3% and 32.3% were observed.

Similar to that discussed in Figure 2.1, abundant overlapping other product ions could be present at the same nominal m/z to those of rearrangement ions, which contributed to the calculated rearrangement product ion ratios in the low resolution LTQ MS/MS spectra, and influenced (either positively or negatively) the results from automated PTM assignment algorithms (see below). For example, Figure 2.11 B shows an expanded region of the mass spectrum from Figure 2.11 A (acquired on the LTQ) that was initially assigned as the b_5 ion due to this cleavage occurring N-terminal to a proline residue, such that the rearrangement ratio for the $b_5^{\square}/b_5$ ion pair was calculated as being only 9.22%. However, Figure 2.11 C, showing the same region of the high resolution mass spectrum acquired using the LTQ Orbitrap Velos, revealed the

presence of a dominant $b_7^{\Delta\Delta}$ (*i.e.*, b_7-$2H_3PO_4$, m/z 619.3301) ion, with the b_5 ion (m/z 619.1627) present only at very low abundance. Therefore, the actual rearrangement ratio for the $b_5^{\square}/b_5$ ion pair was 47.8%. For other peptides, where product ions were found to overlap with rearrangement ions rather than the original ions, the calculated rearrangement ratio in the LTQ spectrum were larger than the true values (e.g., as discussed in Figure 2.1).

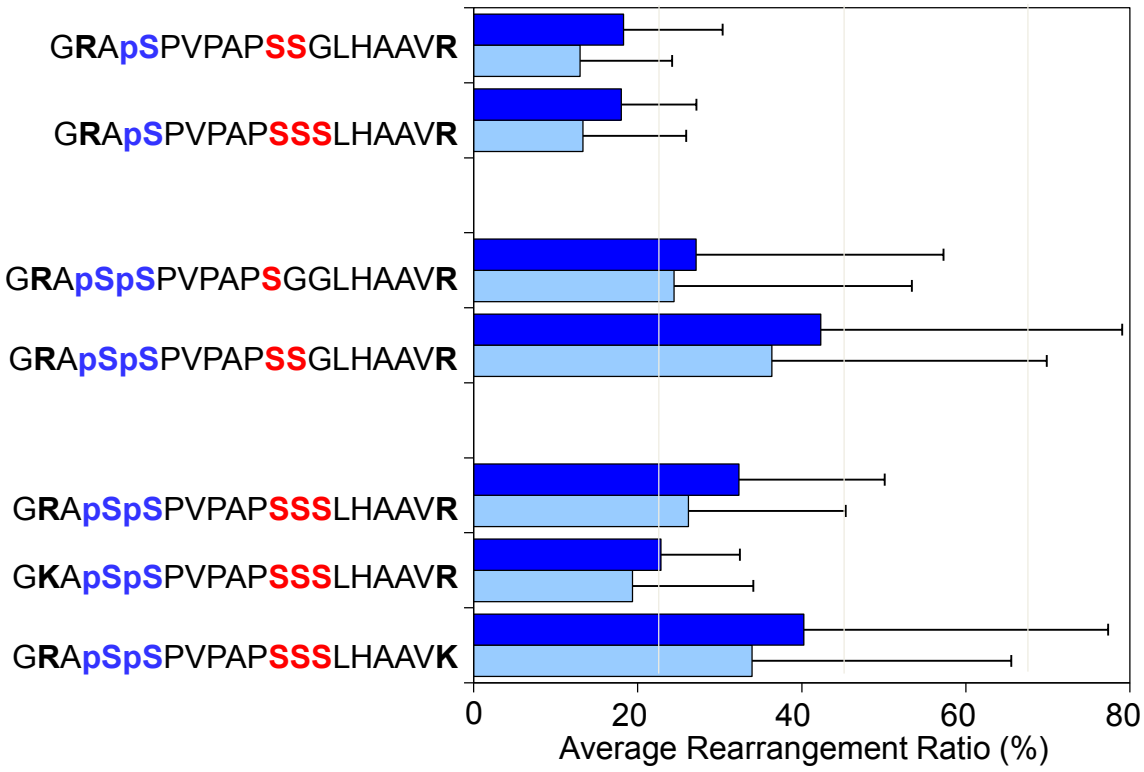

Figure 2.10 Average % phosphate group rearrangement for the doubly protonated ($[M+2H]^{2+}$) precursor ions of the synthetic phosphopeptide library $GX_1AX_2PVPAPX_3LHAAVX_4$, where X_1 = R or K; X_2 = pS or pSpS; X_3 = SGG, SSG or SSS and X_4 = R or K, acquired by ion trap CID-MS/MS using ESI-LTQ (dark blue) or ESI-LTQ Velos (light blue) mass spectrometers. Average ratios were calculated from all observed $y^{\blacksquare}$, $y^{\blacksquare\blacksquare}$ and y-type product ions. Error bars show the standard deviation of the individual % phosphate group rearrangements determined from each product ion.

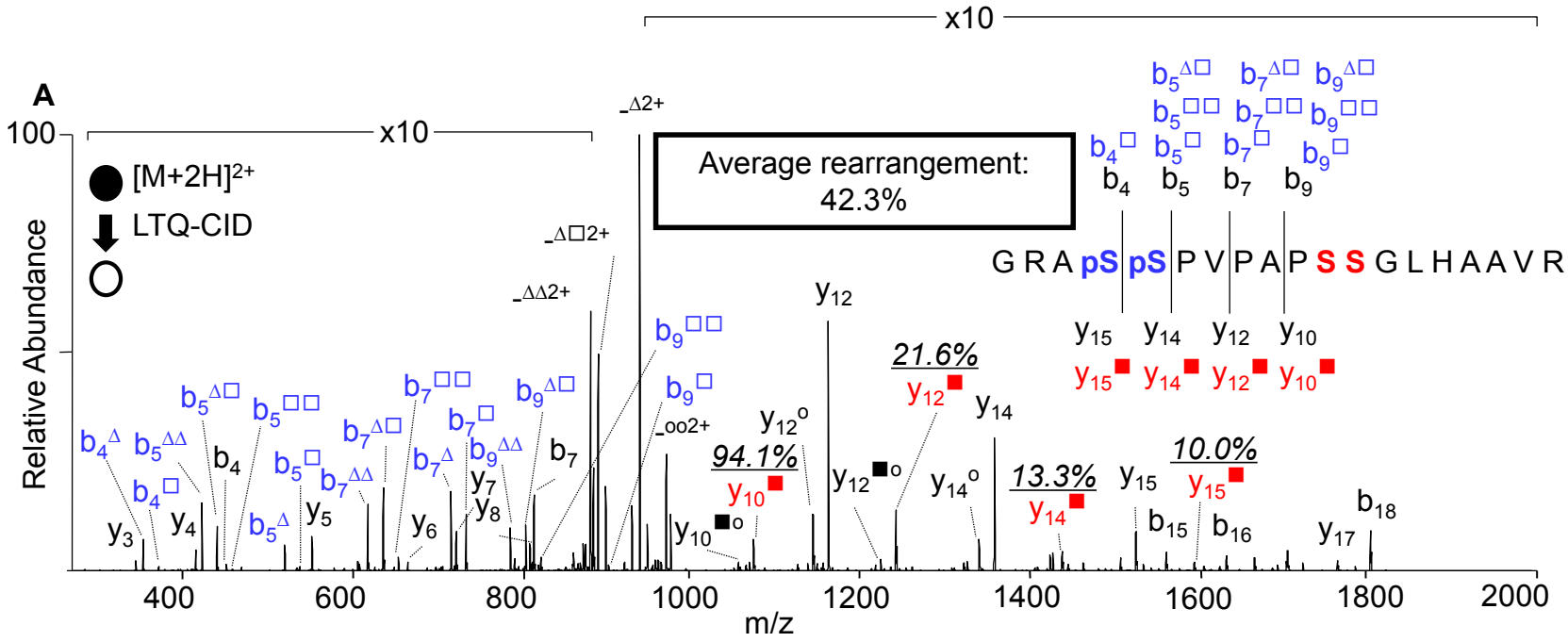

Figure 2.11 ESI-LTQ ion trap CID-MS/MS of the doubly protonated precursor ion from the doubly phosphorylated peptide GRApSpSPVPAPSSLHAAVR. Panel (A) shows the full product ion mass spectrum. An expanded region of the product ion spectrum from panel (A) is shown in panel (B), while panel (C) shows an expanded region of the high resolution product ion spectrum acquired using an LTQ Orbitrap Velos mass spectrometer. ■ = +80Da (+HPO_3); Δ = –98Da (–H_3PO_4 or –(H_2O+HPO_3)); □ = –80Da (–HPO_3); ° = –18Da (–H_2O).

Figure 2.11 (Cont'd)

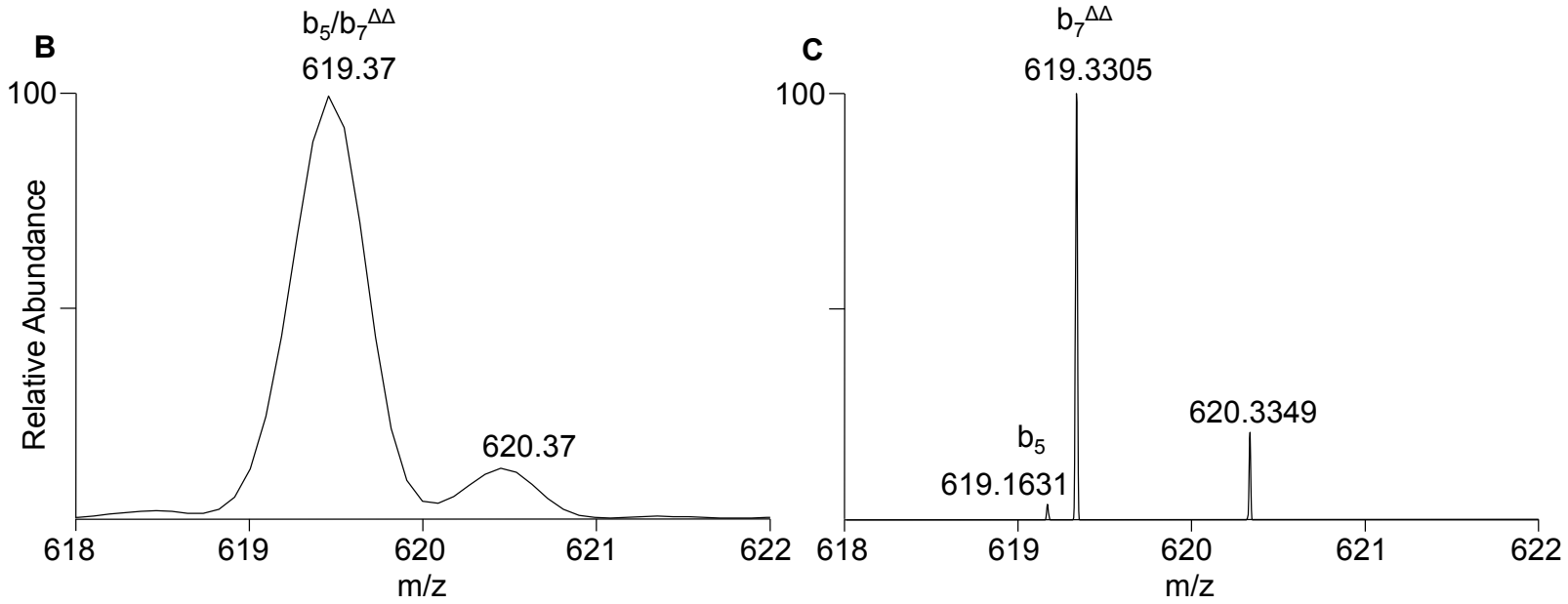

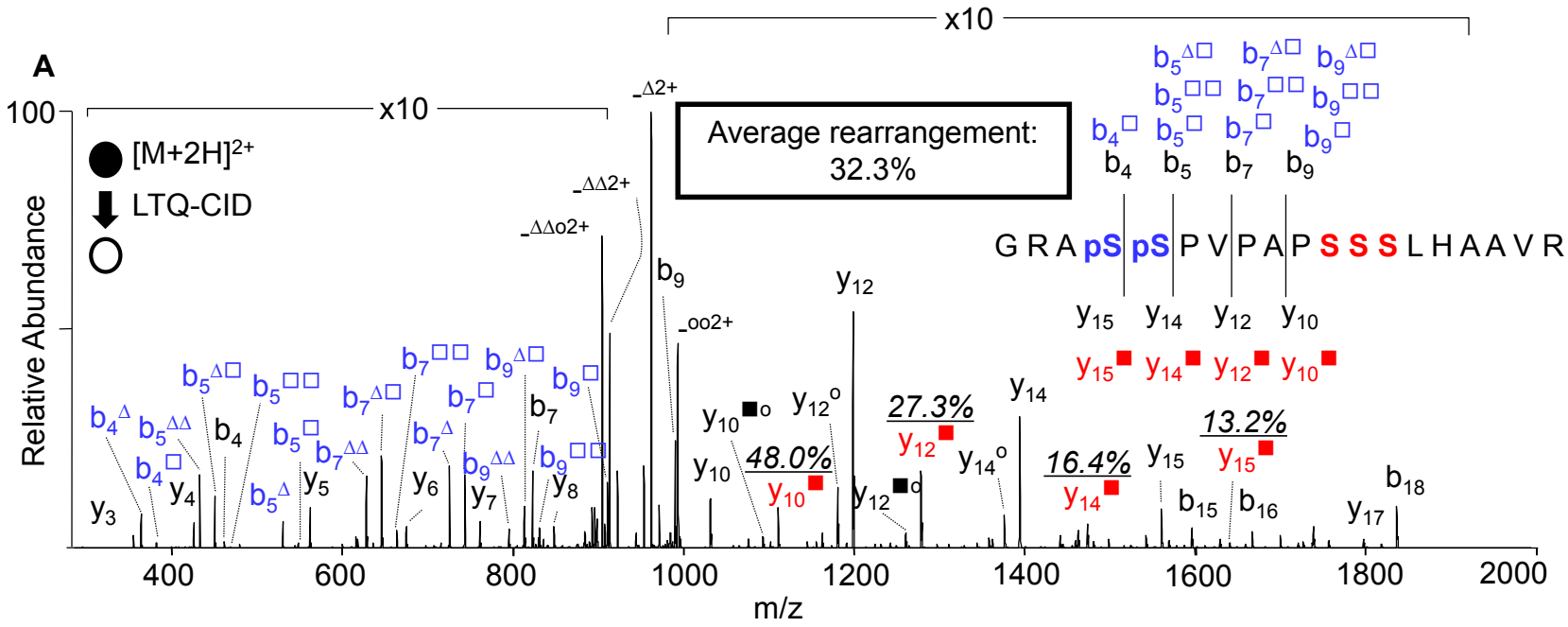

Figure 2.12 ESI-LTQ ion trap CID-MS/MS of the doubly protonated precursor ion from the doubly phosphorylated peptides (A) GRApSpSPVPAPSSSLHAAVR and (B) GRApSpSPVPAPSSSLHAAVK. ■ = +80Da (+HPO_3); Δ = –98Da (–H_3PO_4 or –(H_2O+HPO_3)); □ = –80Da (–HPO_3); ° = –18Da (–H_2O).

Figure 2.12 (Cont'd)

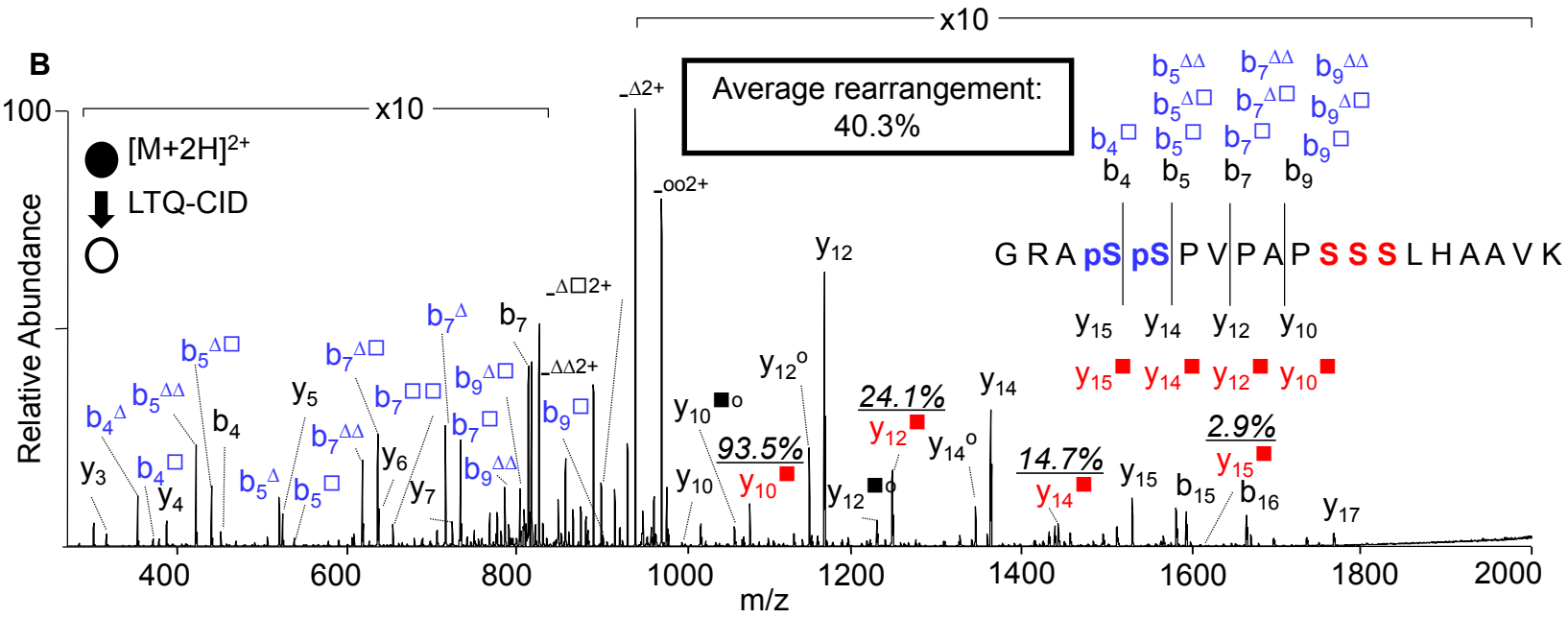

Similar to that observed for the peptides containing one donor and one acceptor, substitution of an arginine residue with lysine, *i.e.*, GKApSpSPVPAPSSSLHAAVR and GRApSpSPVPAPSSSLHAAVK (Figure 2.12 B) did not significantly affect the amplitude of the rearrangement reaction, despite changing the proton mobility from non-mobile to partially mobile (Figure 2.10). Finally, CID-MS/MS of each of the peptides from their triply protonated precursor ions (*i.e.*, partially mobile or mobile protonation states) did not yield any rearrangement, despite the greater numbers of donor and acceptors that were present.

2.2.3.4 CID-MS/MS Ion Activation Timescale

In an earlier study, it was reported that where the abundance of product ions resulting from phosphate group transfer reactions decreased as a function of decreasing activation time in the linear ion trap or in a triple quadrupole[187]. Consistenly, ions subjected to CID-MS/MS in the LTQ Orbitrap Velos mass spectrometer, in which ion activation occurs in a shorter timeframe (default 10 ms) due to the presence of a higher helium bath gas pressure compared to the LTQ (30 ms default ion activation timescale), yielded lower average % rearrangement ratios (compare the light blue (LTQ Velos) and dark blue bars (LTQ) in Figure 2.6 and Figure 2.10).

2.2.4 Competing Fragmentation or Rearrangement Reactions can Result in Erroneous CID-MS/MS Phosphorylation Site Localizations in Phosphopeptides Containing Multiple Donors and Acceptors

The results above clearly indicate that multiply protonated peptides in both non-mobile and partially mobile protonation states can undergo significant rearrangement

reactions, and that the presence of multiple donors and acceptors within a given peptide results in a greater extent of rearrangement. Interestingly, in a previously published phosphoproteome analysis study[262], which used trypsin as the enzyme for digestion, 33.5% of the phosphopeptides identified by CID-MS/MS were from precursor ions in either non-mobile or partially mobile protonation states. If the partially mobile peptides with charge states ≥ 3+ are excluded (*i.e.*, those from which no significant rearrangement is expected to see), the number of peptides become 21.9% of the total. Of these, 85.4% had at least one acceptor in addition to the phosphorylated (*i.e.*, potential donor) amino acid, 63.4% had at least two acceptors and 56.7% had at least two donors and one acceptor. Notably, 43.3% had at least two donors and two acceptors, representing 9.5% of the total peptides identified. These phosphopeptides, *i.e.*, those with multiple donors and/or acceptors, are more likely to undergo significant rearrangement reactions that could affect localization of their phosphorylation sites. In another data set in which Lys-C was used for digestion[259], 15.9% of the phosphopeptides identified by CID were classified as non-mobile (all charge states) or partially mobile (charge states ≤ 2+). Among these peptides, 29.0% had at least two donors and two acceptors (*i.e.*, 4.6% of the total peptides identified).

The Ascore algorithm is widely used for assigning phosphorylation sites in phosphoproteome-wide datasets of CID-MS/MS spectra[253, 259], so it was used here to evaluate whether rearrangement reactions could potentially affect the ability to confidently assign the correct phosphorylation sites. Ascore values greater than 13 have been reported to provide 95% confidence for phosphorylation site localization, while Ascore values greater than 19 provide 99% confidence[253]. Analysis of all the peptides

in this study, acquired by LTQ CID-MS/MS from their triply protonated precursor ions (either partially mobile or mobile protonation states), in which no significant phosphate group rearrangement reaction product ions were observed, each resulted in confident assignment (*i.e.*, high Ascore values) of the correct phosphorylation sites (Table 2.1) at the end of this chapter)[253]. Analysis of the same spectra using the PhosphoScore algorithm, whose Dscore has previously been shown to provide good agreement with Ascore[254], also yielded confident and correct assignment for all the triply protonated precursor ions. In contrast, analysis of the same peptides acquired from their doubly protonated precursor ions (either non-mobile or partially mobile protonation states), yielded a range of Ascore and Dscore values, with many instances of either (i) non-confident assignments (*i.e.*, low Ascore and Dscores), despite using high quality MS/MS spectra in each case, or (ii) confident (*i.e.*, high Ascore and Dscores) but *incorrectly* assigned phosphorylation site localizations (Table 2.1).

To assess the extent to which the magnitude of the rearrangement reactions affected the confidence of phosphorylation site assignments using the Ascore and PhosphoScore algorithms, the ratios of the Ascore and PhosphoScore values for the triply and doubly protonated precursor ions (*i.e.*, the ratio of Ascore 3+/Ascore 2+ and Dscore 3+/Dscore 2+) were calculated for each phosphopeptide in the library, then plotted against the average % rearrangement reaction values experimentally determined from the doubly protonated ions (Figure 2.13). Given that the triply protonated ions were each correctly assigned with high Ascore and Dscore values, a high Ascore/Dscore 3+/+2 ratio therefore corresponds to a low relative Ascores and Dscore for the doubly protonated ion, *i.e.*, a decreased confidence associated with their

phosphorylation site localization. Interestingly, a trend toward increasing Ascore and Dscore 3+/+2 ratios with increased rearrangement was observed in Figure 2.13, again indicating that the rearrangement reactions can negatively contribute to the confidence values obtained from these PTM scoring algorithms.

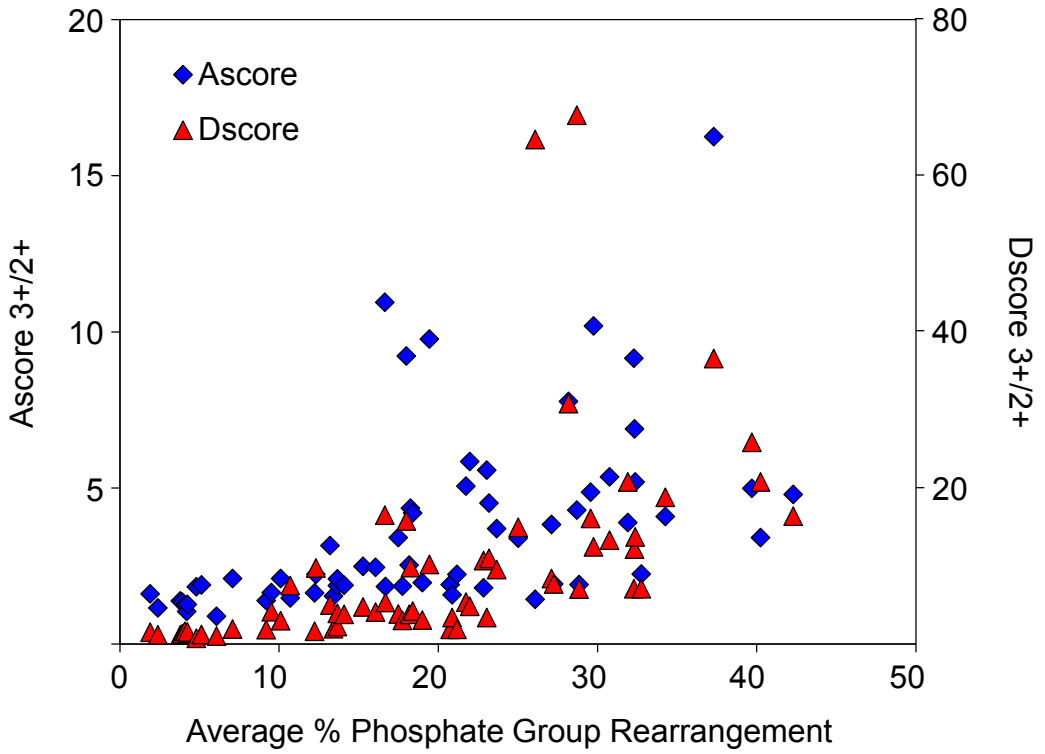

Figure 2.13 Average % phosphate group rearrangement versus Ascore and Dscore ratios for the LTQ CID-MS/MS doubly protonated ($[M+2H]^{2+}$) precursor ions from the synthetic phosphopeptide library $GX_1AX_2PVPAPX_3LHAAVX_4$, where X_1 = R, K or G; X_2 = pS, pSpS, pT, pY or pYpY; X_3 = SGG , TGG, YGG, SSG or SSS and X_4 = R, K or G. The x-axis shows the average % phosphate group rearrangement for each peptide. The y-axis shows the ratio of Ascore (blue) and Dscore (red) values determined from the triply and doubly protonated precursor ions (*i.e.*, the ratio of Ascore 3+/2+ or Dscore 3+/2+) for each phosphopeptide in the library.

Interestingly, the GRApTPVPAPSGGLHAAVR peptide from Figure 2.3, (non-mobile, average rearrangement 17.5%) was confidently but incorrectly assigned as GRATPVPAPpSGGLHAAVR, with an Ascore value of 31.05. In this case, the presence of the M+1 isotope peaks of the y_{10}^{o}, y_{12}^{o} and y_{14}^{o} ions, that were erroneously assigned as $y_9^{\blacksquare}$, $y_{11}^{\blacksquare}$ and $y_{13}^{\blacksquare}$ ions due to 'overlapping' at the same nominal m/z values, the $b_4^{\square}$, $b_6^{\square}$ and $b_8^{\square}$ ions that arose from both the rearrangement phosphate group transfer and competing direct HPO_3 loss fragmentation pathways), and the actual $y_{10}^{\blacksquare}$, $y_{12}^{\blacksquare}$, and $y_{14}^{\blacksquare}$ rearrangement ions, each contributed to the incorrect assignment. In another example, analysis of the doubly protonated (partially mobile) GRApSpSPVPAPSSSLHAAVK peptide ($y_{10}^{\blacksquare}$, $y_{12}^{\blacksquare}$, $y_{14}^{\blacksquare}$, $y_{15}^{\blacksquare}$, $b_5^{\square}$, $b_7^{\square}$ and $b_9^{\square}$ ions; average rearrangement 40.25%) resulted in a confident, but incorrect assignment as GRApSSPVPAPSpSSLHAAVK, with Ascore values of 19.33 for the incorrectly assigned C-terminal pS), and 38.87 for the correctly assigned N-terminal pS. Thus, for both these examples, despite the rearrangement ions being less abundant than those of the original (*i.e.*, un-rearranged) sequence ions, when observed along with erroneously assigned 'overlapping' ions, these ions do clearly play a significant role in the resulting incorrect phosphorylation site assignments.

2.3 Conclusions

The observation of abundant product ions arising from unanticipated competing fragmentation or rearrangement reactions during the ion activation period of an MS/MS or MS^3 experiment may potentially limit the success of bioinformatic approaches used for peptide identification and the characterization and localization of post translational modifications, if these reactions are not accounted for in the *in silico* 'rules' used by the

search algorithms. Here, it was demonstrated that the combined loss of metaphosphate and water that can occur as a competing isobaric mass fragmentation pathway with the loss of phosphoric acid during CID-MS/MS. This competing fragmentation pathways can lead to erroneous phosphorylation site assignments upon analysis of the CID-MS^3 spectra acquired from their $[M+nH-98Da]^{n+}$ product ions using automated PTM site localization algorithms. Furthermore, it was shown that abundant product ions formed via intramolecular phosphate group rearrangement reactions can be formed during CID-MS/MS of doubly protonated precursor ions under non-mobile or partially mobile conditions, particularly for peptides containing multiple phosphorylated 'donor' and non-phosphorylated 'acceptor' residues, and that peptides with these classifications are prevalent within large scale phosphoproteome analysis datasets. Thus, albeit not the sole determining factor that leads to decreased confidence or incorrect phosphorylation site localizations, and likely to affect only a subset of doubly protonated non-mobile or partially mobile precursor ions, it is clear that that rearrangement reactions can play a significant contributing role in decreased confidence or erroneous CID-MS/MS phosphorylation site localizations using current automated PTM site scoring algorithms. The results from this study therefore provide a framework for identifying the peptide sequences and precursor ion proton mobility classifications, for which closer scrutiny or validation of current bioinformatic algorithm phosphoproteome analysis search results are warranted. Furthermore, the results from this and other 'fundamental' gas-phase peptide fragmentation studies should be considered in any future efforts aimed at the development of improved bioinformatics tools for the characterization of protein post translational modifications.

	$[M+2H]^{2+}$							
	Avg % Rearrangement		ms^2-Ascore		ms^2-Dscore		ms^3-Dscore	
Sequence	LTQ	LTQ Velos	Ascore	Indicated Sequence	Dscore	Indicated Sequence	Dscore	Indicated Sequence
GRApYPVPAPSGGLHAAVR	21.75	17.08	29.65	-Y*-S-	0.0310	-Y#-S-	1.0000	**-Y-S*-**
GRApYPVPAPTGGLHAAVR	16.07	11.74	51.82	-Y*-T-	0.0383	-Y#-T-		
GRApYPVPAPYGGLHAAVR	13.68	8.36	67.36	-Y*-Y-	0.0474	-Y#-Y-		
GRApTPVPAPSGGLHAAVR	17.49	14.74	31.05	**-T-S*-**	0.0276	-T#-S-	0.0140	**-T-S*-**
GRApTPVPAPTGGLHAAVR	12.32	8.24	58.66	-T*-T-	0.0140	-T#-T-		
GRApTPVPAPYGGLHAAVR	10.10	4.94	67.36	-T*-Y-	0.0616	-T#-Y-		
GRApSPVPAPSGGLHAAVR	13.20	9.81	27.23	**-S-S*-**	0.0191	-S#-S-	0.0268	-S*-S-
GRApSPVPAPTGGLHAAVR	9.21	4.96	67.36	-S*-T-	0.0555	-S#-T-		
GRApSPVPAPYGGLHAAVR	7.08	3.24	67.36	-S*-Y-	0.0693	-S#-Y-	1.0000	-S*-Y-
GRApYPVPAPSGGLHAAVK	23.05	16.90	26.07	-Y*-S-	0.0463	-Y#-S-	1.0000	**-Y-S*-**
GRApYPVPAPSGGLHAAVG	13.43	4.34	56.74	-Y*-S-	0.0802	-Y#-S-	1.0000	**-Y-S*-**
GKApYPVPAPSGGLHAAVR	21.98	13.73	17.14	-Y*-S-	0.0307	-Y#-S-	1.0000	**-Y-S*-**
GGApYPVPAPSGGLHAAVR	3.81	2.48	78.89	-Y*-S-	0.1374	-Y#-S-		
GRASPVPAPpYGGLHAAVR	21.18	17.93	77.13	-S-Y*-	0.0916	-S-Y#-	1.0000	**-S*-Y-**

Table 2.1 Summary of Ascore LTQ MS/MS and Dscore LTQ MS/MS and MS^3 phosphorylation site localization results for a library of synthetic phosphopeptide sequences. (Ascore: * indicates the assigned phosphorylation site; Dscore: # indicates the assigned phosphorylation site for MS/MS; * indicates the assigned site for MS^3; Ascore/Dscore sequences are indicated in bold text if they were incorrectly assigned; Ascore/Dscore values are indicated in bold text if they were not confidently (>95% confidence) assigned; When two phosphorylation sites exist, the assigned site is labeled in red text.)

Table 2.1 (Cont'd)

	$[M+3H]^{3+}$					
	ms^2-Ascore		ms^2-Dscore		ms^3-Dscore	
Sequence	Ascore	Indicated Sequence	Dscore	Indicated Sequence	Dscore	Indicated Sequence
GRApYPVPAPSGGLHAAVR	149.65	-Y*-S-	0.1644	-Y#-S-		
GRApYPVPAPTGGLHAAVR	126.40	-Y*-T-	0.1546	-Y#-T-		
GRApYPVPAPYGGLHAAVR	139.42	-Y*-Y-	0.1822	-Y#-Y-		
GRApTPVPAPSGGLHAAVR	105.36	-T*-S-	0.1040	-T#-S-	0.1027	-T*-S-
GRApTPVPAPTGGLHAAVR	130.11	-T*-T-	0.1352	-T#-T-		
GRApTPVPAPYGGLHAAVR	140.21	-T*-Y-	0.1803	-T#-Y-		
GRApSPVPAPSGGLHAAVR	85.53	-S*-S-	0.0945	-S#-S-	0.1406	-S*-S-
GRApSPVPAPTGGLHAAVR	92.70	-S*-T-	0.0978	-S#-T-		
GRApSPVPAPYGGLHAAVR	140.21	-S*-Y-	0.1296	-S#-Y-	1.0000	-S*-Y-
GRApYPVPAPSGGLHAAVK	144.78	-Y*-S-	0.1539	-Y#-S-		
GRApYPVPAPSGGLHAAVG	86.04	-Y*-S-	0.1533	-Y#-S-		
GKApYPVPAPSGGLHAAVR	99.90	-Y*-S-	0.1465	-Y#-S-		
GGApYPVPAPSGGLHAAVR	108.05	-Y*-S-	0.1511	-Y#-S-		
GRASPVPAPpYGGLHAAVR	171.07	-S-Y*-	0.1661	-S-Y#-	1.0000	**-S*-Y-**

Table 2.1 (Cont'd)

	$[M+2H]^{2+}$							
	Avg % Rearrangement		ms^2-Ascore		ms^2-Dscore		ms^3-Dscore	
Sequence	LTQ	LTQ Velos	Ascore	Indicated Sequence	Dscore	Indicated Sequence	Dscore	Indicated Sequence
GGASPVPAPpYGGLHAAVR	4.81	0.95	61.56	-S-Y*-	0.1828	-S-Y#-		
GRASPVPAPpYGGLHAAVG	6.08	1.09	106.94	-S-Y*-	0.1251	-S-Y#-		
GRAYPVPAPpSGGLHAAVR	4.20	1.79	126.46	-Y-S*-	0.1151	-Y-S#-	1.0000	**-Y-S*-**
GKApSPVPAPSGGLHAAVR	20.75	15.87	53.18	-S*-S-	0.0469	-S#-S-	0.0551	-S*-S-
GRApYPVPAPTGGLHAAVK	18.41	13.07	33.00	-Y*-T-	0.0338	-Y#-T-		
GRApYPVPAPYGGLHAAVK	15.27	9.96	57.18	-Y*-Y-	0.0413	-Y#-Y-		
GRApTPVPAPSGGLHAAVK	16.69	13.35	67.36	-T*-S-	0.0295	-T#-S-	0.0219	**-T-S*-**
GRApTPVPAPTGGLHAAVK	13.67	9.40	67.36	-T*-T-	0.0450	-T#-T-		
GRApTPVPAPYGGLHAAVK	17.75	7.72	67.36	-T*-Y-	0.0426	-T#-Y-		
GRApSPVPAPSGGLHAAVK	14.10	9.45	67.36	-S*-S-	0.0380	-S#-S-	**0.0035**	-S*-S-
GRApSPVPAPTGGLHAAVK	10.71	6.53	67.36	-S*-T-	0.0156	-S#-T-		
GRApSPVPAPYGGLHAAVK	9.52	5.17	67.36	-S*-Y-	0.0352	-S#-Y-		
GRApYPVPAPTGGLHAAVG	19.00	7.89	34.55	-Y*-T-	0.0463	-Y#-T-		
GRApYPVPAPYGGLHAAVG	4.24	1.18	79.31	-Y*-Y-	0.1164	-Y#-Y-		

Table 2.1 (Cont'd)

	$[M+3H]^{3+}$					
	ms^2-Ascore		ms^2-Dscore		ms^3-Dscore	
Sequence	Ascore	Indicated Sequence	Dscore	Indicated Sequence	Dscore	Indicated Sequence
GGASPVPAPpYGGLHAAVR	111.46	-S-Y*-	0.1252	-S-Y#-		
GRASPVPAPpYGGLHAAVG	93.90	-S-Y*-	0.1184	-S-Y#-		
GRAYPVPAPpSGGLHAAVR	129.99	-Y-S*-	0.1494	-Y-S#-	1.0000	**-Y-S*-**
GKApSPVPAPSGGLHAAVR	100.39	-S*-S-	0.0842	-S#-S-	0.0968	-S*-S-
GRApYPVPAPTGGLHAAVK	137.85	-Y*-T-	0.1400	-Y#-T-		
GRApYPVPAPYGGLHAAVK	141.11	-Y*-Y-	0.1927	-Y#-Y-		
GRApTPVPAPSGGLHAAVK	123.14	-T*-S-	0.1549	-T#-S-	0.1223	-T*-S-
GRApTPVPAPTGGLHAAVK	125.14	-T*-T-	0.0975	-T#-T-		
GRApTPVPAPYGGLHAAVK	123.79	-T*-Y-	0.1263	-T#-Y-		
GRApSPVPAPSGGLHAAVK	125.57	-S*-S-	0.1421	-S#-S-	0.1025	-S*-S-
GRApSPVPAPTGGLHAAVK	97.84	-S*-T-	0.1155	-S#-T-		
GRApSPVPAPYGGLHAAVK	109.64	-S*-Y-	0.1424	-S#-Y-		
GRApYPVPAPTGGLHAAVG	67.40	-Y*-T-	0.1394	-Y#-T-		
GRApYPVPAPYGGLHAAVG	99.71	-Y*-Y-	0.1737	-Y#-Y-		

Table 2.1 (Cont'd)

	[M+2H]$^{2+}$							
	Avg % Rearrangement		ms^2-Ascore		ms^2-Dscore		ms^3-Dscore	
Sequence	LTQ	LTQ Velos	Ascore	Indicated Sequence	Dscore	Indicated Sequence	Dscore	Indicated Sequence
GRApTPVPAPSGGLHAAVG	5.14	2.02	50.22	-T*-S-	0.0829	-T#-S-	**0.0037**	**-T-S*-**
GRApTPVPAPTGGLHAAVG	4.08	1.05	89.93	-T*-T-	0.0764	-T#-T-		
GRApTPVPAPYGGLHAAVG	12.24	0.62	67.36	-T*-Y-	0.0832	-T#-Y-		
GRApSPVPAPSGGLHAAVG	3.93	1.04	84.45	-S*-S-	0.1076	-S#-S-	0.0545	-S*-S-
GRApSPVPAPTGGLHAAVG	2.40	0.80	68.94	-S*-T-	0.0941	-S#-T-		
GRApSPVPAPYGGLHAAVG	1.92	0.33	68.68	-S*-Y-	0.0915	-S#-Y-		
GRApSPVPAPSSGLHAAVR	18.27	12.95	18.42	**-S-S*SG-**	**0.0087**	-S#-SSG-	0.0111	-S*-SSG-
GKApSPVPAPSSGLHAAVR	26.09	20.17	51.82	-S*-SSG-	**0.0011**	-S#-SSG-	0.0389	-S*-SSG-
GRApSPVPAPSSGLHAAVK	16.65	13.22	**8.58**	**-S-S*SG-**	**0.0063**	-S#-SSG-	0.0139	**-S-S*SG-**
GRApSPVPAPSSSLHAAVR	18.00	13.32	**9.34**	**-S-SSS*-**	**0.0057**	-S#-SSS-	0.0126	**-S-SSS*-**
GKApSPVPAPSSSLHAAVR	28.84	22.90	46.77	**-S-S*SS-**	0.0126	**-S-S#SS-**	0.0443	-S*-SSS-
GRApSPVPAPSSSLHAAVK	19.45	14.07	**9.34**	**-S-S*SS-**	**0.0090**	-S#-SSS-	0.0183	**-S-SSS*-**
GRApYPVPAPSSGLHAAVR	27.25	23.63	58.98	-Y*-SSG-	0.0188	-Y#-SSG-	0.0212	**-Y-SS*G-**
GKApYPVPAPSSGLHAAVR	26.54	16.42	**11.51**	**-Y-SS*G-**	**0.0002**	**-Y-S#SG-**	**0.0097**	**-Y-SS*G-**
GRApYPVPAPSSGLHAAVK	32.29	20.42	**11.95**	**-Y-S*SG-**	0.0208	-Y#-SSG-	0.0187	**-Y-S*SG-**

Table 2.1 (Cont'd)

	$[M+3H]^{3+}$					
	ms^2-Ascore		ms^2-Dscore		ms^3-Dscore	
Sequence	Ascore	Indicated Sequence	Dscore	Indicated Sequence	Dscore	Indicated Sequence
GRApTPVPAPSGGLHAAVG	94.40	-T*-S-	0.0968	-T#-S-	0.0693	-T*-S-
GRApTPVPAPTGGLHAAVG	110.74	-T*-T-	0.1183	-T#-T-		
GRApTPVPAPYGGLHAAVG	109.51	-T*-Y-	0.1319	-T#-Y-		
GRApSPVPAPSGGLHAAVG	111.58	-S*-S-	0.1339	-S#-S-	0.0596	-S*-S-
GRApSPVPAPTGGLHAAVG	78.62	-S*-T-	0.1053	-S#-T-		
GRApSPVPAPYGGLHAAVG	109.51	-S*-Y-	0.1324	-S#-Y-		
GRApSPVPAPSSGLHAAVR	79.84	-S*-SSG-	0.0848	-S#-SSG-	0.1280	-S*-SSG-
GKApSPVPAPSSGLHAAVR	73.56	-S*-SSG-	0.0736	-S#-SSG-	0.0865	-S*-SSG-
GRApSPVPAPSSGLHAAVK	93.81	-S*-SSG-	0.1032	-S#-SSG-	0.0692	-S*-SSG-
GRApSPVPAPSSSLHAAVR	86.04	-S*-SSS-	0.0887	-S#-SSS-	0.1206	-S*-SSS-
GKApSPVPAPSSSLHAAVR	88.05	-S*-SSS-	0.0881	-S#-SSS-	0.0970	-S*-SSS-
GRApSPVPAPSSSLHAAVK	91.10	-S*-SSS-	0.0913	-S#-SSS-	0.1127	-S*-SSS-
GRApYPVPAPSSGLHAAVR	112.70	-Y*-SSG-	0.1435	-Y#-SSG-		
GKApYPVPAPSSGLHAAVR	107.70	-Y*-SSG-	0.1500	-Y#-SSG-		
GRApYPVPAPSSGLHAAVK	109.20	-Y*-SSG-	0.1457	-Y#-SSG-		

Table 2.1 (Cont'd)

	$[M+2H]^{2+}$							
	Avg % Rearrangement		ms^2-Ascore		ms^2-Dscore		ms^3-Dscore	
Sequence	LTQ	LTQ Velos	Ascore	Indicated Sequence	Dscore	Indicated Sequence	Dscore	Indicated Sequence
GRApYPVPAPSSSLHAAVR	30.76	24.52	18.42	**-Y-S*SS-**	0.0116	**-Y-S#SS-**	**0.0010**	**-Y-SSS*-**
GKApYPVPAPSSSLHAAVR	25.01	16.82	28.65	-Y*-SSS-	0.0109	**-Y-S#SS-**	**0.0025**	**-Y-SSS*-**
GRApYPVPAPSSSLHAAVK	34.27	20.58	16.22	**-Y-SS*S-**	**0.0030**	-Y#-SSS-	0.0101	**-Y-S*SS-**
GRApSpSPVPAPSGGLHAAVR	27.11	24.43	27.88	**-S*S-S*-**	0.0137	-S#S#-S-	**0.0033**	-S*S#-S-
			16.22	**-S*S-S*-**				
GKApSpSPVPAPSGGLHAAVR	32.75	22.36	32.40	-S*S*-S-	0.0138	-S#S#-S-	**0.0041**	**-S#S-S*-**
			56.14	-S*S*-S-				
GRApSpSPVPAPSGGLHAAVK	18.17	18.11	37.02	-S*S*-S-	0.0309	-S#S#-S-	**0.0038**	**-SS#-S*-**
			50.11	-S*S*-S-				
GRApSpSPVPAPSSGLHAAVR	42.30	36.36	**12.43**	**-S*S-S*SG-**	**0.0055**	**-S#S-S#SG-**	**0.0006**	**-S*S-SS#G-**
			16.22	**-S*S-S*SG-**				
GKApSpSPVPAPSSGLHAAVR	20.87	12.25	51.82	-S*S*-SSG-	0.0237	-S#S#-SSG-	**0.0030**	-S#S*-SSG-
			78.64	-S*S*-SSG-				
GRApSpSPVPAPSSGLHAAVK	29.58	26.91	**12.43**	**-S*S-SS*G-**	**0.0070**	**-S#S-SS#G-**	**0.0007**	-S*S#-SSG-
			28.87	**-S*S-SS*G-**				

Table 2.1 (Cont'd)

	$[M+3H]^{3+}$					
	ms^2-Ascore		ms^2-Dscore		ms^3-Dscore	
Sequence	Ascore	Indicated Sequence	Dscore	Indicated Sequence	Dscore	Indicated Sequence
GRApYPVPAPSSSLHAAVR	98.27	-Y*-SSS-	0.1538	-Y#-SSS-		
GKApYPVPAPSSSLHAAVR	96.64	-Y*-SSS-	0.1630	-Y#-SSS-		
GRApYPVPAPSSSLHAAVK	66.08	-Y*-SSS-	0.0569	-Y#-SSS-		
GRApSpSPVPAPSGGLHAAVR	82.06	-S*S*-SSS-	0.1138	-S#S#-S-	**0.0008**	-S#S*-S-
	76.01	-S*S*-SSS-				
GKApSpSPVPAPSGGLHAAVR	84.87	-S*S*-S-	0.0968	-S#S#-S-	0.0307	-S#S*-S-
	103.02	-S*S*-S-				
GRApSpSPVPAPSGGLHAAVK	106.89	-S*S*-S-	0.1152	-S#S#-S-	**0.0017**	**-S#S-S*-**
	106.80	-S*S*-S-				
GRApSpSPVPAPSSGLHAAVR	68.86	-S*S*-SSG-	0.0893	-S#S#-SSG-	**0.0008**	-S#S*-SSG-
	64.99	-S*S*-SSG-				
GKApSpSPVPAPSSGLHAAVR	90.11	-S*S*-SSG-	0.0790	-S#S#-SSG-	0.0201	-S#S*-SSG-
	108.21	-S*S*-SSG-				
GRApSpSPVPAPSSGLHAAVK	86.53	-S*S*-SSG-	0.1126	-S#S#-SSG-	**0.0018**	**-S#S-S*SG-**
	79.19	-S*S*-SSG-				

Table 2.1 (Cont'd)

	$[M+2H]^{2+}$							
	Avg % Rearrangement		ms^2-Ascore		ms^2-Dscore		ms^3-Dscore	
Sequence	LTQ	LTQ Velos	Ascore	Indicated Sequence	Dscore	Indicated Sequence	Dscore	Indicated Sequence
GRApSpSPVPAPSSSLHAAVR	32.32	26.17	**9.34**	**-S*S-SS*S-**	**0.0077**	**-S#S-S#SS-**	0.0103	**-S*S-S#SS-**
			16.22	**-S*S-SS*S-**				
GKApSpSPVPAPSSSLHAAVR	22.85	19.36	46.79	-S*S*-SSS-	**0.0072**	**-S#S-S#SS-**	**0.0014**	-S#S*-SSS-
			61.59	-S*S*-SSS-				
GRApSpSPVPAPSSSLHAAVK	40.25	33.95	19.33	**-S*S-SS*S-**	**0.0050**	**-S#S-SSS#-**	**0.0030**	**-SS#-SSS*-**
			28.87	**-S*S-SS*S-**				
GRApYpYPVPAPSGGLHAAVR	23.20	19.13	34.05	-Y*Y*-S-	0.0122	-Y#Y#-S-	**0.0093**	**-YY#-S*-**
			46.76	-Y*Y*-S-				
GKApYpYPVPAPSGGLHAAVR	23.66	17.62	37.02	-Y*Y*-S-	0.0140	**-Y#Y-S#-**	**0.0008**	**-Y#Y-S*-**
			52.56	-Y*Y*-S-				
GRApYpYPVPAPSGGLHAAVK	28.18	21.89	53.60	**-Y*Y-S*-**	**0.0044**	-Y#Y#-S-	**0.0003**	**-Y#Y-S*-**
			16.10	**-Y*Y-S*-**				

Table 2.1 (Cont'd)

	$[M+3H]^{3+}$					
	ms^2-Ascore		ms^2-Dscore		ms^3-Dscore	
Sequence	Ascore	Indicated Sequence	Dscore	Indicated Sequence	Dscore	Indicated Sequence
GRApSpSPVPAPSSSLHAAVR	82.04	-S*S*-SSS-	0.0933	-S#S#-SSS-	**0.0048**	-S#S*-SSS-
	80.54	-S*S*-SSS-				
GKApSpSPVPAPSSSLHAAVR	83.46	-S*S*-SSS-	0.0765	-S#S#-SSS-	0.0154	-S#S*-SSS-
	110.61	-S*S*-SSS-				
GRApSpSPVPAPSSSLHAAVK	80.58	-S*S*-SSS-	0.1044	-S#S#-SSS-	**0.0097**	-S*S#-SSS-
	75.34	-S*S*-SSS-				
GRApYpYPVPAPSGGLHAAVR	186.15	-Y*Y*-S-	0.1333	-Y#Y#-S-		
	165.29	-Y*Y*-S-				
GKApYpYPVPAPSGGLHAAVR	156.75	-Y*Y*-S-	0.1329	-Y#Y#-S-		
	163.83	-Y*Y*-S-				
GRApYpYPVPAPSGGLHAAVK	204.37	-Y*Y*-S-	0.1353	-Y#Y#-S-		
	188.40	-Y*Y*-S-				

Table 2.1 (Cont'd)

	[M+2H]$^{2+}$							
	Avg % Rearrangement		ms^2-Ascore		ms^2-Dscore		ms^3-Dscore	
Sequence	LTQ	LTQ Velos	Ascore	Indicated Sequence	Dscore	Indicated Sequence	Dscore	Indicated Sequence
GRApYpYPVPAPSSGLHAAVR	31.90	29.78	25.97	-Y*Y*-SSG-	**0.0068**	**-Y#Y-S#SG-**	**0.0058**	**-YY#-S*SG-**
			41.21	-Y*Y*-SSG-				
GKApYpYPVPAPSSGLHAAVR	28.71	22.24	25.05	**-Y*Y-S*SG-**	**0.0020**	**-Y#Y-S#SG-**	**0.0026**	**-YY#-SS*G-**
			32.40	**-Y*Y-S*SG-**				
GRApYpYPVPAPSSGLHAAVK	29.76	23.54	13.24	**-Y*Y-S*SG-**	0.0106	-Y#Y#-SSG-	**0.0001**	**-Y#Y-S*SG-**
			16.10	**-Y*Y-S*SG-**				
GRApYpYPVPAPSSSLHAAVR	39.69	32.32	37.02	**-Y*Y-S*SS-**	**0.0056**	**-Y#Y-S#SS-**	0.0102	**-YY-S#SS*-**
			19.16	**-Y*Y-S*SS-**				
GKApYpYPVPAPSSSLHAAVR	32.36	24.01	28.75	-Y*Y*-SSS-	0.0112	-Y#Y#-SSS-	**0.0012**	**-YY#-S*SS-**
			52.27	-Y*Y*-SSS-				
GRApYpYPVPAPSSSLHAAVK	37.31	28.36	**6.47**	**-Y*Y-SS*S-**	**0.0030**	**-Y#Y-S#SS-**	**0.0012**	**-Y#Y-SSS*-**
			19.16	**-Y*Y-SS*S-**				

Table 2.1 (Cont'd)

	$[M+3H]^{3+}$					
	ms^2-Ascore		ms^2-Dscore		ms^3-Dscore	
Sequence	Ascore	Indicated Sequence	Dscore	Indicated Sequence	Dscore	Indicated Sequence
GRApYpYPVPAPSSGLHAAVR	125.76	-Y*Y*-SSG-	0.1413	-Y#Y#-SSG-		
	120.15	-Y*Y*-SSG-				
GKApYpYPVPAPSSGLHAAVR	120.67	-Y*Y*-SSG-	0.1341	-Y#Y#-SSG-		
	120.74	-Y*Y*-SSG-				
GRApYpYPVPAPSSGLHAAVK	153.64	-Y*Y*-SSG-	0.1311	-Y#Y#-SSG-		
	140.73	-Y*Y*-SSG-				
GRApYpYPVPAPSSSLHAAVR	138.91	-Y*Y*-SSS-	0.1455	-Y#Y#-SSS-		
	118.61	-Y*Y*-SSS-				
GKApYpYPVPAPSSSLHAAVR	196.45	-Y*Y*-SSS-	0.1525	-Y#Y#-SSS-		
	183.34	-Y*Y*-SSS-				
GRApYpYPVPAPSSSLHAAVK	161.9	-Y*Y*-SSS-	0.1100	-Y#Y#-SSS-		
	142.90	-Y*Y*-SSS-				

CHAPTER THREE

Quantification of Competing H_3PO_4 versus HPO_3+H_2O Neutral Losses from Regioselective ^{18}O-Labeled Phosphopeptides

3.1 Introduction

As discussed in chapter one, product ions with neutral loss of 98 Da are often dominant in the CID-MS/MS spectra of protonated phosphopeptide ions, which suppresses the abundances of other product ions containing information on the phosphorylation site(s). However, CID-MS^3 of these product ions can be performed to obtain additional sequence information for localizing phosphorylation sites[181, 183, 184, 263-265]. The original phosphorylation site(s) of the peptide can be assigned based on the observed location of dehydration sites in the product ions formed by CID-MS^3. Unfortunately, however, the neutral loss of 98 Da could result from either the direct loss of phosphoric acid (H_3PO_4) from the phosphorylated residue (*i.e.*, pathway A in Scheme 3.1) or the combined losses of meta-phosphate (HPO_3) from the phosphorylated residue and water (H_2O) from another site within the peptide (pathway B in Scheme 3.1). Pathway A forms product ions containing dehydration at the original phosphorylation site of the peptide while pathway B generates product ions containing dehydration at other sites of the peptide. Furthermore, the Ser and Thr hydroxyl side chains, carboxylic acid functional groups, and a carbonyl oxygen of the backbone amide bonds may all contribute to the water loss in pathway B[180]. Therefore, if

---

The results described in this chapter were published in: Cui, L., Yapici, I., Borhan, B. and Reid, G.E., Quantification of Competing H_3PO_4 versus HPO_3+H_2O Neutral Losses from Regioselective ^{18}O-Labeled Phosphopeptide Ions. *J. Am. Soc. Mass Spectrom* **2014**, 25, 141-148.

the combined loss pathway contributes dominantly to this neutral loss, using the dehydration site to localize phosphorylation sites via MS^3 can produce an incorrect result.

CID-MS^3 of $[M+nH-98Da]^{n+}$ product ions from CID-MS/MS of the protonated phosphopeptides have previously been analyzed. The existence of the combined losses pathway has been confirmed by the presence of product ions containing dehydration that were not at the original sites of phosphorylation[180, 187]. However, these dehydration product ions are often of not equal abundance, which makes the quantification of the combined losses pathway infeasible. The best way to experimentally quantify these two competing pathways is through isotope labeling. Isotope labeling has been advantageous in prior studies of peptide fragmentation mechanisms. For example, regioselective deuterium labeling has previously been used to confirm that direct phosphate group loss from protonated phosphopeptides occurs via a "charge directed" S_N2 neighboring group participation reaction mechanism[180], while ^{18}O labeling of the carboxyl group has been employed to identify the sources of water losses during peptide fragmentation[81].

In this chapter, a series of phosphopeptides containing regioselective ^{18}O labeling at the phosphoester bonds, prepared by a new synthesis strategy described in chapter four, were examined. This synthesis strategy first involves the solution-phase synthesis of Ser and Thr amino acids with ^{18}O incorporated into their side chain hydroxyl groups, which are subsequently phosphorylated after introduction of the labeled amino acids to the peptide sequence using solid phase peptide synthesis methods. As shown in Scheme 3.1, the observation of a neutral loss of 100 Da from

regioselective ^{18}O-labeled phosphopeptides upon CID-MS/MS is indicative of the direct loss of H_3PO_4 from the phosphorylated residue, while the loss of 98 Da is indicative of the combined losses pathway. Thus, by simply comparing the intensity of these two ions, these competing fragmentation pathways can be quantified. The regioselective ^{18}O labeled pS and pT containing peptides were adapted from, and relatively representative of, peptide sequences previously reported in large-scale phosphoproteomics studies[173, 259]. [259]The pY peptides were not investigated here as -98 Da neutral losses from these peptides can only occur via the combined loss pathway, as previously reported[266].

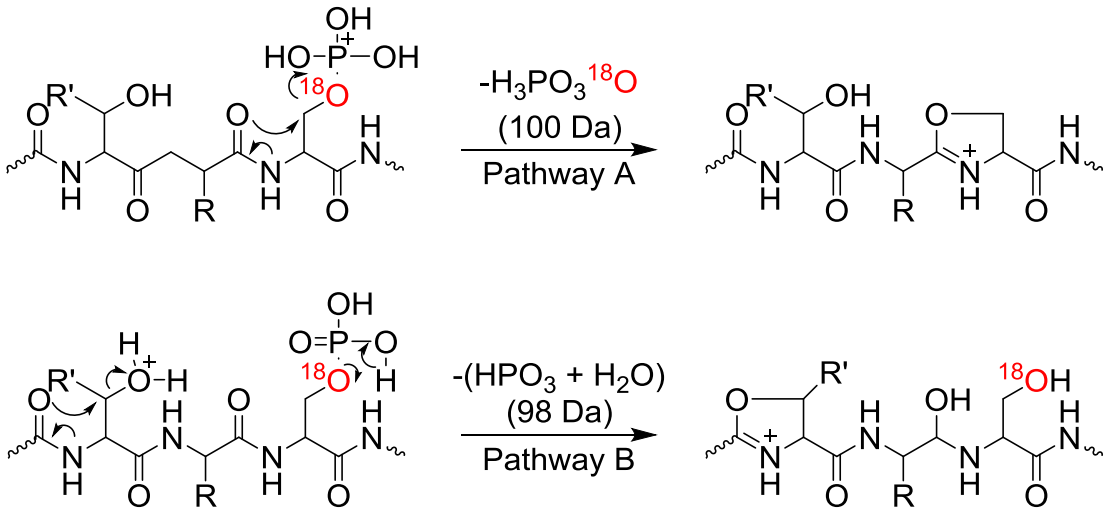

Scheme 3.1 Competing pathways for the CID-MS/MS gas-phase fragmentation reactions of protonated phosphopeptide ions. (A) Competition between H_3PO_4 loss side chain fragmentation and amide bond cleavage pathways, (B) competition within side chain fragmentation pathways involving the loss of H_3PO_4 or the combined losses of HPO_3 and H_2O, and (C) intramolecular phosphate group (HPO_3) transfer (*i.e.*, rearrangement or 'scrambling').

3.2 Results and Discussion

3.2.1 Quantification of Competing Fragmentation Pathways

Figure 3.1 shows the ion trap CID-MS/MS spectra of two doubly protonated phosphopeptide precursor ions: GRApSPVPAPSGGLHAAVR (Figure 3.1 A) and ALQAPHSPpTK (Figure 3.1 B) adapted from the sequences of peptides from hypothetical protein LOC57648 and pre-B-cell leukemia transcription factor interacting protein 1, respectively, that were previously reported from a large scale phosphoproteome analysis dataset [173]. In CID-MS/MS of these two peptides, the lack of observable ^{18}O labeled y and b ions which do not contain phosphorylation sites indicated that no ^{18}O scrambling occurred during the peptide synthesis process.

The blue inserts (Figure 3.1 A(i) and Figure 3.1 B(i)) to each spectrum show the isolation spectra for the two peptides, demonstrating that no M+2 isotope ions of the ^{18}O-labeled peptides were present, while the red inserts show expanded regions of the product ion spectra containing the -98 and -100 Da neutral loss products. Note that m/z 890.96 in Figure 3.1 A(i) is the M+1 isotope of the doubly protonated precursor ion of the phosphopeptide lacking ^{18}O, due to the original Ser amino acid having an ^{18}O-incorporation of 91%. The presence of this M+1 isotope ion gave rise to two concerns. Firstly, the dissociation of this ion produces a -98 Da neutral loss product ion at m/z 841.97 which overlaps with M+1 isotope product ion from the direct neutral loss fragmentation pathway (-100 Da) of the ^{18}O labeled peptide (m/z 891.46). As it presents at approx. 9% relative abundance compared to the monoisotopic ion of the ^{18}O-labeled peptide, the apparent abundance of the M+1 isotope of -100 Da neutral loss product ions from the ^{18}O labeled peptide was effectively increased. However, this does not

affect the quantification of the two competing fragmentation pathways, as only the phosphopeptide monoisotopic ions were employed for quantification. Furthermore, the presence of this M+1 isotope ion also indicates the presence of the M+2 isotope of the unlabeled phosphopeptide at m/z 891.46. The M+2 isotope ion again produces a -98 Da neutral loss product ion at m/z 842.47, which overlaps with the monoisotopic product ion from the combined neutral loss fragmentation pathway (-98 Da) of the ^{18}O labeled peptide. Fortunately, the contribution of this ion to the observed abundance of the combined neutral loss pathway of the ^{18}O-labeled peptides is less than 5% (M+2 isotope of this ion is approx. 50% relative to its M+1 isotope) and is negligible.

In Figure 3.1A(ii), m/z 841.47 corresponds to the monoisotopic ion of the fragmentation pathway resulting in the direct neutral loss of the phosphate group, while m/z 842.47 arises from the combined neutral loss pathway. The abundances of these product ions indicate that only 37% of the phosphate side chain neutral loss from GRApSPVPAPSGGLHAAVR results from the direct loss (*i.e.*, pathway A in Scheme 3.1), while 63% results from the combined losses (*i.e.*, pathway B in Scheme 3.1). In contrast, in Figure 3.1 B(ii), the abundances of the product ions at m/z 516.29 and 517.29 from the ALQAPHSPpTK peptide indicate that 93.5% of the neutral loss is derived from the direct loss pathway. Interestingly, the two competing fragmentation pathways occur to different extents in these two peptides. Notably, GRApSPVPAPSGGLHAAVR contains two Arg residues, so its doubly protonated precursor ion is in a non-mobile protonated state[71]. The doubly protonated precursor ions of the ALQAPHSPpTK peptide, however, are in a partially mobile protonated state,

suggestive of the effect of precursor ion proton mobility on these competing side chain fragmentation reactions.

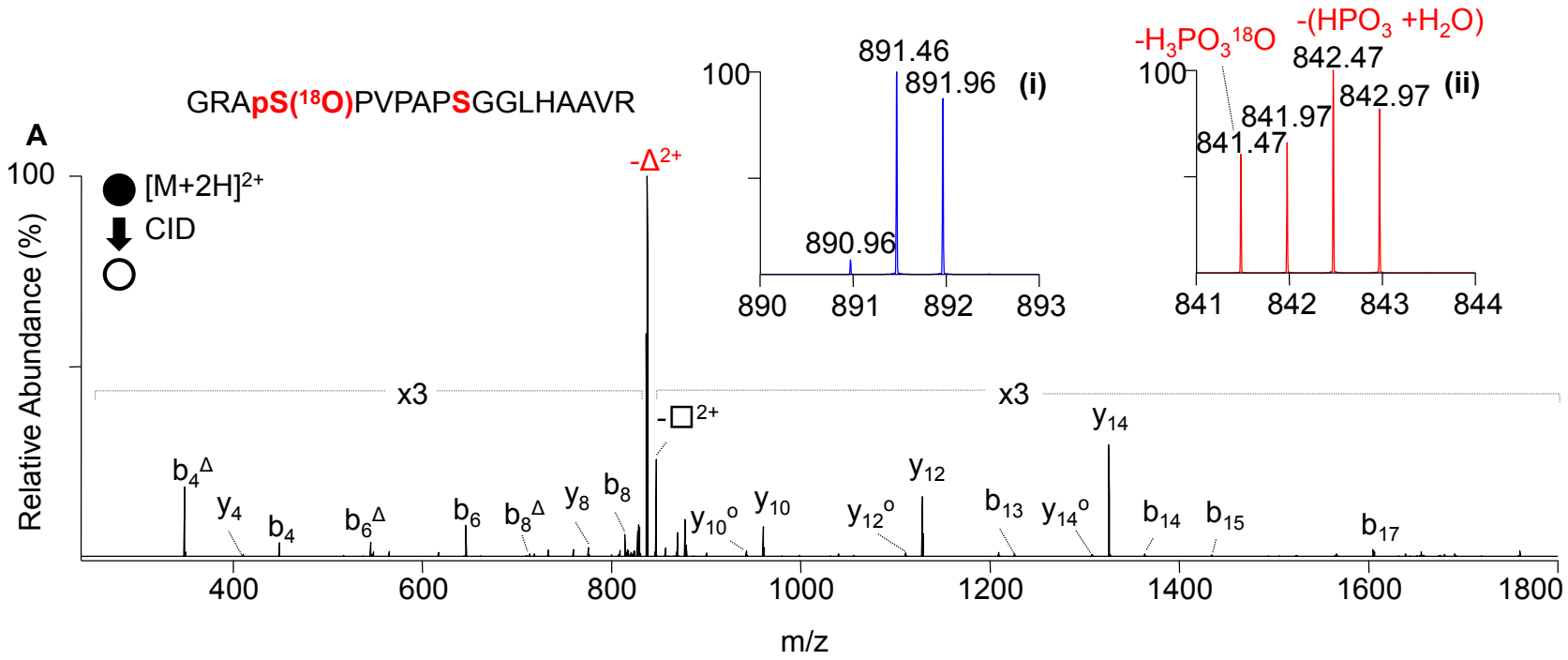

Figure 3.1 (A) CID-MS/MS product ion spectra for the doubly protonated precursor ions of the phosphopeptides GRApSPVPAPSGGLHAAVR. The blue colored inserts (i) show the isolation spectra for the precursor ions, while the red colored inserts (ii) show expanded regions of the spectra for the neutral losses of $H_3PO_3{}^{18}O$ and (HPO_3+H_2O). Δ = –100/98 Da (–$H_3PO_3{}^{18}O$ or –(HPO_3+H_2O)); □ = –80 Da (–HPO_3); ° = –18 Da (–H_2O); * = –17 Da (–NH_3). (B) CID-MS/MS product ion spectra for the doubly protonated precursor ions of the phosphopeptides ALQAPHSPpTK. The blue colored inserts (i) show the isolation spectra for the precursor ions, while the red colored inserts (ii) show expanded regions of the spectra for the neutral losses of $H_3PO_3{}^{18}O$ and (HPO_3+H_2O). Δ = –100/98 Da (–$H_3PO_3{}^{18}O$ or –(HPO_3+H_2O)); □ = –80 Da (–HPO_3); ° = –18 Da (–H_2O); * = –17 Da (–NH_3).

Figure 3.1 (Cont'd)

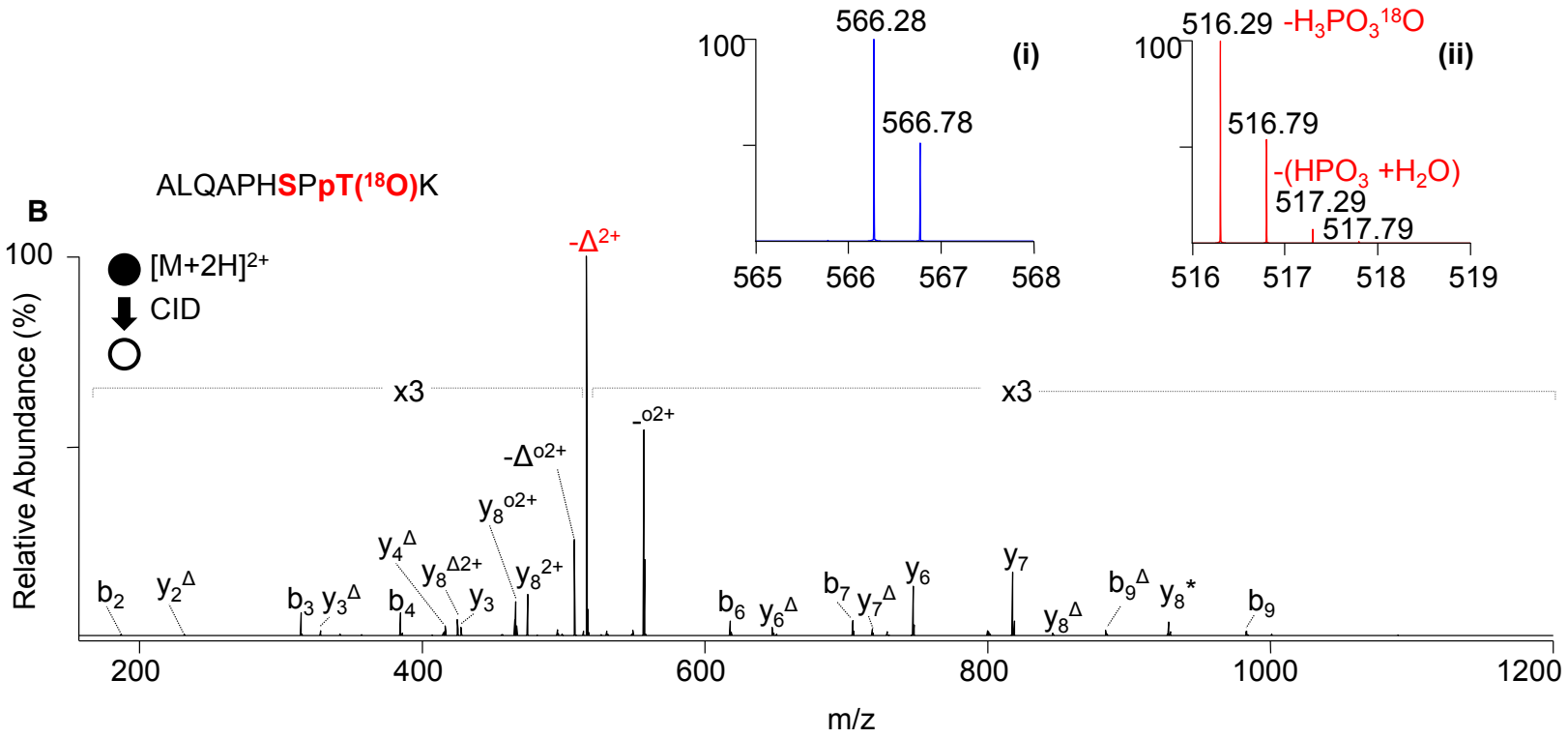

3.2.2 Examination of Factors that Influence the Competing Side Chain Fragmentation Pathways

In order to systematically evaluate the influence of proton mobility, and to determine the effect of the phosphoamino acid identity (*i.e.*, pS or pT) on the competition between the direct and combined side chain neutral loss fragmentation pathways, a series of ^{18}O labeled pS and ^{18}O pT peptides were synthesized, then their doubly and singly protonated precursor ions analyzed by CID-MS/MS. Quantification of the competing fragmentation pathways for the singly and doubly protonated precursor ions are shown in Figure 3.2. The red bars and green bars in Figure 3.2 show the percentage of the combined losses, while the gray bars indicate the percentage of the direct loss pathway. The proton mobility of each peptide precursor ion is noted on the right hand side of the bars, where N, P and M represent non-mobile, partially mobile and mobile proton precursor ions, respectively.

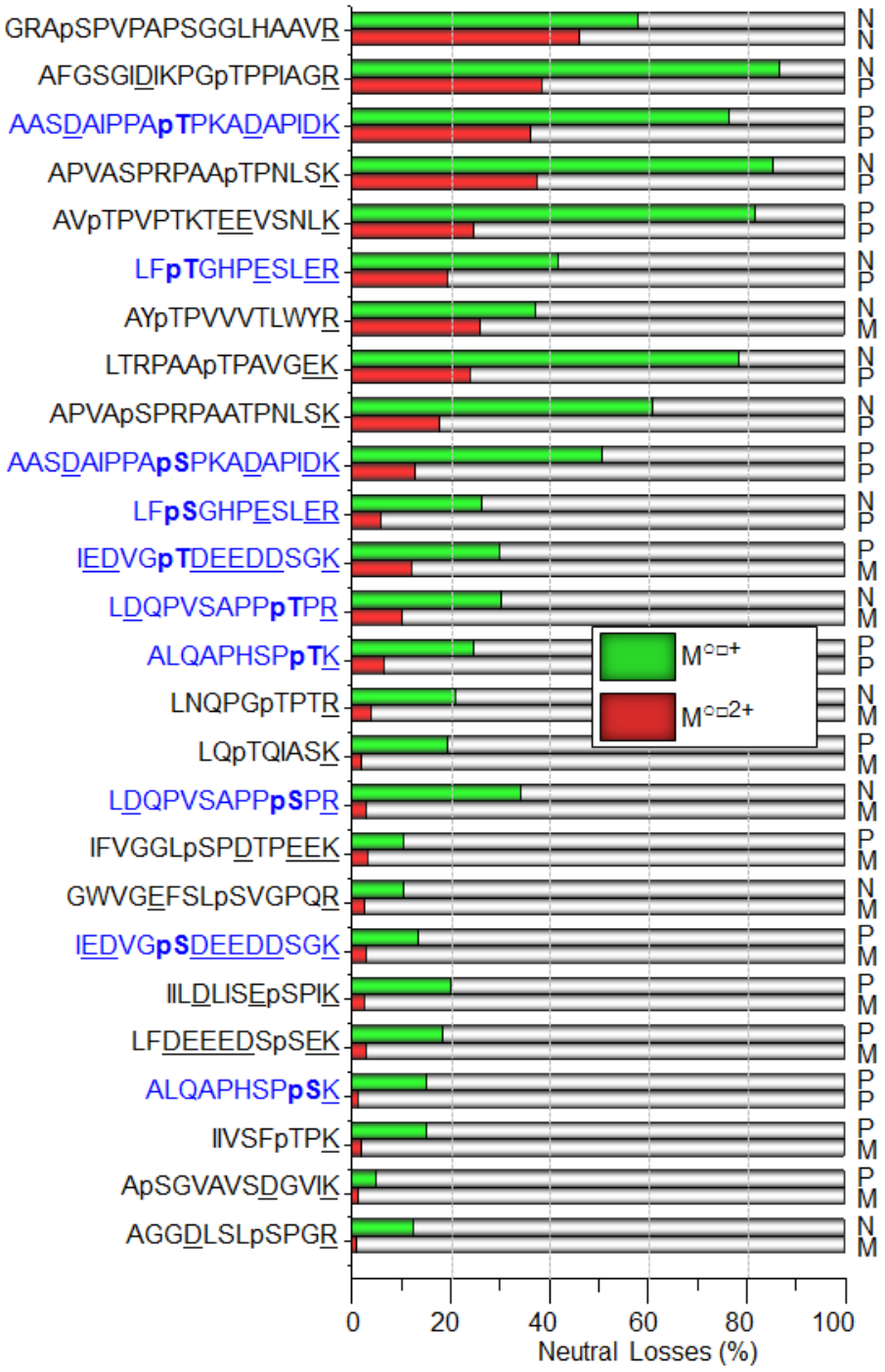

Figure 3.2 Quantification of competing neutral loss pathways from CID-MS/MS of singly and doubly protonated ^{18}O labeled pS and pT phosphopeptide ions. Green and red bars indicate the % of the combined losses, while gray bars indicate the % of direct losses. Peptide pairs labeled in blue have same basic sequences but differ in the identity of the phosphorylated residue (*i.e.*, pS and pT). □ = –80 Da ($–HPO_3$); ○ = –18 Da ($–H_2O$). M: Mobile Proton; P: Partially Mobile Proton; N: Non-mobile Proton.

As previously described, there are two factors that influence the proton mobility of a peptide: the number of ionizing protons and the number of basic residues present in the peptide in chapter 2. For the peptides examined here, the peptides in the upper part of Figure 3.2 generally contain more basic residues. Therefore, for the same charge state precursor ions, a clear trend is observed for decreasing combined losses with increasing proton mobility. Similarly, the combined losses pathway was found to be more prevalent for the singly protonated precursor ions, consistent with their decreased proton mobility compared to the doubly protonated precursors with the same peptide sequence. Based on these results, the extent of the two competing neutral loss pathways upon ion trap CID-MS/MS is directly correlated to the proton mobility of the peptide precursor ion *i.e.*, the more non-mobile the peptide precursor ion, the greater the extent of combined losses is observed.

There are five pairs of peptides in Figure 3.2 whose sequences are labeled in blue text, that differ only in the identity of the ^{18}O-labeled phosphorylated residue *i.e.*, pS and pT. Interestingly, the pT containing peptides were each observed to undergo side chain losses via the combined fragmentation pathway to a greater extent than their corresponding pS containing peptides. This finding is consistent with a previous finding that the loss of H_3PO_4 from pT containing peptide is hindered compared to pS[180], presumably due to the presence of the β-methyl group on its side chain making this direct loss fragmentation pathway less favorable compared to the combined loss fragmentation pathway. Furthermore, it has been recently reported that the observation of dehydration within product ions not containing the former phosphorylated residue are

more abundant in the CID-MS^3 spectra of pT containing peptides compared to pS, consistent with the discussion above.

3.2.3 Competing Fragmentation Pathways in HCD-MS/MS

HCD in the multipole collision cell of the LTQ Orbitrap Velos is increasingly being employed in proteomics studies[63, 267]. Due to the shorter ion activation time scale associated with HCD, the phosphate group neutral loss from a given phosphopeptide is typically not as dominant, and thus less problematic for phosphopeptide sequence assignment and phosphorylation site localization. HCD-MS/MS was performed on all 26 synthesized phosphopeptides, where the collision energy of HCD was individually optimized such that the precursor ion abundance was reduced to approximately equivalent to that of the most abundant product ion in order to minimize secondary fragmentation of the products. Figure 3.3 shows the HCD-MS/MS spectra for the same two peptides as described in Figure 3.1. In addition to neutral loss of the phosphoamino acid residue side chain being reduced for these peptides upon performing HCD-MS/MS compared to CID-MS/MS, the percentage of side chain loss occurring via the combined loss fragmentation pathway was also significantly lower under HCD-MS/MS conditions. For example, the combined loss from the GRApSPVPAPSGGLHAAVR peptide decreased from 63.1% to 32.3%, and from 6.5% to 4.6% for the ALQAPHSPpTK peptide. Indeed, a clear trend toward decreased combined losses under HCD-MS/MS conditions was observed for all 26 phosphopeptides analyzed in this study (Figure 3.4). Some of the peptides here did not line up perfectly as CID-MS/MS in terms of the trend of increasing combined losses with decreasing proton mobility. This is probably due to the fact that collision energy of HCD was optimized individually while that of CID used a

universal setting for all peptides. Nevertheless, the combination of lower abundant side chain neutral losses and a decreased extent of combined neutral losses observed as a function of the shorter ion activation time scale of HCD, together with the fact that HCD produces similar sequence ion information as CID, are clearly indicative that HCD should be considered as a more favorable dissociation method for phosphopeptide analysis.

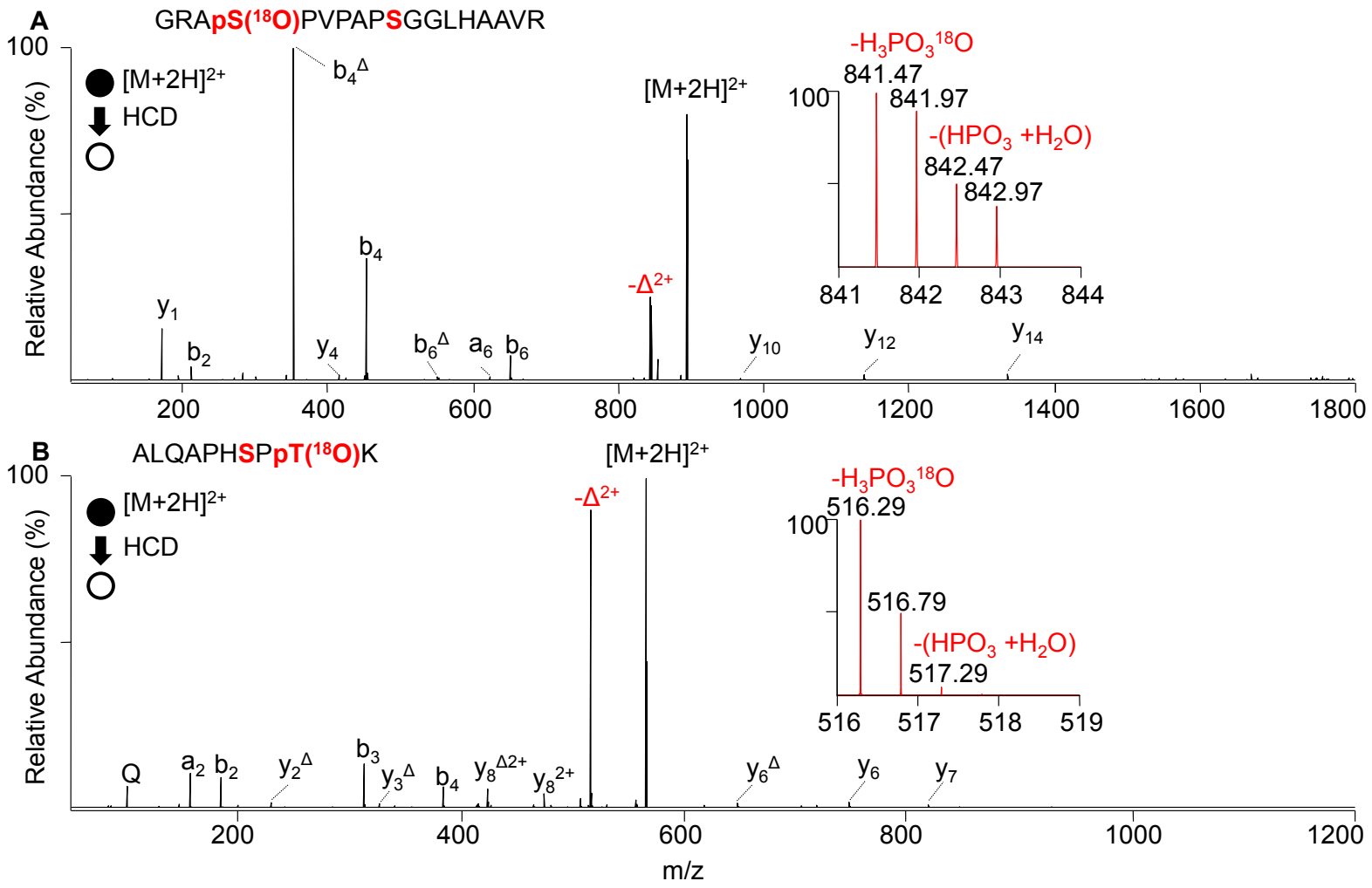

Figure 3.3 HCD-MS/MS product ion spectra for the doubly protonated precursor ions of the phosphopeptides (A) GRApSPVPAPSGGLHAAVR and (B) ALQAPHSPpTK. The red colored inserts show expanded regions of the spectra for the neutral losses of $H_3PO_3{}^{18}O$ and (HPO_3+H_2O). Δ = –100/98 Da (–$H_3PO_3{}^{18}O$ or –(HPO_3+H_2O)).

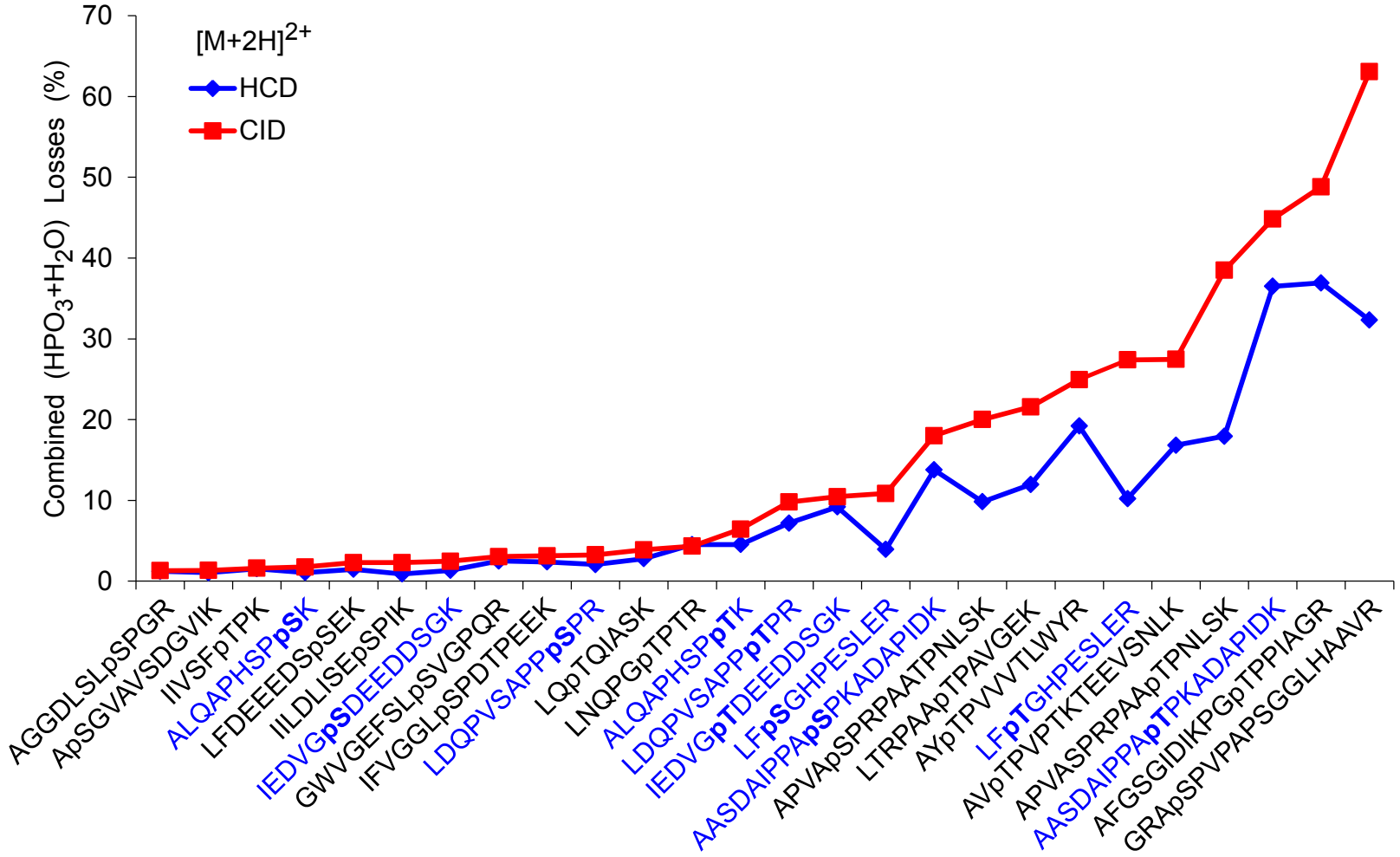

Figure 3.4 Comparison of the % combined neutral losses from CID-MS/MS (red) and HCD-MS/MS (blue) of the doubly protonated ^{18}O labeled pS and pT phosphopeptide ions.

3.2.4 The Source of Water in the Combined Neutral Loss Pathway

Undoubtedly, HPO_3 losses in the combined neutral loss fragmentation pathway described above originate from the phosphorylated amino acid residues. However, there are several potential sources for the observed loss of water. If water loss originates from the side chain hydroxyl groups of Ser or Thr residues, CID-MS^3 of the -98 Da neutral loss ions will produce product ions indicating that the dehydrated site is from the Ser or Thr residues instead of pS or pT within the original phosphopeptide, which subsequently provides incorrect phosphorylation site localization. However, other studies have shown that the water loss could also originate from the carboxylic acid functional groups of the C-terminus or side chains of the peptide, or from the peptide backbone[81]. Indeed, several of these pathways may contribute to the dehydration process simultaneously.

In order to determine the contribution of the carboxylic acid functional groups, the CID-MS/MS fragmentation behavior of each of the phosphopeptides after conversion to their methyl esters was examined. Upon performing this modification, the carboxylic groups are unable to contribute to any water losses. Then, quantification of the two competing neutral loss pathways was again performed for these peptide methyl esters, as shown in Figure 3.5. There were only a few cases in which the percentage of the combined losses from the methyl esterified peptides decreased significantly compared to their original unmodified forms, indicating that the carboxylic acid functional groups were not a major source of the water losses in the combined loss fragmentation pathway. For example, for the doubly protonated precursor ions, only the LFpSGHPESLER, LFpTGHPESLER, AASDAIPPApSPKADAPIDK,

AASDAIPPApTPKADAPIDK, AFGSGIDIKPGpTPPIAGR and GRApSPVPAPSGGLHAAVR peptides exhibited an approx. 5% or greater decrease (4.9%, 8.0%, 4.9%, 8.4%, 10.3% and 16.7%, respectively).

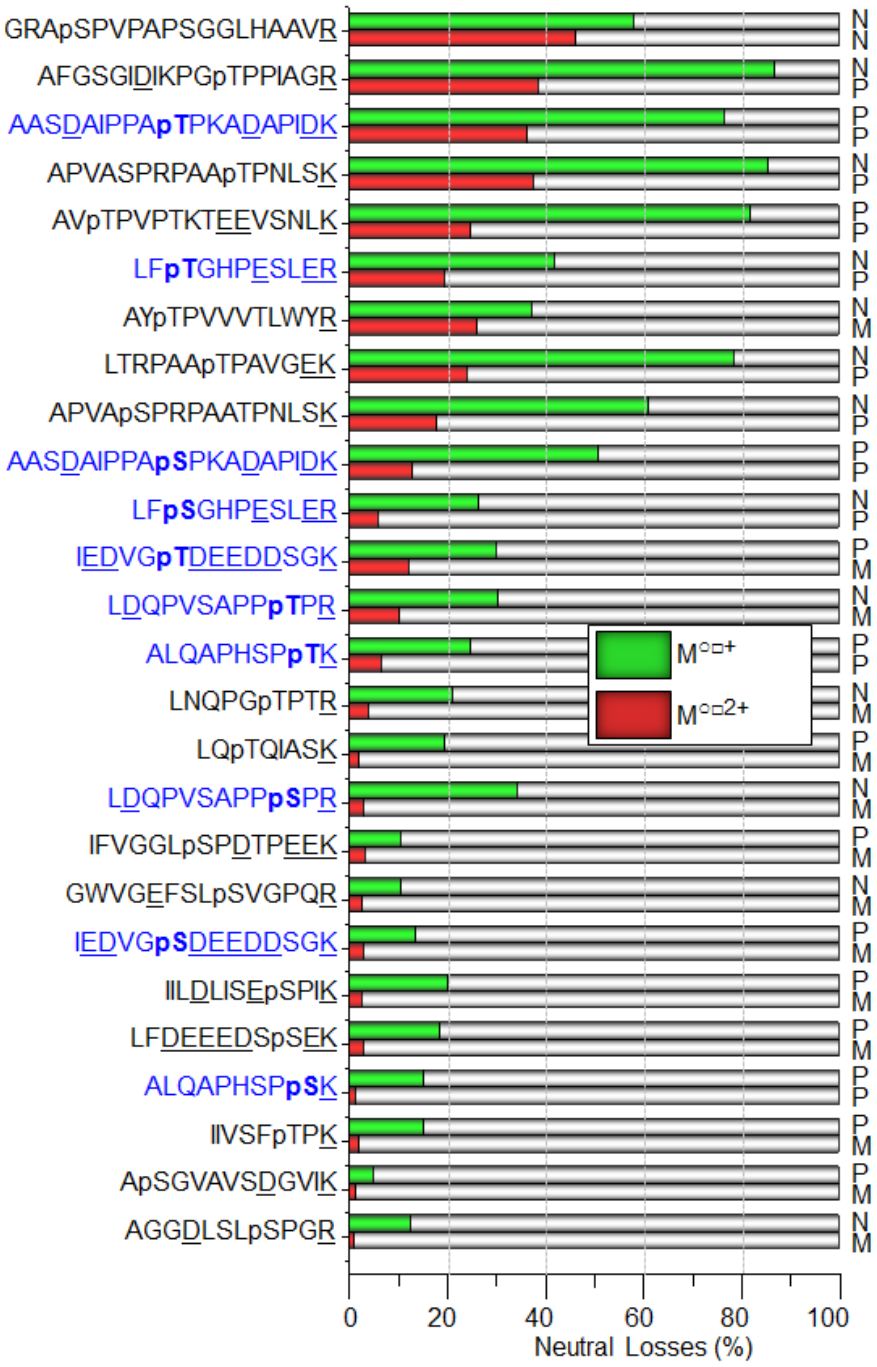

Figure 3.5 Quantification of competing neutral loss pathways from CID-MS/MS of singly and doubly protonated ^{18}O labeled pS and pT phosphopeptide methyl esters. The underlined residues were methyl esterified. Green and red bars indicate the % of the combined losses, while gray bars indicate the % of direct losses. Peptide pairs labeled in blue have same basic sequences but differ in the identity of the phosphorylated residue (*i.e.*, pS and pT). □ = –80 Da ($–HPO_3$); ° = –18 Da ($–H_2O$). M: Mobile Proton; P: Partially Mobile Proton; N: Non-mobile Proton.

It was next investigated the extent to which the water loss in the combined neutral loss pathway originated from the peptide backbone. To this end, an ^{18}O labeled peptide AAADAIPPApTPKADAPIDK lacking side chain hydroxyl groups was synthesized. The observed water loss upon CID-MS/MS of this peptide can only originate from the peptide carboxylic acid groups or the peptide amide backbone. As shown in Figure 3.6, the amount of combined neutral losses decreased to 36.6% compared to 44.9% (refer to Figure 3.2) in the Ser-containing AASDAIPPApTPKADAPIDK peptide. Given that substitution of Ser with Ala in AASDAIPPApTPKADAPIDK did not change its fragmentation pattern in CID-MS/MS, as shown in the CID-MS/MS spectra of AASDAIPPApTPKADAPIDK and AAADAIPPApTPKADAPIDK in Figure 3.5, this result indicated that only approx. 18.5% of the combined neutral loss pathway involved the Ser side chain for the AASDAIPPApTPKADAPIDK peptide. Upon methyl esterification and CID-MS/MS of the AAADAIPPApTPKADAPIDK peptide, the combined neutral losses decreased further from 36.6% to 26.3% (Figure 3.7), indicating that the water loss in the combined loss fragmentation pathway for the AASDAIPPApTPKADAPIDK peptide originated from a combination of losses from the Ser (approx. 18.5%), the carboxylic acids (approx. 22.9%) and the amide bond of the peptide backbone (approx. 58.6%).

As the peptide amino acid composition is expected to significantly influence the peptide fragmentation pattern, it may be deduced that the extent of dehydration occurring from the various sites will vary from peptide to peptide. However, any of these sites, *i.e.*, the Ser and Thr hydroxyl side chains, carboxylic acid groups, and the backbone amide bonds, competing with the direct loss pathway to generate dehydration

sites can potentially complicate localization of the correct phosphorylation sites via MS^3. For example, if dehydration originates from 5-18^{th} residues of GRApTPVPAPSGGLHAAVR during CID-MS/MS, product ions that contain the 10^{th} Ser in CID-MS^3 of product ion $[M+2H-98Da]^{2+}$ from CID-MS/MS are indicative of phosphorylation occurring at the Ser instead of Thr. Indeed, as precious shown in chapter two, y_8^o, y_{10}^o and y_{12}^o ions were observed more abundant than y_8, y_{10} and y_{12} ions in CID-MS^3 of product ion $[M+2H-98Da]^{2+}$ from CID-MS/MS of GRApTPVPAPSGGLHAAVR. Consequently, phosphorylation was assigned to the Ser residue using the phosphorylation localization algorithm designed for CID-MS^3.

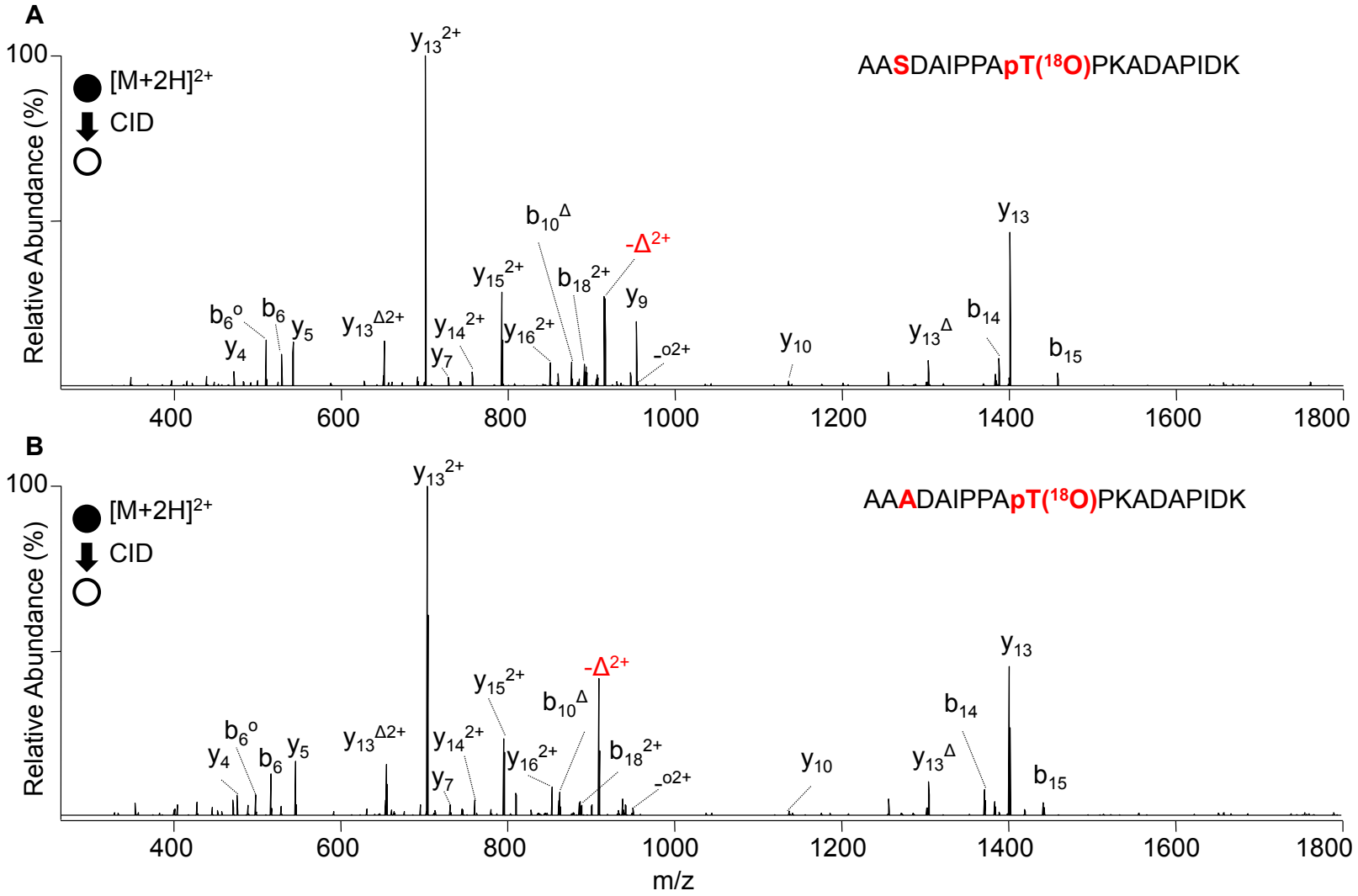

Figure 3.6 CID-MS/MS product ion spectra for the doubly protonated precursor ions of the phosphopeptides (A) AASDAIPPApTPKADAPIDK and (B) AAADAIPPApTPKADAPIDK. Δ = –100/98 Da ($–H_3PO_3{}^{18}O$ or $–(HPO_3+H_2O)$); ° = –18 Da ($–H_2O$).

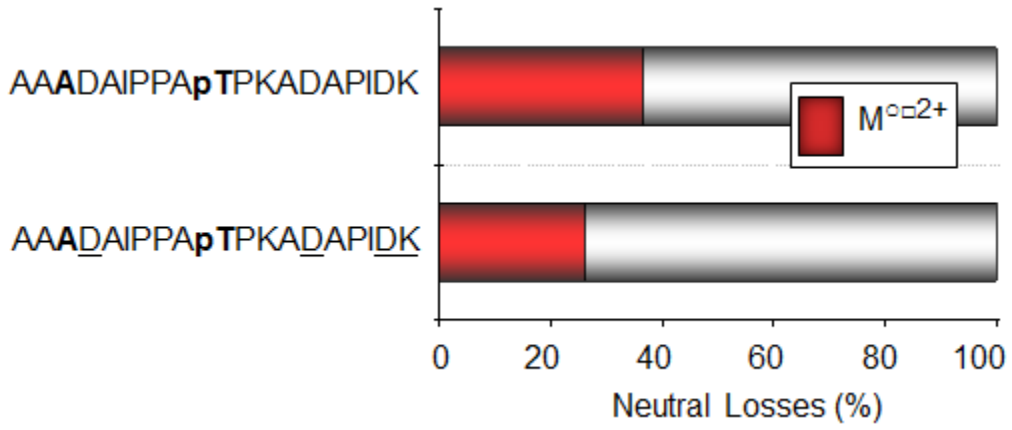

Figure 3.7 Quantification of competing neutral loss pathways from CID-MS/MS of doubly protonated ^{18}O labeled AAADAIPPApTPKADAPIDK and AAADAIPPApTPKADAPIDK methyl ester phosphopeptide ions. The underlined residues were methyl esterified. Red bars indicate the % of the combined losses, while gray bars indicate the % of direct losses. □ = –80 Da ($–HPO_3$); ° = –18 Da ($–H_2O$).

3.3 Conclusions

The competition between the two phosphoamino acid side chain fragmentation pathways for protonated phosphopeptide ions, *i.e.*, $-H_3PO_4$ versus $-(HPO_3+H_2O)$ varies according to the properties of the peptide. Precursor ion proton mobility plays a significant role in this competition, with non-mobile and partially-mobile phosphopeptide ions exhibiting a greater proclivity for combined HPO_3+H_2O losses, *i.e.*, the same category of phosphopeptides that produces dominant -98 Da neutral loss ions upon ion trap CID-MS/MS, which are most likely to be subjected to further dissociation by CID-MS^3. For phosphopeptides that differ only in the identity of the phosphoamino acid, pT containing peptides exhibit more abundant combined neutral losses compared to pS containing peptides. HCD-MS/MS results in less dominant phosphate group neutral losses and a simultaneous decrease in the problematic combined neutral loss fragmentation pathway, highlighting the importance of HCD as a beneficial dissociation technique for phosphopeptide sequencing. Hydroxyl groups, carboxylic acid groups and the amide bonds of the peptide backbone all contribute to the water loss in the combined neutral losses pathway; however, their extent of contribution varies according to the peptide amino acid compositions.

In summary, the data reported in this chapter is strongly suggestive against the use of ion trap CID-MS^3 for phosphorylation site localization, particularly for phosphopeptides under conditions of limited proton mobility, and for pT containing peptides, whereas HCD-MS/MS is preferred.

CHAPTER FOUR

Experimental Methods for Chapters Two and Three

4.1 Materials

All aqueous solutions were prepared using deionized water purified by a Barnstead nanopure diamond purification system (Dubuque, IA). N-α-Fmoc protected amino acid building blocks with acid-labile orthogonal side-chain protection, where appropriate, were purchased from EMD Biosciences (Darmstadt, Germany) and are listed in Table 4.1 Boc-glycine-OH, Boc-alanine-OH, Boc-isoleucine-OH, Boc-leucine-OH, methyl (2S, 3R)-threoninate hydrochloride, 9-fluorenylmethyl N-succinimidyl carbonate, dibenzyl-*N*,*N*-diisopropylphosphoamidite and preloaded Wang-resins were also purchased from EMD Bioscience. Reagent grade O-(Benzotriazol-1-yl)-N,N,N',N'-tetramethyluronium tetrafluoroborate (TBTU) and N-Hydroxybenzotriazole (HOBt) were from Peptides International (Louisville, KY). 2,5-DHB (HPLC grade), piperidine (biotech grade), N,N-diisopropylethylamine (DIPEA, biotech grade), triisopropylsilane (TIS, 99%) and reagent grade triphenylmethyl chloride, butyldimethylsilyl chloride, imidazole and triethylamine were purchased from Sigma Aldrich (St. Louis, MO). Methyl aziridine-2-carboxylate (97%) was from TCI America (Portland, OR). $H_2{}^{18}O$ (98%) was obtained from Medical Isotopes (Pelham, NH). AG® 1-X8 anion exchange resin (hydroxyl form, 1.3 mmol/mL) was from Bio-rad (Hercules, CA). Dichloromethane (DCM, 99.5%), acetic acid (99.7%) and acetic anhydride (97%) were from Mallinckrodt Chemicals (Phillipsburg, NJ). Dimethylformamide (DMF, 99.8%) (further dried with 4Å molecular sieves) and Silica Gel 60 Å (230-400 mesh) were purchased from Jade Scientific (Canton, MI). Trifluoroacetic acid (TFA, LC grade) was from Thermo Scientific (San

Jose, CA). Methanol (99.8%) and ethyl acetate(99.5%) were from VWR BDH chemicals (West Chester, PA). Acetonitrile (ACN, HPLC grade) and diethyl ether (99.9%) were purchased from EMD Chemicals (Gibbstown, NJ). All other reagents were commercially available and used without further purification.

Table 4.1 Common amino acid building blocks used for solid-phase peptide synthesis.

Amino Acid	Abbreviation		Solid Phase Peptide Synthesis Building Block
	3 Letter	1 Letter	
Alanine	Ala	A	Fmoc-Ala-OH
Arginine	Arg	R	Fmoc-Arg(Pbf)-OH
Asparagine	Asn	N	Fmoc-Asn(Trt)-OH
Aspartic Acid	Asp	D	Fmoc-Asp(OtBu)-OH
Cysteine	Cys	C	Fmoc-Cys(Trt)-OH
Glutamic Acid	Glu	E	Fmoc-Glu(OtBu)-OH
Glutamine	Gln	Q	Fmoc-Gln(Trt)-OH
Glycine	Gly	G	Fmoc-Gly-OH
Histidine	His	H	Fmoc-His(Trt)-OH
Isoleucine	Ile	I	Fmoc-Ile-OH
Leucine	Leu	L	Fmoc-Leu-OH
Lysine	Lys	K	Fmoc-Lys(Boc)-OH
Methionine	Met	M	Fmoc-Met-OH
Phenylalanine	Phe	F	Fmoc-Phe-OH
Phosphoserine	pSer	pS	Fmoc-Ser(PO(OBzl)OH)-OH
Phosphothreonine	pThr	pT	Fmoc-Thr(PO(OBzl)OH)-OH
Phosphotyrosine	pTyr	pY	Fmoc- Ser(PO(OBzl)OH)-OH
Proline	Pro	P	Fmoc-Pro-OH
Serine	Ser	S	Fmoc-Ser(tBu)-OH
Threonine	Thr	T	Fmoc-Thr(tBu)-OH
Tryptophan	Trp	W	Fmoc-Trp(Boc)-OH
Tyrosine	Tyr	Y	Fmoc-Tyr(tBu)-OH
Valine	Val	V	Fmoc-Val-OH

4.2 Phosphopeptides

All phosphopeptides were prepared by Fmoc-based solid-phase peptide synthesis using an automated peptide synthesizer, as described in detail below. Detailed experimental methods for synthesis of regioselectively ^{18}O labeled pS and pT peptides are also shown as follows.

4.2.1 Fmoc Solid-Phase Peptide Synthesis (SPPS)

4.2.1.1 Apparatuses

All peptides were synthesized using an Intavis model ResPep SL automated peptide synthesizer (Koeln, Germany). 1 μmol scale synthesis was prepared in a 96 well plate with glass fibre filters in each well.

4.2.1.2 Synthesis

Generally, peptide synthesis was completed at a 1 μmol scale. The N-α-Fmoc protected C-terminal residue was bound to the Wang-resin and swelled in DMF (200 μL) for 15 min with continuous mixing then washed with 4 x 600 μL DMF. C-terminal elongation of the peptide was completed via repetitive Fmoc deprotection and amino acid coupling until the target peptide sequence was achieved. Following the synthesis, cleavage of peptides from the resin and acid-labile orthogonal protecting groups was performed. All the solutions used by the peptide synthesizer were pre-made before synthesis and kept at room temperature during the synthesis.

4.2.1.2.1 Fmoc Deprotection

Deprotection of the resin-bound peptide *N*-terminal Fmoc group to form a free amine *N*-terminus was achieved by incubating in 25 μL 25% piperidine in DMF for 5 min and then repeated for another 10 min for the first 6 residues from the C-terminus of the

peptides. The incubation times were increased to 15 min and 15 min starting from the 7th residue. The peptidyl resin was then washed with 2 x 400 µL and 6 x 260 µL DMF.

4.2.1.2.2 Amino Acid Coupling

N-α-Fmoc amino acid derivatives were pre-dissolved in dry DMF to a concentration of 0.6 M. 8.5 µL (51 µmol) of the derivative solutions were pre-activated by mixing with DIPEA (2.5 µL) and a DMF solution consisting of 0.5 M TBTU, 0.5 M HOBt (8 µL). Coupling of the pre-activated building blocks to the peptidyl resin was completed by incubation for 20 min. The process was repeated to increase the coupling efficiency. The length of the coupling time was dependent on the position of the amino acid. Couplings for the 1-6th, 7-12th and >12th residues were performed 20, 30 and 40 min respectively.

Directly following the coupling, unreacted free amines were capped by incubating in 5% acetic anhydride in DMF (25 µL) for 5 min. The peptidyl resin was then washed with 2 x 400 µL and 5 x 260 µL DMF.

4.2.1.2.3 Resin Cleavage and Deprotection of Acid-Labile Orthogonal Protecting Groups

Upon completion of the target peptide sequence, a final triple Fmoc deprotection was performed. The peptidyl resin was dried by washing with 3 x 600 µL ethanol and 3 x 80 µL DCM. Then the peptide was cleaved from the resin along with any acid-labile orthogonal side chain protecting groups by continuous mixing with a cleavage solution (1 mL) for 3 hr. The composition of the cleavage solution was dependent upon the composition of the peptidyl resin. Normally, 95% TFA / 2.5% H_2O / 2.5% TIS solution was used unless the peptide contained Cys(Trt) or Met residues, where 94.5% TFA /

2.5% H_2O / 2.5% EDT / 1% TIS solution was prepared for the cleavage. The cleavage solution was added to each well and the whole plate was sealed in a device that was made specifically for the cleavage. After 3 hr incubation with continuous mixing, the cleavage solutions were dried down under nitrogen flow, which was followed by adding cold diethyl ether (0.5 mL) and 25% acetic acid (aq) solution (0.5 mL). The aqueous phase was separated from the organic layer and then lyophilized. Lyophilized crude peptides were used without further purification.

4.2.2 Synthesis of Regioselective ^{18}O-Labeled Phospho-serine and threonine Peptides

Regioselective ^{18}O-labeled amino acid derivatives were prepared by solution phase synthesis. The overall synthesis procedure is shown in Scheme 4.1 and experimental details are described in the following sections. In general, methyl-aziridine-2-carboxylate was converted to ^{18}O labeled Ser under strong acidic condition by reaction with 15% perchloric acid in $H_2{}^{18}O$[268]. The α-amino group of the synthesized Serine(^{18}O) was then subjected to Fmoc protection using 9-fluorenylmethyl N-succinimidyl carbonate. The hydroxyl group of the resultant Fmoc-Serine(^{18}O) was then selectively protected with tert-butyldimethylsilyl chloride to generate Fmoc-Serine(^{18}O-TBDMS)[180, 269].

Methyl (2*S*, 3*R*)-threoninate hydrochloride was first protected by triphenylmethyl chloride at the α-amino group. The resulting product, methyl (2*S*, 3*R*)-N-triphenylmethylthreoninate was converted to methyl (2*S*, 3*S*)-N-triphenylmethyl-3-methylaziridine-2-carboxylate by adding triethylamine and methanesulfonyl chloride. After cleaving the triphenylmethyl protection group by trifluoroacetic acid, methyl (2*S*,

3*S*)-3-methylaziridine-2-carboxylate trifluoroacetate was obtained. Fmoc-Threonine(^{18}O-TBDMS) was then prepared using the same procedures as those described above for Fmoc-Serine(^{18}O-TBDMS)[270, 271].

The tert-butyldimethylsilyl protected amino acids Fmoc-Serine(^{18}O-TBDMS) and Fmoc-L-Threonine(^{18}O-TBDMS) were then introduced into peptide sequences using standard Fmoc peptide synthesis protocols, followed by on-resin deprotection of the Ser side chain and functionalization of the resin bound hydroxyl group using dibenzyl-N,N-diisopropylphosphoramidite[180]. Finally, oxidation, peptide cleavage, and extraction from the resin afforded the product phosphopeptides. Detailed experimental methods for this procedure are below.

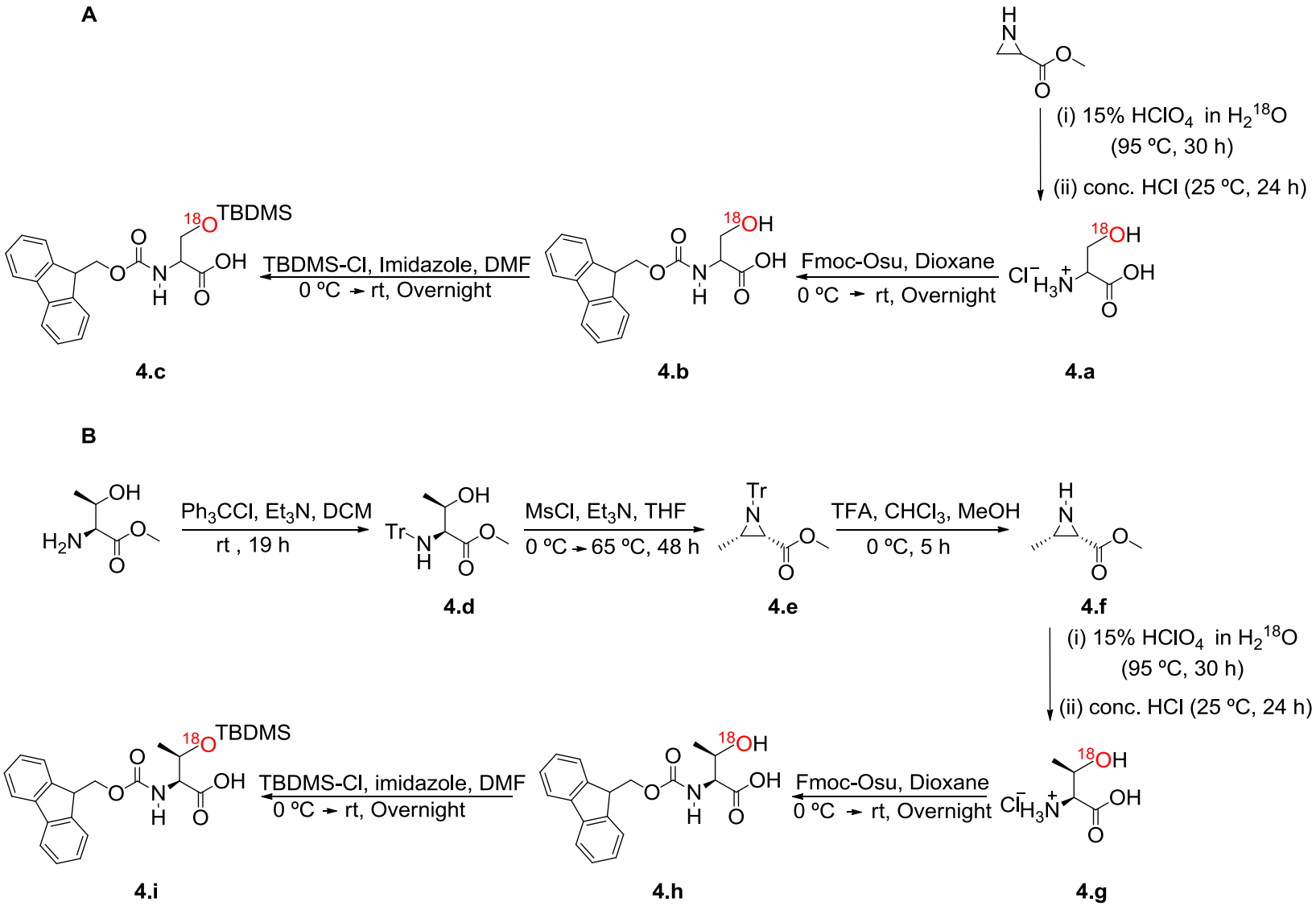

Scheme 4.1 Synthesis process for Fmoc-Serine(^{18}O-TBDMS) (A) and Fmoc-L-Threonine(^{18}O-TBDMS) (B).

4.2.2.1 Synthesis of Serine(^{18}O) (4.a)

4.a was prepared using a method adapted from a previous report in the literature[268]. Methyl aziridine-2-carboxylate (224 mg, 2.21 mmol) was dissolved in 15% (w/w) perchloric acid (2 mL) prepared by adding 70% (w/w) perchloric acid (286 µL) to $H_2{}^{18}O$ (1714 µL). After the reaction mixture was stirred in a sealed tube at 95 ºC for 30 h, it was neutralized with NH_4OH. The resulting mixture was diluted with water (40 mL) and combined with anion exchange resin for purification. The mixture with resin was stirred for 1 h. The aqueous phase was decanted and the resin was washed with water. Finally, 5% aqueous acetic acid was added to elute the product. The eluant was dried down under nitrogen flow and the product was obtained as a white solid, which was then dissolved in concentrated HCl (5 mL) and kept at room temperature overnight to achieve 99% back exchange from ^{18}O to ^{16}O of the carboxylic group. The resulting mixture was dried down under nitrogen flow. The product, Ser(^{18}O) hydrochloride (**4.a**) (Scheme 4.1 A) was obtained as a crude white solid (317.0 mg, quantitative yield) and was used without further purification. High resolution ESI-MS confirmed the protonated product at m/z=108.0541 (calc. 108.0542) and with 91% ^{18}O incorporation. Ion trap CID-MS/MS resulted in major product ions at m/z=62.0489 (-(H_2O+CO)) and 88.0394 (-$H_2{}^{18}O$). The lack of observable ions at m/z=60.0446 (*i.e.*, -$H_2{}^{18}O$ +CO) indicated that the ^{18}O labeling was on the hydroxyl group[80].

4.2.2.2 Synthesis of Fmoc-Serine(^{18}O) (4.b)

4.a was dissolved in 10% Na_2CO_3 (aq) (10 mL) and 1,4-dioxane (5 mL) and treated dropwise with the 9-fluorenylmethyl N-succinimidyl carbonate (733.3 mg, 2.17 mmol) in 1,4-dioxane (10 mL) at 0 ºC. After 1 h at 0 ºC, the mixture was warmed to

room temperature and then stirred overnight. The resulting mixture was diluted with cold water (20 mL) and extracted with ether (2×20 mL). The aqueous layer was acidified with 5% HCl (aq) solution followed by extraction with ethyl acetate (2 × 30 mL). The combined organic phases were dried with $MgSO_4$, filtered, and concentrated *in vacuo* to yield an off-white solid Fmoc-Serine(^{18}O) (**4.b**) (546.1 mg, 1.66 mmol, 75.0% yield); $[\alpha]_D^{20}$ 0.0º (*c* 1.0, DMF)#; ^{1}H NMR (500 MHz, $(CD_3)_2CO$): δ 3.90 (1H, β- *CH*H, *dd*, *J* =11.0, 4.0 Hz), 3.98 (1H, β- *CH*H, *dd*, *J* =11, 4.5 Hz), 4.40 -4.24 (4 H, Fmoc-$CHCH_2O$, α-CH, *m*,), 6.54 (1H, NH, *d*, *J* = 8.5 Hz), 7.33 (2H, *ddd*, *J* = 8.5, 7.5, 1 Hz), 7.41 (2H, *t*, *J* = 7.5 Hz), 7.74 (2H, *dd*, *J* = 7.5, 3.5 Hz), 7.86 (2H, *d*, *J* = 7.5 Hz); ^{13}C NMR* (125 MHz, $(CD_3)_2CO$): 172.36, 157.15, 145.16, 145.09, 142.16, 128.6, 128.03, 126.25, 120.86, 67.46, 63.11, 57.31, 48.05[180, 269].

4.2.2.3 Synthesis of Fmoc-Serine(^{18}O-TBDMS) (4.c)

A solution of **4.b** (546.1 mg, 1.66 mmol) in dry DMF (6 mL) was treated with *tert*-butyldimethylsilyl chloride (440.8 mg, 2.93 mmol) and imidazole (459.7 mg, 6.75 mmol) at 0 ºC while stirring under nitrogen atmosphere. The reaction mixture was kept at 0 ºC for 1 h, and then stirred at room temperature overnight. The solution was diluted with 1 N HCl (aq.) (13 mL) and extracted with ether (2×20 mL). The combined organic layers were concentrated *in vacuo* and the resulting residue was partitioned between 10% LiBr (aq.) solution (13 mL) and diethyl ether (2×20 mL). The combined organics were dried with $MgSO_4$, filtered, and concentrated *in vacuo*. The crude was purified by silica gel column. An initial mobile phase composition of 5% ethyl acetate, 95% hexanes was used to elute impurities followed by elution of the product with 80% ethyl acetate, 20% hexanes. The *tert*-butyldimethylsilyl protected product Fmoc-Serine(^{18}O-TBDMS) (**4.c**)

(432.9 mg, 0.98mmol, 59.0%) was recovered as a yellow oil. ^{1}H NMR (500 MHz, $(CD_3)_2CO$): δ 0.082 (3H, *s*), 0.089 (3H, *s*), 0.898 (9H, s), 3.98 (1H, β- *CH*H, *dd*, *J* =10.0, 3.5 Hz), 4.10 (1H, β- *CH*H, *dd*, *J* =10.5, 4.0 Hz), 4.26 (2H, Fmoc-CH, *t*, *J* = 7.0 Hz), 4.40 -4.31 (3 H, Fmoc-CH_2O, α-CH, *m*,), 6.43 (1H, NH, *d*, *J* = 9.0 Hz), 7.33 (2H, *t*, *J* = 7.5 Hz), 7.41 (2H, *t*, *J* = 7.5 Hz), 7.72 (2H, *dd*, *J* = 6.5, 3.5 Hz), 7.86 (2H, *d*, *J* = 7.5 Hz); ^{13}C NMR* (125 MHz, $(CD_3)_2CO$): 172.01, 156.89, 145.19, 145.07, 142.19, 128.62, 128.03, 126.25, 126.22, 120.89, 67.48, 64.36, 57.04, 48.06, 26.27, 18.94, -5.20, -5.27[180].

4.2.2.4 Synthesis of Methyl (*2S*, *3R*)-N-triphenylmethylthreoninate (4.d)

Methyl (*2S*, *3R*)-threoninate hydrochloride (2.0 g, 11.8 mmol) was suspended in dichloromethane (35 mL). Under nitrogen atmosphere, triethylamine (3.3 mL, 23.5 mmol) was added dropwise, leading to a milky solution. The resulting solution was cooled to 0 ºC and triphenylmethyl chloride (3.28 g, 11.8 mmol) powder was added portion wise over 5 min. The mixture was then stirred at room temperature for 21 h. The reaction mixture was washed with 10% citric acid (2×10 mL) and then water (2×10 mL). The organic phase was dried over Na_2SO_4, filtered, and concentrated *in vacuo* to yield a yellow oil, methyl (*2S*, *3R*)-N-triphenylmethylthreoninate (**4.d**) (Scheme 4.1B). The crude product was used without further purification.

4.2.2.5 Synthesis of Methyl (*2S*, *3R*)-N-triphenylmethylthreoninate (4.e)

Compound **4.d** was dissolved in tetrahydrofuran (30 mL) and the solution was cooled to 0 ºC. Triethylamine (3.5 mL, 24.8 mmol) was added dropwise over 5 min, which was then followed by the addition of methanesulfone chloride (0.9 mL, 11.5 mmol) over 2 min under nitrogen. The reaction mixture was stirred at 0 ºC for 30 min

and then refluxed for 48 h. The solvent was then removed *in vacuo* to leave a residue which was dissolved in ethyl acetate (25 mL) and washed with 10% aqueous citric acid solution (3×5 mL) followed by saturated aqueous sodium bicarbonate solution (2×5 mL) with back washing. The combined organic phases were dried over Na_2SO_4, filtered, and concentrated *in vacuo*, resulting in a white solid, Methyl (*2S*, *3S*)-N-triphenylmethyl-3-methylaziridine-2-carboxylate (**4.e**) (3.46 g, 9.7 mmol, 82%). ^{1}H NMR (500 MHz, (CD_3Cl): δ 1.35 (3H, *d, J* = 5.5 Hz), 1.61 (1H, *quintet, J* = 5.5 Hz), 1.86 (1H, *d, J* = 6.0 Hz), 3.17 (1H, *d*, *J* = 8.0 Hz), 3.73 (3H, *s*), 7.22-7.18 (3H, *m*), 7.26 (6H, *t, J* = 7.0 Hz), 7.50 (6H, *d, J* = 8.0 Hz); ^{13}C NMR (125 MHz, (CD_3Cl): δ 170.69, 143.91, 129.4, 127.59, 126.83, 75.01, 51.77, 35.96, 34.70, 13.32 [270].

4.2.2.6 Synthesis of Methyl (2*S*, 3*S*)-3-methylaziridine-2-carboxylate trifluoroacetate (4.f)

To a solution of **4.e** (3.46 g, 9.7 mmol) in chloroform and methanol (1:1/v:v, 20 mL) was added trifluoroacetic acid (10 mL) under 0 ºC. The mixture was stirred at this temperature for 3 h. The reaction mixture was concentrated under nitrogen flow and then dried under vacuum. The residue was evaporated with diethyl ether to remove the trifluoroacetic acid residue and then partitioned in diethyl ether (40 mL) and water (30 mL). The ether layer was extracted with water (3×10 mL). The aqueous phases were combined and dried down under nitrogen flow over night. The resulting crude yellow oil, Methyl (2*S*, 3*S*)-3-methylaziridine-2-carboxylate trifluoroacetate (**4.f**), was obtained (2.69 g, quantitative yield) and was used without further purification. ^{1}H NMR (500 MHz, (CD_3Cl): 1.49 (3H, *d*, *J* = 6.0 Hz), 3.27 (1H, *qd*, *J* =7.8, 6.0 Hz), 3.70 (1H, *d*, *J* = 7.8 Hz

), 3.86 (3H, *s*), 8.62 (1H, broad *s*); ^{13}C NMR (125 MHz, (CD_3Cl): 169.99, 161.78, 161.47, 116.93, 114.63, 53.77, 37.14, 36.19, 9.80 .

4.2.2.7 Synthesis of L-Threonine(^{18}O) (4.g)

4.g was prepared by following the same protocol that was applied for the synthesis of **4.a**. **4.g** was obtained as a white solid in 91.4% yield from **4.f**. High resolution ESI-MS confirmed the protonated product at m/z=122.0697 (calc. 122.0698) and with 74% ^{18}O incorporation. Ion trap CID-MS/MS of the ion at m/z=122.0697 showed major fragments at m/z=76.0645(-(H_2O+CO)) and 102.0550 (-$H_2{}^{18}O$). Lack of observable ions at m/z=74.0603 (*i.e.*, -$H_2{}^{18}O$+CO) indicated that the ^{18}O labeling was on the hydroxyl group.

4.2.2.8 Synthesis of Fmoc-L-Threonine(^{18}O) (4.h)

4.h was prepared following the same protocol that was applied for the synthesis of **4.b**. **4.h** was obtained as a white solid in 85.9% yield from **4.g**. $[\alpha]_D^{20}$ -13.0º (*c* 1.0, DMF)*#; ^{1}H NMR (500 MHz, $(CD_3)_2CO$): δ 1.25 (3H, *d*, *J* = 6.5 Hz) , 4.40-4.20 (5 H, Fmoc-$CHCH_2O$, α-CH, β- *C*H *m*,), 6.29 (1H, NH, *d*, *J* = 7.5 Hz), 7.33 (2H, *t*, *J* = 8.0 Hz), 7.41 (2H, *t*, *J* = 7.5 Hz), 7.75 (2H, *t*, *J* = 6.5 Hz), 7.86 (2H, *d*, *J* = 7.0 Hz); ^{13}C NMR (125 MHz, $(CD_3)_2CO$): 172.52, 157.59, 145.24, 145.09, 142.21, 128.63, 128.06, 126.04, 126.29, 120.89, 68.07, 67.50, 60.47, 48.13, 20.72.

4.2.2.9 Synthesis of Fmoc-L-Threonine(^{18}O-TBDMS) (4.i)

4.i was prepared following the same protocol that was applied for the synthesis of **4.c**. **4.i** was obtained as a white solid in 61.2% yield from **4.h**. ^{1}H NMR (500 MHz, $(CD_3)_2CO$): δ 0.081 (3H, *s*), 0.12 (3H, *s*), 0.9 (9H, s), 1.25 (3H, *d*, *J* = 6.5 Hz), 4.4-4.2 (4 H, *m*), 4.54 (1H, *m*), 6.15 (1H, NH, *d*, *J* = 9.5 Hz), 7.32 (2H, *t*, *J* = 7.5 Hz), 7.41 (2H, *t*, *J*

= 7.5 Hz), 7.72 (2H, *t*, *J* = 8.0 Hz), 7.86 (2H, *d*, *J* = 7.5 Hz). ^{13}C NMR (125 MHz, $(CD_3)_2CO$): 172.26, 157.51, 145.23, 145.04, 142.21, 128.64, 128.04, 126.01, 126.24, 120.91, 69.88, 67.50, 60.69, 48.12, 26.23, 21.27, 18.74, 18.63, -4.14, -4.89.

*: Data collected for this compound was obtained on its non-isotope labeled form which was prepared using the same conditions as for the isotope labeled compound.

#: Optical rotation confirmed that Fmoc-Serine(^{18}O) consisted of D,L enantiomers while Fmoc-Threonine(^{18}O) mainly consisted of L isomer. The influence of amino acid chirality on CID-MS/MS peptide fragmentation was evaluated on an example peptide (*i.e.* GRApSPVPAPSGGLHAAVR). The result showed that there were no significant differences between the normalized intensities of all the ions observed in CID-MS^3 of the -98 Da neutral loss ions from CID-MS/MS of L-phosphoserine containing and D,L-phosphothreonine containing GRApSPVPAPSGGLHAAVR. (Average standard deviation from mean = 1.6%, data not shown). Therefore, fragmentation of the pS(^{18}O) and pT(^{18}O) containing peptides can be fairly compared.

4.2.3 On-resin SPPS of Regioselective ^{18}O-Labeled Phospho-serine and -threonine Peptides

The side chain protected phospho-serine and -threonine peptides were synthesized as described above in section 4.2.1 using **4.c** for Ser and **4.i** for Thr incorporation and Boc-Gly/Iso/Leu/Ala-OH as the *N*-terminal amino acids. The peptidyl resin (1 μmol) was dried by washing with 3 x 600 μL ethanol and 3 x 80 μL DCM. Selective deprotection of the serine silyl protecting group was completed by incubation of the dried peptidyl resin with a solution of tetrabutylammonium fluoride trihydrate ($TBAF{\cdot}3H_2O$, 1.05 mg, 3.3 μmol) in dimethylacetamide (DMA) (80 μL) for 4 h. The

above procedure was repeated for another incubation of 14 h. The peptidyl resin was then washed with DMA (3 x 200 µL) and DCM (3 x 200 µL) and dried overnight *in vacuo*. A 0.45 M tetrazole solution in acetonitrile (190 µL, 85.7 µmol) was mixed with dry DMF (110 µL) and dibenzyl-N,N-diisopropylphosphoramidite (21.5 mg, 62.9 µmol). The solution was then added to the peptidyl resin and incubated for 2 hr at room temperature under a N_2 (g) atmosphere. The above reaction was repeated for another 2 hr incubation. The resin was washed with DMF (2 x 200 µL) followed by oxidation with 6 M *t*-butyl hydroperoxide (50 µL, 0.28 mmol) for 0.5 hr twice, resulting in desired phosphopeptides. The resin was then washed with DMF, ethanol and DCM. Cleavage and extraction of the peptides followed the description in section 4.2.1.2.3 affording the finial phosphopeptides.

4.3 Multistage Tandem Mass Spectrometry Analysis of Phosphopeptides

4.3.1 Phosphopeptide Sample Preparation

All peptide samples were prepared in 50% methanol, 49% water, 1% acetic acid (v/v/v) for subsequent mass spectrometry analyses and stored at -20 °C. For matrix-assisted laser desorption/ionization (MALDI) analysis, 10 pmol (0.5 µL of 20 µM solution) peptide was mixed with 0.5 µL of a 2,5-DHB matrix solution (50 mg/mL in 50% acetonitrile, 49% water and 1% formic acid) directly on the MALDI plate.

4.3.2 Mass Spectrometry

Phosphopeptides were analyzed using (i) a Thermo Scientific LTQ Orbitrap Velos Mass Spectrometer equipped with an Advion BioSciences Triversa Nanomate nESI source (Ithaca, NY), (ii) a Thermo Scientific LTQ Mass Spectrometer interfaced with an Advion BioSciences Triversa Nanomate nESI source (Ithaca, NY), and (iii) a

Thermo Scientific LTQ XL Mass Spectrometer (San Jose, CA) equipped with a MALDI source. External calibration of the instruments was performed using standard Thermo calibration mixtures. For nESI analysis, 10 µL of the sample solution was loaded for infusion by the Nanomate. The spray voltage was maintained at 1.4 kV and gas pressure was 0.3 psi. The temperature for ion transfer tube of LTQ and LTQ Orbitrap Velos was set to 180°C and 250 °C, respectively. The S-lens of the LTQ Orbitrap Velos was set to 57%. For MALDI analysis, a laser energy of 12 µJ was used. The LTQ Orbitrap Velos MS/MS spectra were acquired using a mass analyzer resolution of 60,000.

Positive ionization mode collision induced dissociation (CID)-MS/MS performed on the LTQ and LTQ XL mass spectrometers used standard excitation conditions (q=0.25, activation time=30 ms, normalized collision energy ((NCE)=35%). Positive ionization mode CID-MS/MS experiments performed on the LTQ Orbitrap Velos used standard excitation conditions (q=0.25, activation time=10 ms, NCE=35%). Ion activation conditions for positive ionization mode higher energy collision induced dissociation (HCD)-MS/MS on the LTQ Orbitrap Velos were q=0.25 and activation time=0.1 ms. NCE was optimized individually for each peptide precursor ion.

All MS/MS and MS^3 experiments performed by CID were on selected precursor ions. Isolation widths for the singly, doubly and triply protonated precursor ions were 3.0, 2.5 and 2.0 respectively. Depending on precursor ion abundances, all spectra shown were typically averaged over 200 scans.

4.4 Quantitative Analysis

4.4.1 Quantitative Analysis of Product Ion Abundances in Phosphate Group Rearrangement Reactions (Chapter Two)

All scans from each MS/MS or MS^3 acquisition were averaged prior to analysis to reduce scan-to-scan variance in ion abundances when determining the % rearrangements observed for each peptide ion, as well as to improve signal-to-noise and minimize the influence of poor spectral quality on the variability of the scores obtained following phosphorylation site assignment using the Ascore and PhosphoScore algorithms. Two types of rearranged product ions can be formed when rearrangement occurs via transfer of a phosphate group from a 'donor' (*i.e.*, phosphorylated) amino acid residue to an 'acceptor' amino acid residue; (i) a product ion containing the 'acceptor' amino acid residue with m/z +80 Da higher (*i.e.*, $+HPO_3$) than that of the 'non-rearranged' product ion, and (ii) a product ion containing the 'donor' phosphoamino acid residue, with m/z 80 Da lower (*i.e.*, $-HPO_3$) than that of the 'non-rearranged' product ion. However, the latter ions may also potentially be formed via the direct loss of HPO_3, or via the combined losses of HPO_3 and H_2O, where the loss of H_2O occurs from a different region of the peptide that is not contained in the observed fragment ion. Here, therefore, the extent of phosphate group rearrangement resulting from CID-MS/MS of each peptide precursor ion was manually calculated by expressing the abundance of each observed rearranged product ion (matching to within a tolerance of ± 0.2 m/z for the LTQ XL and LTQ, and ± 0.002 m/z for the LTQ Orbitrap Velos) as a fraction of the summed abundances of the rearranged and non-rearranged products (e.g., $y_n^{+80}/(y_n^{+80}+y_n)$ and $b_n^{-80}/(b_n^{-80}+b_n)$, or $y_n^{+80}/(y_n^{+80}+y_n)$ only). Then, the average of the individual % rearrangement values was determined for each peptide precursor ion

charge state. The Ascore and PhosphoScore algorithms were both used to automatically assign a confidence level for phosphorylation site localization from the CID-MS/MS data, while the PhosphoScore algorithm was used for assigning phosphorylation sites from the MS^3 data. The default settings were used for each algorithm.

4.4.2 Quantitative Analysis of Competing Fragmentation Pathways for Product Ions with Neutral Loss of 98 Da (Chapter Three)

All scans from each MS/MS acquisition were averaged prior to analysis to reduce scan-to-scan variance in ion abundances, as well as to improve signal-to-noise. Here, the percentage of the combined loss fragmentation pathway upon MS/MS of each peptide precursor ion was calculated by expressing the abundance of the -98 Da mono-isotope neutral loss product ion (matching to within a tolerance of ± 0.2 m/z for the LTQ XL and ± 0.002 m/z for the LTQ Orbitrap Velos) as a fraction of the summed abundances of the -98 Da and -100 Da monoisotopic neutral loss product ions.

CHAPTER FIVE

Characterization of Full Length, Truncated and Oxidized Variants of Parathyroid Hormone and Development of an Immuno-LC-MS/MS Assay for their Detection in Biological Samples

5.1 Introduction

Parathyroid hormone (PTH) plays a critical role in the regulation of circulating calcium concentration in plasma. Maintaining normal concentrations of circulating calcium is essential for the function of certain proteins responding to calcium concentration, which are involved in cell signaling and bone metabolism[272]. PTH regulates circulating calcium concentration through three pathways. In response to decreased calcium concentration detected by a calcium-sensing receptor, more PTH is produced and secreted into the circulatory system, activating PTH receptor type 1 (PTH1R)[273], which consequently, increases the reabsorption of calcium in the kidney, stimulating the release of calcium from bones and promoting the absorption of calcium in the gut regulated by increased synthesis of 1,25-dihyroxyvitamin D in kidney[272]. Increased calcium concentration then participates in a feedback loop to decrease the secretion of PTH. Excessive secretion of PTH can result from abnormalities in the regulation system, which was defined as hyperparathyroidism. Secondary hyperparathyroidism has drawn the most attention for its frequent occurrence in patients with chronic kidney disease[274]. Parathyroid responds to lowered calcium concentration to increase secretion of PTH in secondary hyperparathyroidism[272]. After longstanding chronic kidney disease, tertiary hyperparathyroidism can be induced, which is characterized by autonomous secretion of PTH. The causes for primary

hyperparathyroidismin, in which parathyroid glands secrete excessive PTH, remain unclear. However, irradiation was found to be associated with primary hyperparathyroidism[275, 276].

PTH is produced in parathyroid glands involving a two-step cleavage process from a PTH precursor of 115 amino acids[277, 278]. The intact PTH consisting of 84 amino acids (PTH 1-84) is subsequently secreted into the circulatory system. Studies have shown that PTH 1-84 can be converted to other truncated forms through metabolic processes[279, 280]. There are two main types of truncated forms of PTH: PTH 7-84, the most predominant truncated form observed in chronic kidney disease and PTH 1-34. It is believed that PTH1R can be activated upon recognizing the N-terminal residues of the PTH sequence. Studies have shown that PTH 1-34 is biologically active[281] while truncated forms missing the first several N-terminal residues have no biological activities[273].

The successful diagnosis and appropriate treatment of hyperparathyroidism depends on the accurate quantification of the biologically active forms of PTH. Therefore, immunoassays for PTH have been developed for the detection of PTH in serum or plasma samples[273, 282]. There have been three generations of PTH assays developed since the 1960's, when the first PTH assay was developed[283]. The first generation PTH assay employed a single radiolabeled antibody against the C-terminal amino acids of PTH. This type of assay suffers from the limitation of not being able to differentiate between the biological active forms versus N-terminal truncated inactive forms of PTH. Later on, a "sandwich" type second generation PTH assay was developed, in which a pair of PTH antibodies were used[284]. The C-terminal specific

antibody (anti PTH 39-84) was anchored onto polystyrene beads as the capture antibody and an N-terminal specific radiolabeled antibody (anti PTH 1-34) was in solution as the conjugate antibody. The initial aim of this type assay was to detect only the intact PTH. However, it was discovered later that it also had cross reactivity with PTH C-terminal truncated forms, such as PTH 7-84[285], because most N-terminal specific antibodies in this type of assay are raised against PTH 20-25 region which serves as an antigenic site[273]. The PTH 7-84 fragment is known to be accumulated in patients with renal disease to high concentrations[278, 285]. With a significant amount of PTH 7-84 present in the samples, this type of assay cannot accurately detect the biological active forms of PTH. To overcome this limitation, an N-terminal specific antibody (anti PTH 1-6) with better selectivity towards the intact form of PTH 1-84 was employed. Unfortunately, it has been reported that the improved second generation PTH assay has no obvious advantage over the old one[286].

The above immuno-metric PTH assays apparently cannot fulfill the need for accurate detection of intact PTH. A third generation of PTH assay by combining the immuno-affinity approach with LC-MS has recently been introduced[274, 277, 278]. The PTH was first extracted from plasma by employing a C-terminal specific antibody. The extracted PTH was then either digested in situ or eluted from the immuno-affinity beads followed by digestion. The digested PTH peptides mixture was analyzed by LC-MS or LC-MS/MS. By identifying and quantifying peptides of interest, the concentration of the specific form of PTH in the sample can be determined. This third generation PTH assay eliminates the interferences of other truncated forms and thus can accurately quantify the intact PTH 1-84[277]. Moreover, by monitoring the peptides from the PTH C-

terminal truncated forms, the amount of PTH 7-84 can also be successfully quantified [278]. Unfortunately, the third generation of PTH assays have not be able to detect biologically active forms of truncated PTH, such as PTH 1-34. This limitation can be easily overcame by employing a N-terminal specific antibody for extracting the PTH from the sample.

There are two methionine residues at position 8 (M8) and 18 (M18) of the PTH sequence, which can be oxidized when subjected to oxidative stress[287, 288]. As discussed in chapter one, oxidation of methionine residues within a protein can affect the protein activity. It has been reported that PTH loses its biological activity upon methionine oxidation[274, 288-290]. A recent study using the second generation PTH assay showed that only 7%-34% of PTH in patients with late-stage renal disease was free of oxidation. Patients with late-stage renal disease are usually on hemodialysis and are potentially more susceptible to oxidative stress[274].

Here, an improved third generation PTH assay named immuno-LC-MS/MS assay was developed with the capability of simultaneously quantifying intact PTH 1-84, truncated PTH 7-84 and their oxidized variants. ^{15}N labeled PTH 1-84 and PTH 7-84 were employed as internal standards, as well as the $^{13}C_6{}^{15}N_1$Leu labeled oxidized PTH tryptic peptides. Plasma samples from patients that were on dialysis were analyzed by newly developed immuno-LC-MS/MS assay, and by three other traditional second generation PTH assays (assay A and B use anti PTH 1-34 antibodies while assay C uses anti PTH 1-6 antibody). By comparing the results from these four different assays, it can be determined whether the secondary PTH assays have a significant cross-reactivity with biological inactive oxidized forms of PTH. Additionally, the oxidation

kinetics of both PTH 1-84 and 7-84 was studied, and oxidized PTH variants were purified by HPLC and characterized by CID-MS/MS.

5.2 Results and Discussion

5.2.1 Characterization of Full Length and Truncated PTH by LC-MS Bottom-up Approach

Due to the presence of various other proteins and the low abundance of PTH (pg/mL) in plasma, direct analysis of intact PTH by LC-MS based shotgun proteomics is nearly impossible. Fortunately, the detection of enzymatic PTH peptides is more sensitive and more amenable for analysis of PTH in biological samples. In this study, the ultimate interest is to simultaneously characterize and quantify PTH 1-84, PTH 7-84 and their different oxidized forms. Therefore among the enzymatic peptides, those containing the M8 and M18 residues are required. Three enzymes were evaluated for this purpose, which were trypsin, Arg-C and Glu-C. Theoretically, Arg-C and Glu-C should each yield a single peptide containing both M8 and M18 residues. This would be beneficial for differentiating the PTH M8(oxidation)M18 with PTH M8M18(oxidation) forms.

To ensure complete digestion of the protein mixture from real patient samples, 1:1 ratio of enzymes and PTH 1-84 was used for the digestion. All digestions were performed at 37 ºC for 4 hours. Under those conditions, it was found that Arg-C cleaved not only at the C-terminal of Arg residues but also at the C-terminal of Lys residues, and thus generated a peptide profile similar to that of trypsin (data not shown). Non-specific cleavage could yield two sets of peptides (PTH 1-20 versus PTH 1-13 and PTH 14-20) that need to be included in methionine oxidation quantification, which consequently

complicated the analysis of PTH oxidized variants. Thus Arg-C was concluded to not be a good enzyme for quantitative analysis of PTH.

LC-MS analysis of trypsin and Glu-C digested PTH 1-84 is shown in Figure 5.1 and Figure 5.2. 10 mM NH_4HCO_3 was used as digestion buffer for trypsin while PBS buffer was used for Glu-C. One hundred fmol of digested sample was injected for LC-MS analysis. Panel A in Figure 5.1 shows the overall LC chromatography. Panel B, C and D are the extracted MS ion currents for triply charged PTH 1-13, doubly charged 14-20 and triply charged 1-20 peptide ions respectively. PTH 1-13 and 14-20 are the peptides of interest for quantification. No significant signal was present for PTH 1-20 confirming that the trypsin digestion was complete without missed cleavage, at least in this region. The insert spectra (i) and (ii) are averaged MS scans for peptides eluted at 15.62 min and 10.29 min from the LC column, which include PTH 1-13 and 14-20. Both of these two peptide peaks are among the major peaks in the LC chromatogram. Similarly, in Figure 5.2, panel A shows the overall LC chromatography of Glu-C digested PTH and panel B is the extracted MS ion current for the quadruply charged PTH 5-19 peptide ion. The insert spectrum in Figure 5.2 shows the averaged MS scans for peptides eluting at 14.97 min, which include PTH 5-19. Comparison between Figure 5.1 and Figure 5.2 shows that the MS intensity of PTH 1-13 and 14-20 is one order of magnitude higher than that of PTH 5-19. Therefore, for the issue of sensitivity, trypsin is a better choice for digesting PTH than Glu-C. However, PTH 5-19 includes both of the methionine residues and can be used for differentiating the PTH M8(oxidation)M18 from PTH M8M18(oxidation) forms. Depending on the purpose of the study, either of the enzymes can be employed for PTH digestion.

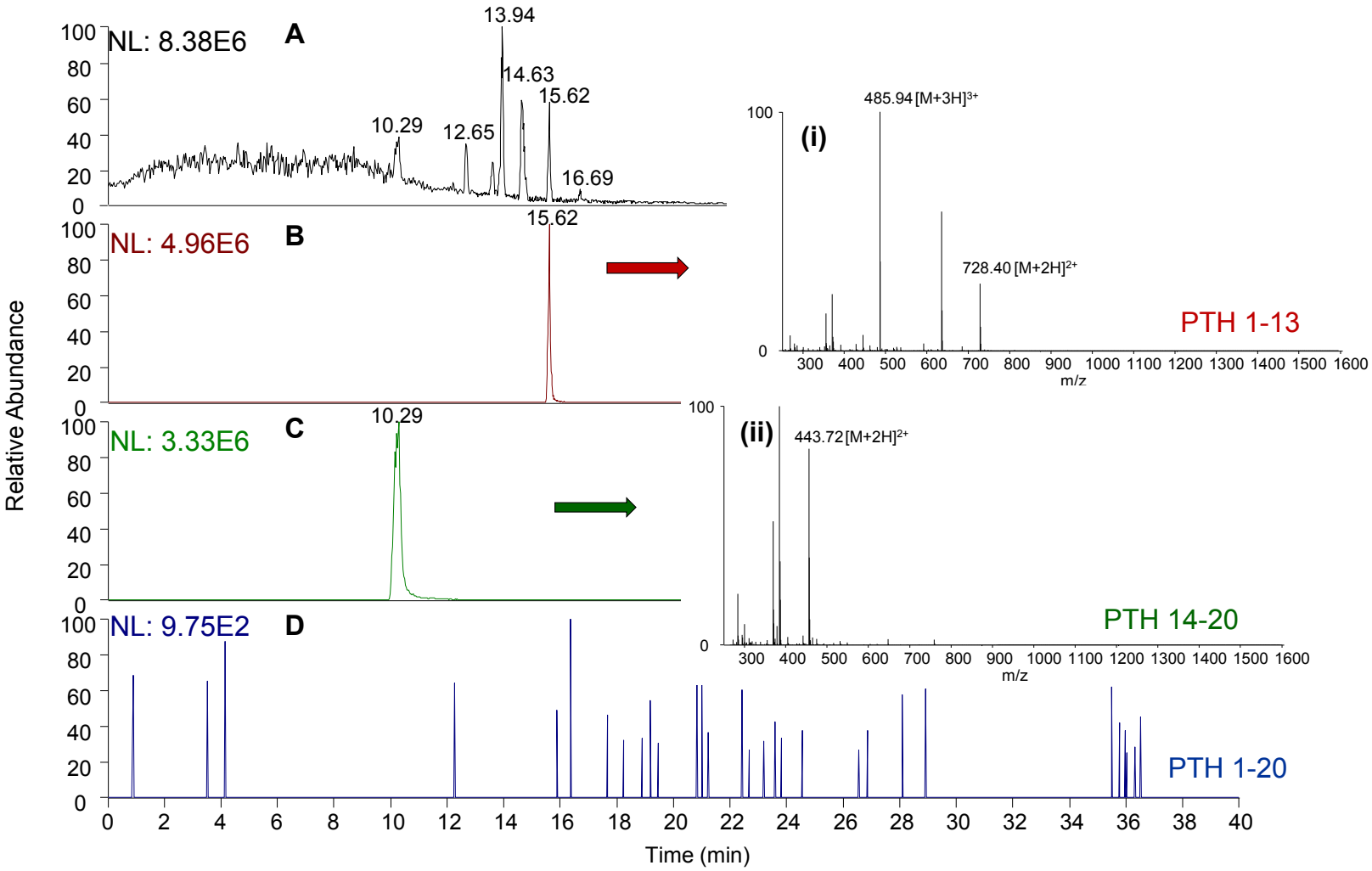

Figure 5.1 LC-MS of trypsin digested PTH 1-84. (A) General LC chromatography of trypsin digested PTH 1-84; (B) Extracted MS ion current for triply charged PTH 1-13; (C) Extracted MS ion current for doubly charged PTH 14-20; (D) Extracted MS ion current for PTH 1-20; Insert (i) shows the averaged MS scans for PTH 1-13 while (i) shows the averaged MS scans for PTH 14-20.

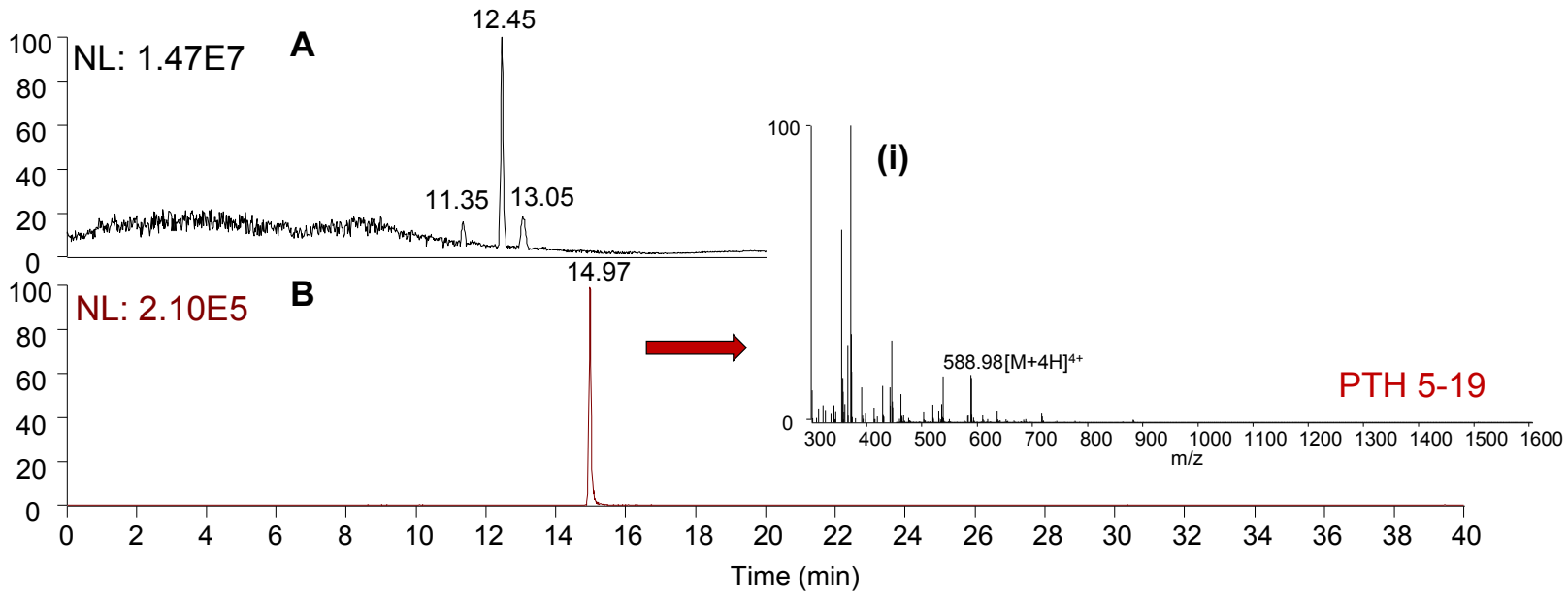

Figure 5.2 LC-MS of Glu-C digested PTH 1-84. (A) General LC chromatography of Glu-C digested PTH 1-84; (B) Extracted MS ion current for quadruply charged PTH 5-19; Insert spectrum shows the averaged MS scans for PTH 5-19.

5.2.2 Oxidation Profiles of Full Length and Truncated PTH

To investigate and mimic the oxidation kinetics of both PTH 1-84 and PTH 7-84 *in vivo*, the full length and truncated PTH were subject to H_2O_2 oxidation in PBS buffer *in vitro* at 37 ºC for different lengths of time. PTH 1-84 and PTH 7-84 were combined into one sample for oxidation in order to eliminate any potential sample handling bias. Figure 5.3 shows the oxidation profiles for both PTH 1-84 (A) and PTH 7-84 (B). Given that enough pure PTH 1-84 and 7-84 were available, Glu-C was used for digestion of PTH to achieve a better understanding of how each of the oxidized forms evolves during *in vitro* oxidation. Four hundred fmol of digests from each condition were injected for LC-MS analysis.

The MS intensity of quadruply charged PTH 5-19 and PTH 7-19 (for PTH 7-84) peptide ions and their oxidized forms were used for calculating the composition percentage as the y axis in Figure 5.3, assuming that the native forms of PTH 5-19 and PTH 7-19 ionize similarly to their oxidative forms. Even if their ionization efficiencies were different, the relative amount of each PTH variant at different time points can still be compared with one another. Note that at time point 0, oxidized forms of PTH 5-19 and 7-19 were detected, which shows that oxidation can be introduced during sample handling without H_2O_2 oxidation. As shown in Figure 5.3, for both PTH 1-84 and PTH 7-84, the M8 residue is more accessible to oxidation than the M18 residue. The M8 residue of PTH 7-84 is even more easily oxidized than that of PTH 1-84. The oxidation profiles for both full length and truncated PTH reach a plateau after 4 h. Notably, no significant amount of PTH 1-84M8(O)M18(2O), PTH 1-84M8(2O)M18(O) or PTH 1-84M8(2O)M(2O) were observed, even at the time point of 24 h. In contrast, PTH 7-

84M8(O)M18(2O) and PTH 7-84M8(2O)M(O) were detected after 30 min of oxidation for PTH 7-84, but both of their percentages stay flat at about 10% after 1 h. PTH 7-84M8(O)M18(2O) and PTH 7-84M8(2O)M(O) are presented as one value because they were not resolved in the LC chromatography. No significant amount of PTH 7-84M8(2O)M(2O) was detected. Comparing the oxidation profiles of PTH 1-84 to 7-84, it is seen that PTH 7-84 is more accessible to oxidation, which could be due to the fact the M8 residue of PTH 7-84 is less protected without the first 6 residues. The oxidation profile of PTH 1-84 is consistent with previous results[288] while that of PTH 7-84 is first reported here.

Harsh oxidation conditions, such as using 5 M H_2O_2 (30% H_2O_2 is about 10 M) in PBS buffer and 5 M H_2O_2 in 0.1 M acetic acid for an oxidation time of 2 h were also investigated for oxidation of PTH 1-84. It was found that the overall intensity for each of the PTH 1-84 forms was decreased by one order of magnitude after using these harsh conditions compared with 12 mM H_2O_2 in PBS buffer (data not shown). This probably was caused by the partial degradation of PTH under these conditions. Again, no significant amount of PTH 1-84M8(O)M18(2O), PTH 1-84M8(2O)M18(O) or PTH 1-84M8(2O)M(2O) were observed. Given that oxidation stress *in vivo* is very unlikely to be harsher than the above conditions, it is concluded that only methionine sulfoxides should be considered in quantification of PTH and its oxidative forms.

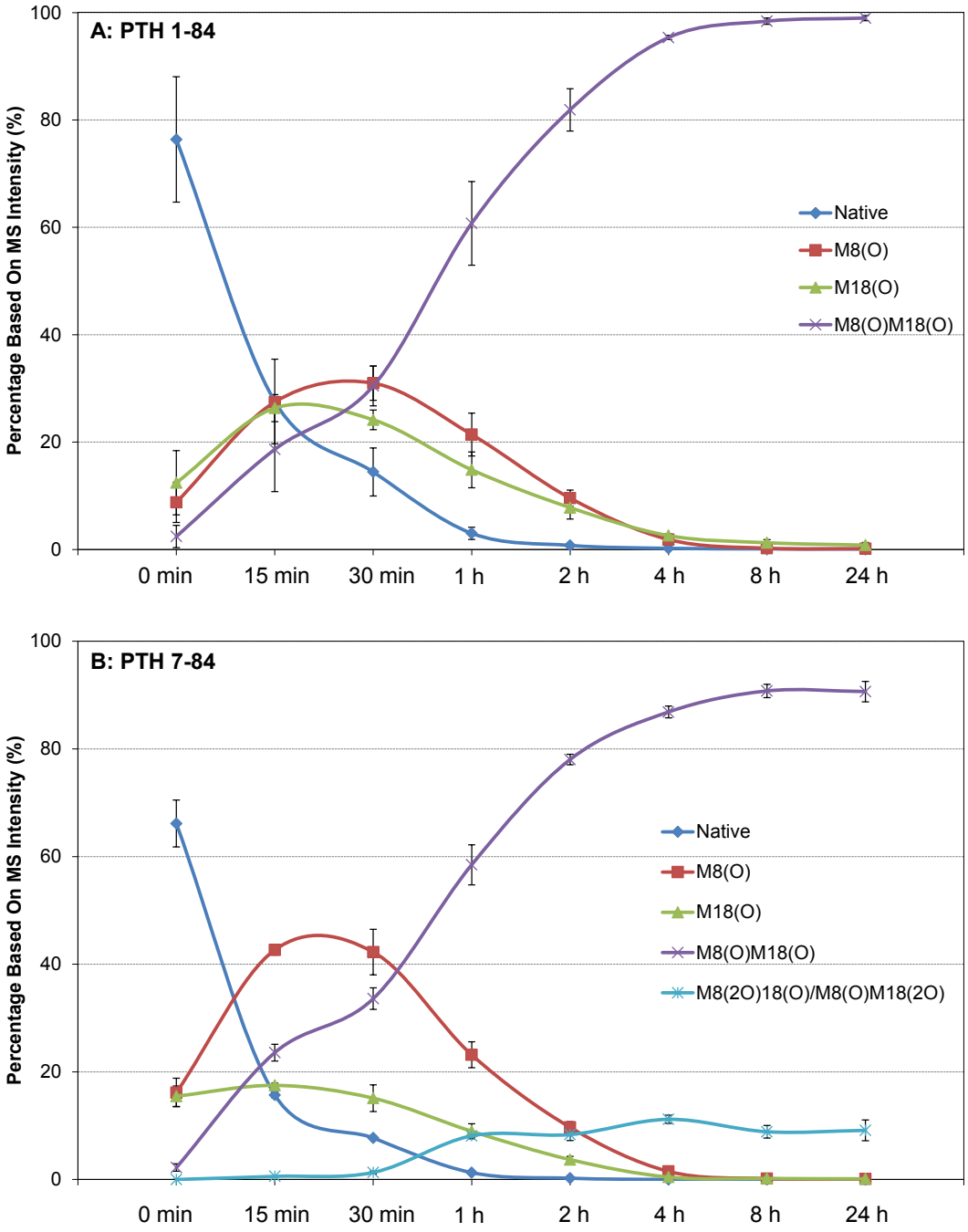

Figure 5.3 Oxidation profiles of PTH 1-84 (A) and PTH 7-84 (B). Oxidation was performed in PBS buffer with 12 mM H_2O_2 at 37 ºC. The length of time is shown as the x-axis while y-axis shows the percentage of each of the forms at certain time point calculated based on the MS intensity of quadruply charged PTH 5-19 (A) and PTH 7-19 (B) ions.

5.2.3 Separation of Full Length, Truncated and Oxidized Variants of PTH

In preparation of pure oxidative variants (with methionine sulfoxide) of full length and truncated PTH, PTH 1-84 and 7-84 native forms were oxidized using the conditions described in section 5.2.2 for 1 h and 30 min respectively. As shown in Figure 5.4, the oxidized forms of PTH 1-84 were well resolved by RP-HPLC. However, oxidized forms of PTH 7-84 were not easily separated, especially PTH 7-84M18(O) and PTH 7-84M8(O) forms. Therefore, a much shallower elution gradient was used for separation of the oxidized variants of PTH 7-84. The identity of each chromatographic peak was determined by CID-MS/MS as described below in section 5.2.4.

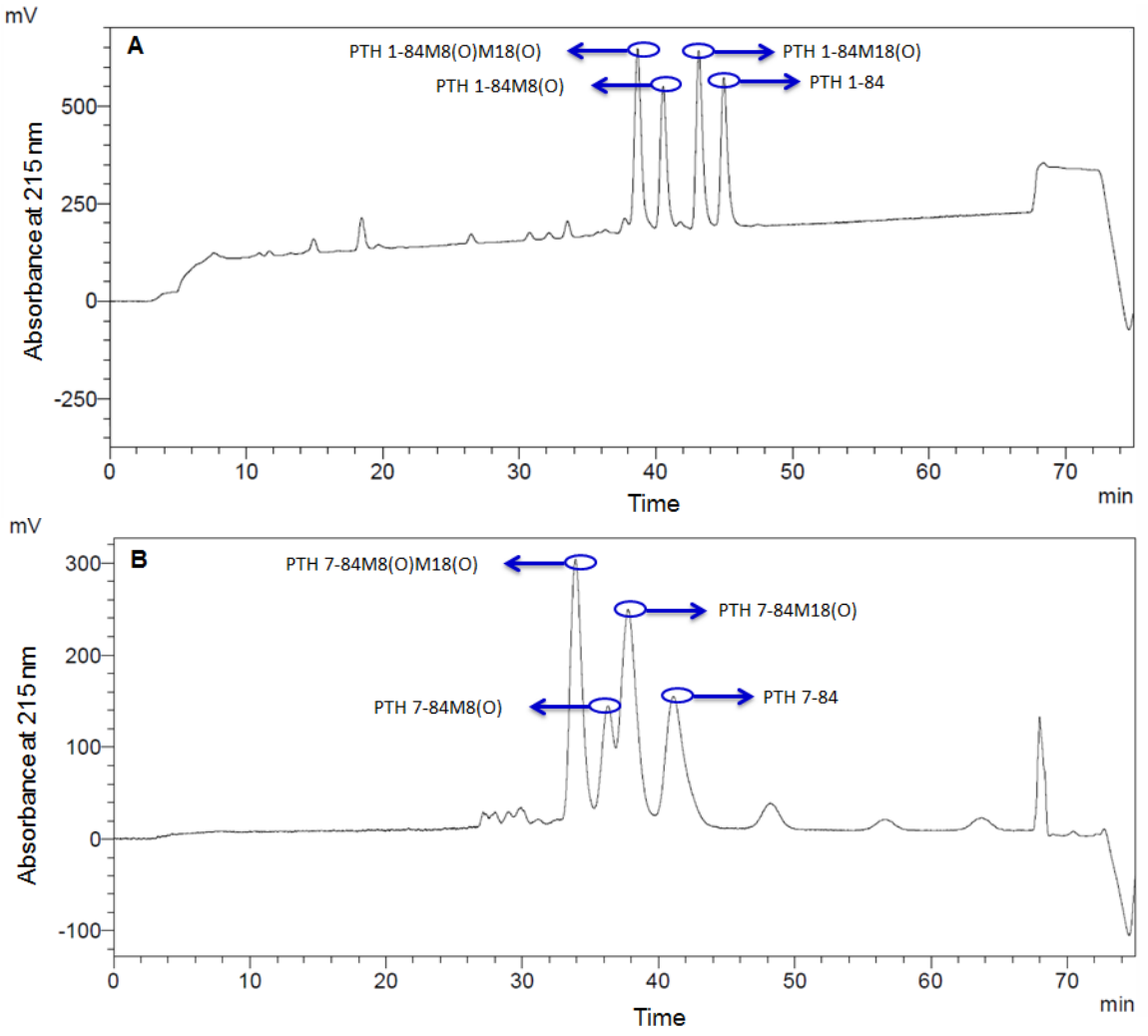

Figure 5.4 HPLC separation of native and oxidized forms of PTH 1-84 (A) and PTH 7-84 (B). Oxidation was performed in PBS buffer with 12 mM H_2O_2 at 37 ºC for 1 h for PTH 1-84 and 30 min for PTH 7-84.

5.2.4 MS and CID-MS/MS for Top-down Characterization of Full Length, Truncated and Oxidized Variants of PTH

HPLC purified native and oxidized forms of PTH 1-84 and PTH 7-84 were characterized by ESI-MS and CID-MS/MS using a Thermo Scientific Orbitrap Velos mass spectrometer at a resolution of 60,000, as shown in Figure 5.5 and Figure 5.6. The native form of PTH 1-84, PTH 1-84M8(O)/PTH 1-84M18(O), and PTH 1-84M8(O)M18(O) can be differentiated from each other by the mass shift +16 Da or +32 Da in MS level. However, to differentiate PTH 1-84M8(O) from PTH 1-84M18(O) and to confirm that the +32 Da shift is from two methionine sulfoxides instead of methionine sulfone, MS/MS is needed for further structural information. Therefore, CID-MS/MS was performed on the $[M+11H]^{11+}$ precursor ion of PTH 1-84, PTH 7-84 and their oxidized variants. This charge state was chosen for CID-MS/MS for two reasons: it was one of the most abundant charge states in MS and CID-MS/MS of these ions not only provided efficient fragmentation, but also yielded fragments that could be used to localize and identify the sites of methionine oxidation. For instance, b_{13} ions in CID-MS/MS of PTH 1-84M8(O) (Figure 5.5 B) and PTH 1-84M18(O) (Figure 5.5 C) have a mass difference of 16 Da. By identifying the mass of this ion, it can be determined which methionine residue of the precursor ion was oxidized. By identifying a +16 Da mass shift on the b_{13} ion and a +32 Da mass shift on b_{30}^{4+} ion, the composition of PTH 1-84 +32 Da can be characterized as PTH 1-84M8(O)M18(O) (Figure 5.5 D). Similarly, the b_4 and b_5 product ions in the CID-MS/MS spectrum of PTH 7-84 and its oxidized forms (Figure 5.6) can be used to pinpoint the existence and position of the methionine oxidation.

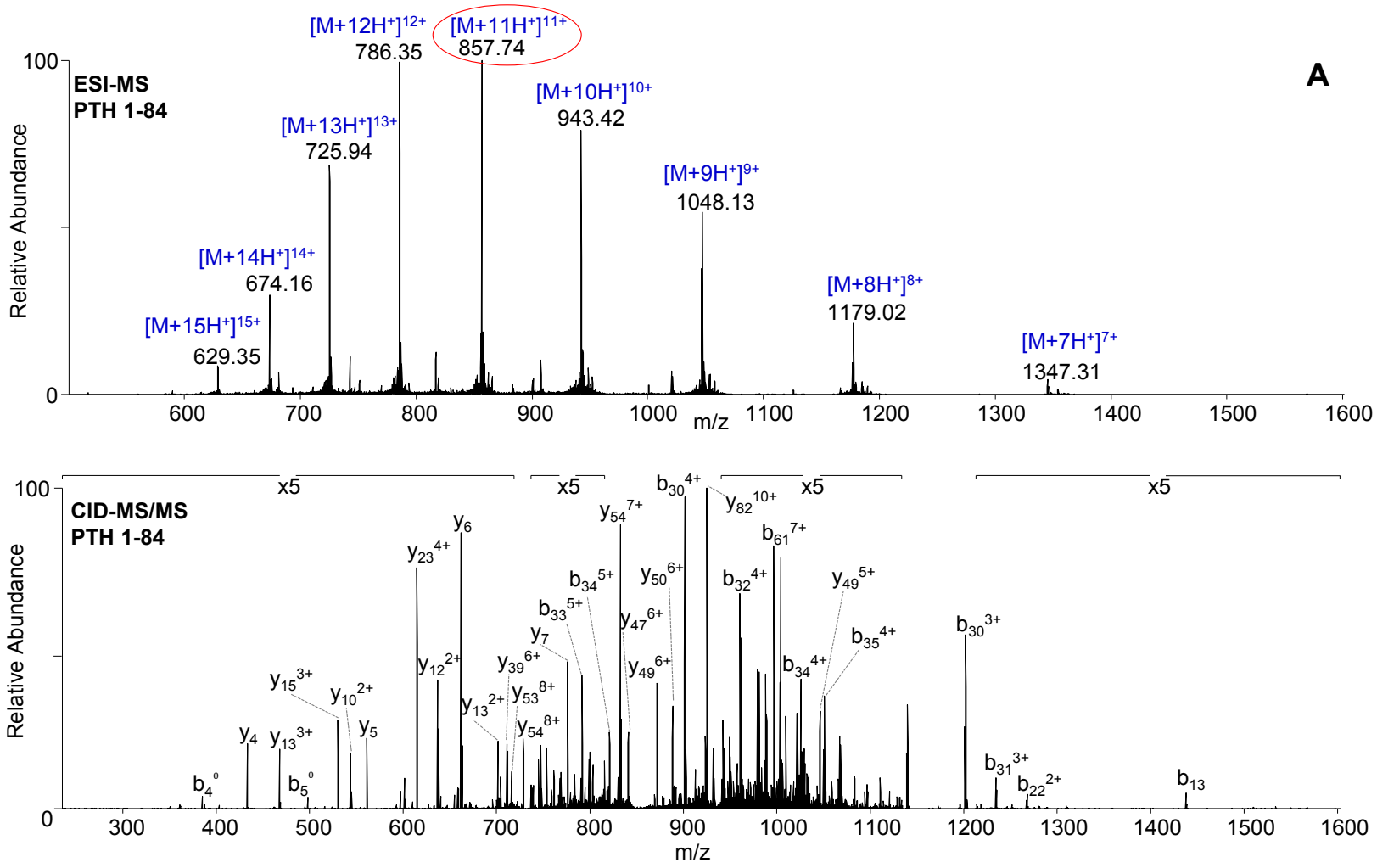

Figure 5.5 ESI-MS and CID-MS/MS of $[M+11H]^{11+}$ of PTH 1-84 (A), PTH 1-84M8(O) (B), PTH 1-84M18(O) (C) and PTH 1-84M8(O)M18(O) (D). The b ions labeled in red can be used for localizing methionine sulfoxide(s).

Figure 5.5 (Cont'd)

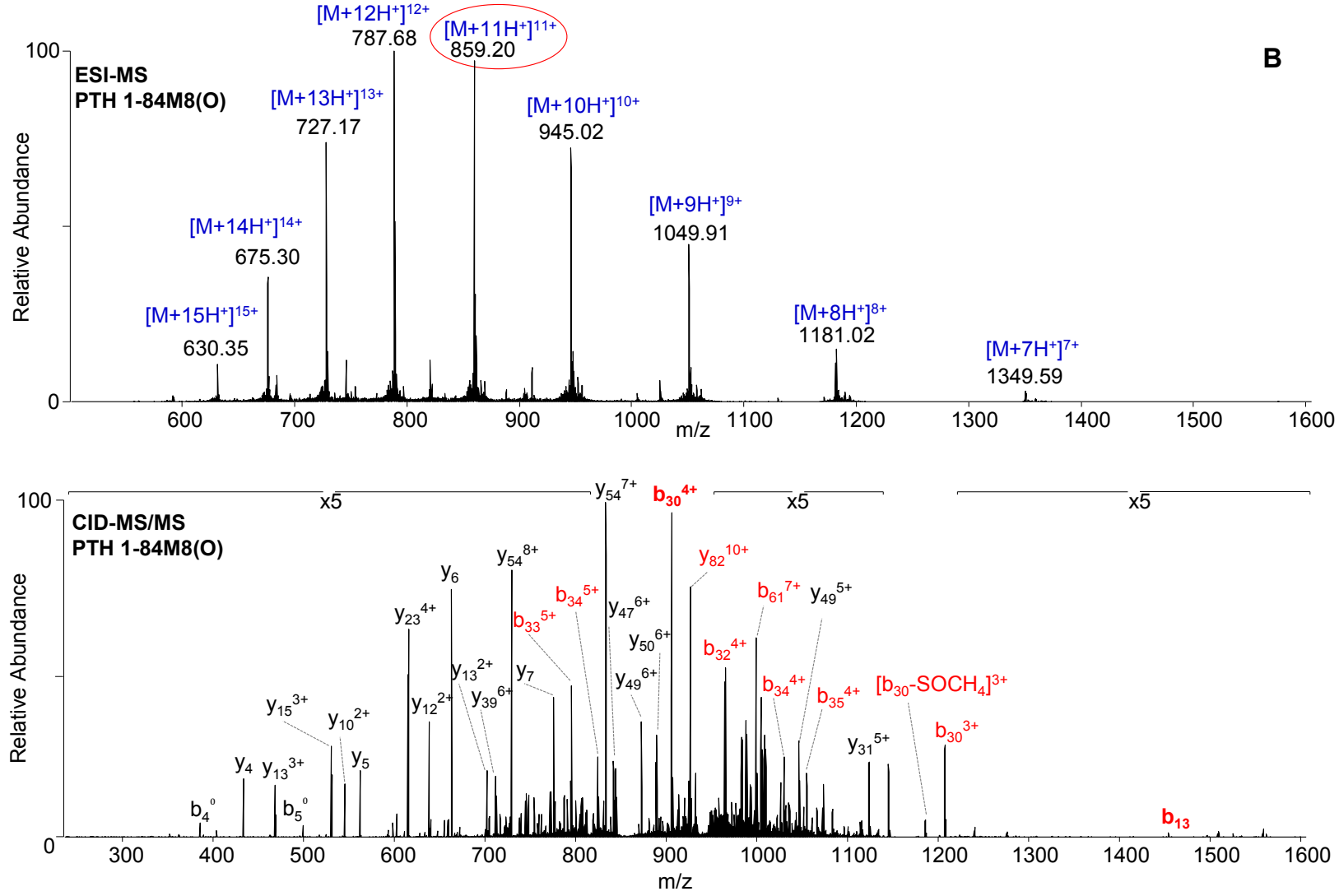

Figure 5.5 (Cont'd)

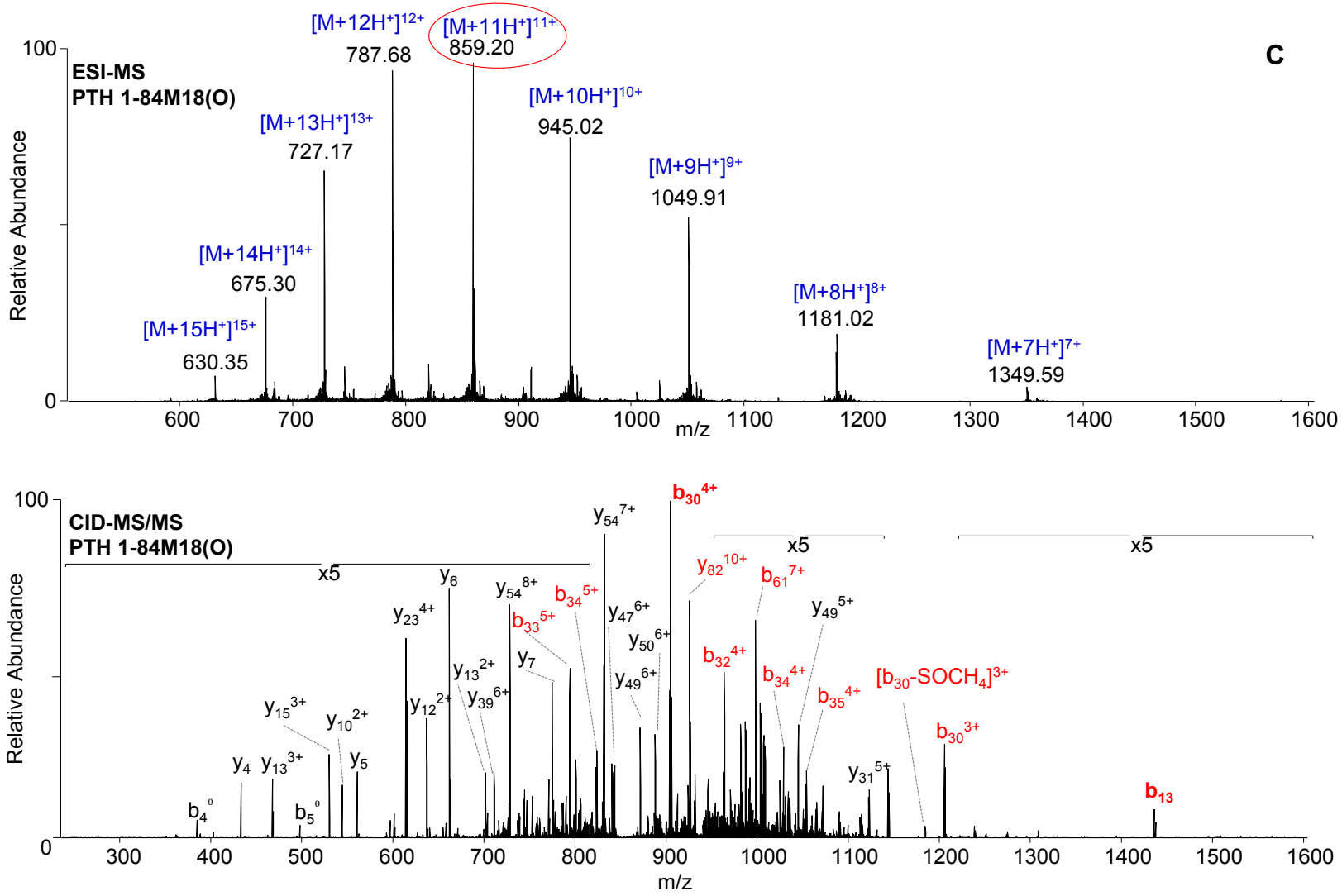

Figure 5.5 (Cont'd)

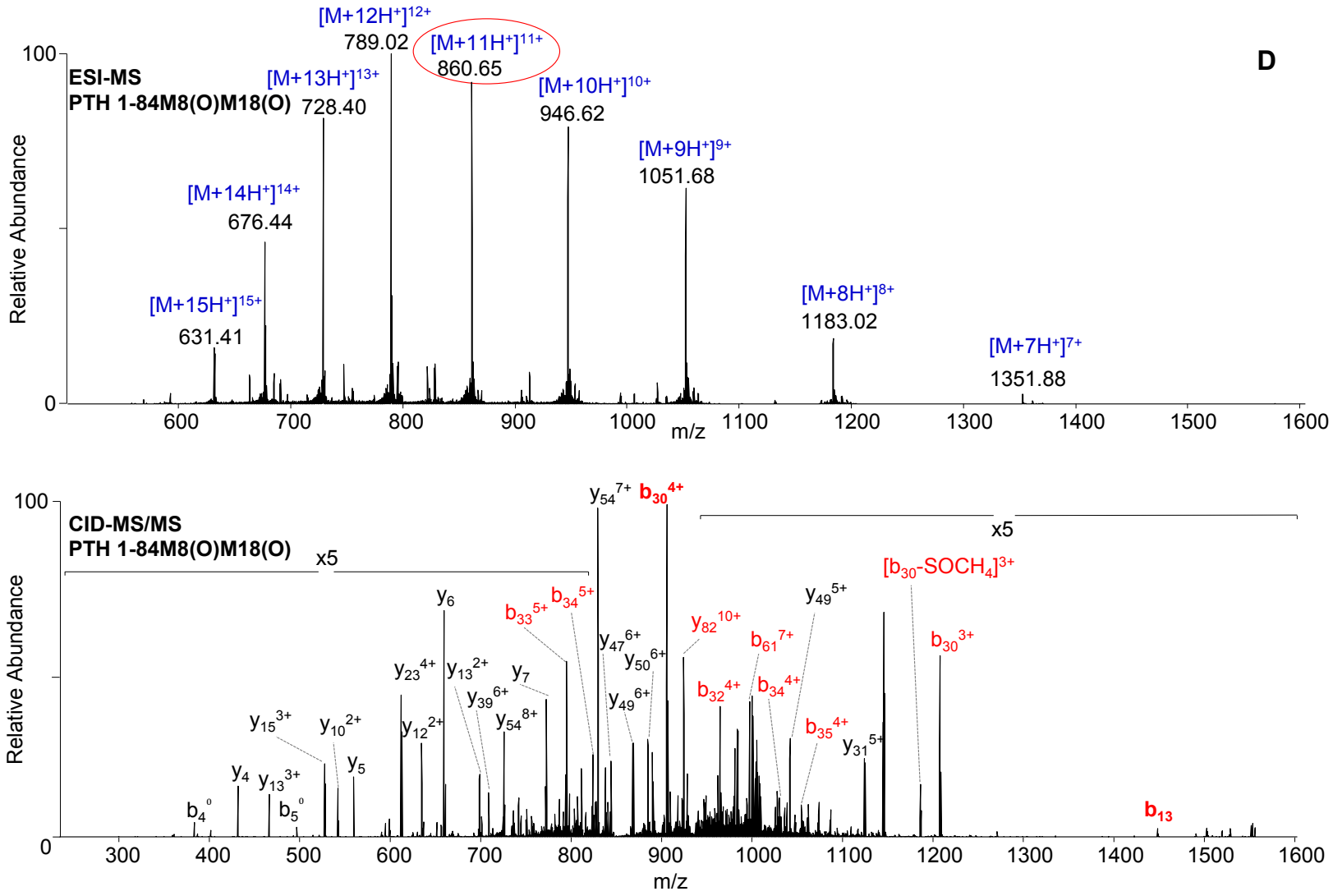

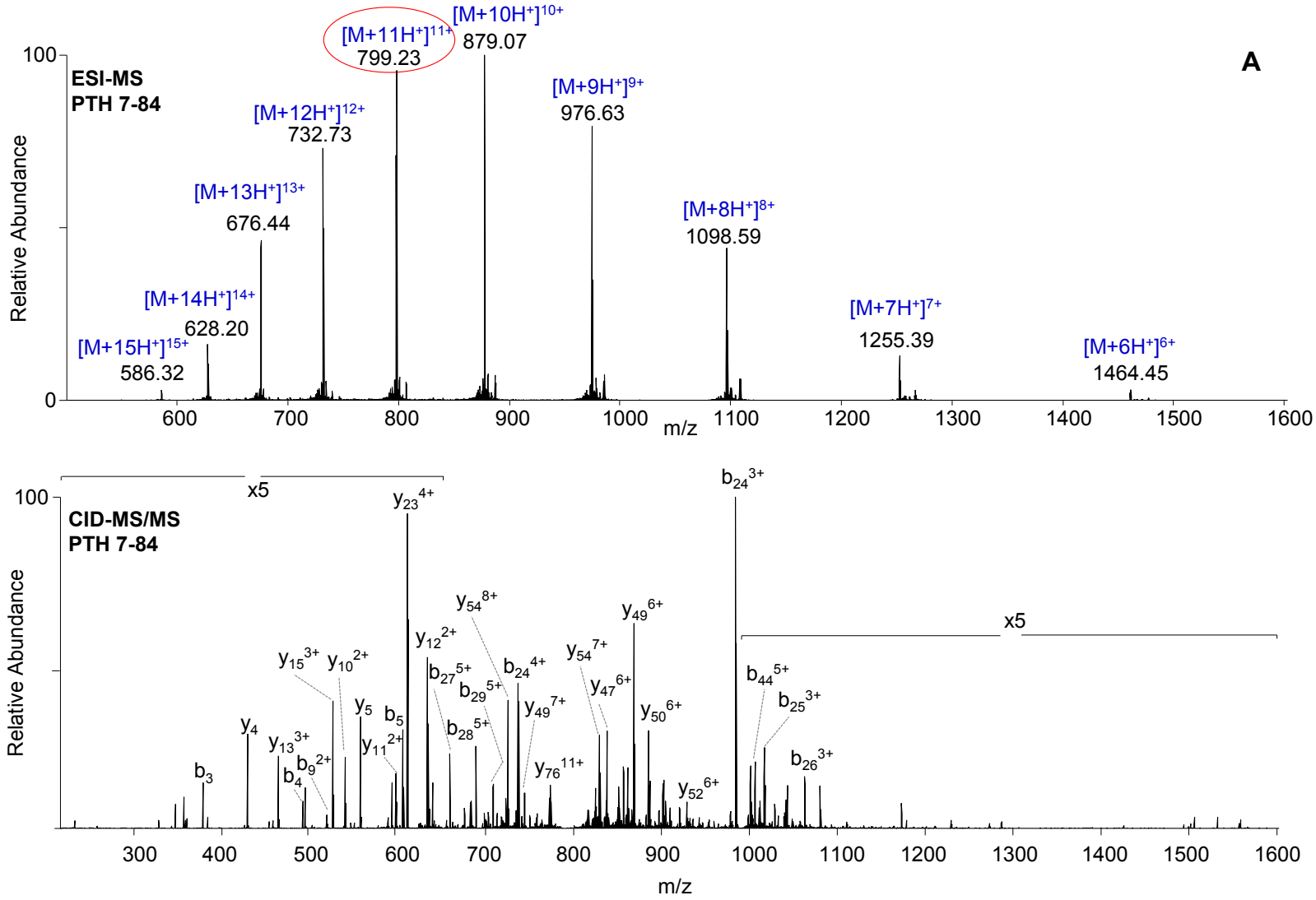

Figure 5.6 ESI-MS and CID-MS/MS of $[M+11H]^{11+}$ of PTH 7-84 (A), PTH 7-84M8(O) (B), PTH 7-84M18(O) (C) and PTH 7-84M8(O)M18(O) (D). The b ions labeled in red can be used for localizing methionine sulfoxide(s).

Figure 5.6 (Cont'd)

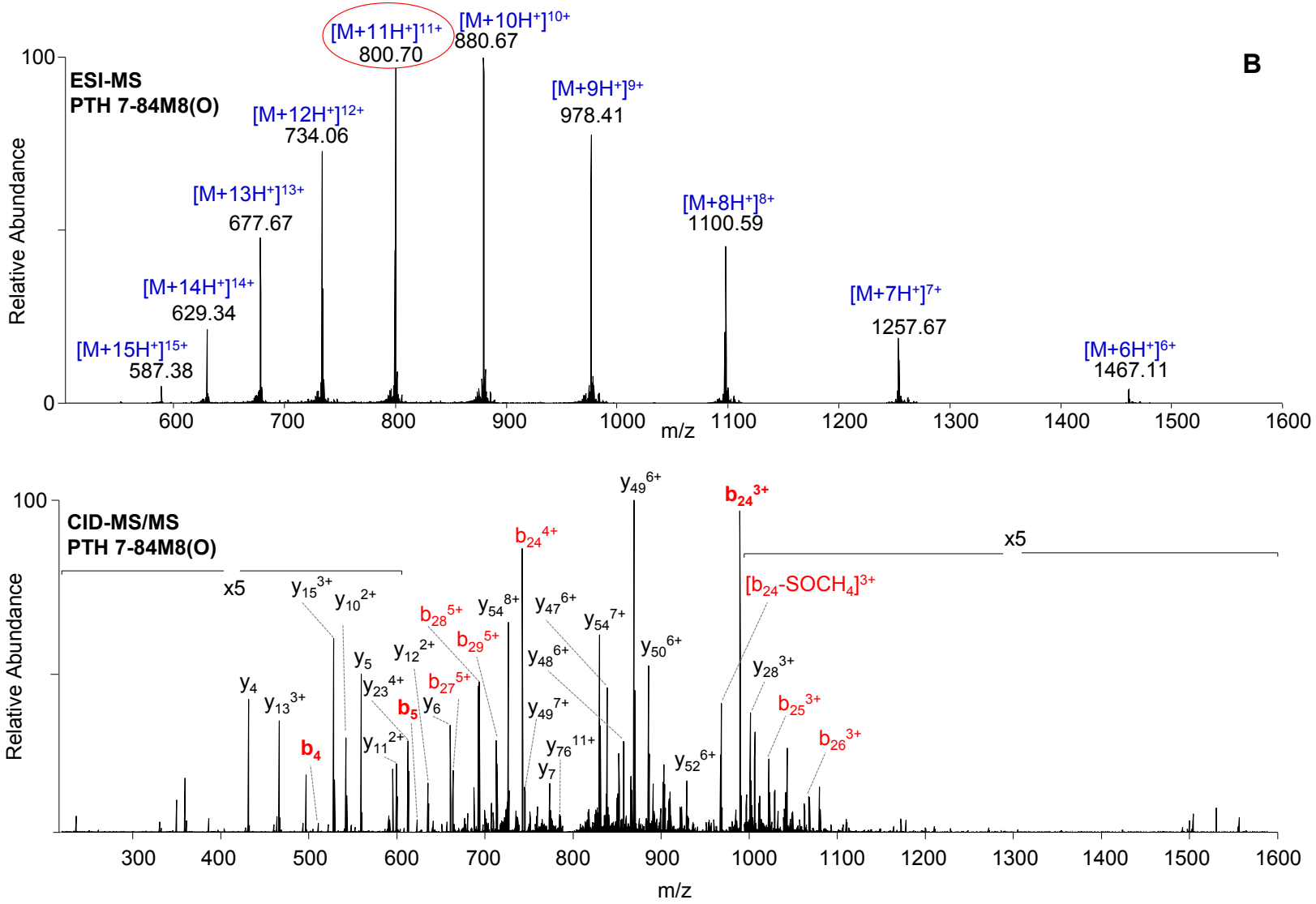

Figure 5.6 (Cont'd)

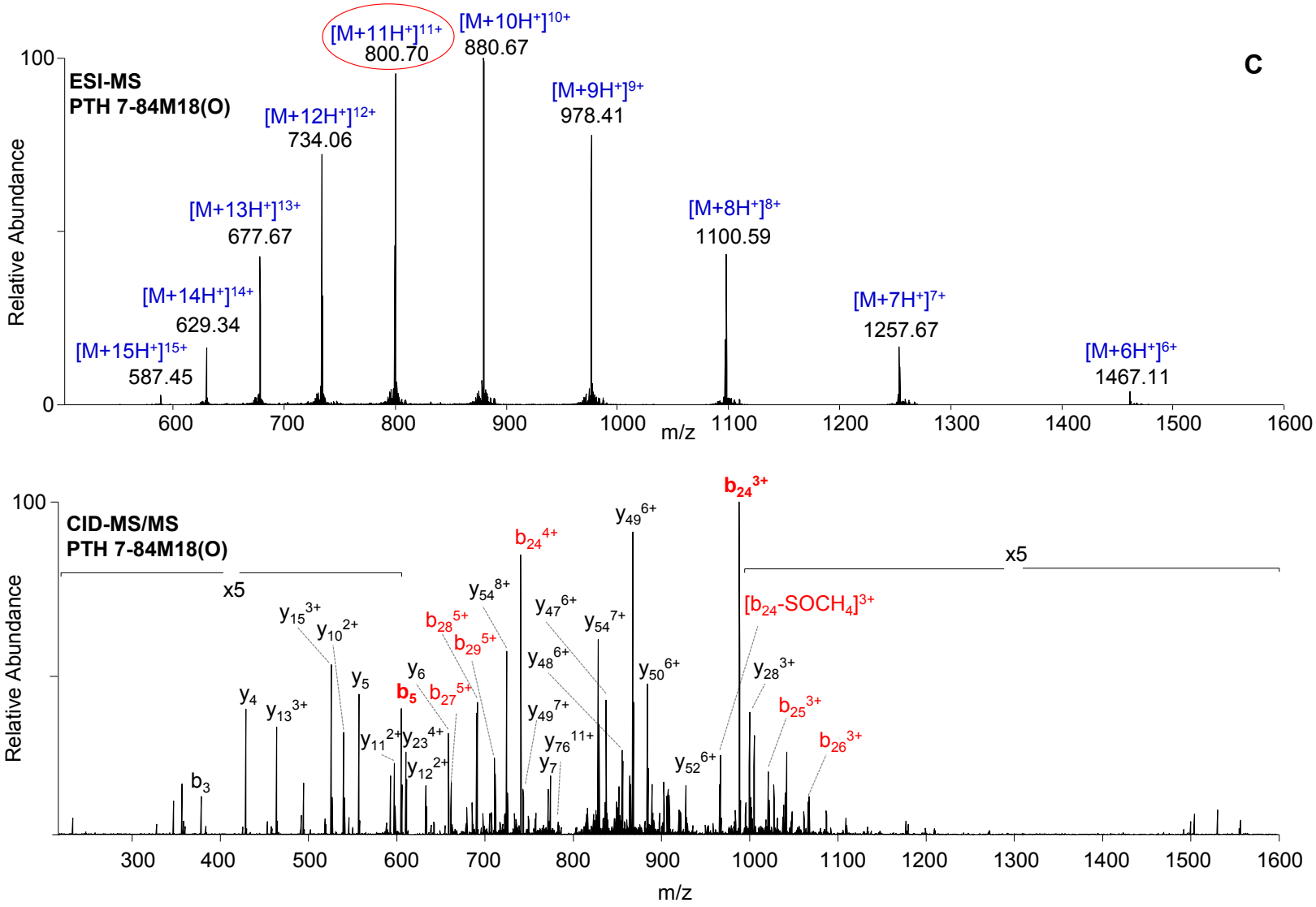

Figure 5.6 (Cont'd)

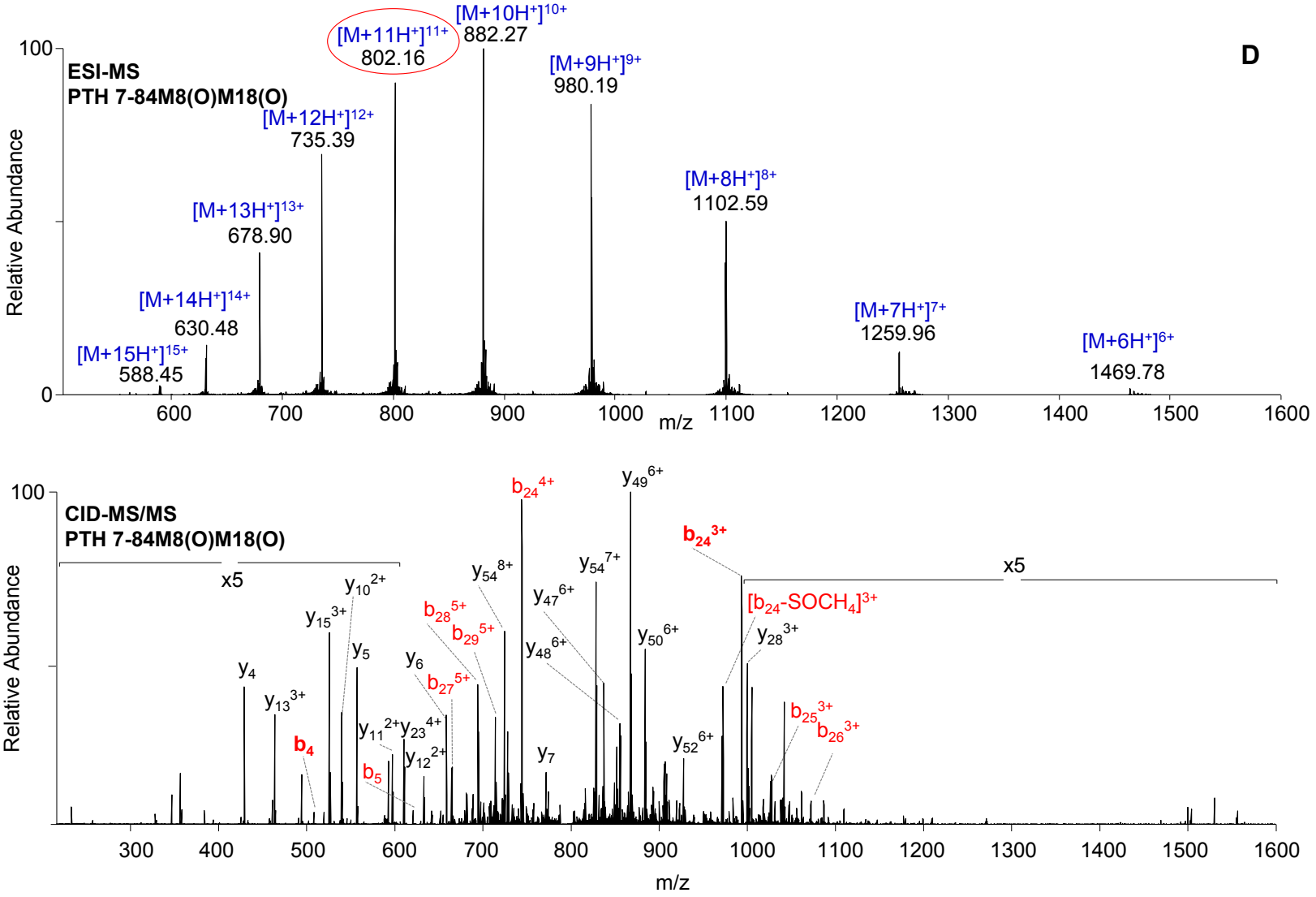

5.2.5 Development of an Immuno-LC-MS/MS Assay for Full Length, Truncated and Oxidized Variants of PTH in Biological Samples

5.2.5.1 Optimized Immuno-LC-MS/MS Assay Workflow

An immuno-affinity enrichment approach was employed in this study to simplify the background and to enrich PTH before LC-MS/MS analysis. As shown in Figure 5.7, the internal standards, ^{15}N labeled 1-84 and 7-84 were first added to the human plasma samples to correct for any potential PTH losses during sample handling to achieve more accurate quantification. Pmp beads coated with a goat anti PTH 39-84 antibody were used to pull out all forms of PTH containing residues 39-84, which would include PTH 1-84, 7-84 and their oxidized forms. Subsequently, the plasma was removed after binding. Optimal conditions used for washing and elution of the pmp beads were critical for decreasing the sample background without sacrificing the recovery yield of the PTH after the immuno-affinity enrichment. These conditions can be found in chapter five.

The eluents were then digested by trypsin. Trypsin was chosen here as resultant PTH peptides were more sensitive to be detected as discussed in 5.2.1. Finally, isotope labeled synthetic PTH peptide standards, $^{13}C_6{}^{15}N_1$Leu_PTH 1-13M(O), $^{13}C_6{}^{15}N_1$Leu_PTH 7-13M(O), and $^{13}C_6{}^{15}N_1$Leu_PTH 14-20M(O), were added into the digests as standards for quantifying the oxidized forms of PTH 1-84 and 7-84 before being subjected to LC-MS/MS analysis.

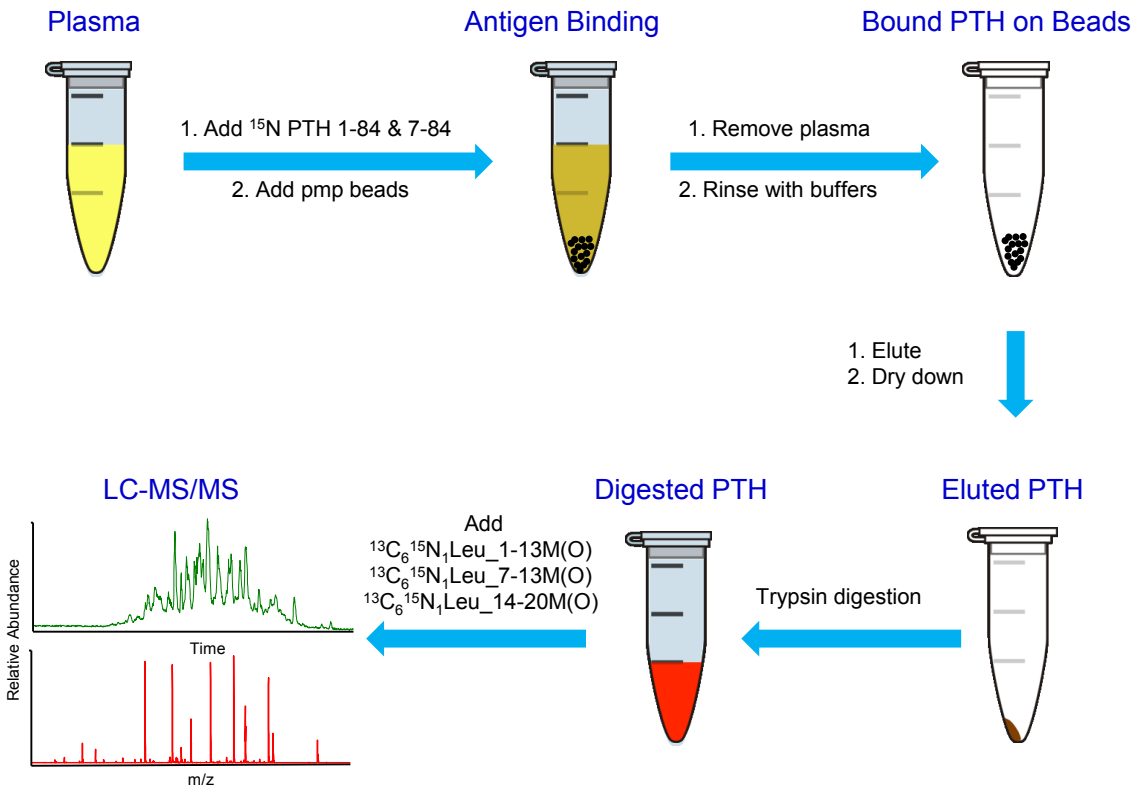

Figure 5.7 Workflow for the Immuno-LC-MS/MS PTH Assay

5.2.5.2 Linear Response of Immuno-LC-MS/MS Assay for PTH

In the immuno-LC-MS/MS assay, 500 pg each of PTH 1-84 of ^{15}N labeled PTH 1-84 and 7-84 were added into the sample as internal standards for quantification of PTH. Given that the actual concentration of PTH in real biological samples varies, it is essential to make sure that the immuno-LC-MS/MS assay has a relatively wide linear range which includes the concentration of the added ^{15}N labeled internal standards. Thus different amounts of PTH 1-84 WHO standard, *i.e.* 0 pg, 5 pg, 10 pg (in triplicate), 20 pg, 50 pg (in triplicate), 100 pg, 200 pg, 500 pg (in triplicate), 1000pg, 2000 pg, were separately added into 1 mL of PTH depleted plasma (usually the patient plasma available for analysis is about 1mL) then analyzed by immuno-LC-MS/MS. Figure 5.8 shows the response of the assay to PTH 1-84 represented by PTH 1-13 and 14-20 peptides. The x-axis shows the initial concentration of PTH in the sample and the y-axis shows the monitored fragment ion intensity in CID-MS/MS of PTH 1-13 (A) and PTH 14-20 (B). It can be deduced from these two curves that immuno-LC-MS/MS assay for PTH responds linearly in the range of 5-2000 pg/mL.

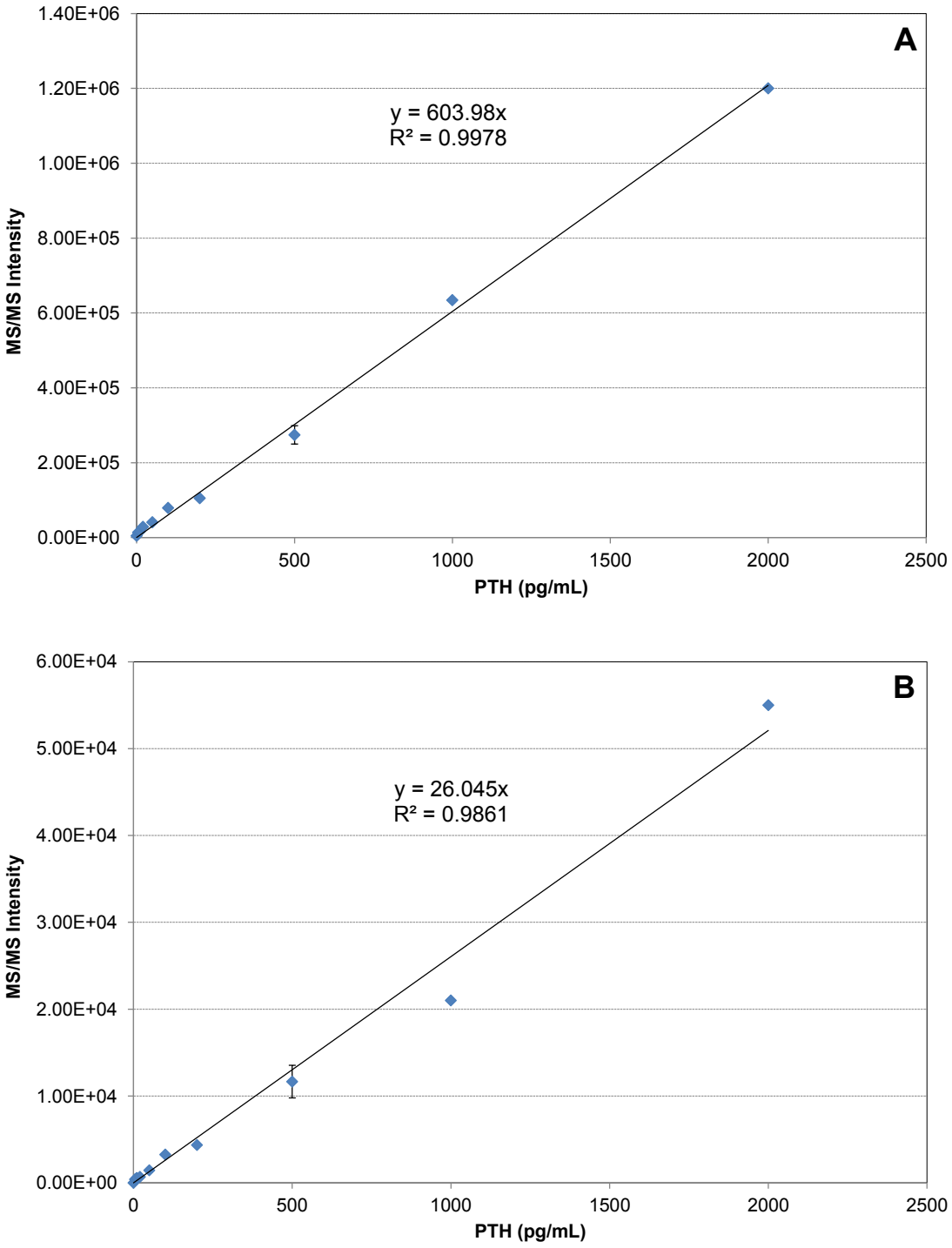

Figure 5.8 Response curves of immuno-LC-MS/MS for PTH 1-84 represented by PTH 1-13 (A) and PTH 14-20 (B). The x-axis is the initial concentration of PTH in the sample and the y-axis is the monitored fragment ion (y_{11}^{2+} for PTH 1-13 and y_5^+ for PTH 14-20) intensity in CID-MS/MS.

5.2.5.3 Quantification of Full Length, Truncated and Oxidized Variants of PTH in Patient Samples

5.2.5.3.1 Data Processing for Immuno-LC-MS/MS

Using the optimized conditions for the immuno-LC-MS/MS assay, a series of patient samples were then analyzed. Figure 5.9 shows the LC-MS/MS raw data for the monitored peptides of interest, which include the tryptic peptides from the PTH in the patient plasma, the ^{15}N labeled peptides from the internal standards ^{15}N_PTH 1-84 and 7-84, and the $^{13}C_6{}^{15}N_1$Leu labeled peptides, from three different patient samples. For each peptide, the ion current of the most abundant product ion was extracted. The most abundant product ions in each case are listed in Table 6.1. Note that all these three patient samples show a large amount of methionine oxidation, which clearly shows the effectiveness of this newly developed assay in quantifying the oxidized variants of PTH.

Figure 5.9 A includes the extracted ion current for PTH 1-13M(2O). This shows that methionine sulfone exists at low abundance, and is less than 5% of the observed methionine sulfoxide in this sample. In other patient samples without significant amount of PTH 1-13M(O), PTH 1-13M(2O) was not even distinguished from the background noise. Similar phenomena were observed for PTH 7-13M(2O) and PTH 14-20M(2O). Therefore, the amount of methionine sulfone present in the biological samples was not significant. Thus there was no need to include methionine sulfone in quantification of oxidized variants of PTH.

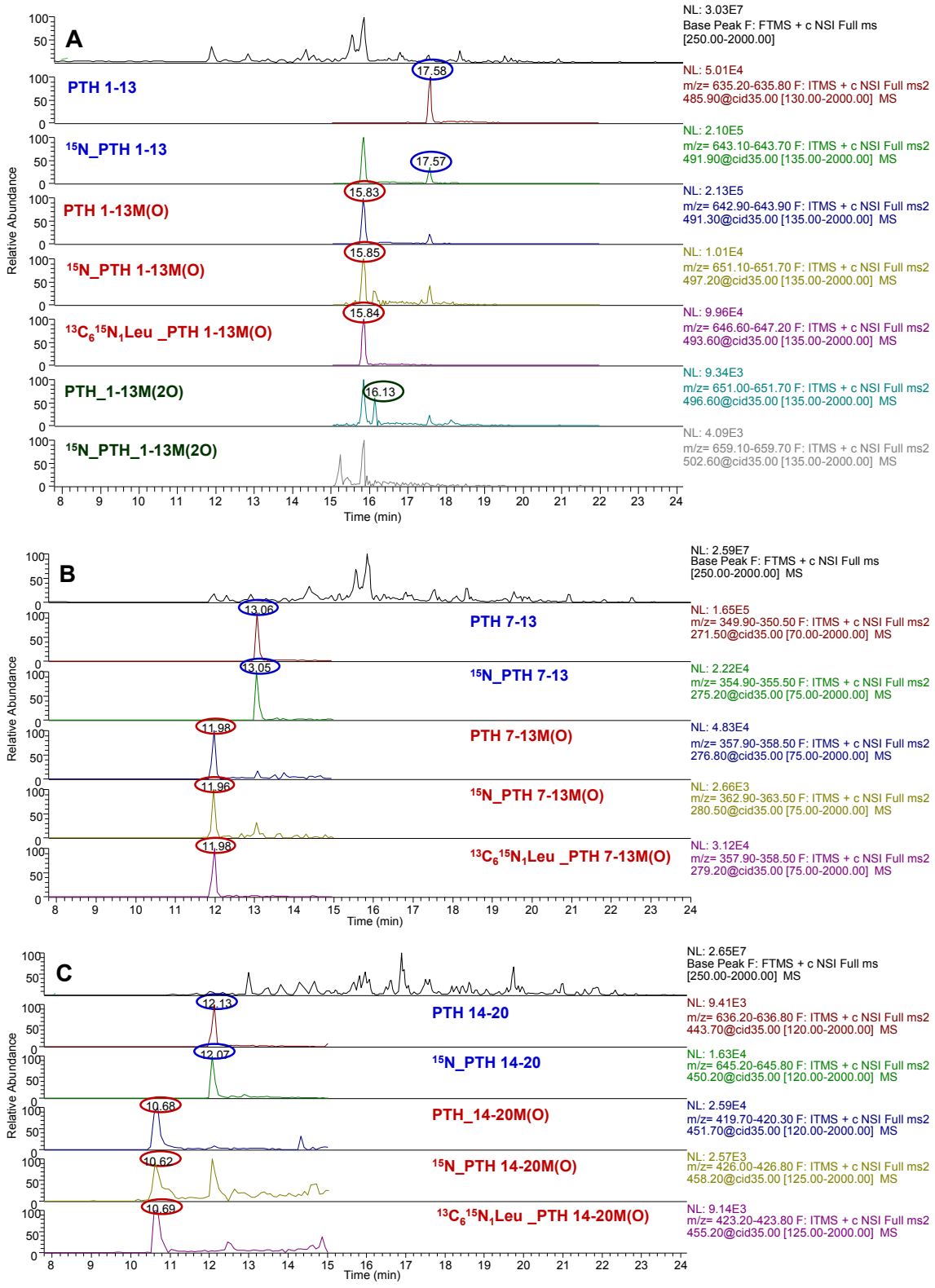

Figure 5.9 LC-MS/MS extracted currents for monitored fragments of PTH 1-13 and PTH 1-13M(O) (A); PTH 7-13 and PTH 7-13M(O) (B); PTH 14-20 (C) and PTH 14-20M(O) (C).

The raw data was processed using the detailed procedures described in 6.7.2 and yielded the PTH concentrations in pg/mL. Examples are shown in Figure 5.10. PTH 1-13 represents the concentration of PTH 1-84, PTH 7-13 represents the concentration of PTH 7-84, and PTH 14-20 represents the sum concentration of PTH 1-84, PTH 7-84 and any other forms of PTH containing residues 14-84. PTH 1-13M(O) represents the concentration of any full length PTH with oxidation at M8 residue, PTH 7-13M(O) represents the concentration of any truncated PTH with oxidation at M8 residue, PTH 14-20M(O) represents the concentration of any full length and truncated PTH with oxidation at M18 residue. The last three columns show results obtained from different second generation PTH assays. Different PTH capture and conjugate antibodies were used in these assays. Interestingly, with a large amount of oxidation present in the sample, the values obtained from the second PTH assays were much lower compared with the levels of PTH detected by immuno-LC-MS/MS assay as shown in Figure 5.10 B. This observance is discussed in more detail below.

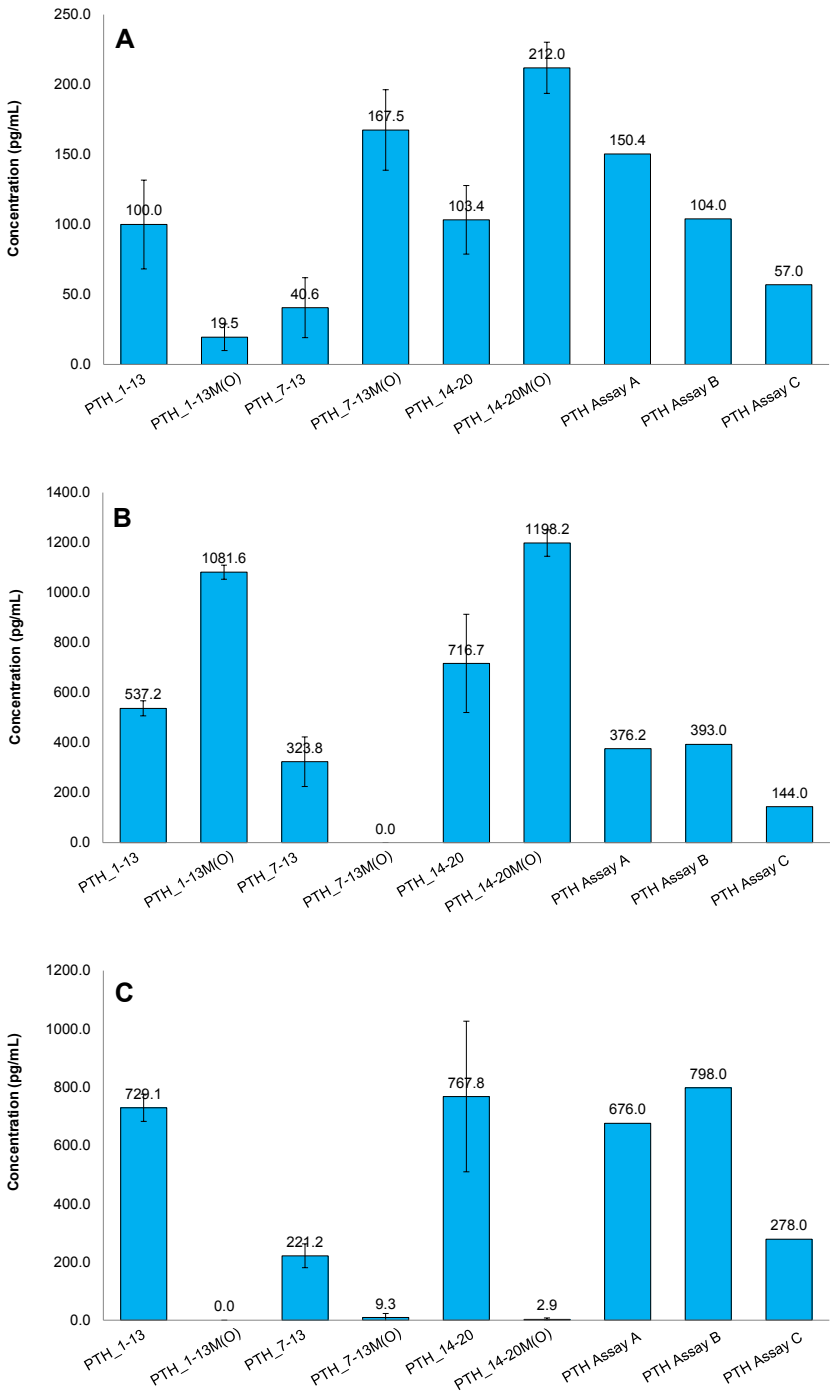

Figure 5.10 Immuno-LC-MS/MS assay results from patient samples

5.2.5.3.2 Recovery Yields of Full Length, Truncated and Oxidized Variants of PTH in Immuno-LC-MS/MS Assay

To evaluate whether different variants of PTH have similar recovery yields in immuno-LC-MS/MS assay, 500 pg of PTH 1-84, 1-84M8(O), 1-84M18(O) and 1-84M8(O)M18(O) were added into the PTH depleted plasma separately along with equivalent amount of ^{15}N labeled PTH 1-84. These samples were then analyzed by the immuno-LC-MS/MS assay. Three peptides that were common to all these variants were monitored and fragmented by CID-MS/MS, *i.e.* PTH 21-25, PTH 53-65 and PTH 66-80. By comparing the intensity of monitored product ions of these three peptides from the PTH variants to those from the ^{15}N labeled PTH 1-84, the relative recovery yield of each variant could be obtained as shown in Figure 5.11. Similarly, 7-84M8(O)M18(O) was compared against ^{15}N labeled PTH 7-84 to yield its relative recovery yield. Generally, there were no apparent differences between oxidized and native forms of PTH 1-84 or PTH 7-84 in terms of recovery. This result was not surprising given that the pmp beads used in this assay were bound with antibody that would interact with the 39-84 residues of PTH. Therefore the changes in the non-binding residues did not affect the binding.

Since there were no significant biases in recovery among different variants of PTH, the overall recovery of the immuno-LC-MS/MS assay was then calculated using PTH 1-84M8(O)M18(O). The intensity of monitored fragments of PTH 1-13M(O) and PTH 14-20M(O) was compared with that of isotopic standard peptides $^{13}C_6{}^{15}N_1$Leu_PTH 1-13M(O) and $^{13}C_6{}^{15}N_1$Leu_PTH 14-20M(O) respectively. The recovery yield was calculated as 66% and was employed for quantifying the oxidized forms of peptides in the assay.

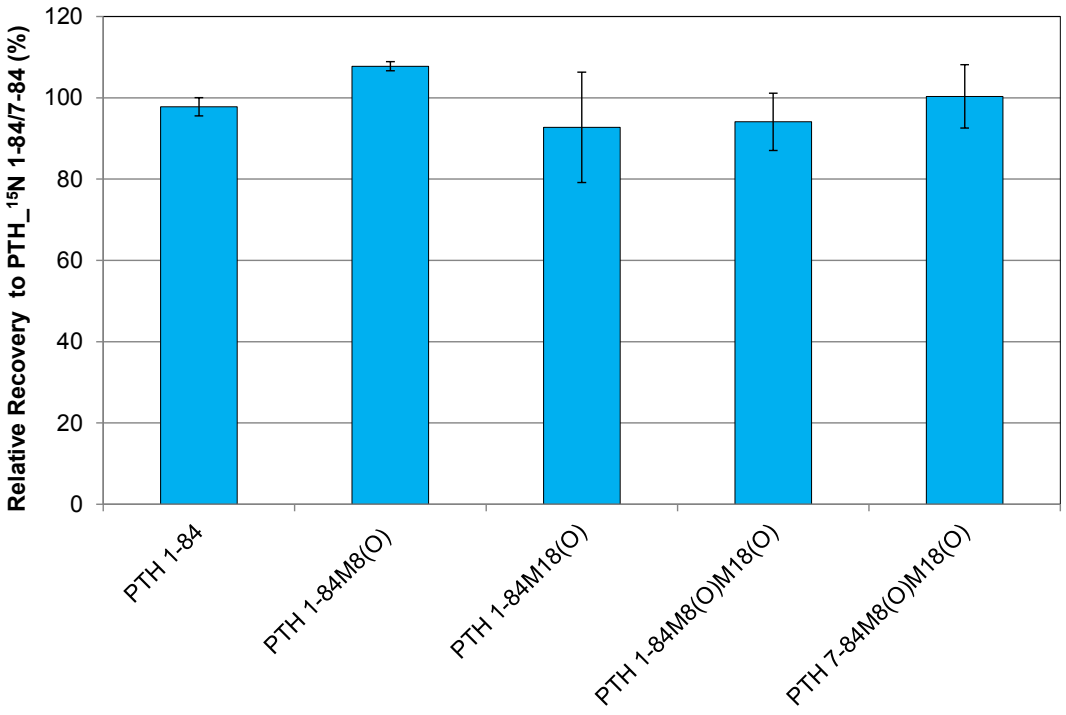

Figure 5.11 The relative recoveries of different variants of PTH in immuno-LC-MS/MS

5.2.5.3.3 *In vivo* versus *in Vitro* Oxidation of PTH

Three sets of clinical samples were analyzed by the assay developed in this study. Plasma was collected from patients that were on dialysis, and provided by DiaSorin Inc.. There were 41 samples from site 1 (samples set A) and 33 samples from site 2 (samples set B and C). The three samples in Figure 5.10 showing significant amount of oxidation were all from set A. Interestingly, samples in set A had more overall oxidation than those from set B and C. As shown in Figure 5.12, only two samples from set B had a percentage of oxidation greater than 11%. The percentage of oxidation was calculated by taking the sum concentration of PTH 1-13M(O), PTH 7-13M(O) and PTH 14-20M(O) divided by the sum concentration of all native and oxidized peptides. The PTH oxidation could come from *in vivo* or *in vitro* oxidation. However, given that the difference in the amount of oxidation was correlated to the sites where the samples were collected, the extensive oxidation observed in sample set A was probably introduced during the on-site sample handling process, i. e. most of the oxidation in set A was due to *in vitro* oxidation.

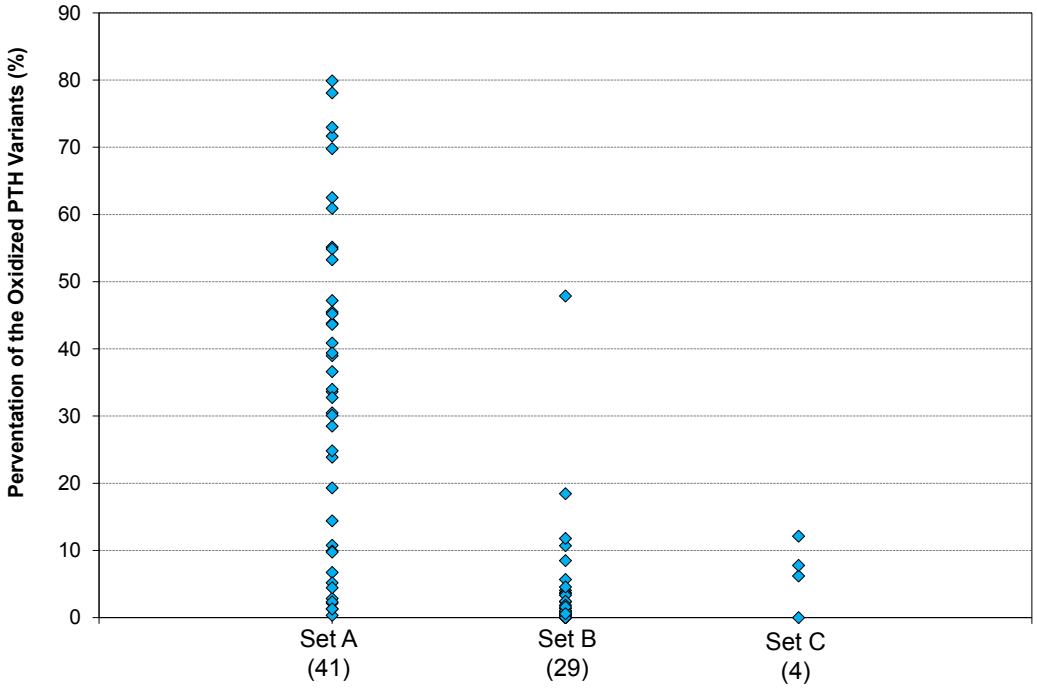

Figure 5.12 Oxidation of PTH in different sets of patient samples. The percentage of oxidation was calculated by taking the sum concentration of PTH 1-13M(O), PTH 7-13M(O) and PTH 14-20M(O) divided by the sum concentration of all native and oxidized peptides. There were 41 samples in set A collected from site 1, and 29 samples in set B and 4 samples in set C collected from site 2.

5.2.5.3.4 The Effect of Oxidation on Second Generation PTH Assays

To evaluate the effect of oxidation on the second PTH assays, the percentage of oxidation for 41 samples in set A was plotted against the difference in concentration between the PTH 1-13 value obtained from the immuno-LC-MS/MS assay and that of the second generation assay, as shown in Figure 5.13. The x-axis shows the percentage of oxidation while the y-axis shows the concentration difference, in pg/mL. Only set A samples were chosen for this evaluation because samples in the other two sets did not show a significant amount of oxidation. Additionally, evaluation within one set of samples excluded any other interferences. As the second generation assays were aiming to detect the biologically active form of PTH 1-84, PTH 1-13 representing PTH 1-84 in the immuno-LC-MS/MS assay was chosen for the evaluation. When less than 30% oxidation was present, the results from assay C had a reasonable good correlation with the immuno-LC-MS/MS results. On the other hand, the amount of PTH 1-84 tended to be overrepresented by assays A and B compared to the immuno-LC-MS/MS results. The reason could be that in the secondary PTH assays, the C-terminal specific antibody anchored to the beads were able to capture all forms of PTH and their N-terminal specific antibodies were not specific enough to only recognize the PTH 1-84.Therefore the results from assay A and B were higher than their real values. Assay C used a N-terminal specific antibody that was against the 1-6th residues of the PTH 1-84, which was believed to be more specific to PTH 1-84 than the N-terminal specific antibodies used by assay B and C. This could explain why assay C had closer match with immuno-LC-MS/MS results when no significant amount of oxidation was present. However, with greater than 30% of oxidation present, the amount of PTH 1-84 tended to be

underrepresented by assay A, B and C. This might be due to that high amount of oxidized variants of PTH may compete with the native form of PTH to bind with the conjugate antibodies occupying the sites which the native form of PTH should have bound to. If the oxidized variants of PTH are not binding to the conjugate antibodies firmly, which are then washed off after incubation, less amount of PTH 1-84 would be detected.

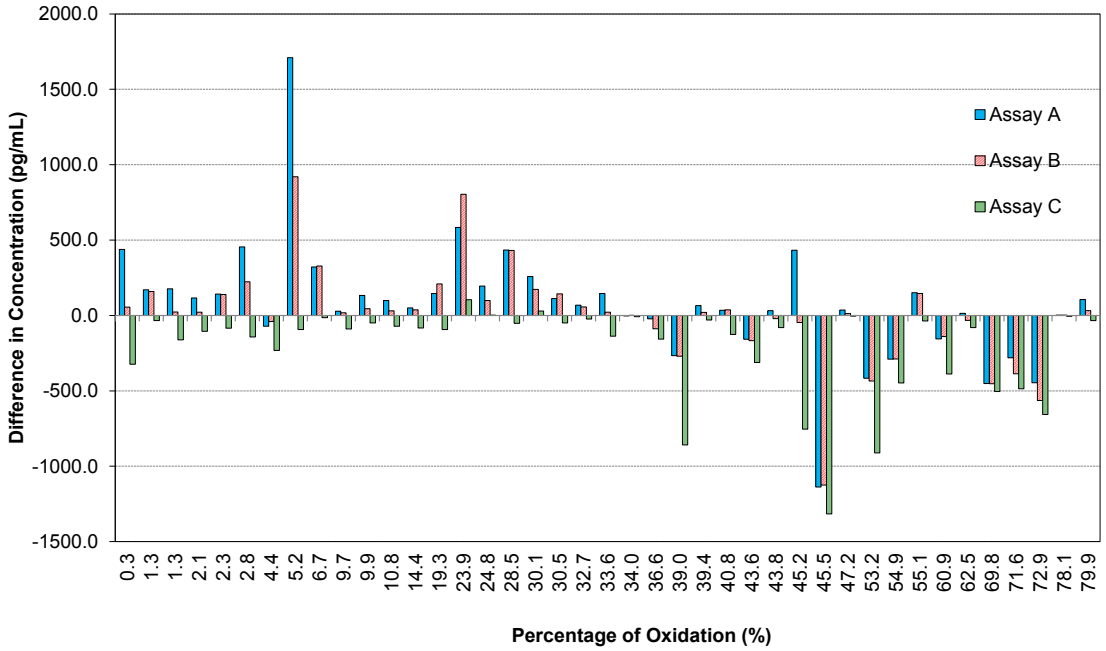

Figure 5.13 The effect of oxidation on the PTH detection of traditional PTH assays. X-axis shows the percentage of oxidation while the y-axis shows the concentration differences in pg/mL. The percentage of oxidation was calculated by taking sum concentration of PTH 1-13M(O), PTH 7-13M(O) and PTH 14-20M(O) divided by the sum concentration of all native and oxidized peptides. The concentration difference was calculated by subtracting the concentration of PTH 1-13 obtained in the immuno-LC-MS/MS assay from the detected PTH concentration in the traditional assay.

5.3 Conclusions

Oxidation at methionine 8 and 18 residues of PTH sequence are known to alter the activity of PTH. In this chapter, the oxidation profiles of both full length and truncated PTH were investigated. Both “bottom-up” approach and “top-down” approach were employed for characterizing and quantifying oxidized variants from *in vitro* oxidation of PTH. The results showed that the M8 residue was more accessible for oxidation than M18. Furthermore, PTH 7-84 was more easily oxidized than PTH 1-84. No forms of PTH containing methionine sulfone were found upon oxidation of PTH 1-84, and only small percentages observed upon oxidation of PTH 7-84. Oxidized variants of PTH can be separated by off-line HPLC and characterized by ESI-MS and CID-MS/MS.

An immuno-LC-MS/MS assay enabling simultaneous detection and quantification of native and oxidized variants of PTH was developed. Different heavy isotope-labeled standards were employed for accurate quantitative analysis of PTH. Immuno-LC-MS/MS assay of clinical samples collected from different sites showed very different results in terms of percentage of oxidation. Samples with significant amount of PTH oxidation were all from one site, suggesting that oxidation is likely due to variance in sample handling processes. Analysis of more samples from other sites would be helpful to confirm this conclusion. Results from immuno-LC-MS/MS assay and second generation assays for analyzing samples with oxidized variants of PTH were compared. Second generation assays tended to underreport the intact PTH concentration when oxidized PTH variants present in the sample were greater than 30%. To evaluate the direct effect of oxidation on second generation assays, each of the pure oxidized forms of PTH should be added to PTH depleted plasma in known concentration and subjected

to analysis by second generation assays. The readings from these assays can then be compared with the real concentrations to determine their cross reactivity with oxidized variants of PTH.

CHAPTER SIX

Experimental Methods for Chapter Five

6.1 Materials

N-α-Fmoc protected amino acid building blocks with acid-labile orthogonal side-chain protection, where appropriate, were purchased from EMD Biosciences (Darmstadt, Germany) and are listed in Table 4.1. N-α-Fmoc-L- methionine-DL-sulfoxide and preloaded Wang-resins were also purchased from EMD Bioscience. N-α-Fmoc-L-Leucine (U-$^{13}C_6$, 97-99%; ^{15}N, 97-99%) was purchased from Cambridge Isotope Laboratories. Inc (Tewksbury, MA). Reagent grade O-(Benzotriazol-1-yl)-N,N,N',N'-tetramethyluronium tetrafluoroborate (TBTU) and N-Hydroxybenzotriazole (HOBt) were from Peptides International (Louisville, KY). N,N-diisopropylethylamine (DIPEA, biotech grade), triisopropylsilane (99%), DL-dithiothreitol (98%) ammonium bicarbonate (reagent grade), Dulbecco's Phosphate Buffered Saline (PBS, power), tris(hydroxymethyl)aminomethane hydrochloride (Tris•HCl), and water (H_2O, HPLC grade) were purchased from Sigma Aldrich (St. Louis, MO). Dichloromethane (DCM, 99.5%), acetic acid (99.7%) and acetic anhydride (97%) were from Mallinckrodt Chemicals (Phillipsburg, NJ). Dimethylformamide (DMF, 99.8%) was purchased from Jade Scientific (Canton, MI) and further dried with 4Å molecular sieves. Hydrogen Peroxide (H_2O_2, % wt: 30% in water) was from Fisher Scientific (Fair Lawn, NJ). Trifluoroacetic acid (TFA, LC grade) was from Thermo Scientific (San Jose, CA). Formic acid (FA, 96%) was purchased from Spectrum Chemical (Gardena, CA). Methanol (99.8%) was from VWR BDH chemicals (West Chester, PA). Acetonitrile (ACN, HPLC grade) and diethyl ether (99.9%) were purchased from EMD Chemicals (Gibbstown,

NJ). Glu-C (sequence grade), Arg-C (sequence grade) and Trypsin (sequence grade) used for enzymatic digestion were purchased from Promega Corporation (Madison, WI). ^{15}N labeled recombinant human parathyroid hormone (PTH) 1-84 and 7-84 were purchased from Cell Sciences (Canton, MA). Recombinant human PTH 1-84 and 7-84 were purchased from ProSpec (East Brunswick, NJ). World health organization (WHO) international standard human recombinant PTH 1-84 was from National Institute for Biological Standards and Control (NIBSC, Potters Bar, UK). Pmp beads were prepared in house at DiaSorin (Stillwater, MN) from Dynabeads® Magnetic Beads (Life Technologies, Grand Island, NY) coated with a goat anti-PTH (39-84) antibody. All other reagents were commercially available and used without further purification.

6.2 Isotope-labeled Peptides

$^{13}C_6{}^{15}N_1$Leu labeled SVSEIQ<u>L</u>M(O)HNLGK, H<u>L</u>NSM(O)ER, and <u>L</u>M(O)HNLGK peptides (underlined Leu was isotope labeled) were prepared in house by Fmoc-based solid-phase peptide synthesis on an automated peptide synthesizer, as described in detail the following sections.

6.2.1 Fmoc Solid-Phase Peptide Synthesis (SPPS)

6.2.1.1 Apparatuses

All peptides were synthesized using an Intavis model ResPep SL automated peptide synthesizer (Koeln, Germany). 2.5 µmol scale synthesis was performed in a 96 well plate with a glass fiber filter in each well.

6.2.1.2 Synthesis

Generally, peptide synthesis was completed at a 2.5 µmol scale. The N-α-Fmoc protected *C*-terminal residue was bound to the Wang-resin and was swelled in DMF

(200 µL) for 15 min with continuous mixing, then washed with 4 x 600 µL DMF. *C*-terminal elongation of the peptide was completed via repetitive Fmoc deprotection and amino acid coupling until the target peptide sequence was achieved. Following the synthesis, cleavage of peptides from the resin and acid-labile orthogonal protecting groups was performed. All solutions used by the peptide synthesizer were pre-made before the synthesis and kept under room temperature during the synthesis. The procedures of Fmoc deprotection, amino acid coupling, resin cleavage and deprotection of acid-labile orthogonal protecting groups are the same as those described in chapter four, section 4.2.1.2. Instead of using normal N-α-Fmoc-L-Leucine, N-α-Fmoc-L-Leucine (U-$^{13}C_6$, 97-99%; ^{15}N, 97-99%) was incorporated into the peptide sequences. The residue that was isotope-labeled in underlined in the sequences.

6.2.1.3 Peptide Purification

The synthetic $^{13}C_6{}^{15}N_1$Leu labeled peptides SVSEIQ<u>L</u>M(O)HNLGK, H<u>L</u>NSM(O)ER, and <u>L</u>M(O)HNLGK were purified by Reversed Phase-High Performance Liquid Chromatography (RP-HPLC) (Shimadzu, model LC-20AB, Columbia, MD) using a Vydac Protein and Peptide C18 column (150 mm x 10 mm, 10 µm) (Grace Davison Discovery Sciences, Hesperia, CA). Peptides were eluted at 4 mL/min with UV detection at 215 nm using a 60 min linear gradient from 0-100% B (Solvent A: 0.1% (aq) TFA and solvent B: 0.089% (aq) TFA with 60% ACN). The retention times for SVSEIQ<u>L</u>M(O)HNLGK, H<u>L</u>NSM(O)ER and <u>L</u>M(O)HNLGK were 20.25 min, 9.25 min and 11.75 min respectively.

6.3 Comparison of Different Proteolytic Enzymes for PTH Digestion

6.3.1 Trypsin Digestion

500 ng WHO_PTH 1-84 was dissolved in 47.5 µL 10 mM NH_4HCO_3. 500 ng of trypsin in 2 µL water was added into the solution which was then incubated at 37^{0}C for 4 h. The digestion was quenched by adding 0.5 µL acetic acid. The digested sample was then diluted to a concentration of 50 nM using 0.1% FA in H_2O and 2 µL was injected for LC-MS/MS analysis.

6.3.2 Glu-C Digestion

500 ng WHO_PTH1-84 was dissolved in 44.5 µL PBS buffer. 500 ng of Glu-C in 5 µL water was added into the solution which was then incubated at 37^{0}C for 4 h. The digestion was quenched by adding 0.5 µL acetic acid. The digested sample was then diluted to a concentration of 50 nM using 0.1% FA in H_2O and 2 µL was injected for LC-MS/MS analysis.

6.3.3 Arg-C Digestion

500 ng WHO_PTH 1-84 was dissolved in 39.5 µL 10 mM NH_4HCO_3. 500 ng of Arg-C in 5 µL Tris-HCl buffer and 5 µL activation buffer (50 mM DTT in 10 mM NH_4HCO_3) were added into the solution which was then incubated at 37^{0}C for 4 h. The digestion was quenched by adding 0.5 µL acetic acid. The digested sample was finally diluted to a concentration of 50 nM using 0.1% FA in H_2O and 2 µL was injected for LC-MS/MS analysis for LC-MS/MS analysis.

6.4 Oxidation Profiles of PTH

6.4.1 *In Vitro* Oxidation of WHO_PTH 1-84 and ^{15}N_PTH 7-84

10 µg of WHO_PTH 1-84 and 10 µg of ^{15}N_PTH 7-84 were dissolved in 100 µl PBS buffer. Then 5 µL of 250 mM of H_2O_2 was added to the solution resulting in a H_2O_2 concentration of 12 mM. 9.5 µL of the solution was drawn out before adding 250 mM of

H_2O_2 as control for 0 min oxidation. The solution was incubated at 37 ^{0}C. At 15 min, 30 min, 1 h, 2 h, 4 h, 8 h and 24 h, 10 µL of the solution was drawn out and quenched by adding 2 µL 31.25 µg/ml catalase in PBS buffer. After incubating for 5 min at room temperature to make sure that the catalytic reaction went to completion, each of the samples was dried down under vacuum for 40 min using a Savant Savant SpeedVac concentrator (Thermo Fisher Scientific, San Jose, CA).

6.4.2 *In Vitro* Intensive Oxidation of ProSpec_PTH 1-84

Each of 5 aliquots of ProSpec_PTH 1-84 (1 µg) was dissolved in 10 µl PBS buffer. 0.5 µL of 250 mM H_2O_2, 10 µL of 333 M H_2O_2, 10 µL of 1.67 M H_2O_2 and 10 µL of 10 M H_2O_2 were added to 4 of the aliquots, respectively. The 4 aliquots, with final H_2O_2 concentrations of 12 mM, 167mM, 833 mM and 5 M, were incubated at 37 ^{0}C for 2 h. Finally, all 5 aliquots were then freeze dried for 3 h.

6.4.3 Glu-C Digestion of Oxidized PTH

In the dried down samples containing oxidized PTH, 48.5 µL of PBS and 100 ng Glu-C dissolved in 1 µL of water were added. The solutions were then incubated at 37 ^{0}C for 4 h and quenched by adding 0.5 µL acetic acid. The digested samples were diluted to a concentration of 100 nM using 0.1% FA in H_2O prior to LC-MS analysis.

6.5 Preparation and Purification of Oxidized Variants of PTH

6.5.1 Oxidation of ProSpec_ PTH 1-84 and ProSpec_PTH 7-84

4×2 mg of ProSpec_PTH 1-84 or PTH 7-84 were dissolved in 800 µl PBS buffer. 40 µL of 250 mM of H_2O_2 was then added to the solution, which made the final concentration of H_2O_2 12 mM. After incubating at 37 ^{0}C for 1 h (30 min for 7-84), the oxidation was quenched by adding 160 µL of 31.25 µg/ml catalase in PBS buffer. The

above solution was incubated for 5 min at room temperature to make sure that the catalytic reaction went to completion. The solution was finally introduced to off-line HPLC for purification of different oxidized variants.

6.5.2 Purification of Oxidized ProSpec_PTH Variants

The products, PTH M8(O)M18(O), PTH M8(O), PTH M18(O) and PTH from oxidation of ProSpec_PTH were purified via RP-HPLC (Shimadzu, model LC-20AB, Columbia, MD) using a Vydac Protein and Peptide C18 column (150 mm x 10 mm, 10 µm) (Grace Davison Discovery Sciences, Hesperia, CA). The PTH 1-84 oxidized mixtures were eluted at 4 mL/min with UV detection at 215 nm using the following gradient elution conditions: 0-5 min, 0-30% solvent B; 5-65 min, 30-65% solvent B (Solvent A: 0.1% (aq) TFA; solvent B: 0.089% (aq) TFA with 60% ACN). The retention times for PTH 1-84M8(O)M18(O), PTH 1-84M18(O), PTH 1-84M8(O) and PTH 1-84 were 37.8 min, 40.0 min, 42.5 min and 44.6 min respectively. The PTH 7-84 oxidized mixtures were eluted using the following gradient elution conditions: 0-5 min, 0-45% solvent B; 5-65 min, 45-50% solvent B. The retention times for PTH 7-84M8(O)M18(O), PTH 7-84M18(O), PTH 7-84M8(O) and PTH 7-84 were 33.9 min, 36.3 min, 37.8 min and 41.1 min.

6.6 Quantification of the ^{15}N_PTH and PTH Variants

6.6.1 Trypsin Digestion of WHO_PTH and ^{15}N_PTH

Two aliquots of 500 ng WHO_PTH dissolved in 2 µL water were prepared. 500 ng ^{15}N_PTH 1-84 (based on the values provided by the vendor) in 2 µL water and 500 ng ^{15}N_PTH 7-84 (based on the values provided by the vendor) in 2 µL water were added into each WHO-PTH aliquot separately. In each sample, 43.5 µL 10 mM

NH_4HCO_3, 500 ng of trypsin in 2 µL water were added, which were then incubated at 37^0C for 4 h. The digestions were quenched by adding 0.5 µL acetic acid. The digested samples were finally diluted to a concentration of 100 nM using 0.1% TFA / 2% ACN in H_2O and 4 µL was injected for LC-MS/MS analysis.

6.6.2 Trypsin Digestion of ^{15}N_PTH and PTH Variants

500 ng PTH 1-84, PTH 1-84M8(O) PTH 1-84M18(O) and PTH 1-84M8(O)M18(O) (purified by off-line HPLC and weighed), were dissolved in 47.5 µL 10 mM NH_4HCO_3 individually along with 500 ng ^{15}N_PTH 1-84 (corrected amount by referencing to WHO_PTH 1-84). 500 ng of trypsin in 2 µL water was added into each solution then incubated at 37^0C for 4 h. The digestions were quenched by adding 0.5 µL acetic acid. The digested samples were finally diluted to a concentration of 100 nM using 0.1% TFA / 2% ACN in H_2O and added each isotope labeled PTH peptide $^{13}C_6{}^{15}N_1$Leu_PTH 1-13M(O), $^{13}C_6{}^{15}N_1$Leu_PTH 7-13M(O) and $^{13}C_6{}^{15}N_1$Leu_PTH 14-20M(O were added to a concentration of 100 nM, and 4 µL was injected for LC-MS/MS analysis. (PTH 7-84, PTH 7-84M8(O) PTH 7-84M18(O) and PTH 7-84M8(O)M18(O) were also processed using the above procedure with ^{15}N_PTH 7-84 added as reference).

6.7 Immuno-LC-MS/MS Assay for PTH

6.7.1 Immuno-affinity Enrichment of PTH in Plasmas

20 µL containing 500 pg each of 25 pg/µL ^{15}N PTH 1-84 and ^{15}N PTH 7-84 (corrected amount by referencing to WHO_PTH 1-84) in PTH depleted plasma were added to each plasma sample. 350 µg (50 µL) pmp beads were then added into the patient plasma and incubated at room temperature for with gentle rotation. Plasma was then removed using a DynaMag™-2 Magnet (Life Technologies, Grand Island, NY) to

capture the pmp beads. Following washes with 1 mL PBS, 1 mL 35% ACN and 1 mL PBS, 10 min each with gentle rotation, a final wash with 1 mL of 10 mM NH_4HCO_3 was performed. Bound PTH was then eluted with 100 µL 3.5% ACN / 0.9% FA after 10 min incubation with gentle rotation. The eluent was dried down under vacuum for 2 h using a Savant SpeedVac concentrator.

6.7.2 Recovery Yields of PTH Variants in Immuno-LC-MS/MS

500 pg PTH 1-84, PTH 1-84M8(O) PTH 1-84M18(O) and PTH 1-84M8(O)M18(O) (corrected amount by referencing to ^{15}N_PTH 1-84), were added into PTH depleted plasma individually along with 500 pg ^{15}N_ PTH 1-84. 350 µg (50 µL) pmp beads were then added into each plasma sample which then incubated at room temperature for 1 h. The plasma was then removed using a DynaMag™-2 Magnet. Following washes with 1 mL PBS, 1 mL 35% ACN and 1 mL PBS, 10 min each, a final wash with 1 mL of 10 mM NH_4HCO_3 was performed. Bound PTH was eluted with 100 µL 3.5% ACN / 0.9% FA after 10 min incubation with gentle rotation. The eluents were dried down under vacuum for 2 h using a Savant SpeedVac concentrator

6.7.3 Trypsin Digestion of Enriched PTH by Immuno-affinity Approach

In the dried down samples containing eluted PTH, 47.5 µL of 10 mM NH_4HCO_3 and 500 ng trypsin dissolved in 2 µL of water were added. The solutions were incubated at 37 ^0C for 4 h, and the digestion was quenched by adding 0.5 µL acetic acid. Following the addition of 3 µL of 17.67 nM isotope labeled PTH peptides ($^{13}C_6{}^{15}N_1$Leu_PTH 1-13M(O), $^{13}C_6{}^{15}N_1$Leu_PTH 7-13M(O) and $^{13}C_6{}^{15}N_1$Leu_PTH 14-20M(O)) mixture, 0.5 µL of 10% TFA and 1 µL of ACN, the digested samples were dried down under vacuum for 2 h using a Savant SpeedVac concentrator. The dried

down digests were finally reconstituted in 53 µL 0.1% TFA / 2% ACN in H_2O and 5 µL was injected for LC-MS/MS analysis.

6.8 Mass Spectrometry

6.8.1 ESI-MS and CID-MS/MS Analysis of $^{13}C_6{}^{15}N_1$Leu Labeled Peptides and Purified Oxidized PTH Variants

$^{13}C_6{}^{15}N_1$Leu labeled peptides and purified oxidized PTH variants were analyzed using a Thermo Scientific LTQ Orbitrap Velos Mass Spectrometer (San Jose, CA) equipped with an Advion BioSciences Triversa Nanomate nESI source (Ithaca, NY). External calibration of the instruments was performed using standard Thermo calibration mixtures. For nESI analysis, 10 µL of the sample solution was loaded for infusion by the Nanomate. The spray voltage was maintained at 1.4 kV and gas pressure was 0.3 psi. The temperature of the ion transfer tube was set at 250 °C. The S-lens of the LTQ Orbitrap Velos was set to 57%. The LTQ Orbitrap Velos MS and MS/MS spectra were acquired at resolution power of 60,000. CID-MS/MS was performed on selected precursor ions used standard excitation conditions (q=0.25, activation time=10 ms, normalized collision energy ((NCE)=35%). Isolation widths for $^{13}C_6{}^{15}N_1$Leu labeled peptides and purified oxidized PTH variants protonated precursor ions were m/z 2.5 and 2.0, respectively. Full scans were taken at an AGC target value 1.0×10^6 and 100 ms maximum injection time in MS. CID-MS/MS scans were taken at an AGC target value 5.0×10^4 and 300 ms maximum injection time. All spectra shown were typically averaged over 50 scans.

6.8.2 LC-ESI-MS and LC-ESI-MS/MS Analysis of PTH Digests in Immuno-LC-MS/MS Assay

LC-ESI-MS and CID-MS/MS analyses were performed using a Thermo Scientific LTQ Orbitrap Velos mass spectrometer coupled to an Advance nESI source and Agilent 1260 Infinity Binary LC System (Agilent Technologies, Santa Clara, CA). Analyses were performed using automated methods created by the Xcalibur software (Thermo Fisher Scientific, San Jose, CA). 2-5 µL of each sample with various concentrations (refer to sample preparation sections for individual concentrations and volumes) in 0.1% FA or 0.1% TFA / 2% ACN in H_2O were loaded using 1260 Infinity High Performance Micro Autosampler (Agilent Technologies, Santa Clara, CA) onto a Peptide Opti-trap Cap (0.5 mm x 1.3 mm, Optimize Technologies, Oregon City, OR) at a flow rate at 2 µL/min using 0.1% FA / 2% ACN in H_2O as the loading buffer. After 5 min loading time, the peptides concentrated on the trap were eluted onto a fused silica capillary column packed with Magic C18AQ (3 µm, 200 Å, 0.2 mm I.D. x 50 mm in length, Bruker, Billerica, MA) at a flow rate of 2 µL/min using a linear 20 min gradient from 2% to 60% solvent B (Solvent A: 0.1% FA in H_2O; solvent B: 0.1% FA in ACN). After gradient separation, the system was cleaned with 90% solvent B for 6 min followed by equilibrium with 98% solvent A for 8 min.

The spray voltage of the LTQ Orbitrap Velos mass spectrometer was maintained at 1.7 kV. The ion transfer tube of the mass spectrometer was set at 200 °C, and the S-lens is set at 57%. The full MS scans were acquired at m/z 250 - 2000 for tryptic PTH peptides and m/z 300 – 2000 for Glu-C digested PTH peptides at a power resolving 60,000. Full scans were taken at an AGC target value 1.0×10^6 and with 300 ms maximum injection time in FT. CID-MS/MS scans were taken at AGC target value 1.0×10^4 and 100 ms maximum injection time in the ion trap. All spectra were recorded in

centroid mode. The mass spectrometer was programmed to operate with an inclusion list containing the m/z values of tryptic PTH peptide precursor ions in Table 6.1. In studying the recovery yields of PTH variants, PTH 21-25 ($[M+2H]^{2+}$, m/z 351.70), ^{15}N_PTH 21-25 ($[M+2H]^{2+}$, m/z 356.69), PTH 53-65 ($[M+3H]^{3+}$, m/z 518.94), ^{15}N_PTH 53-65 ($[M+3H]^{3+}$, m/z 526.26), PTH 66-80 ($[M+3H]^{3+}$, m/z 520.61) and ^{15}N_PTH 66-80 ($[M+3H]^{3+}$, m/z 526.60) were also added to the inclusion list. For CID-MS/MS analysis, these precursor ions in the survey MS scan were selectively isolated with an isolation window of m/z 2.5. The isolated ions were fragmented with standard excitation conditions (q=0.25, activation time=10 ms, NCE=35%).

Table 6.1 Tryptic PTH peptide 'inclusion list' precursor ions, retention times and 'targeted' CID-MS/MS product ions.

PTH Peptide Precursor Ion	PTH Peptide Sequence	Inclusion List Window (Retention Time)	Precursor ion m/z			Monitored Most Abundant MS/MS Fragment Ion		
			Native	^{15}N	$^{13}C_6{}^{15}N_1$Leu	Native	^{15}N	$^{13}C_6{}^{15}N_1$Leu
PTH 1-13 $[M+3H]^{3+}$	SVSEIQLMHNLGK	15.01-20.00 min (17.6 min)	485.93	491.91	488.26	y_{11}^{2+} 635.34	y_{11}^{2+} 643.34	y_{11}^{2+} 638.84
PTH 1-13M(O) $[M+3H]^{3+}$	SVSEIQLM(O)HNLGK	15.01-20.00 min (15.8 min)	491.26	497.24	493.60	y_{11}^{2+} 643.34	y_{11}^{2+} 651.34	y_{11}^{2+} 646.84
PTH 1-13M(2O)[1] $[M+3H]^{3+}$	SVSEIQLM(2O)HNLGK	15.01-20.00 min (16.1 min)	496.59	502.57	498.93	y_{11}^{2+} 651.34	y_{11}^{2+} 659.34	y_{11}^{2+} 654.84
PTH 14-20 $[M+2H]^{2+}$	HLNSMER	8.00-15.00 min (12.1 min)	443.71	450.19	447.22	y_5^{+} 636.27	y_5^{+} 645.27	y_5^{+} 636.27
PTH 14-20M(O) $[M+2H]^{2+}$	HLNSM(O)ER	8.01-15.00 min (10.7 min)	451.71	458.19	455.22	$-CH_3SOH^{2+}$ 419.72	$-CH_3SOH^{2+}$ 426.22	$-CH_3SOH^{2+}$ 423.22
PTH 14-20M(2O) $[M+2H]^{2+}$	HLNSM(2O)ER	8.01-15.00 min (10.9 min)	459.71	466.19	463.22	y_5^{+} 668.27	y_5^{+} 677.27	y_5^{+} 668.27
PTH 7-13M $[M+3H]^{3+}$	LMHNLGK	8.01-15.00 min (13.1 min)	271.49	275.14	273.83	y_6^{2+} 350.18	y_6^{2+} 355.18	y_6^{2+} 350.18
PTH 7-13M(O) $[M+3H]^{3+}$	LM(O)HNLGK	8.01-15.00 min (12.0 min)	276.82	280.47	279.16	y_6^{2+} 358.18	y_6^{2+} 363.18	y_6^{2+} 358.18
PTH 7-13M(2O)[1] $[M+3H]^{3+}$	LM(2O)HNLGK	8.01-15.00 min (12.2 min)	282.15	285.81	284.49	y_6^{2+} 366.18	y_6^{2+} 371.18	y_6^{2+} 366.18

6.9 Data Analysis

6.9.1 *In Vitro* Oxidation Profiles of PTH Methionine Residues

PTH 5-19 from Glu-C digestion of PTH 1-84 was used as the representative peptide for quantification of PTH 1-84 oxidation while PTH 7-19 from Glu-C digestion of PTH 7-84 was used as the representative peptide for quantification of PTH 7-84 oxidation. At each time point of oxidation, the percentage composition of each native or oxidized PTH form was calculated by expressing the MS abundance of quadruply charged corresponding native or oxidized PTH 5-19/7-19 peptide ions as a fraction of the summed MS abundances of all quadruply charged native and oxidized PTH 5-19/7-19 peptide ions.

6.9.2 Determination of the Actual Quantity of ^{15}N_PTH and PTH Variants

PTH 21-25, PTH 53-65 and PTH 66-80 from trypsin digestion of the different variants of PTH were used as representative peptides for determining the actual amount of ^{15}N_PTH and PTH variants referenced to the WHO_PTH 1-84 standard. The MS abundance of each peptide ion was compared with that of the reference sample to yield a relative ratio (PTH 21-25 ($[M+2H]^{2+}$, m/z 351.70), PTH 53-65 ($[M+3H]^{3+}$, m/z 518.94) and PTH 66-80 ($[M+3H]^{3+}$, m/z 520.61) were compared to ^{15}N_PTH 21-25 ($[M+2H]^{2+}$, m/z 356.69), ^{15}N_PTH 53-65 ($[M+3H]^{3+}$, m/z 526.26) and ^{15}N_PTH 66-80 ($[M+3H]^{3+}$, m/z 526.60)). The average ratio of the three peptides was used for calculating the actual amount ^{15}N_PTH and PTH variants in the sample.

6.9.3 Recovery Yields of PTH Variants in Immuno-LC-MS/MS

PTH 21-25, PTH 53-65 and PTH 66-80 from trypsin digestion of the different variants of PTH were used as representative peptides for calculating their relative

recovery yields to ^{15}N_PTH in the immuno-LC-MS/MS assay. The abundances of y_3^+ (m/z 474.28), y_6^+ (m/z 728.36) and y_{13}^{2+} (m/z 680.36) for CID-MS/MS of PTH 21-25, PTH 53-65 and PTH 66-80 peptide ions of each PTH variant were compared to the abundances of y_3^+ (m/z 481.28), y_6^+ (m/z 737.36) and y_{13}^{2+} (m/z 688.36) in CID-MS/MS of ^{15}N_PTH 21-25, ^{15}N_PTH 53-65 and ^{15}N_PTH 66-80 of ^{15}N_PTH 1-84/7-84, respectively, to yield relative recovery ratios. The average ratio of the three peptides was used for calculating the relative recovery ratio of each PTH variant.

The overall recovery yield of the immuno-LC-MS/MS assay was calculated using PTH 1-84M8(O)M18(O). The abundance of monitored fragments of PTH 1-13M(O) and PTH 14-20M(O) was compared with that of isotopic standard peptides $^{13}C_6{}^{15}N_1$Leu_PTH 1-13M(O) and $^{13}C_6{}^{15}N_1$Leu_PTH 14-20M(O), respectively, to yield the assay recovery yield. The recovery yield obtained was 66% and was employed for quantifying PTH oxidized variants in the assay.

6.9.4 Quantification of PTH Native and Oxidized Variants in Patient Plasma

PTH 1-13, 1-13M(O) and 1-13M(2O) from trypsin digestion of PTH 1-84 and its oxidized variants were used as the representative peptides for quantification of PTH 1-84 and its oxidized variants while PTH 7-13, 7-13M(O) and 7-13M(2O) from trypsin digestion of PTH 7-84 and its oxidized variants were used as the representative peptides for quantification of PTH 7-84 and its oxidized variants. PTH 14-20, 14-20M(O) and 14-20M(2O) from trypsin digestion of PTH 1-84 or PTH 7-84 and its oxidized variants were used as the representative peptides for quantification of both PTH 1-84 and PTH 7-84 and their oxidized variants. Other variants of PTH might exist in the sample but were not included for quantification in this method.

Ion abundances of monitored fragments in CID-MS/MS of the unlabeled (*i.e.*, sample) and ^{15}N labeled PTH 1-13, 7-13 and 14-20 peptides were extracted. The monitored fragments for each peptide in CID-MS/MS are recorded in Table 6.1. The ratio of unlabeled/ ^{15}N-labeled was calculated, then multiplied by 500 pg (multiplied by 1000 pg for the 14-20 peptide) and divided by the patient sample volume to yield sample concentration (pg/mL).

For the oxidized peptides, ion abundances of monitored fragments in CID-MS/MS of the unlabeled (*i.e.*, sample) and ^{15}N-labeled PTH 1-13M(O), 7-13M(O) and 14-20M(O) peptides, and the isotope labeled $^{13}C_6{}^{15}N_1$Leu_1-13M(O), $^{13}C_6{}^{15}N_1$Leu_7-13M(O) and $^{13}C_6{}^{15}N_1$Leu_14-20M(O) synthetic peptides, were extracted. The monitored fragments for each peptide in MS/MS are recorded in Table 6.1 The ion abundances of monitored fragments in CID-MS/MS of the unlabeled oxidized peptides were corrected to account for any oxidation occurring during sample handling (determined as the abundance of the unlabeled oxidized peptides - ((^{15}N-labeled(ox) peptide / ^{15}N-labeled(non-oxidized) peptide) x unlabeled (non-oxidized) peptide). Then, the corrected MS/MS ion abundances of the oxidized peptides (*i.e.*, sample) were divided by the abundance of the $^{13}C_6{}^{15}N_1$Leu labeled synthetic peptides, then multiplied by 500 pg and divided by the patient sample volume, then divided by recovery yield (66%) of PTH in immuno-LC-MS/MS assay to yield sample concentration (pg/mL).

BIBLIOGRAPHY

BIBLIOGRAPHY

1. O'Donovan, C., Apweiler, R., Bairoch, A., The human proteomics initiative (HPI). *Trends in Biotechnology* **2001**, 19, 178-181.

2. Thelen, J.J., Miernyk, J.A., The proteomic future: Where mass spectrometry should be taking us. *Biochemical Journal* **2012**, 444, 169-181.

3. Yates, J.R., Ruse, C.I., Nakorchevsky, A., Proteomics by mass spectrometry: Approaches, advances, and applications. *Annual Review of Biomedical Engineering* **2009**, 11, 49-79.

4. Karas, M., Bachmann, D., Hillenkamp, F., Influence of the wavelength in high-irradiance ultraviolet-laser desorption mass-spectrometry of organic-molecules. *Analytical Chemistry* **1985**, 57, 2935-2939.

5. Fenn, J.B., Mann, M., Meng, C.K., Wong, S.F., Whitehouse, C.M., Electrospray Ionization for mass-spectrometry of large biomolecules. *Science* **1989**, 246, 64-71.

6. Aebersold, R., Mann, M., Mass spectrometry-based proteomics. *Nature* **2003**, 422, 198-207.

7. Gygi, S.P., Corthals, G.L., Zhang, Y., Rochon, Y., Aebersold, R., Evaluation of two-dimensional gel electrophoresis-based proteome analysis technology. *Proceedings of the National Academy of Sciences of the United States of America* **2000**, 97, 9390-9395.

8. Vestal, M.L., The future of biological mass spectrometry. *Journal of the American Society for Mass Spectrometry* **2011**, 22, 953-959.

9. Swaney, D.L., Wenger, C.D., Coon, J.J., Value of using multiple proteases for large-scale mass spectrometry-based proteomics. *Journal of Proteome Research* **2010**, 9, 1323-1329.

10. Baud, F., Karlin, S., Measures of residue density in protein structures. *Proceedings of the National Academy of Sciences of the United States of America* **1999**, 96, 12494-12499.

11. Brewis, I.A., Brennan, P., Proteomics technologies for the global identification and quantification of proteins. *Advances in Protein Chemistry and Structural Biology* **2010**, 80, 1-44.

12. Washburn, M.P., Wolters, D., Yates, J.R., 3rd, Large-scale analysis of the yeast proteome by multidimensional protein identification technology. *Nature Biotechnology* **2001**, 19, 242-247.

13. Hernandez-Borges, J., Aturki, Z., Rocco, A., Fanali, S., Recent applications in nanoliquid chromatography. *Journal of Separation Science* **2007**, 30, 1589-1610.

14. Huang, M.Z., Cheng, S.C., Cho, Y.T., Shiea, J., Ambient ionization mass spectrometry: A tutorial. *Analytica Chimica Acta* **2011**, 702, 1-15.

15. Takats, Z., Wiseman, J.M., Gologan, B., Cooks, R.G., Mass spectrometry sampling under ambient conditions with desorption electrospray ionization. *Science* **2004**, 306, 471-473.

16. Monge, M.E., Harris, G.A., Dwivedi, P., Fernandez, F.M., Mass spectrometry: Recent advances in direct open air surface sampling/ionization. *Chemical Reviews* **2013**, 113, 2269-2308.

17. Second, T.P., Blethrow, J.D., Schwartz, J.C., Merrihew, G.E., MacCoss, M.J., Swaney, D.L., Russell, J.D., Coon, J.J., Zabrouskov, V., Dual-pressure linear ion trap mass spectrometer improving the analysis of complex protein mixtures. *Analytical Chemistry* **2009**, 81, 7757-7765.

18. Hu, Q.Z., Noll, R.J., Li, H.Y., Makarov, A., Hardman, M., Cooks, R.G., The Orbitrap: a new mass spectrometer. *Journal of Mass Spectrometry* **2005**, 40, 430-443.

19. Michalski, A., Damoc, E., Lange, O., Denisov, E., Nolting, D., Muller, M., Viner, R., Schwartz, J., Remes, P., Belford, M., Dunyach, J.J., Cox, J., Horning, S., Mann, M., Makarov, A., Ultra high resolution linear ion trap orbitrap mass spectrometer (Orbitrap Elite) facilitates top down LC MS/MS and versatile peptide fragmentation Modes. *Molecular & Cellular Proteomics* **2012**, 11.

20. Michalski, A., Damoc, E., Hauschild, J.P., Lange, O., Wieghaus, A., Makarov, A., Nagaraj, N., Cox, J., Mann, M., Horning, S., Mass spectrometry-based proteomics using Q Exactive, a high-performance benchtop quadrupole orbitrap mass spectrometer. *Molecular & Cellular Proteomics* **2011**, 10.

21. Hebert, A.S., Richards, A.L., Bailey, D.J., Ulbrich, A., Coughlin, E.E., Westphall, M.S., Coon, J.J., The one hour yeast proteome. *Molecular & Cellular Proteomics* **2014**, 13, 339-347.

22. Gu, X., Deng, C., Yan, G., Zhang, X., Capillary array reversed-phase liquid chromatography-based multidimensional separation system coupled with MALDI-TOF-TOF-MS detection for high-throughput proteome analysis. *Journal of Proteome Research* **2006**, 5, 3186-3196.

23. Ko, K.H., Kwon, C.I., Park, S.H., Han, N.Y., Lee, H.K., Kim, E.H., Hahm, K.B., Application of matrix-assisted laser desorption/ionization time-of-flight imaging mass spectrometry (MALDI-TOF IMS) for premalignant gastrointestinal lesions. *Clin Endosc* **2013**, 46, 611-619.

24. Clark, A.E., Kaleta, E.J., Arora, A., Wolk, D.M., Matrix-assisted laser desorption ionization-time of flight mass spectrometry: A fundamental shift in the routine practice of clinical microbiology. *Clinical Microbiology Reviews* **2013**, 26, 547-603.

25. Ginter, J.M., Zhou, F., Johnston, M.V., Generating protein sequence tags by combining cone and conventional collision induced dissociation in a quadrupole time-of-flight mass spectrometer. *Journal of the American Society for Mass Spectrometry* **2004**, 15, 1478-1486.

26. Garcia, B.A., What does the future hold for top down mass spectrometry? *Journal of the American Society for Mass Spectrometry* **2010**, 21, 193-202.

27. Thevis, M., Loo, R.R.O., Loo, J.A., Mass spectrometric characterization of transferrins and their fragments derived by reduction of disulfide bonds. *Journal of the American Society for Mass Spectrometry* **2003**, 14, 635-647.

28. Mortz, E., OConnor, P.B., Roepstorff, P., Kelleher, N.L., Wood, T.D., McLafferty, F.W., Mann, M., Sequence tag identification of intact proteins by matching tandem mass spectral data against sequence data bases. *Proceedings of the National Academy of Sciences of the United States of America* **1996**, 93, 8264-8267.

29. Loo, J.A., Quinn, J.P., Ryu, S.I., Henry, K.D., Senko, M.W., Mclafferty, F.W., High-resolution tandem mass-spectrometry of large biomolecules. *Proceedings of the National Academy of Sciences of the United States of America* **1992**, 89, 286-289.

30. Jones, A.W., Cooper, H.J., Dissociation techniques in mass spectrometry-based proteomics. *Analyst* **2011**, 136, 3419-3429.

31. Ge, Y., Lawhorn, B.G., ElNaggar, M., Strauss, E., Park, J.H., Begley, T.P., McLafferty, F.W., Top down characterization of larger proteins (45 kDa) by electron capture dissociation mass spectrometry. *Journal of the American Chemical Society* **2002**, 124, 672-678.

32. Kelleher, N.L., Lin, H.Y., Valaskovic, G.A., Aaserud, D.J., Fridriksson, E.K., McLafferty, F.W., Top down versus bottom up protein characterization by tandem high-resolution mass spectrometry. *Journal of the American Chemical Society* **1999**, 121, 806-812.

33. Durbin, K.R., Fellers, R.T., Ntai, L., Kelleher, N.L., Compton, P.D., Autopilot: An online data acquisition control system for the enhanced high-throughput characterization of intact proteins. *Analytical Chemistry* **2014**, 86, 1485-1492.

34. Ahlf, D.R., Compton, P.D., Tran, J.C., Early, B.P., Thomas, P.M., Kelleher, N.L., Evaluation of the compact high-field orbitrap for top-down proteomics of human cells. *Journal of Proteome Research* **2012**, 11, 4308-4314.

35. Scigelova, M., Makarov, A., Orbitrap mass analyzer - Overview and applications in proteomics. *Proteomics* **2006**, 6, 16-21.

36. Makarov, A., Denisov, E., Dynamics of ions of intact proteins in the orbitrap mass analyzer. *Journal of the American Society for Mass Spectrometry* **2009**, 20, 1486-1495.

37. Eng, J.K., Mccormack, A.L., Yates, J.R., An approach to correlate tandem mass-spectral data of peptides with amino-acid-sequences in a protein database. *Journal of the American Society for Mass Spectrometry* **1994**, 5, 976-989.

38. Perkins, D.N., Pappin, D.J.C., Creasy, D.M., Cottrell, J.S., Probability-based protein identification by searching sequence databases using mass spectrometry data. *Electrophoresis* **1999**, 20, 3551-3567.

39. Geer, L.Y., Markey, S.P., Kowalak, J.A., Wagner, L., Xu, M., Maynard, D.M., Yang, X.Y., Shi, W.Y., Bryant, S.H., Open mass spectrometry search algorithm. *Journal of Proteome Research* **2004**, 3, 958-964.

40. Craig, R., Beavis, R.C., TANDEM: Matching proteins with tandem mass spectra. *Bioinformatics* **2004**, 20, 1466-1467.

41. Frank, A., Pevzner, P., PepNovo: De novo peptide sequencing via probabilistic network modeling. *Analytical Chemistry* **2005**, 77, 964-973.

42. Ma, B., Zhang, K.Z., Hendrie, C., Liang, C.Z., Li, M., Doherty-Kirby, A., Lajoie, G., PEAKS: powerful software for peptide de novo sequencing by tandem mass spectrometry. *Rapid Communications in Mass Spectrometry* **2003**, 17, 2337-2342.

43. Wells, J.M., McLuckey, S.A., Collision-induced dissociation (CID) of peptides and proteins. *Biological Mass Spectrometry* **2005**, 402, 148-185.

44. Zubarev, R.A., Kelleher, N.L., McLafferty, F.W., Electron capture dissociation of multiply charged protein cations. A nonergodic process. *Journal of the American Chemical Society* **1998**, 120, 3265-3266.

45. Cooper, H.J., Hakansson, K., Marshall, A.G., The role of electron capture dissociation in biomolecular analysis. *Mass Spectrometry Reviews* **2005**, 24, 201-222.

46. Syka, J.E.P., Coon, J.J., Schroeder, M.J., Shabanowitz, J., Hunt, D.F., Peptide and protein sequence analysis by electron transfer dissociation mass spectrometry. *Proceedings of the National Academy of Sciences of the United States of America* **2004**, 101, 9528-9533.

47. Brodbelt, J.S., Shedding light on the frontier of photodissociation. *Journal of the American Society for Mass Spectrometry* **2011**, 22, 197-206.

48. Brodbelt, J.S., Wilson, J.J., Infrared multiphoton dissociation in quadrupole Ion traps. *Mass Spectrometry Reviews* **2009**, 28, 390-424.

49. Brodbelt, J.S., Photodissociation mass spectrometry: New tools for characterization of biological molecules. *Chemical Society Reviews* **2014**, 43, 2757-2783.

50. Reilly, J.P., Ultraviolet photofragmentation of biomolecular ions. *Mass Spectrometry Reviews* **2009**, 28, 425-447.

51. Cooks, R.G., Collision-induced dissociation - readings and commentary. *Journal of Mass Spectrometry* **1995**, 30, 1215-1221.

52. Thomson, J.J., Rays of positive electricity and their application to chemical analysis, Longmans, Green, London, **1913**.

53. Jennings, K.R., Collision-induced decompositions of aromatic molecular ions. *Int. J. Mass. Spectrom. Ion Phys.* **1968**, 1, 227-235.

54. McLafferty, F.W., Bryce, T.A., Metastable-ion characteristics - characterization of isomeric molecules. *Chemical Communications* **1967**, 1215-1217.

55. McLuckey, S.A., Goeringer, D.E., Slow heating methods in tandem mass spectrometry. *Journal of Mass Spectrometry* **1997**, 32, 461-474.

56. McLuckey, S.A., Mentinova, M., Ion/neutral, ion/electron, ion/photon, and ion/ion interactions in tandem mass spectrometry: Do we need them all? Are they enough? *Journal of the American Society for Mass Spectrometry* **2011**, 22, 3-12.

57. Paizs, B., Suhai, S., Fragmentation pathways of protonated peptides. *Mass Spectrometry Reviews* **2005**, 24, 508-548.

58. Biemann, K., Contributions of mass-spectrometry to peptide and protein-structure. *Biomedical and Environmental Mass Spectrometry* **1988**, 16, 99-111.

59. Roepstorff, P., Fohlman, J., Proposal for a common nomenclature for sequence ions in mass-spectra of peptides. *Biomedical Mass Spectrometry* **1984**, 11, 601-601.

60. Palumbo, A.M., Smith, S.A., Kalcic, C.L., Dantus, M., Stemmer, P.M., Reid, G.E., Tandem mass spectrometry strategies for phosphoproteome analysis. *Mass Spectrometry Reviews* **2011**, 30, 600-625.

61. Downard, K.M., Biemann, K., The effect of charge-state and the localization of charge on the collision-induced dissociation of peptide ions. *Journal of the American Society for Mass Spectrometry* **1994**, 5, 966-975.

62. Thomson, B.A., Douglas, D.J., Corr, J.J., Hager, J.W., Jolliffe, C.L., Improved collisionally activated dissociation efficiency and mass resolution on a triple quadrupole mass-spectrometer system. *Analytical Chemistry* **1995**, 67, 1696-1704.

63. Olsen, J.V., Macek, B., Lange, O., Makarov, A., Horning, S., Mann, M., Higher-energy C-trap dissociation for peptide modification analysis. *Nature Methods* **2007**, 4, 709-712.

64. Tabb, D.L., Smith, L.L., Breci, L.A., Wysocki, V.H., Lin, D., Yates, J.R., Statistical characterization of ion trap tandem mass spectra from doubly charged tryptic peptides. *Analytical Chemistry* **2003**, 75, 1155-1163.

65. Breci, L.A., Tabb, D.L., Yates, J.R., Wysocki, V.H., Cleavage N-terminal to proline: Analysis of a database of peptide tandem mass spectra. *Analytical Chemistry* **2003**, 75, 1963-1971.

66. Gu, C.G., Tsaprailis, G., Breci, L., Wysocki, V.H., Selective gas-phase cleavage at the peptide bond terminal to aspartic acid in fixed-charge derivatives of asp-containing peptides. *Analytical Chemistry* **2000**, 72, 5804-5813.

67. Yu, W., Vath, J.E., Huberty, M.C., Martin, S.A., Identification of the facile gas-phase cleavage of the Asp-Pro and Asp-Xxx peptide-bonds in matrix-assisted laser-desorption time-of-flight mass-spectrometry. *Analytical Chemistry* **1993**, 65, 3015-3023.

68. Huang, Y.Y., Wysocki, V.H., Tabb, D.L., Yates, J.R., The influence of histidine on cleavage C-terminal to acidic residues in doubly protonated tryptic peptides. *International Journal of Mass Spectrometry* **2002**, 219, 233-244.

69. Wysocki, V.H., Tsaprailis, G., Smith, L.L., Breci, L.A., Special feature: Commentary - mobile and localized protons: A framework for understanding peptide dissociation. *Journal of Mass Spectrometry* **2000**, 35, 1399-1406.

70. Lee, S.W., Kim, H.S., Beauchamp, J.L., Salt bridge chemistry applied to gas-phase peptide sequencing: Selective fragmentation of sodiated gas-phase peptide ions adjacent to aspartic acid residues. *Journal of the American Chemical Society* **1998**, 120, 3188-3195.

71. Kapp, E.A., Schutz, F., Reid, G.E., Eddes, J.S., Moritz, R.L., O'Hair, R.A.J., Speed, T.P., Simpson, R.J., Mining a tandem mass spectrometry database to determine the trends and global factors influencing peptide fragmentation. *Analytical Chemistry* **2003**, 75, 6251-6264.

72. Loo, J.A., Edmonds, C.G., Smith, R.D., Tandem mass-spectrometry of very large molecules .2. Dissociation of multiply charged proline-containing proteins from electrospray ionization. *Analytical Chemistry* **1993**, 65, 425-438.

73. Dongre, A.R., Jones, J.L., Somogyi, A., Wysocki, V.H., Influence of peptide composition, gas-phase basicity, and chemical modification on fragmentation efficiency: Evidence for the mobile proton model. *Journal of the American Chemical Society* **1996**, 118, 8365-8374.

74. Cox, K.A., Gaskell, S.J., Morris, M., Whiting, A., Role of the site of protonation in the low-energy decompositions of gas-phase peptide ions. *Journal of the American Society for Mass Spectrometry* **1996**, 7, 522-531.

75. Tsaprailis, G., Nair, H., Zhong, W., Kuppannan, K., Futrell, J.H., Wysocki, V.H., A mechanistic investigation of the enhanced cleavage at histidine in the gas-phase dissociation of protonated peptides. *Analytical Chemistry* **2004**, 76, 2083-2094.

76. Tsaprailis, G., Nair, H., Somogyi, A., Wysocki, V.H., Zhong, W.Q., Futrell, J.H., Summerfield, S.G., Gaskell, S.J., Influence of secondary structure on the fragmentation of protonated peptides. *Journal of the American Chemical Society* **1999**, 121, 5142-5154.

77. Gehrig, P.M., Roschitzki, B., Rutishauser, D., Reiland, S., Schlapbach, R., Phosphorylated serine and threonine residues promote site-specific fragmentation of singly charged, arginine-containing peptide ions. *Rapid Communications in Mass Spectrometry* **2009**, 23, 1435-1445.

78. Balta, B., Aviyente, V., Lifshitz, C., Elimination of water from the carboxyl group of GlyGlyH(+). *Journal of the American Society for Mass Spectrometry* **2003**, 14, 1192-1203.

79. Reid, G.E., Simpson, R.J., O'Hair, R.A.J., Probing the fragmentation reactions of protonated glycine oligomers via multistage mass spectrometry and gas phase ion molecule hydrogen/deuterium exchange. *International Journal of Mass Spectrometry* **1999**, 191, 209-230.

80. Reid, G.E., Simpson, R.J., O'Hair, R.A.J., Leaving group and gas phase neighboring group effects in the side chain losses from protonated serine and its derivatives. *Journal of the American Society for Mass Spectrometry* **2000**, 11, 1047-1060.

81. Ballard, K.D., Gaskell, S.J., Dehydration of peptide [M+H]+ Ions in the gas-phase. *Journal of the American Society for Mass Spectrometry* **1993**, 4, 477-481.

82. Csonka, I.P., Paizs, B., Lendvay, G., Suhai, S., Proton mobility and main fragmentation pathways of protonated lysylglycine. *Rapid Communications in Mass Spectrometry* **2001**, 15, 1457-1472.

83. Dookeran, N.N., Yalcin, T., Harrison, A.G., Fragmentation reactions of protonated alpha-amino acids. *Journal of Mass Spectrometry* **1996**, 31, 500-508.

84. Harrison, A.G., Fragmentation reactions of protonated peptides containing glutamine or glutamic acid. *Journal of Mass Spectrometry* **2003**, 38, 174-187.

85. Froelich, J.M., Reid, G.E., The Effect of Post-translational and process-induced modifications on the multistage gas-phase fragmentation reactions of protonated peptides. *Combinatorial Chemistry & High Throughput Screening* **2009**, 12, 175-184.

86. Csonka, I.P., Paizs, B., Lendvay, G., Suhai, S., Proton mobility in protonated peptides: a joint molecular orbital and RRKM study. *Rapid Communications in Mass Spectrometry* **2000**, 14, 417-431.

87. Paizs, B., Lendvay, G., Vekey, K., Suhai, S., Formation of b(2)(+) ions from protonated peptides: an ab initio study. *Rapid Communications in Mass Spectrometry* **1999**, 13, 525-533.

88. Gronert, S., Li, K.H., Horiuchi, M., Manipulating the fragmentation patterns of phosphopeptides via gas-phase boron derivatization: Determining phosphorylation sites in peptides with multiple serines. *Journal of the American Society for Mass Spectrometry* **2005**, 16, 1905-1914.

89. Leymarie, N., Zaia, J., Effective use of mass spectrometry for glycan and glycopeptide structural analysis. *Analytical Chemistry* **2012**, 84, 3040-3048.

90. Dalpathado, D.S., Desaire, H., Glycopeptide analysis by mass spectrometry. *Analyst* **2008**, 133, 731-738.

91. Reid, G.E., Roberts, K.D., Kapp, E.A., Simpson, R.J., Statistical and mechanistic approaches to understanding the gas-phase fragmentation behavior of methionine sulfoxide containing peptides. *Journal of Proteome Research* **2004**, 3, 751-759.

92. Froelich, J.M., Reid, G.E., Mechanisms for the proton mobility-dependent gas-phase fragmentation reactions of S-alkyl cysteine sulfoxide-containing peptide ions. *Journal of the American Society for Mass Spectrometry* **2007**, 18, 1690-1705.

93. Steen, H., Mann, M., Similarity between condensed phase and gas phase chemistry: Fragmentation of peptides containing oxidized cysteine residues and its implications for proteomics. *Journal of the American Society for Mass Spectrometry* **2001**, 12, 228-232.

94. Yague, J., Nunez, A., Boix, M., Esteller, M., Alfonso, P., Casal, J.I., Oxidation of carboxyamidomethyl cysteine may add complexity to protein identification. *Proteomics* **2005**, 5, 2761-2768.

95. Chowdhury, S.M., Munske, G.R., Ronald, R.C., Bruce, J.E., Evaluation of low energy CID and ECD fragmentation behavior of mono-oxidized thio-ether bonds in peptides. *Journal of the American Society for Mass Spectrometry* **2007**, 18, 493-501.

96. Harrison, A.G., Young, A.B., Bleiholder, C., Suhai, S., Paizs, B., Scrambling of sequence information in collision-induced dissociation of peptides. *Journal of the American Chemical Society* **2006**, 128, 10364-10365.

97. Yague, J., Paradela, A., Ramos, M., Ogueta, S., Marina, A., Barahona, F., de Castro, J.A.L., Vazquez, J., Peptide rearrangement during quadrupole ion trap fragmentation: Added complexity to MS/MS spectra. *Analytical Chemistry* **2003**, 75, 1524-1535.

98. Vachet, R.W., Bishop, B.M., Erickson, B.W., Glish, G.L., Novel peptide dissociation: Gas-phase intramolecular rearrangement of internal amino acid residues. *Journal of the American Chemical Society* **1997**, 119, 5481-5488.

99. Tang, X.J., Thibault, P., Boyd, R.K., Fragmentation reactions of multiply-protonated peptides and implications for sequencing by tandem mass-spectrometry with low-energy collision-induced dissociation. *Analytical Chemistry* **1993**, 65, 2824-2834.

100. Harrison, A.G., Peptide sequence scrambling through cyclization of b(5) Ions. *Journal of the American Society for Mass Spectrometry* **2008**, 19, 1776-1780.

101. Yalcin, T., Khouw, C., Csizmadia, I.G., Peterson, M.R., Harrison, A.G., Why are B ions stable species in peptide spectra? *Journal of the American Society for Mass Spectrometry* **1995**, 6, 1165-1174.

102. Yalcin, T., Csizmadia, I.G., Peterson, M.R., Harrison, A.G., The structure and fragmentation of B-n (n>=3) ions in peptide spectra. *Journal of the American Society for Mass Spectrometry* **1996**, 7, 233-242.

103. Jia, C.X., Qi, W., He, Z.M., Cyclization reaction of peptide fragment ions during multistage collisionally activated decomposition: An inducement to lose internal amino-acid residues. *Journal of the American Society for Mass Spectrometry* **2007**, 18, 663-678.

104. Saminathan, I.S., Wang, X.S., Guo, Y.Z., Krakovska, O., Voisin, S., Hopkinson, A.C., Siu, K.W.M., The extent and effects of peptide sequence scrambling via formation of macrocyclic b Ions in model proteins. *Journal of the American Society for Mass Spectrometry* **2010**, 21, 2085-2094.

105. Yu, L., Tan, Y.L., Tsai, Y., Goodlett, D.R., Polfer, N.C., On the relevance of peptide sequence permutations in shotgun proteomics studies. *Journal of Proteome Research* **2011**, 10, 2409-2416.

106. Bowie, J.H., Brinkworth, C.S., Dua, S., Collision-induced fragmentations of the (M-H)(-) parent anions of underivatized peptides: An aid to structure determination and some unusual negative ion cleavages. *Mass Spectrometry Reviews* **2002**, 21, 87-107.

107. Bilusich, D., Bowie, J.H., Fragmentations of (M-H)(-) Anions of underivatised peptides. Part 2: Characteristic cleavages of Ser and Cys and of disulfides and other post-translational modifications, together with some unusual internal processes. *Mass Spectrometry Reviews* **2009**, 28, 20-34.

108. Bilusich, D., Brinkworth, C.S., McAnoy, A.M., Bowie, J.H., The fragmentations of [M-H](-) anions derived from underivatised peptides. The side-chain loss of H2S from Cys. A joint experimental and theoretical study. *Rapid Communications in Mass Spectrometry* **2003**, 17, 2488-2494.

109. Wang, T.F., Andreazza, H.J., Bilusich, D., Bowie, J.H., Negative ion fragmentations of deprotonated peptides containing post-translational modifications. An unusual cyclisation/rearrangement involving phosphotyrosine; a joint experimental and theoretical study. *Rapid Communications in Mass Spectrometry* **2009**, 23, 1669-1677.

110. Andreazza, H.J., Wang, T.F., Bilusich, D., Hoffmann, P., Bowie, J.H., Negative ion fragmentations of deprotonated peptides containing post-translational modifications: Diphosphorylated systems containing Ser, Thr and Tyr. A characteristic phosphate/phosphate cyclisation. A joint experimental and theoretical study. *Rapid Communications in Mass Spectrometry* **2009**, 23, 1825-1833.

111. Andreazza, H.J., Fitzgerald, M., Bilusich, D., Hoffmann, R., Hoffmann, P., Elchinger, P.C.H., Bowie, J.H., Characteristic negative ion fragmentations of deprotonated peptides containing post-translational modifications: mono-phosphorylated Ser, Thr and Tyr. A joint experimental and theoretical study. *Rapid Communications in Mass Spectrometry* **2008**, 22, 3305-3312.

112. Edelson-Averbukh, M., Pipkorn, R., Lehmann, W.D., Phosphate group-driven fragmentation of multiply charged phosphopeptide anions. Improved recognition of peptides phosphorylated at serine, threonine, or tyrosine by negative ion electrospray tandem mass spectrometry. *Analytical Chemistry* **2006**, 78, 1249-1256.

113. Nwosu, C.C., Strum, J.S., An, H.J., Lebrilla, C.B., Enhanced detection and identification of glycopeptides in negative ion mode mass spectrometry. *Analytical Chemistry* **2010**, 82, 9654-9662.

114. Cooper, H.J., Hakansson, K., Marshall, A.G., The role of electron capture dissociation in biomolecular analysis. *Mass Spectrom Rev* **2005**, 24, 201-222.

115. Zubarev, R.A., Horn, D.M., Fridriksson, E.K., Kelleher, N.L., Kruger, N.A., Lewis, M.A., Carpenter, B.K., McLafferty, F.W., Electron capture dissociation for structural characterization of multiply charged protein cations. *Analytical Chemistry* **2000**, 72, 563-573.

116. Palumbo, A.M., Smith, S.A., Kalcic, C.L., Dantus, M., Stemmer, P.M., Reid, G.E., Tandem mass spectrometry strategies for phosphoproteome analysis. *Mass Spectrom Rev* **2011**.

117. Zubarev, R.A., Reactions of polypeptide ions with electrons in the gas phase. *Mass Spectrometry Reviews* **2003**, 22, 57-77.

118. Zhurov, K.O., Fornelli, L., Wodrich, M.D., Laskay, U.A., Tsybin, Y.O., Principles of electron capture and transfer dissociation mass spectrometry applied to peptide and protein structure analysis. *Chem Soc Rev* **2013**, 42, 5014-5030.

119. Sawicka, A., Skurski, P., Hudgins, R.R., Simons, J., Model calculations relevant to disulfide bond cleavage via electron capture influenced by positively charged groups. *Journal of Physical Chemistry B* **2003**, 107, 13505-13511.

120. Syrstad, E.A., Turecek, F., Toward a general mechanism of electron capture dissociation. *Journal of the American Society for Mass Spectrometry* **2005**, 16, 208-224.

121. Sweet, S.M., Cooper, H.J., Electron capture dissociation in the analysis of protein phosphorylation. *Expert Rev Proteomics* **2007**, 4, 149-159.

122. Bakhtiar, R., Guan, Z., Electron capture dissociation mass spectrometry in characterization of post-translational modifications. *Biochem Biophys Res Commun* **2005**, 334, 1-8.

123. Zubarev, R.A., Kruger, N.A., Fridriksson, E.K., Lewis, M.A., Horn, D.M., Carpenter, B.K., McLafferty, F.W., Electron capture dissociation of gaseous multiply-charged proteins is favored at disulfide bonds and other sites of high hydrogen atom affinity. *Journal of the American Chemical Society* **1999**, 121, 2857-2862.

124. Horn, D.M., Ge, Y., McLafferty, F.W., Activated ion electron capture dissociation for mass spectral sequencing of larger (42 kDa) proteins. *Analytical Chemistry* **2000**, 72, 4778-4784.

125. Yoo, H.J., Wang, N., Zhuang, S.Y., Song, H.T., Hakansson, K., Negative-ion electron capture dissociation: Radical-driven fragmentation of charge-increased gaseous peptide anions. *Journal of the American Chemical Society* **2011**, 133, 16790-16793.

126. McLuckey, S.A., Huang, T.Y., Ion/ion reactions: New chemistry for analytical MS. *Analytical Chemistry* **2009**, 81, 8669-8676.

127. Turecek, F., Chen, X.H., Hao, C.T., Where does the electron go? Electron distribution and reactivity of peptide cation radicals formed by electron transfer in the gas phase. *Journal of the American Chemical Society* **2008**, 130, 8818-8833.

128. Coon, J.J., Ueberheide, B., Syka, J.E.P., Dryhurst, D.D., Ausio, J., Shabanowitz, J., Hunt, D.F., Protein identification using sequential ion/ion reactions and tandem mass spectrometry. *Proceedings of the National Academy of Sciences of the United States of America* **2005**, 102, 9463-9468.

129. Good, D.M., Wirtala, M., McAlister, G.C., Coon, J.J., Performance characteristics of electron transfer dissociation mass spectrometry. *Molecular & Cellular Proteomics* **2007**, 6, 1942-1951.

130. Kim, M.S., Pandey, A., Electron transfer dissociation mass spectrometry in proteomics. *Proteomics* **2012**, 12, 530-542.

131. Coon, J.J., Collisions or electrons? protein sequence analysis in the 21st century. *Analytical Chemistry* **2009**, 81, 3208-3215.

132. Wiesner, J., Premsler, T., Sickmann, A., Application of electron transfer dissociation (ETD) for the analysis of posttranslational modifications. *Proteomics* **2008**, 8, 4466-4483.

133. Swaney, D.L., McAlister, G.C., Wirtala, M., Schwartz, J.C., Syka, J.E.P., Coon, J.J., Supplemental activation method for high-efficiency electron-transfer dissociation of doubly protonated peptide precursors. *Analytical Chemistry* **2007**, 79, 477-485.

134. Rumachik, N.G., McAlister, G.C., Russell, J.D., Bailey, D.J., Wenger, C.D., Coon, J.J., Characterizing peptide neutral losses induced by negative electron-transfer dissociation (NETD). *Journal of the American Society for Mass Spectrometry* **2012**, 23, 718-727.

135. Coon, J.J., Shabanowitz, J., Hunt, D.F., Syka, J.E., Electron transfer dissociation of peptide anions. *Journal of the American Society for Mass Spectrometry* **2005**, 16, 880-882.

136. Huzarska, M., Ugalde, I., Kaplan, D.A., Hartmer, R., Easterling, M.L., Polfer, N.C., Negative electron transfer dissociation of deprotonated phosphopeptide anions: choice of radical cation reagent and competition between electron and proton transfer. *Analytical Chemistry* **2010**, 82, 2873-2878.

137. Kjeldsen, F., Silivra, O.A., Ivonin, I.A., Haselmann, K.F., Gorshkov, M., Zubarev, R.A., C-alpha-C backbone fragmentation dominates in electron detachment dissociation of gas-phase polypeptide polyanions. *Chemistry-A European Journal* **2005**, 11, 1803-1812.

138. Budnik, B.A., Haselmann, K.F., Zubarev, R.A., Electron detachment dissociation of peptide di-anions: An electron-hole recombination phenomenon. *Chemical Physics Letters* **2001**, 342, 299-302.

139. van der Rest, G., He, F., Emmett, M.R., Marshall, A.G., Gaskell, S.J., Gas-phase cleavage of PTC-derivatized electrosprayed tryptic peptides in an FT-ICR trapped-ion cell: Mass-based protein identification without liquid chromatographic separation. *Journal of the American Society for Mass Spectrometry* **2001**, 12, 288-295.

140. Little, D.P., Speir, J.P., Senko, M.W., Oconnor, P.B., Mclafferty, F.W., Infrared multiphoton dissociation of large multiply-Charged ions for biomolecule sequencing. *Analytical Chemistry* **1994**, 66, 2809-2815.

141. Zimmerman, J.A., Watson, C.H., Eyler, J.R., Multiphoton ionization of laser-desorbed neutral molecules in a fourier-transform ion-cyclotron resonance mass-spectrometer. *Analytical Chemistry* **1991**, 63, 361-365.

142. Stephenson, J.L., Booth, M.M., Shalosky, J.A., Eyler, J.R., Yost, R.A., Infrared multiple-photon dissociation in the quadrupole ion-trap via a multipass optical arrangement. *Journal of the American Society for Mass Spectrometry* **1994**, 5, 886-893.

143. Madsen, J.A., Brodbelt, J.S., Comparison of infrared multiphoton dissociation and collision-induced dissociation of supercharged peptides in ion traps. *Journal of the American Society for Mass Spectrometry* **2009**, 20, 349-358.

144. Gardner, M.W., Smith, S.I., Ledvina, A.R., Madsen, J.A., Coon, J.J., Schwartz, J.C., Stafford, G.C., Brodbelt, J.S., Infrared multiphoton dissociation of peptide cations in a dual pressure linear ion trap mass spectrometer. *Analytical Chemistry* **2009**, 81, 8109-8118.

145. Hashimoto, Y., Hasegawa, H., Waki, L., High sensitivity and broad dynamic range infrared multiphoton dissociation for a quadrupole ion trap. *Rapid Communications in Mass Spectrometry* **2004**, 18, 2255-2259.

146. Payne, A.H., Glish, G.L., Thermally assisted infrared multiphoton photodissociation in a quadrupole ion trap. *Analytical Chemistry* **2001**, 73, 3542-3548.

147. Hashimoto, Y., Hasegawa, H., Yoshinari, K., Waki, I., Collision-activated infrared multiphoton dissociation in a quadrupole ion trap mass spectrometer. *Analytical Chemistry* **2003**, 75, 420-425.

148. Ly, T., Julian, R.R., Ultraviolet photodissociation: Developments towards applications for mass-spectrometry-based proteomics. *Angewandte Chemie-International Edition* **2009**, 48, 7130-7137.

149. Madsen, J.A., Boutz, D.R., Brodbelt, J.S., Ultrafast ultraviolet photodissociation at 193 nm and its applicability to proteomic workflows. *Journal of Proteome Research* **2010**, 9, 4205-4214.

150. Madsen, J.A., Kaoud, T.S., Dalby, K.N., Brodbelt, J.S., 193-nm photodissociation of singly and multiply charged peptide anions for acidic proteome characterization. *Proteomics* **2011**, 11, 1329-1334.

151. Parthasarathi, R., He, Y., Reilly, J.P., Raghavachari, K., New insights into the vacuum UV photodissociation of peptides. *Journal of the American Chemical Society* **2010**, 132, 1606-1610.

152. Thompson, M.S., Cui, W.D., Reilly, J.P., Fragmentation of singly charged peptide ions by photodissociation at lambda=157 nm. *Angewandte Chemie-International Edition* **2004**, 43, 4791-4794.

153. Zhang, L.Y., Reilly, J.P., Peptide de novo sequencing using 157 nm photodissociation in a tandem time-of-flight mass spectrometer. *Analytical Chemistry* **2010**, 82, 898-908.

154. Fung, Y.M.E., Kjeldsen, F., Silivra, O.A., Chan, T.W.D., Zubarev, R.A., Facile disulfide bond cleavage in gaseous peptide and protein cations by ultraviolet photodissociation at 157 nm. *Angewandte Chemie-International Edition* **2005**, 44, 6399-6403.

155. Oh, J.Y., Moon, J.H., Kim, M.S., Sequence- and site-specific photodissocniation at 266nm of protonated synthetic polypeptides containing a tryptophanyl residue. *Rapid Communications in Mass Spectrometry* **2004**, 18, 2706-2712.

156. Vasicek, L., Brodbelt, J.S., Enhancement of ultraviolet photodissociation efficiencies through attachment of aromatic chromophores. *Analytical Chemistry* **2010**, 82, 9441-9446.

157. Schreiber, T.B., Mausbacher, N., Breitkopf, S.B., Grundner-Culemann, K., Daub, H., Quantitative phosphoproteomics--an emerging key technology in signal-transduction research. *Proteomics* **2008**, 8, 4416-4432.

158. Hunter, T., Signaling - 2000 and beyond. *Cell* **2000**, 100, 113-127.

159. Stein, A., Pache, R.A., Bernado, P., Pons, M., Aloy, P., Dynamic interactions of proteins in complex networks: a more structured view. *FEBS J* **2009**, 276, 5390-5405.

160. Cohen, P., The regulation of protein function by multisite phosphorylation--a 25 year update. *Trends Biochem Sci* **2000**, 25, 596-601.

161. Tamayev, R., Zhou, D.W., D'Adamio, L., The interactome of the amyloid beta precursor protein family members is shaped by phosphorylation of their intracellular domains. *Molecular Neurodegeneration* **2009**, 4, 1-14.

162. Lawrence, M.C., Jivan, A., Shao, C., Duan, L., Goad, D., Zaganjor, E., Osborne, J., McGlynn, K., Stippec, S., Earnest, S., Chen, W., Cobb, M.H., The roles of MAPKs in disease. *Cell Res* **2008**, 18, 436-442.

163. Hershko, D.D., Shapira, M., Prognostic role of p27Kip1 deregulation in colorectal cancer. *Cancer* **2006**, 107, 668-675.

164. Brambilla, E., Gazzeri, S., Lantuejoul, S., Coll, J.L., Moro, D., Negoescu, A., Brambilla, C., p53 mutant immunophenotype and deregulation of p53 transcription pathway (Bcl2, Bax, and Waf1) in precursor bronchial lesions of lung cancer. *Clin Cancer Res* **1998**, 4, 1609-1618.

165. Takai, N., Hamanaka, R., Yoshimatsu, J., Miyakawa, I., Polo-like kinases (Plks) and cancer. *Oncogene* **2005**, 24, 287-291.

166. Kewalramani, G., An, D., Kim, M.S., Ghosh, S., Qi, D., Abrahani, A., Pulinilkunnil, T., Sharma, V., Wambolt, R.B., Allard, M.F., Innis, S.M., Rodrigues, B., AMPK control of myocardial fatty acid metabolism fluctuates with the intensity of insulin-deficient diabetes. *Journal of Molecular and Cellular Cardiology* **2007**, 42, 333-342.

167. Arber, S., Barbayannis, F.A., Hanser, H., Schneider, C., Stanyon, C.A., Bernard, O., Caroni, P., Regulation of actin dynamics through phosphorylation of cofilin by LIM-kinase. *Nature* **1998**, 393, 805-809.

168. Heredia, L., Helguera, P., de Olmos, S., Kedikian, G., Sola Vigo, F., LaFerla, F., Staufenbiel, M., de Olmos, J., Busciglio, J., Caceres, A., Lorenzo, A., Phosphorylation of actin-depolymerizing factor/cofilin by LIM-kinase mediates amyloid beta-induced degeneration: a potential mechanism of neuronal dystrophy in Alzheimer's disease. *The Journal of Neuroscience* **2006**, 26, 6533-6542.

169. Zeigler, M.E., Chi, Y., Schmidt, T., Varani, J., Role of ERK and JNK pathways in regulating cell motility and matrix metalloproteinase 9 production in growth factor-

stimulated human epidermal keratinocytes. *Journal of Cellular Physiology* **1999**, 180, 271-284.

170. Reinders, J., Sickmann, A., State-of-the-art in phosphoproteomics. *Proteomics* **2005**, 5, 4052-4061.

171. Nita-Lazar, A., Saito-Benz, H., White, F.M., Quantitative phosphoproteomics by mass spectrometry: past, present, and future. *Proteomics* **2008**, 8, 4433-4443.

172. Schmelzle, K., Kane, S., Gridley, S., Lienhard, G.E., White, F.M., Temporal dynamics of tyrosine phosphorylation in insulin signaling. *Diabetes* **2006**, 55, 2171-2179.

173. Olsen, J.V., Blagoev, B., Gnad, F., Macek, B., Kumar, C., Mortensen, P., Mann, M., Global, in vivo, and site-specific phosphorylation dynamics in signaling networks. *Cell* **2006**, 127, 635-648.

174. Swaney, D.L., Wenger, C.D., Thomson, J.A., Coon, J.J., Human embryonic stem cell phosphoproteome revealed by electron transfer dissociation tandem mass spectrometry. *Proceedings of the National Academy of Sciences of the United States of America* **2009**, 106, 995-1000.

175. Dunn, J.D., Reid, G.E., Bruening, M.L., Techniques for phosphopeptide enrichment prior to analysis by mass spectrometry. *Mass Spectrometry Reviews* **2010**, 29, 29-54.

176. Grimsrud, P.A., Swaney, D.L., Wenger, C.D., Beauchene, N.A., Coon, J.J., Phosphoproteomics for the masses. *ACS Chem Biol* **2010**, 5, 105-119.

177. Kweon, H.K., Hakansson, K., Selective zirconium dioxide-based enrichment of phosphorylated peptides for mass spectrometric analysis. *Analytical Chemistry* **2006**, 78, 1743-1749.

178. Larsen, M.R., Thingholm, T.E., Jensen, O.N., Roepstorff, P., Jorgensen, T.J., Highly selective enrichment of phosphorylated peptides from peptide mixtures using titanium dioxide microcolumns. *Molecular & Cellular Proteomics* **2005**, 4, 873-886.

179. Pinkse, M.W., Uitto, P.M., Hilhorst, M.J., Ooms, B., Heck, A.J., Selective isolation at the femtomole level of phosphopeptides from proteolytic digests using 2D-NanoLC-ESI-MS/MS and titanium oxide precolumns. *Analytical Chemistry* **2004**, 76, 3935-3943.

180. Palumbo, A.M., Tepe, J.J., Reid, G.E., Mechanistic insights into the multistage gas-phase fragmentation behavior of phosphoserine- and phosphothreonine-containing peptides. *Journal of Proteome Research* **2008**, 7, 771-779.

181. Chang, E.J., Archambault, V., McLachlin, D.T., Krutchinsky, A.N., Chait, B.T., Analysis of protein phosphorylation by hypothesis-driven multiple-stage mass spectrometry. *Analytical Chemistry* **2004**, 76, 4472-4483.

182. Jiang, X., Han, G., Feng, S., Ye, M., Yao, X., Zou, H., Automatic validation of phosphopeptide identifications by the MS2/MS3 target-decoy search strategy. *Journal of Proteome Research* **2008**, 7, 1640-1649.

183. Schroeder, M.J., Shabanowitz, J., Schwartz, J.C., Hunt, D.F., Coon, J.J., A neutral loss activation method for improved phosphopeptide sequence analysis by quadrupole ion trap mass spectrometry. *Analytical Chemistry* **2004**, 76, 3590-3598.

184. Villen, J., Beausoleil, S.A., Gygi, S.P., Evaluation of the utility of neutral-loss-dependent MS3 strategies in large-scale phosphorylation analysis. *Proteomics* **2008**, 8, 4444-4452.

185. Yu, L.R., Zhu, Z.Y., Chan, K.C., Issaq, H.J., Dimitrov, D.S., Veenstra, T.D., Improved titanium dioxide enrichment of phosphopeptides from HeLa cells and high confident phosphopeptide identification by cross-validation of MS/MS and MS/MS/MS spectra. *J. Proteome Res.* **2007**, 6, 4150-4162.

186. Beausoleil, S.A., Jedrychowski, M., Schwartz, D., Elias, J.E., Villen, J., Li, J.X., Cohn, M.A., Cantley, L.C., Gygi, S.P., Large-scale characterization of HeLa cell nuclear phosphoproteins. *Proc. Natl. Acad. Sci. USA* **2004**, 101, 12130-12135.

187. Palumbo, A.M., Reid, G.E., Evaluation of gas-phase rearrangement and competing fragmentation reactions on protein phosphorylation site assignment using collision induced dissociation-MS/MS and MS3. *Analytical Chemistry* **2008**, 80, 9735-9747.

188. Janek, K., Wenschuh, H., Bienert, M., Krause, E., Phosphopeptide analysis by positive and negative ion matrix-assisted laser desorption/ionization mass spectrometry. *Rapid Commun Mass Spectrom* **2001**, 15, 1593-1599.

189. Edelson-Averbukh, M., Shevchenko, A., Pipkorn, R., Lehmann, W.D., Gas-phase intramolecular phosphate shift in phosphotyrosine-containing peptide monoanions. *Analytical Chemistry* **2009**, 81, 4369-4381.

190. Good, D.M., Wirtala, M., McAlister, G.C., Coon, J.J., Performance characteristics of electron transfer dissociation mass spectrometry. *Molecular & Cellular Proteomics* **2007**, 6, 1942-1951.

191. Molina, H., Horn, D.M., Tang, N., Mathivanan, S., Pandey, A., Global proteomic profiling of phosphopeptides using electron transfer dissociation tandem mass spectrometry. *Proceedings of the National Academy of Sciences of the United States of America* **2007**, 104, 2199-2204.

192. Huzarska, M., Ugalde, I., Kaplan, D.A., Hartmer, R., Easterling, M.L., Polfer, N.C., Negative electron transfer dissociation of deprotonated phosphopeptide anions: choice of radical cation reagent and competition between electron and proton transfer. *Analytical Chemistry* **2010**, 82, 2873-2878.

193. Apweiler, R., Hermjakob, H., Sharon, N., On the frequency of protein glycosylation, as deduced from analysis of the SWISS-PROT database. *Biochimica Et Biophysica Acta-General Subjects* **1999**, 1473, 4-8.

194. Dwek, R.A., Glycobiology: Toward understanding the function of sugars. *Chemical Reviews* **1996**, 96, 683-720.

195. Patrie, S.M., Roth, M.J., Kohler, J.J., Introduction to glycosylation and mass spectrometry. *Ovarian Cancer: Methods and Protocols* **2013**, 951, 1-17.

196. Budnik, B.A., Lee, R.S., Steen, J.A., Global methods for protein glycosylation analysis by mass spectrometry. *Biochim Biophys Acta* **2006**, 1764, 1870-1880.

197. Rudd, P.M., Elliott, T., Cresswell, P., Wilson, I.A., Dwek, R.A., Glycosylation and the immune system. *Science* **2001**, 291, 2370-2376.

198. Taniguchi, N., Human disease glycomics/proteome initiative (HGPI). *Molecular & Cellular Proteomics* **2008**, 7, 626-627.

199. Dube, D.H., Bertozzi, C.R., Glycans in cancer and inflammation. Potential for therapeutics and diagnostics. *Nature Reviews Drug Discovery* **2005**, 4, 477-488.

200. Morelle, W., Michalski, J.C., The mass spectrometric analysis of glycoproteins and their glycan structures. *Current Analytical Chemistry* **2005**, 1, 29-57.

201. Nilsson, B., Analysis of protein glycosylation by mass spectrometry. *Molecular Biotechnology* **1994**, 2, 243-280.

202. Morelle, W., Canis, K., Chirat, F., Faid, V., Michalski, J.C., The use of mass spectrometry for the proteomic analysis of glycosylation. *Proteomics* **2006**, 6, 3993-4015.

203. Hofsteenge, J., Muller, D.R., Debeer, T., Loffler, A., Richter, W.J., Vliegenthart, J.F.G., New-type of linkage between a carbohydrate and a protein - C-glycosylation of a specific tryptophan residue in human rnase U-S. *Biochemistry* **1994**, 33, 13524-13530.

204. Geng, M., Zhang, X., Bina, M., Regnier, F., Proteomics of glycoproteins based on affinity selection of glycopeptides from tryptic digests. *Journal of Chromatography B* **2001**, 752, 293-306.

205. Kaji, H., Saito, H., Yamauchi, Y., Shinkawa, T., Taoka, M., Hirabayashi, J., Kasai, K., Takahashi, N., Isobe, T., Lectin affinity capture, isotope-coded tagging and mass spectrometry to identify N-linked glycoproteins. *Nature Biotechnology* **2003**, 21, 667-672.

206. Bunkenborg, J., Pilch, B.J., Podtelejnikov, A.V., Wisniewski, J.R., Screening for N-glycosylated proteins by liquid chromatography mass spectrometry. *Proteomics* **2004**, 4, 454-465.

207. Qiu, R.Q., Regnier, F.E., Use of multidimensional lectin affinity chromatography in differential glycoproteomics. *Analytical Chemistry* **2005**, 77, 2802-2809.

208. Harvey, D.J., Identification of protein-bound carbohydrates by mass spectrometry. *Proteomics* **2001**, 1, 311-328.

209. Patel, T., Bruce, J., Merry, A., Bigge, C., Wormald, M., Jaques, A., Parekh, R., Use of hydrazine to release in intact and unreduced form both N-linked and O-linked oligosaccharides from glycoproteins. *Biochemistry* **1993**, 32, 679-693.

210. Patel, T.P., Parekh, R.B., Release of oligosaccharides from glycoproteins by hydrazinolysis. *Guide to Techniques in Glycobiology* **1994**, 230, 57-66.

211. Iyer, R.N., Carlson, D.M., Alkaline borohydride degradation of blood group-H substance. *Arch Biochem Biophys* **1971**, 142, 101-&.

212. Mechref, Y., Novotny, M.V., Structural investigations of glycoconjugates at high sensitivity. *Chemical Reviews* **2002**, 102, 321-369.

213. Zhang, L., Reilly, J.P., Extracting both peptide sequence and glycan structural information by 157 nm photodissociation of N-linked glycopeptides. *Journal of Proteome Research* **2009**, 8, 734-742.

214. Vekey, K., Ozohanics, O., Toth, E., Jeko, A., Revesz, A., Krenyacz, J., Drahos, L., Fragmentation characteristics of glycopeptides. *International Journal of Mass Spectrometry* **2013**, 345, 71-79.

215. Demelbauer, U.M., Zehl, M., Plematl, A., Allmaier, G., Rizzi, A., Determination of glycopeptide structures by multistage mass spectrometry with low-energy collision-induced dissociation: comparison of electrospray ionization quadrupole ion trap and matrix-assisted laser desorption/ionization quadrupole ion trap reflectron time-of-flight approaches. *Rapid Communications in Mass Spectrometry* **2004**, 18, 1575-1582.

216. Olivova, P., Chen, W.B., Chakraborty, A.B., Gebler, J.C., Determination of N-glycosylation sites and site heterogeneity in a monoclonal antibody by electrospray quadrupole ion-mobility time-of-flight mass spectrometry. *Rapid Communications in Mass Spectrometry* **2008**, 22, 29-40.

217. Bykova, N.V., Rampitsch, C., Krokhin, O., Standing, K.G., Ens, W., Determination and characterization of site-specific N-glycosylation using MALDI-Qq-TOF tandem mass spectrometry: Case study with a plant protease. *Analytical Chemistry* **2006**, 78, 1093-1103.

218. Hogan, J.M., Pitteri, S.J., Chrisman, P.A., McLuckey, S.A., Complementary structural information from a tryptic N-linked glycopeptide via electron transfer ion/ion reactions and collision-induced dissociation. *Journal of Proteome Research* **2005**, 4, 628-632.

219. Mirgorodskaya, E., Roepstorff, P., Zubarev, R.A., Localization of O-glycosylation sites in peptides by electron capture dissociation in a fourier transform mass spectrometer. *Analytical Chemistry* **1999**, 71, 4431-4436.

220. Hakansson, K., Cooper, H.J., Emmett, M.R., Costello, C.E., Marshall, A.G., Nilsson, C.L., Electron capture dissociation and infrared multiphoton dissociation MS/MS of an N-glycosylated tryptic peptide to yield complementary sequence information. *Analytical Chemistry* **2001**, 73, 4530-4536.

221. Alley, W.R., Mechref, Y., Novotny, M.V., Characterization of glycopeptides by combining collision-induced dissociation and electron-transfer dissociation mass spectrometry data. *Rapid Communications in Mass Spectrometry* **2009**, 23, 161-170.

222. Wu, S.L., Huehmer, A.F.R., Hao, Z.Q., Karger, B.L., On-line LC-MS approach combining collision-induced dissociation (CID), electron-transfer dissociation (ETD), and CID of an isolated charge-reduced species for the trace-level characterization of proteins with post-translational modifications. *Journal of Proteome Research* **2007**, 6, 4230-4244.

223. Seipert, R.R., Dodds, E.D., Clowers, B.H., Beecroft, S.M., German, J.B., Lebrilla, C.B., Factors that influence fragmentation behavior of N-linked glycopeptide ions. *Analytical Chemistry* **2008**, 80, 3684-3692.

224. Dodds, E.D., Gas-phase dissociation of glycosylated peptide ions. *Mass Spectrometry Reviews* **2012**, 31, 666-682.

225. Deguchi, K., Ito, H., Takegawa, Y., Shinji, N., Nakagawa, H., Nishimura, S.I., Complementary structural information of positive- and negative-ion MSn spectra of glycopeptides with neutral and sialylated N-glycans. *Rapid Communications in Mass Spectrometry* **2006**, 20, 741-746.

226. Deguchi, K., Ito, H., Baba, T., Hirabayashi, A., Nakagawa, H., Fumoto, M., Hinou, H., Nishimura, S.I., Structural analysis of O-glycopeptides employing negative- and positive-ion multi-stage mass spectra obtained by collision-induced and electron-capture dissociations in linear ion trap time-of-flight mass spectrometry. *Rapid Communications in Mass Spectrometry* **2007**, 21, 691-698.

227. Ko, B.J., Brodbelt, J.S., 193 nm ultraviolet photodissociation of deprotonated sialylated oligosaccharides. *Analytical Chemistry* **2011**, 83, 8192-8200.

228. Madsen, J.A., Ko, B.J., Xu, H., Iwashkiw, J.A., Robotham, S.A., Shaw, J.B., Feldman, M.F., Brodbelt, J.S., Concurrent automated sequencing of the glycan and peptide portions of O-linked glycopeptide anions by ultraviolet photodissociation mass spectrometry. *Analytical Chemistry* **2013**, 85, 9253-9261.

229. Shacter, E., Quantification and significance of protein oxidation in biological samples. *Drug Metab Rev* **2000**, 32, 307-326.

230. Bakhtiar, R., Guan, Z., Electron capture dissociation mass spectrometry in characterization of peptides and proteins. *Biotechnol Lett* **2006**, 28, 1047-1059.

231. Spickett, C.M., Pitt, A.R., Protein oxidation: role in signalling and detection by mass spectrometry. *Amino Acids* **2012**, 42, 5-21.

232. Stadtman, E.R., Moskovitz, J., Levine, R.L., Oxidation of methionine residues of proteins: Biological consequences. *Antioxidants & Redox Signaling* **2003**, 5, 577-582.

233. Stadtman, E.R., Van Remmen, H., Richardson, A., Wehr, N.B., Levine, R.L., Methionine oxidation and aging. *Biochimica Et Biophysica Acta-Proteins and Proteomics* **2005**, 1703, 135-140.

234. Froelich, J.M., Reid, G.E., The origin and control of ex vivo oxidative peptide modifications prior to mass spectrometry analysis. *Proteomics* **2008**, 8, 1334-1345.

235. Jiang, X.Y., Smith, J.B., Abraham, E.C., Identification of a MS-MS fragment diagnostic for methionine sulfoxide. *Journal of Mass Spectrometry* **1996**, 31, 1309-1310.

236. Guan, Z.Q., Yates, N.A., Bakhtiar, R., Detection and characterization of methionine oxidation in peptides by collision-induced dissociation and electron capture dissociation. *Journal of the American Society for Mass Spectrometry* **2003**, 14, 605-613.

237. Vaudel, M., Sickmann, A., Martens, L., Current methods for global proteome identification. *Expert Review of Proteomics* **2012**, 9, 519-532.

238. Gentzel, M., Kocher, T., Ponnusamy, S., Wilm, M., Preprocessing of tandem mass spectrometric data to support automatic protein identification. *Proteomics* **2003**, 3, 1597-1610.

239. Hastings, C.A., Norton, S.M., Roy, S., New algorithms for processing and peak detection in liquid chromatography/mass spectrometry data. *Rapid Communications in Mass Spectrometry* **2002**, 16, 462-467.

240. Senko, M.W., Beu, S.C., Mclafferty, F.W., Determination of monoisotopic masses and ion populations for large biomolecules from resolved isotopic distributions. *Journal of the American Society for Mass Spectrometry* **1995**, 6, 229-233.

241. Zhang, Z.Q., Marshall, A.G., A universal algorithm for fast and automated charge state deconvolution of electrospray mass-to-charge ratio spectra. *Journal of the American Society for Mass Spectrometry* **1998**, 9, 225-233.

242. Hernandez, P., Muller, M., Appel, R.D., Automated protein identification by tandem mass spectrometry: Issues and strategies. *Mass Spectrometry Reviews* **2006**, 25, 235-254.

243. Matthiesen, R., Methods, algorithms and tools in computational proteomics: A practical point of view. *Proteomics* **2007**, 7, 2815-2832.

244. Lopez-Ferrer, D., Martinez-Bartolome, S., Villar, M., Campillos, M., Martin-Maroto, F., Vazquez, J., Statistical model for large-scale peptide identification in databases from tandem mass spectra using SEQUEST. *Analytical Chemistry* **2004**, 76, 6853-6860.

245. Sadygov, R.G., Cociorva, D., Yates, J.R., Large-scate database searching using tandem mass spectra: Looking up the answer in the back of the book. *Nature Methods* **2004**, 1, 195-202.

246. Cox, J., Neuhauser, N., Michalski, A., Scheltema, R.A., Olsen, J.V., Mann, M., Andromeda: A peptide search engine integrated into the MaxQuant environment. *Journal of Proteome Research* **2011**, 10, 1794-1805.

247. Kim, S., Bandeira, N., Pevzner, P.A., Spectral profiles, a novel representation of tandem mass spectra and their applications for de novo peptide sequencing and identification. *Molecular & Cellular Proteomics* **2009**, 8, 1391-1400.

248. Tabb, D.L., Saraf, A., Yates, J.R., GutenTag: High-throughput sequence tagging via an empirically derived fragmentation model. *Analytical Chemistry* **2003**, 75, 6415-6421.

249. Tabb, D.L., Ma, Z.Q., Martin, D.B., Ham, A.J.L., Chambers, M.C., DirecTag: Accurate sequence tags from peptide MS/MS through statistical scoring. *Journal of Proteome Research* **2008**, 7, 3838-3846.

250. Tanner, S., Shu, H.J., Frank, A., Wang, L.C., Zandi, E., Mumby, M., Pevzner, P.A., Bafna, V., InsPecT: Identification of posttransiationally modified peptides from tandem mass spectra. *Analytical Chemistry* **2005**, 77, 4626-4639.

251. Na, S., Bandeira, N., Paek, E., Fast multi-blind modification search through tandem mass spectrometry. *Molecular & Cellular Proteomics* **2012**, 11, M111.010199.

252. Chalkley, R.J., Clauser, K.R., Modification site localization scoring: Strategies and performance. *Molecular & Cellular Proteomics* **2012**, 11, 3-14.

253. Beausoleil, S.A., Villen, J., Gerber, S.A., Rush, J., Gygi, S.P., A probability-based approach for high-throughput protein phosphorylation analysis and site localization. *Nature Biotechnology* **2006**, 24, 1285-1292.

254. Ruttenberg, B.E., Pisitkun, T., Knepper, M.A., Hoffert, J.D., PhosphoScore: An open-source phosphorylation site assignment tool for MSn data. *Journal of Proteome Research* **2008**, 7, 3054-3059.

255. Taus, T., Kocher, T., Pichler, P., Paschke, C., Schmidt, A., Henrich, C., Mechtler, K., Universal and confident phosphorylation site localization using phosphoRS. *Journal of Proteome Research* **2011**, 10, 5354-5362.

256. Savitski, M.M., Lemeer, S., Boesche, M., Lang, M., Mathieson, T., Bantscheff, M., Kuster, B., Confident phosphorylation site localization using the Mascot delta score. *Molecular & Cellular Proteomics* **2011**, 10, M110.003830.

257. Chi, A., Bai, D.L., Geer, L.Y., Shabanowitz, J., Hunt, D.F., Analysis of intact proteins on a chromatographic time scale by electron transfer dissociation tandem mass spectrometry. *International Journal of Mass Spectrometry* **2007**, 259, 197-203.

258. Sadygov, R.G., Good, D.M., Swaney, D.L., Coon, J.J., A new probabilistic database search algorithm for ETD spectra. *Journal of Proteome Research* **2009**, 8, 3198-3205.

259. Aguiar, M., Haas, W., Beausoleil, S.A., Rush, J., Gygi, S.P., Gas-phase rearrangements do not affect site localization reliability in phosphoproteomics data sets. *Journal of Proteome Research* **2010**, 9, 3103-3107.

260. Mischerikow, N., Altelaar, A.F.M., Navarro, J.D., Mohammed, S., Heck, A.J.R., Comparative assessment of site assignments in CID and electron transfer dissociation spectra of phosphopeptides discloses limited relocation of phosphate groups. *Molecular & Cellular Proteomics* **2010**, 9, 2140-2148.

261. Mortensen, P., Gouw, J.W., Olsen, J.V., Ong, S.E., Rigbolt, K.T., Bunkenborg, J., Cox, J., Foster, L.J., Heck, A.J., Blagoev, B., Andersen, J.S., Mann, M., MSQuant, an open source platform for mass spectrometry-based quantitative proteomics. *Journal of Proteome Research* **2010**, 9, 393-403.

262. Villen, J., Beausoleil, S.A., Gerber, S.A., Gygi, S.P., Large-scale phosphorylation analysis of mouse liver. *Proceedings of the National Academy of Sciences of the United States of America* **2007**, 104, 1488-1493.

263. Beausoleil, S.A., Jedrychowski, M., Schwartz, D., Elias, J.E., Villen, J., Li, J.X., Cohn, M.A., Cantley, L.C., Gygi, S.P., Large-scale characterization of HeLa cell nuclear phosphoproteins. *Proceedings of the National Academy of Sciences of the United States of America* **2004**, 101, 12130-12135.

264. Jiang, X.N., Han, G.H., Feng, S., Jiang, X.G., Ye, M.L., Yao, X.B., Zou, H.F., Automatic validation of phosphopeptide identifications by the MS2/MS3 target-decoy search strategy. *Journal of Proteome Research* **2008**, 7, 1640-1649.

265. Yu, L.R., Zhu, Z.Y., Chan, K.C., Issaq, H.J., Dimitrov, D.S., Veenstra, T.D., Improved titanium dioxide enrichment of phosphopeptides from HeLa cells and high confident phosphopeptide identification by cross-validation of MS/MS and MS/MS/MS spectra. *Journal of Proteome Research* **2007**, 6, 4150-4162.

266. Annan, R.S., Carr, S.A., Phosphopeptide analysis by matrix-assisted laser desorption time-of-flight mass spectrometry. *Analytical Chemistry* **1996**, 68, 3413-3421.

267. Zhang, Y., Ficarro, S.B., Li, S.J., Marto, J.A., Optimized orbitrap HCD for quantitative analysis of phosphopeptides. *Journal of the American Society for Mass Spectrometry* **2009**, 20, 1425-1434.

268. Axelsson, B.S., Otoole, K.J., Spencer, P.A., Young, D.W., Versatile synthesis of stereospecifically labeled D-amino acids via labeled aziridines - Preparation of (2r,3s)-[3-H-2(1)]-serine and (2r,3r)-[2,3-H-2(2)]-serine (2s,2's,3s,3's-[3,3'-H-2(2)]-cystine and (2s,2's,3r,3'r)-[2,2',3,3'-H-2(4)]-cystine and (2s,3s)-[3-H-2(1)-] and (2s,3r)-[2,3-H-2(2)]-beta-chloroalanine. *Journal of the Chemical Society-Perkin Transactions 1* **1994**, 7, 807-815.

269. Brimble, M.A., Kowalczyk, R., Harris, P.W.R., Dunbar, P.R., Muir, V.J., Synthesis of fluorescein-labelled O-mannosylated peptides as components for synthetic vaccines: comparison of two synthetic strategies. *Organic & Biomolecular Chemistry* **2008**, 6, 112-121.

270. Beresford, K.J.M., Church, N.J., Young, D.W., Synthesis of alpha-amino acids by reaction of aziridine-2-carboxylic acids with carbon nucleophiles. *Organic & Biomolecular Chemistry* **2006**, 4, 2888-2897.

271. Wakamiya, T., Shimbo, K., Shiba, T., Nakajima, K., Neya, M., Okawa, K., Synthesis of threo-3-methylcysteine from threonine. *Bulletin of the Chemical Society of Japan* **1982**, 55, 3878-3881.

272. Fraser, W.D., Hyperparathyroidism. *Lancet* **2009**, 374, 145-158.

273. Vieira, J.G., PTH assays: Understanding what we have and forecasting what we will have. *Journal of Osteoporosis* **2012**, 2012, 523246.

274. Hocher, B., Armbruster, F.P., Stoeva, S., Reichetzeder, C., Gron, H.J., Lieker, I., Khadzhynov, D., Slowinski, T., Roth, H.J., Measuring parathyroid hormone (PTH) in patients with oxidative stress--do we need a fourth generation parathyroid hormone assay? *PLoS One* **2012**, 7, e40242.

275. Beard, C.M., Heath, H., Ofallon, W.M., Anderson, J.A., Earle, J.D., Melton, L.J., Therapeutic radiation and hyperparathyroidism - a case-control study in rochester, minn. *Arch Intern Med* **1989**, 149, 1887-1890.

276. Fujiwara, S., Sposto, R., Ezaki, H., Akiba, S., Neriishi, K., Kodama, K., Hosoda, Y., Shimaoka, K., Hyperparathyroidism among atomic-bomb survivors in hiroshima. *Radiation Research* **1992**, 130, 372-378.

277. Lopez, M.F., Rezai, T., Sarracino, D.A., Prakash, A., Krastins, B., Athanas, M., Singh, R.J., Barnidge, D.R., Oran, P., Borges, C., Nelson, R.W., Selected reaction monitoring-mass spectrometric immunoassay responsive to parathyroid hormone and related variants. *Clinical Chemistry* **2010**, 56, 281-290.

278. Kumar, V., Barnidge, D.R., Chen, L.S., Twentyman, J.M., Cradic, K.W., Grebe, S.K., Singh, R.J., Quantification of serum 1-84 parathyroid hormone in patients with hyperparathyroidism by immunocapture in situ digestion liquid chromatography-tandem mass spectrometry. *Clinical Chemistry* **2010**, 56, 306-313.

279. D'Amour, P., Brossard, J.H., Rousseau, L., Nguyen-Yamamoto, L., Nassif, E., Lazure, C., Gauthier, D., Lavigne, J.R., Zahradnik, R.J., Structure of non-(1-84) PTH fragments secreted by parathyroid glands in primary and secondary hyperparathyroidism. *Kidney International* **2005**, 68, 998-1007.

280. Zhang, C.X., Weber, B.V., Thammavong, J., Grover, T.A., Wells, D.S., Identification of carboxyl-terminal peptide fragments of parathyroid hormone in human plasma at low-picomolar levels by mass spectrometry. *Analytical Chemistry* **2006**, 78, 1636-1643.

281. Potts, J.T., Tregear, G.W., Keutmann, H.T., Niall, H.D., Sauer, R., Deftos, L.J., Dawson, B.F., Hogan, M.L., Aurbach, G.D., Synthesis of a biologically active N-terminal tetratriacontapeptide of parathyroid hormone. *Proceedings of the National Academy of Sciences of the United States of America* **1971**, 68, 63-67.

282. Joly, D., Drueke, T.B., Alberti, C., Houillier, P., Lawson-Body, E., Martin, K.J., Massart, C., Moe, S.M., Monge, M., Souberbielle, J.C., Variation in serum and plasma PTH levels in second-generation assays in hemodialysis patients: a cross-sectional study. *Am J Kidney Dis* **2008**, 51, 987-995.

283. Berson, S.A., Aurbach, G.D., Potts, J.T., Yalow, R.S., Immunoassay of bovine and human parathyroid hormone. *Proceedings of the National Academy of Sciences of the United States of America* **1963**, 49, 613-617.

284. Nussbaum, S.R., Zahradnik, R.J., Lavigne, J.R., Brennan, G.L., Nozawaung, K., Kim, L.Y., Keutmann, H.T., Wang, C.A., Potts, J.T., Segre, G.V., Highly sensitive 2-site immunoradiometric assay of parathyrin, and its clinical utility in evaluating patients with hypercalcemia. *Clinical Chemistry* **1987**, 33, 1364-1367.

285. Lepage, R., Roy, L., Brossard, J.H., Rousseau, L., Dorais, C., Lazure, C., D'Amour, P., A non-(I-84) circulating parathyroid hormone (PTH) fragment interferes significantly with intact PTH commercial assay measurements in uremic samples. *Clinical Chemistry* **1998**, 44, 805-809.

286. Eastell, R., Arnold, A., Brandi, M.L., Brown, E.M., D'Amour, P., Hanley, D.A., Rao, D.S., Rubin, M.R., Goltzman, D., Silverberg, S.J., Marx, S.J., Peacock, M., Mosekilde, L., Bouillon, R., Lewiecki, E.M., Diagnosis of asymptomatic primary hyperparathyroidism: Proceedings of the third international workshop. *Journal of Clinical Endocrinology & Metabolism* **2009**, 94, 340-350.

287. Ji, J.A., Zhang, B., Cheng, W., Wang, Y.J., Methionine, tryptophan, and histidine oxidation in a model protein, PTH: mechanisms and stabilization. *Journal of Pharmaceutical Sciences* **2009**, 98, 4485-4500.

288. Nabuchi, Y., Fujiwara, E., Ueno, K., Kuboniwa, H., Asoh, Y., Ushio, H., Oxidation of recombinant human parathyroid hormone: Effect of oxidized position on the biological activity. *Pharmaceutical Research* **1995**, 12, 2049-2052.

289. Horiuchi, N., Effects of oxidation of human parathyroid-hormone on its biological-activity in continuously infused, thyroparathyroidectomized rats. *Journal of Bone and Mineral Research* **1988**, 3, 353-358.

290. Zull, J.E., Smith, S.K., Wiltshire, R., Effect of methionine oxidation and deletion of amino-terminal residues on the conformation of parathyroid-hormone - circular-dichroism studies. *Journal of Biological Chemistry* **1990**, 265, 5671-5676.